Study of Titanium based Composite Coatings for Resistance against Molten Aluminium Soldering on H13 Tool Steel

A thesis submitted in fulfilment
of the requirements for the degree
of
Doctor of Philosophy in Engineering
at
The University of Waikato

by

ASMA SIDDIQ SALMAN

THE UNIVERSITY OF
WAIKATO
Te Whare Wānanga o Waikato

The University of Waikato
2011

To my father Ch. Muhammad Siddiq and to my mother Musarat Siddiq
with gratitude for their gift of my education
and for teaching me to value it

To my husband Salman and to my children Shaheer and Hafi
with all my love

Acknowledgements

First of all, I would like to thank my supervisor Associate Professor Brian Gabbitas for giving me an opportunity to work on one of the components of the light alloy manufacturing (LAM) research project. I am thankful for his guidance and assistance throughout this chapter of my career. His technical guidance, cooperation, great patience and concern for my best interests, and constantly open door have been integral to furthering my engineering education. I would also like to thank my research co-supervisor Professor Deliang Zhang for the helpful advice.

Special thanks to senior lecturer Dr. Peng Cao, from the University of Auckland (previously post doctorate fellow at the University of Waikato) and research officer Stiliana Raynova for their invaluable discussions, suggestions and great assistance with my experimental work. My sincere thanks to Professor Xiong Dangsheng and Dr. Janliang Li from Nanjing University of Science and Technology, China for their valuable assistance to carry out work regarding tribological properties of coatings in China.

Thanks to all technical staff, Steven Newcombe, Brett Nichol, Helen Turner, Yuanji Zhang, Paul Ewart, Indar Singh, Chris and Brian; administrative staff Mary Dalbeth and science librarian Cheryl Ward for their timely help. I thank all my colleagues in the metallic group for their help and co-operation. My special thanks to Holster Engineering Ltd., Tokoroa for hosting my visits to their spraying facilities.

I would like to thank the Foundation for Research, Science and Technology (FRST), New Zealand, for funding this project and the University of the Punjab Lahore, Pakistan for their financial support. Thanks to New Zealand Postgraduate Study abroad awards (NZPSAA) for their funding to carry out a part of my research work at Nanjing University of Science and Technology, Nanjing, China.

I owe many thanks to my parents, parents-in-law and my four wonderful sisters Dr. Sobia, Dr. Saima, Bushra and Dr. Ayesha for their love, motivation and constant support in every aspect.

Last but not least, I would like to thanks my husband Salman whose love and friendship is very precious, without his constant support and cooperation I could not make it at all. Special thanks to my children Shaheer and Hafi for coping with the hard situation during my studies. Their smiling faces and love at the end of each tiring day gave me surplus energy and strength to go ahead.

Related Publications

Journal publications

1. A. Salman, B. Gabbitas, D. L. Zhang, P. Cao, and S. Raynova, *Characterisation of Ti(Al,O)/Al_2O_3 composite powders and thermally sprayed coatings.* Advanced Materials Research, 2007. **29-30:** 135-138.

2. A. Salman, B. Gabbitas, P. Cao, and D. L. Zhang, *Tribological properties of Ti(Al,O)/Al_2O_3 composite coatings by thermal spraying.* International Journal of Modern Physics B (IJMPB), 2009. **23**(6-7): 1407-1412.

3. B. Gabbitas, A. Salman, D. L. Zhang, and P. Cao, *Review of research work on Ti-based composite coatings.* International Journal of Modern Physics B (IJMPB), 2009. **23**(6-7): 1707-1712.

4. A. Salman, B. Gabbitas, J. Li, and D. L. Zhang, *Tribological properties of thermally sprayed TiAl/Al_2O_3 composite coating.* IOP Conference Series: Materials Science and Engineering, 2009. **4**: 012006.

5. A. Salman, B. Gabbitas, and D. L. Zhang, *Thermal shock properties of Ti(Al,O)/Al_2O_3 and TiAl(O)/Al_2O_3 composite coatings.* Advanced Materials Research. **(Paper accepted)**

6. A. Salman and B. Gabbitas, *The performance of thermally sprayed titanium based composite coatings in molten Al*. Surface and Coatings Technology. **(Paper accepted)**

Conferences proceedings

7. A. Salman, B. Gabbitas, D. L. Zhang, P. Cao, and S. Raynova, *Characterisation of Ti(Al,O)/Al_2O_3 composite powders and thermally sprayed coatings.* In Proc. of 4th International Conference on Advanced Materials Processing (ICAMP-4), December 2006, New Zealand.

8. B. Gabbitas, A. Salman, P. Cao, D. L. Zhang, and S. Raynova, *Performance of Ti(Al,O)/Al_2O_3 Composite Coatings in Molten Aluminium.* In Proc. of 11th World Conference on Titanium, 3-7 June 2007. Kyoto**,** Japan.

9. A. Salman, B. Gabbitas, P. Cao, and D. L. Zhang, *Tribological properties of Ti(Al,O)/Al_2O_3 composite coatings by thermal spraying.* In Proc. of 5th International Conference on Advanced Materials Processing (ICAMP-5), 2-5 September 2008, Harbin**,** China.

10. A. Salman, B. Gabbitas, D. L. Zhang, and P. Cao, *Titanium aluminide/alumina composite powder and thermally sprayed coating.* In Proc. of International Conference on Advanced Materials, Development and Performance (AMDP-2008), 13-15 October 2008, Beijing, China.

11. A. Salman, B. Gabbitas, J. Li, and D. L. Zhang, *Tribological properties of thermally sprayed TiAl/Al_2O_3 composite coating.* In Proc. of Workshop on Microstructure and Performance of Materials (PMPM), 8–9 April 2009, Auckland, New Zealand.

12. A. Salman, B. Gabbitas, D L. Zhang, and P Cao, *Titanium aluminide/alumina composite powder and thermally sprayed coating for resistance to attack from molten aluminium.* In Proc. of SMNZI Materials Conference 2009, 10-11 December 2009, Hamilton, New Zealand.

13. A. Salman, B. Gabbitas, and D. L. Zhang, *Thermal shock properties of Ti(Al,O)/Al_2O_3 and TiAl(O)/Al_2O_3 composite coatings.* International Conference on Structural Integrity and Failure (SIF 2010), 4-7 July 2010, Auckland, New Zealand.

Abstract

The service life of industrial components is limited predominantly by chemical corrosion, mechanical failure or mechanical wear. In the aluminium high pressure die casting industry, liquid aluminium is extremely reactive with the constituents of H13 die steel and has a tendency to form intermetallic layers. This chemical interaction results in sticking of molten metal to the die surface which produces defective castings and also damages the die surface. The use of thermal spray coatings provides protection to the surfaces operating in severe environments. An HVOF thermally sprayed coating has the advantage of having excellent bond strength and very low porosity levels (< 1%). This research work is concerned with producing and evaluating the performance of titanium/alumina based composite coatings to improve the service life of tool steel (H13) used for dies in aluminium high pressure die casting and dummy blocks used in Al extrusion.

In this research work, the powder feedstocks for making the composite coatings were produced by high energy mechanical milling of a mixture of Al and TiO_2 powders in two different molar ratios followed by a thermal reaction process. The feedstock powder was then thermally sprayed using a high velocity oxygen fuel (HVOF) technique on H13 steel substrates to produce $Ti(Al,O)/Al_2O_3$ and $TiAl/Al_2O_3$ composite coatings. The performance of the coatings was assessed in terms of Al soldering, liquid metal corrosion resistance, thermal shock resistance and wear resistance.

In an immersion test, the coated specimens were dipped into molten Al at a temperature of 700 ± 10 °C for different intervals of time. The performance of the coatings was tested in terms of liquid metal corrosion resistance and propensity to Al soldering. The dissolution behaviour of the coatings was evaluated by measuring weight loss after dipping the samples in to molten aluminium. The immersion test results showed that the coated samples have relatively few locations where aluminium soldering (reactive/chemical) occurred, however, an H13 steel surface showed more tendency for aluminium soldering. It was found that composite coatings changed the molten Al attack on H13 tool steel from a generalized to a localized one. No reaction

between molten aluminium and a Ti(Al,O)/Al_2O_3 composite coating was identified. The TiAl/Al_2O_3 composite coating was found to be attacked by molten aluminium as a result of a reaction between the coating and molten aluminium. The metallic phase TiAl in the composite coating is believed to be attacked by the molten Al. A Ti(Al,O)/Al_2O_3 composite coating was found to be a better protective coating than the TiAl/Al_2O_3 composite coating due its stability against molten aluminium attack.

The thermal shock behaviour of the composite coatings was investigated by subjecting the coated coupons to a number of cycles, each cycle consisting of a holding time of 30 seconds in molten aluminium at 700 ± 10 °C followed by quenching into water. The surfaces of the coupons were examined for Al soldering and an evaluation of surface spallation. Any cracks found in the coatings were studied to explain their thermal shock behaviour. A Ti(Al,O)/Al_2O_3 composite coating on H13 tool steel produced from a fine feedstock has better thermal shock resistance than the Ti(Al,O)/Al_2O_3 TiAl/Al_2O_3 composite coatings produced from the agglomerated feedstocks.

The study also describes and compares the tribological properties such as friction and sliding wear rate of the composite coatings both at room and high temperature (700 °C) under dry and lubricating conditions. The wear resistance of the coatings was investigated by a tribometer using a spherical ended alumina, flat ended high speed steel and spherical ended hardened steel pins as counter bodies. The experimental results show that the composite coatings look promising for high temperature applications due to their low wear rate at high temperature. However room temperature applications of the composite coatings can be improved under lubricated conditions.

Successful trials of a Ti(Al,O)/Al_2O_3 composite coated dummy block revealed that the coating has potential as an industrial coating.

Table of Contents

List of Figures

List of Tables

Chapter 1

Introduction

1.1. General background

For over a decade, there has been a lot of interest in metal matrix composites (MMC's), intermetallic matrix composites (IMC's) and interpenetrating phase composites (IPC's) as potential materials for structural applications where good corrosion and wear resistance are required [1, 2]. More recently, research has more focused on interpenetrating phase composites (IPC's), largely due to their unique morphology and improved properties. The composites usually consist of two or more phases which are continuous and interpenetrating within the microstructure. In interpenetrating phase composites (IPCs) a continuous matrix phase is interpenetrated by a continuous reinforced phase. The attractive properties of each constituent thus contribute towards overall improved performance of the composite [2, 3]. Composites of this type are difficult to process using the traditionally employed powder metallurgical routes. In-situ processing enables production of a wide range of thermodynamically compatible interpenetrating phase composites, e.g. composites using the Al/TiO_2 system have received significant attention [2, 4, 5]. There is great interest in extending the performance of Ti alloys, particularly Ti based intermetallics due to the limited high temperature application of Ti base alloys (up to about 600 °C) which is far below the service temperature of 1100 °C for nickel-based superalloys. Consequently, Ti-based intermetallic compounds such as Ti_3Al, TiAl, and $TiAl_3$ are actively under development for their elevated temperature properties and low density, as a potential material to replace nickel-based superalloys [6-8]. The applications of the titanium aluminides are however limited by their poor low temperature ductility and toughness [7, 8]. This has led to the development of a novel powder metallurgy technique for the low cost manufacturing of alumina-aluminide alloys [9]. The process involves the reduction of TiO_2 with Al in an inert atmosphere to form a dense, interpenetrating composite of metal matrix and Al_2O_3. The advantage of intermetallics

containing Al_2O_3 in the form of composites with the interpenetrating networks is that the Al_2O_3 constituent contributes towards good thermal stability, high hardness, good corrosion resistance and wear resistance whereas the intermetallic phase improves the mechanical properties, especially the toughness by allowing plastic deformation [2]. Because of the high hardness of the titanium alloy intermetallics and composites, their application as wear resistant coating materials is appropriate.

1.2. The importance of this study

In recent years there has been significant interest in developing cost effective powder metallurgical processes for titanium alloys. Work on the production and characterisation of titanium based powder alloys and composite powders using Al and TiO_2 powders as raw materials is well established at the University of Waikato, and in-situ fabrication processes for titanium aluminide-alumina composite powders ($Ti_3Al(O)/Al_2O_3$, $Ti(Al,O)Al_2O_3$, $TiAl(O)/Al_2O_3$) have been developed [10, 11]. The next stage in the research effort is the development of cost effective products deriving from the technology developed so far.

Previous research [10, 11, 12, 13] has shown that the bulk material formed composite powders has enhanced oxidation and scale spallation resistance up to 800 °C. However, due to the brittle nature of these composite materials, their application in the bulk form is limited. It has been demonstrated [6] that an in-situ composite system, $Ti_3Al(O)/Al_2O_3$, is easy to manufacture with cheap raw materials. When it is applied to Ti sheet by thermal spraying, this coating also decreases the oxidation rate of Ti at temperatures up to 800 °C. The oxidation kinetics of $Ti(Al,O)/Al_2O_3$, $TiAl/Al_2O_3$ were reported by Zhang [14] at 700 °C for 400 hours in air on a pure titanium substrate. The results of this study showed that the oxide scale that formed on top of the coating was very well bonded to the coating, providing enhanced protection to the base material from further oxidation. Liang [15] studied the reaction kinetics of $Ti(Al,O)/Al_2O_3$, $TiAl/Al_2O_3$ and Ti_3Al/ Al_2O_3 coatings at 800 °C and reported that for all these coatings the oxidation kinetics essentially followed a parabolic law, indicating protective oxidation. The $Ti(Al,O)/Al_2O_3$ coating showed the lowest mass gain while the Ti_3Al/Al_2O_3 coating showed the highest mass gain, with oxidation products at 800 °C in these coatings reported to be TiO_2 and Al_2O_3.

The promising results of Ti based composite coatings for high temperature oxidation resistance, initiated an extension of the work on these coatings to investigate their performance against attack by molten aluminium and their possible application as a coating on aluminium die casting dies and dummy blocks used in aluminium extrusion.

An initial investigation [16] on the performance of coatings from $Ti(Al,O)/Al_2O_3$ composite powder using thermal spraying revealed that coatings showed fairly good performance in the preliminary thermal shock resistance tests and did not display any wetting tendency to molten aluminium. Thermal spraying is attractive among all other deposition processes because of the simplicity of application, versatility of the materials sprayed, high deposition efficiency, cost effectiveness and high wear or corrosion resistance properties. Among the other thermal spray processes HVOF is distinctive due to the combination of high particles velocity and relatively low gas temperature and thus it avoids substrate overheating. The lower temperature of the high velocity oxygen fuel (HVOF) has an advantage of producing coatings similar to the original composition of their starting feedstock powders.

The search for suitable materials that eliminate or minimise molten Al attack against tool steel is important in Al processing industries. To address this issue the contact angle between the die steel and molten Al should be large. In other words die materials should have poor wetability with molten aluminium. Most oxides, carbides and nitrides used to coat tool steel dies satisfy this requirement but they also have a large difference in coefficient of thermal expansion from tool steel.

In this work we chose composite coatings made from feedstock powders of composition $Ti(Al,O)/Al_2O_3$ and $TiAl(O)/Al_2O_3$. A major consideration in this choice was low cost, ease of manufacturing and unique microstructure. Chemical reactions between Al and TiO_2 involve reduction of TiO_2 by Al in an inert atmosphere and formation of titanium-aluminide/alumina interpenetrating composites. The solid state reactions produced during the heating of mechanically milled Al/TiO_2 powders have been reported by Ying et al. [4]. In these composite materials the ceramic phase Al_2O_3 has high temperature stability and it is not wetted by molten aluminium below 1000 °C [17, 18] and no reaction has been observed at alumina-aluminium interfaces between 750 °C-1100 °C [18], while the titanium phase acts as a binder and provides

good adhesion to the substrate. It also acts to accommodate the difference in thermal expansion between the tool steel and alumina. The titanium is also more inert to molten aluminium than iron [19] and is very corrosion resistant in molten aluminium, compared with steels and nickel-base alloys [20, 21].

1.3. Problem statement

In high pressure die casting, the die and cores operate under severe conditions of high pressure and rapid temperature fluctuations and face erosion and corrosion from the fast moving molten aluminium. Under these conditions, molten aluminium reacts with H13 tool steel and develops a weld, a condition is often referred to as soldering in the high pressure die casting industry [22]. A similar problem can also occur on dummy blocks used for aluminium extrusion. This not only makes the casting ejection difficult but also affects the quality of the castings. It also leads to machine downtime and requires frequent die surface polishing. Besides soldering and corrosion, erosion and thermal cracking are important modes of die failure [23]. Die failure is a significant issue for the die casting industry [1, 24].

1.4. Hypothesis, aim and objective of this study

The hypothesis to be investigated was that titanium based composite powders/coatings are suitable materials for improving the resistance against molten aluminium attack of metal dies and dummy blocks used in the aluminium casting and extrusion industry respectively.

1.4.1. Theoretical basis

Die life can be improved by applying an appropriate coating which acts as a physical barrier against soldering. The requirements for die coatings are good wear resistance, good substrate adhesion, good thermal shock resistance, adequate fracture toughness and poor wetability for molten aluminium to prevent soldering.

Continuous research work on die steels and surface treatment/coatings has been conducted over the past 20 years [25]. In the associated literature physical vapour deposition (PVD), thermo-reactive diffusion (TRD) and chemical vapour deposition (CVD) coating techniques are reported to have the potential to prevent soldering [26].

Both Chemical Vapour Deposition (CVD) and thermo-reactive diffusion (TRD) require process temperatures far above the tempering temperature of the tools. Therefore, changes in microstructure and dimensions cannot be avoided and thus involve the post-coating heat-treatment of the steel substrate due to the high process temperature. Moreover it cannot be ensured that the specified shape and dimensions can be maintained. These techniques cannot be seen as promising coating methods in aluminium die casting, especially concerning large and geometrically complex steel moulds and require post-coating heat-treatment of the steel substrate due to the high process temperature.

The PVD coating process has been successful in a wider range of substrates and applications. This success is largely due to its lower process temperatures (93-400 °C) and average coating thicknesses of 2-5 μm. No heat treatment after coating is required due to low process temperature. PVD and CVD coatings are commonly known as thin films when their thickness is less than 10 μm. The thin coatings usually fail as a result of excessively high chemical or mechanical loading, or a combination of both.

Thermal spray coating processes differ from the other coating methods in that they are not atomistic processes in which individual ions or atoms attach to a surface. Instead, liquid droplets, or liquid and solid particles deposit onto a surface. Thermal processes have higher coating deposition rates compared to other physical vapour deposition or chemical vapour deposition coating processes. Thermal spray coatings not only enhance the performance of the materials but also preserve the attributes of the substrate. Another big advantage of thermal spraying is the ability to recoat worn or damaged coatings without changing part properties or dimensions Thermal spraying is an effective and low cost method to apply thick coatings to change the surface properties of the component.

Over the past decade, high velocity thermal spraying has been successfully used to produce dense metal and cermet industrial quality coatings with strong adhesion and minimal decomposition. High velocity oxygen fuel (HVOF) and high velocity air fuel (HVAF) processes typically have some of the highest particle velocities at relatively low gas temperature. The high particle velocities result in high impact energies, thus ensuring excellent bond strength (> 90 MPa) and very low porosity levels (< 1%) of the coatings [27]. Typical thicknesses are in the range 100-300 μm.

The research described in this thesis aims to achieve a comprehensive understanding of thermally sprayed composite coatings produced by $Ti(Al,O)/Al_2O_3$ and $TiAl(O)/Al_2O_3$ composite powders and their resistance to molten Al attack.

1.4.2. Research objectives

(a) To evaluate the constitution and microstructure of composite powders and the coatings made using these powders.

(b) To study the effect of powder composition on the resistance of the coatings against molten aluminium attack/soldering.

(c) To carry out thermal shock resistance tests to assess the integrity of coatings under severe operating conditions.

(d) To evaluate the hardness, friction and wear properties of the coatings at room and high temperature.

1.5. The scope of this study

In this work, feedstock composite powders $Ti(Al,O)/Al_2O_3$ and $TiAl(O)/Al_2O_3$ were produced by high energy milling of mixtures of Al and TiO_2 powders followed by an in-situ combustion reaction. The combustion reacted powders were then thermally sprayed using the high velocity oxygen fuel (HVOF) method on a heat-treated H13 tool steel substrate. The performance of the coatings was assessed in term of soldering tendency, corrosion resistance with molten aluminium after dipping into molten aluminium at a temperature of 700 ± 10 °C. The friction and wear properties of the composite coating were assessed for their possible applications at high and room temperature.

1.6. Thesis outline

The thesis contains eight chapters. Chapter one is a general introduction. Chapter two is a literature review which discusses previous work on the topics of solid state reactions, high energy milling, combustion reactions, die casting, soldering and its prevention by using surface coatings. The chapter has a special focus on the study of various coatings and techniques used for soldering prevention in Al die casting dies.

There is an overview about thermal spraying processes. Chapter three describes the experimental methodologies and materials used in this research work while chapters four to seven present and discuss the experimental results. Chapter four covers the processing and characterisation of the composite powders produced for thermal spraying, chapter five describes the microstructure/characterisation of the thermally sprayed composite coatings produced using a high velocity oxygen fuel (HVOF) spraying technique. Chapter six describes the performance evaluation of the composite coatings on an H13 tool steel substrate against molten Al attack. The industrial trials of a coated dummy block used in Al extrusion are also included in this chapter. Chapter seven presents and discusses the results of tribological measurements such as friction and sliding wear of the composite coatings. Chapter eight includes the conclusions and recommendations for future work.

1.7. References

1. Gabbitas, B., A. Salman, D.L. Zhang, and P. Cao, *Review of research work on Ti-based composite coatings.* International Journal of Modern Physics B, 2009. **23**(6-7): p. 1707-1712.

2. Horvitz, D., I. Gotman, E.Y. Gutmanas, and N. Claussen, *In situ processing of dense Al_2O_3-Ti aluminide interpenetrating phase composites.* Journal of the European Ceramic Society, 2002. **22**(6): p. 947-954.

3. Zhang, X., C. Hong, J. Han, and H. Zhang, *Microstructure and mechanical properties of TiB_2/(Cu, Ni) interpenetrating phase composites.* Scripta Materialia, 2006. **55**(6): p. 565-568.

4. Ying, D.Y., D.L. Zhang, and M. Newby, *Solid-state reactions during heating mechanically milled Al/TiO_2 composite powders.* Metallurgical and Materials Transactions A, 2004. **35**(7): p. 2115-2125.

5. Feng, C.F. and L. Froyen, *Formation of Al_3Ti and Al_2O_3 from an Al-TiO_2 system for preparing in-situ aluminium matrix composites.* Composites Part A: Applied Science and Manufacturing, 2000. **31**(4): p. 385-390.

6. Li, Z.W., W. Gao, D.Y. Ying, and D.L. Zhang, *Improved oxidation resistance of Ti with a thermal sprayed $Ti_3Al(O)$-Al_2O_3 composite coating.* Scripta Materialia, 2003. **48**(12): p. 1649-1653.

7. Froes FH, C. Suryanarayana, and and D.J. Elieze, *Synthesis, properties and applications of titanium aluminides.* Journal of Materials Science, 1992. **27**(19): p. 5113-5140.

8. Sauthoff, G., *Intermetallics*. 1995, Germany: Weinheim: VCH.

9. Claussen, N., D.E. Garcia, and R. Janssen, *Reaction sintering of alumina-aluminide alloys (3A).* Journal of Materials Research, 1996. **11**(11): p. 2884-2888.

10. Zhang, D.L. and M. Newby, *Titanium alloy based dispersion-strengthened composites*. 2001: US6264917.

11. Zhang, D.L., Z.H. Cai, and G. Adam, *The mechanical milling of Al/TiO_2 composite powders.* JOM, 2004. **56**(2): p. 53-56.

12. Li, Z.W., W. Gao, J. Liang, and D.L. Zhang, *Oxidation behaviour of SiC and TiC particulate reinforced Ti_3Al intermetallic matrix composites.* International Journal of Modern Physics-B, 2003. **17**(8/9): p. 1770-1777.

13. Li. Z. W., W. Gao, D.Y. Ying, and D.L. Zhang, *Oxidation behaviour of Ti_3Al-TiC composites.* Materials Letters, 2003. **57**(13-14): p. 1970-1976.

14. Zhang, D., *Titanium based materials technology (NERF Report) in UOWX9909*. 2001-2002.

15. Liang, J., *Application of Titanium based composite powders in producing high performance coatings*, Internal Report, The University of Auckland, 1-19.

16. Zheng, L., *The characterisation of titanium alloy composite powder coatings produced by thermal spraying*. ME thesis, 2005, The University of Waikato: Hamilton. p. 54.

17. Yeomans, J.A., *Studies of ceramics-liquid metal reaction interfaces.* Journal of Materials Science, 1990. **25**(5): p. 2312-2320.

18. Sangghaleh, A. and M. Halali, *An investigation on the wetting of polycrystalline alumina by aluminium.* Journal of Material Processing Technology, 2008. **197**(1-3): p. 156-160.

19. Yan, M. and Z. Fan, *Review: Durability of materials in molten aluminium alloys.* Journal of Materials Science, 2001. **36**: p. 285-295.

20. Batchelor, A.W., N.P. Hung, and T.K. Lee, *Wear of metal stirring rods in molten aluminium and suspensions of aluminina particles in molten aluminium.* Tribology International, 1996. **29**(1): p. 41-50.

21. Mihelich, J. and R.F. Decker, *Apparatus for processing corrosion molten metals*. 1998: US.

22. Yu, M., R. Shivpuri, and R.A. Rapp, *Effects of molten aluminium on H13 dies and coatings.* Journal of Materials Engineering and Performance, 1995. **42**(2): p. 175-181.

23. Shivpuri, R., Y.L. Chu, K. Venkatesan, J.R. Conrad, K. Sridharan, M. Shamim, and R.P. Fetherston, *An evaluation of metallic coatings for erosive wear resistance in die casting applications.* Wear, 1996. **192**(1-2): p. 49-55.

24. Salman, A., B. Gabbitas, P. Cao, D.L. Zhang, and S. Raynova. In Proc. of the *11th World conference on Titanium*. 2007. Kyoto, Japan, p. 689-692.

25. Chou, Y.L., P. Cheng, and R. Shivpuri. *Study of erosive wear in die casting dies: surface treatments and coatings*. In Proc. of the *17th International Die Casting Congress and Exposition*. 1993. Cleveland: T93-073.

26. Chellapilla, S., R.A. Shivpuri, and S. Balasubramaniam. In *Transaction of the 17th International Die Casting Congress*. 1997. *Minneapolis. NADCA*. T97-T101.

27. Pawlowski, L., *The Science and Engineering of thermal spray coatings*. 2008, UK: Willey.

Chapter 2

Literature Review

Metal-ceramic composites (cermets) are regarded as a class of advanced engineering materials with low density, excellent oxidation and corrosion resistance, adequate creep resistance at high temperature, good wear resistance and high hardness [1].

In order to further improve the performance of metal-ceramics composites, more recent research has moved away from traditional composite materials with discrete dispersed addition (fibres, whiskers, particles) to interpenetrating phase composites where the second phase exists in larger quantities [2-4]. The new class of metal-ceramic composites was proposed more than a decade ago [5] and termed as 'Interpenetrating phase composites' (IPCs). The composites belonging to this class have a unique microstructure in which both the metal and ceramics phases are continuous and form a three dimensional interconnected network throughout the structure [5, 6]. This improved structure plays an important role in improving the overall performance and properties of a traditional ceramic. The continuous ceramic phase has the potential to provide higher strength, improved high temperature properties, good wear resistance and thermal stability over traditional ceramics with discrete particles and fibre reinforcements [7]. In the literature Al/Al_2O_3 [4, 8], Ti/Al_2O_3, Ti/SiC, Cu/TiB_2 [6], $Al/TiC/Al_2O_3$ [9] and Ti_3Al/Al_2O_3 [10], $NiAl/Al_2O_3$ Ni_3Al/Al_2O_3 [11] are described as commonly used interpenetrating phase composites.

Traditional techniques such as slip casting, infiltration or thermal processing used for producing cermets do not look promising due to high production cost, long processing time, and heavy equipment requirement for densification purposes [1, 12, 13]. Moreover infiltration techniques, commonly used to produce IPCs have the disadvantage of microstructural inhomogeneities as a result of low wetability between ceramic and the metallic phases and the presence of closed pores within the ceramic material which restricts metal infiltration [6, 9]. Self propagating high-temperature

synthesis (SHS) is described as an alternative method to address the problems due to its low processing cost, purity and high time and energy efficiency. A number of materials such as carbides, nitrides, borides, intermetallics and composites have been produced using this process [1, 14, 15].

There is great interest in titanium/alumina metal ceramic composites as low cost materials for high temperature application. The class has an additional advantage that besides having very good properties such as low density, excellent corrosion and oxidation resistance and good wear resistance, both titanium and alumina have similar coefficient of thermal expansion. This make a significant contribution towards better performance of this class at higher temperature compared with the other commonly used titanium/SiC metal composites [1, 16, 17].

Intermetallic/ceramic composites are another important class for high temperature structural and functional applications. High energy milling is an economical way of producing these types of composites. The process involves intensive mechanical milling of elemental metals with Al_2O_3 or using aluminium with metal oxides [18]. Intermetallics with Al_2O_3 reinforcements have special interest for higher temperature application because the Al_2O_3 constituent contributes towards good thermal stability, high hardness, and good corrosion and wear resistance whereas the intermetallic phase improves the mechanical properties, especially the toughness by allowing plastic deformation [19]. Titanium aluminides/Al_2O_3 cermets are the most promising class among intermetallic/ceramic composites. The intermetallic phase, titanium aluminide (TiAl, Ti_3Al and $TiAl_3$) in these composites contribute towards low densities, excellent oxidation and corrosion resistance, high ductility at higher temperature and an adequate creep resistance [20].

Metal-containing Al_2O_3 composites with interpenetrating networks have been fabricated by various techniques such as pressureless sintering [21-26], reaction squeeze-casting [27, 28], pressure assisted thermal explosion [19, 29], reactive infiltration [30-35], pressure infiltration [11, 36], hot pressing [37, 38] and direct metal oxidation [39, 40]. The main limitation with the established conventional processing routes such as DIMOX (directed metal oxidation) [41] and RMP (reactive melt penetration) [33] is that they are restricted to the manufacturing of Al-containing composites. However, for composites containing more refractory metals, high

temperature processing methods such as gas-pressure infiltration, hot extrusion, hot pressing or HIP [42-44] are commonly used. High processing cost is the main problem with these types of composites. The composites fabricated include Ni_3Al and FeAl with TiC, WC and TiB_2, TiAl-Ti_2AlC and ZrO_2-W.

To address the issue of the high processing cost of composites containing refractory metals a novel powder metallurgy technique was developed [26]. The low cost synthesis of intermetallic/alumina composites with interpenetrating networks was successfully achieved using this process. The process involves mechanical milling of either mixtures of aluminium and metal oxides (TiO_2, Fe_2O_3, Nb_2O_5, ZrO_2, etc) or elemental metals (Al, Fe, Ni, etc) and Al_2O_3 followed by controlled heat treatment or sintering. Aluminides formed as a result of the reduction of metal oxides with aluminium or alternatively by a reaction between elemental metals [18, 26, 30].

2.1. Solid state reaction of Al and TiO_2

The use of reactions between Al and TiO_2 is attractive due to their potential in producing in-situ metal matrix composites (MMCs) and intermetallic matrix composites (IMCs) at low cost. The solid state reactions between Al and TiO_2 have been widely studied over the past ten years [26, 45-47]. The reaction involves reduction of TiO_2 by Al in an inert atmosphere and formation of titanium aluminide/Al_2O_3 interpenetrating phase composite. The metal phase can be a single phase metal matrix or an alloyed Al phase or intermetallic phase based upon amount of aluminium in the starting powder mixture. It is reported that aluminium cannot reduce TiO_2 to pure Ti [47]; rather the formation of titanium aluminide/Al_2O_3 composites is possible through the use of different initial Al/TiO_2 molar ratios. Titanium aluminide phases such as $TiAl_3$, TiAl or Ti_3Al are formed [27]. Ying et al. [47] reported the formation of additional phases such as α-Ti (Al,O), Ti_3Al(O) and TiAl(O) in which a solid solution of oxygen and aluminium in a Ti matrix is formed. Thermodynamically, Al reacts with TiO_2 as follows [27, 48, 49].

$$13Al + 3TiO_2 \longrightarrow 3TiAl_3 + 2Al_2O_3 \quad \text{Eq. 2.1}$$

$$7Al + 3TiO_2 \longrightarrow 3TiAl + 2Al_2O_3 \quad \text{Eq. 2.2}$$

$$5Al + 3TiO_2 \longrightarrow Ti_3Al + 2Al_2O_3 \quad \text{Eq. 2.3}$$

The resulting chemical composition of the aluminides depends upon the ratio of aluminium to metal oxide, as shown in equations 2.1 to 2.3. A wide variety of alumina-aluminde composites with different intermetallic/ceramic ratios can be produced. It is reported that with intermetallic volume fractions above 20%, both phases are continuous and hence exhibit an interpenetrating network [24].

The reaction between Al and TiO_2 can be enhanced by reducing the starting powder size by milling techniques such as ball milling or discus milling. Welham et al. [45] reported the formation of Ti_3Al and Al_2O_3 phases at lower temperature for a powder mixture ball milled for 100 hours under vacuum compared to the un-milled powder mixture. Thus a combination of high energy mechanical milling and heat treatment or sintering can be used to produce in-situ metal matrix composites (MMCs) and intermetallic matrix composite (IMCs) powders with favourable microstructure.

Formation of Ti (Al,O)/ Al_2O_3, TiAl(O) /Al_2O_3, Ti_3Al(O) /Al_2O_3 and $TiAl_3$(O) /Al_2O_3 composites as a result of heat treatment of mechanical milled TiO_2/Al composite powders is reported by Zhang et al. [50] depending on the molar ratio between TiO_2 and Al. The metallic phase in these composites contains considerable amounts of dissolved oxygen (up to 25 at%) due to limited reduction ability of aluminium for TiO_2. The presence of some aluminium in the solid solution was also reported in the Ti metallic phase (eq.2.4). According to this research, TiO_2 and Al react as follows:

$$3TiO_2 + 4Al \longrightarrow 3Ti(Al,O) + 2Al_2O_3 \quad \text{Eq. 2.4}$$

$$3TiO_2 + 7Al \longrightarrow 3TiAl(O) + 2Al_2O_3 \quad \text{Eq. 2.5}$$

$$3TiO_2 + 5Al \longrightarrow Ti_3Al(O) + 2Al_2O_3 \quad \text{Eq. 2.6}$$

The oxygen content in Ti(Al), TiAl and Ti_3Al phases is reported to decrease with increasing aluminium content.

In this project, composite powders were produced using TiO_2 and Al powders (two different molar ratios based on eq 2.4 and eq 2.5) as starting materials using high

energy mechanical milling followed by a self propagating high temperature synthesis (SHS).

2.2. High energy mechanical milling

High energy mechanical milling is a very effective method of producing alloys and composite powders. Milling is usually carried out under an inert atmosphere in order to prevent the oxidation of the powders. Process control agents are normally used to prevent sticking of the powders to the discs or the balls and the inner walls of the bowl and to achieve a proper balance between cold welding and fracture when milling ductile materials.

The most common high energy mills include attritor mills, tumbler mills, vibratory mills, planetary mills and discus mills. A number of methods have been used to mechanically mill powders having a composition range such as Al and TiO_2 [45, 51], TiAl, $TiAl_3$, Ti_3Al [52], Ti, Al and SiC [53], Ti and Al [54, 55], pre-alloyed TiAl and NiAl [56] and PbO, La_2O_3, ZrO_2 and TiO_2 [57].

The alloying and phase transformation processes during mechanical milling largely depends upon the energy transferred to powder particles from the moving media (balls, discs). The energy transferred depends upon a number of parameters such as milling speed, milling temperature, types and size of milling balls or disc to powder weight ratio.

Mechanical milling is described by Murty et al. [58], as a process in which powder particles are subjected to repeated fracturing and cold welding using moving media such as balls. The degree of fracturing and cold welding during milling depends mainly on the mechanical behaviour/nature of the powder systems. Mechanical alloying/milling involves three types of powders systems, described as (i) ductile/ductile (ii) ductile/brittle or (iii) brittle/brittle systems [58].

(i) Ductile/Ductile System

The mechanism of mechanical alloying in a system where both powder blends are ductile in nature was first described by Benjamin and Volin [59]. According to these, mechanical alloying in this system can be dived into five stages. The microstructural

evolution for the system during mechanical milling is schematically described in fig. 2.1.

In the initial stage of mechanical milling equiaxed ductile particles are flattened and forged resulting in plate like particles. In the second stage, plates like particles are welded together and result in a sandwich like microstructure. The third stage is the formation of equiaxed particles as a result of stain hardening and fracturing. The fourth stage is called random welding, leading the formation of a number of lamellar colonies of random orientation within each composite powder particle. In the fifth and last stage a balance is achieved between the welding and fracturing of the particles. With further milling the composite microstructure becomes finer and finer and eventually the lamellae become un-resolvable under an optical microscope [58]. A majority of elemental powder blends, mechanical alloyed fall in this system. The most common among them are Ni-Cr, Cu-Ni, Cu-Zn, Ni-AI, Ti-Al etc.

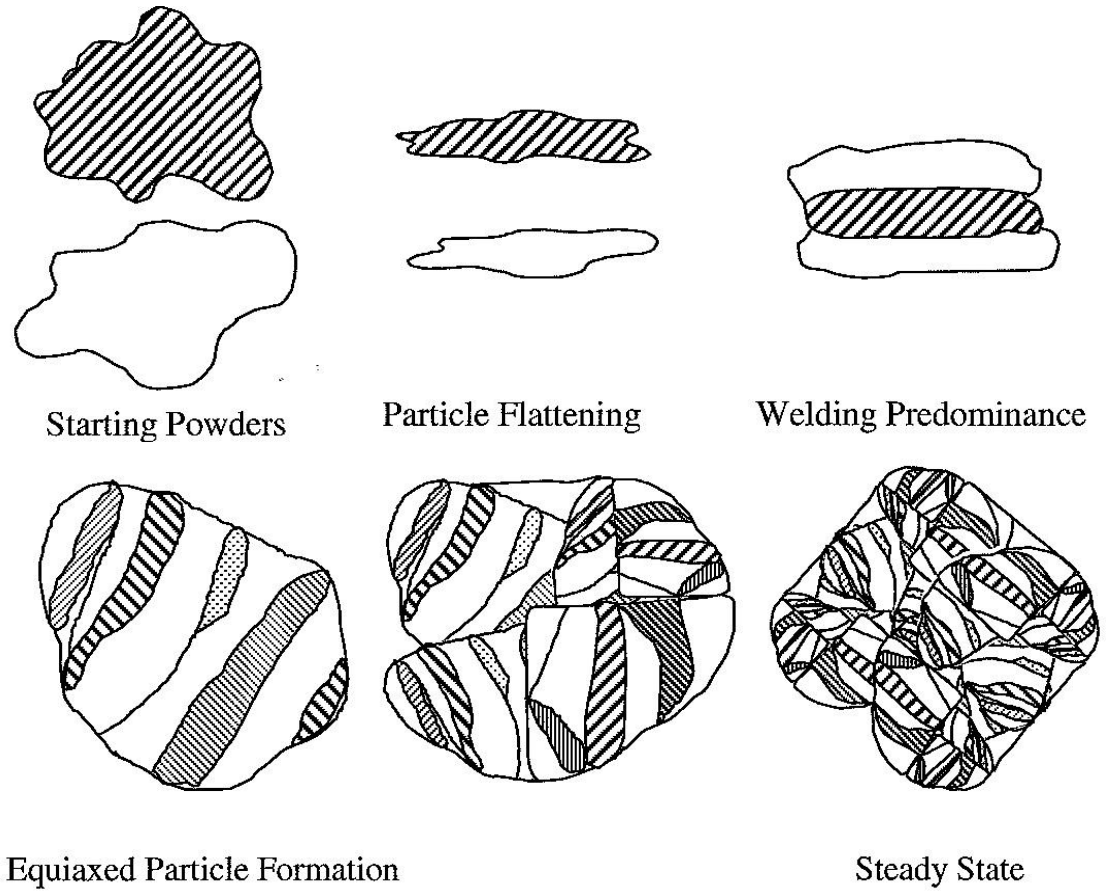

Figure 2.1: Five stages of microstructural evaluation [60, 61].

(ii) Ductile/Brittle System

Ductile/brittle systems typically involve particles of a ductile metal such as Ni or Al and a brittle phase which might be a metal oxide. During milling the ductile particles become flattened and then welded together to form a layered structure. The brittle particles are fragmented and become embedded in the layer ductile particles. As the milling continues, the layered structure becomes more refined until the individual components are un-resolvable. The brittle phase is uniformly distributed in the ductile matrix [58, 59]. NiAl/Al_2O_3, alumindes/Al_2O_3 and alumindes/SiC are the most common among this system. The microstructural evolution for the system during mechanical milling is schematically described in fig. 2.2.

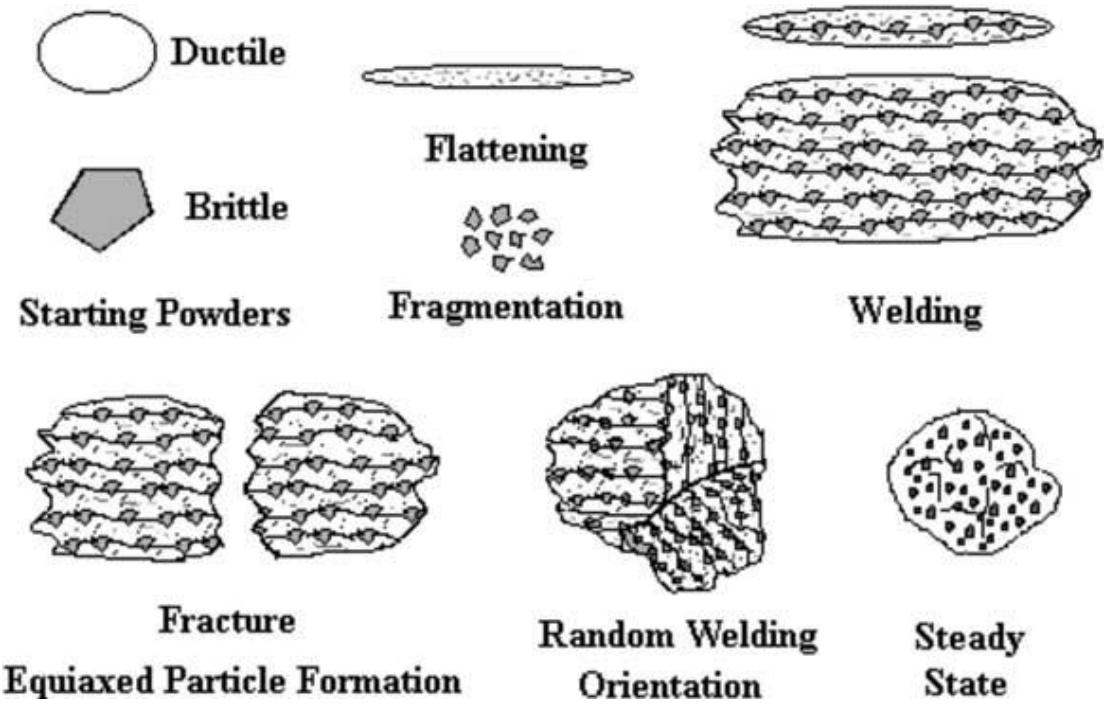

Figure 2.2: The various stages of a ductile-brittle system during mechanical Alloying [61]

(iii) Brittle/Brittle System

The mechanism of alloying is not clearly understood in this system yet. The microstructural features are described to have granular morphology during mechanical alloying which differs markedly from lamellar morphology for ductile/ductile system. Si-Ge is a particular example of such system [58, 62].

A Rocklabs "Split Discus" high energy mill is used in this work to produce composite powders through the shearing and impacting action of a pair of hardened steel discs in a hardened steel bowl. In comparison with the commonly used mills for laboratory investigation such as spex and planetary mills, the discus mill has the advantage that a large amount of powder (more than 0.5 kg per batch) can be milled.

2.3. Combustion synthesis

Combustion synthesis is also known as Self Propagating High Temperature Synthesis (SHS) [19] or thermal explosion [29]. It is an attractive technique for synthesising a variety of advanced materials such as composites, ceramics, intermetallics and functional graded materials with low processing cost.

In combustion synthesis, an external heating source is used for a short period of time to initiate a reaction in the mixture; once the heat is generated the reaction become self supporting and yields final products without requiring any additional heat. A number of characteristics associated with the process are, a self-generated high temperature (800 °C to 3500 °C), relatively rapid propagating combustion fronts (0.1 to 10 cm/sec), high rates of heating (up to 10^6 deg/sec), and thermal gradients (up to 10^7 deg/cm) [63]. The values of temperature, wave velocity, thermal gradients, and rate of heating depend upon the nature of the reactants. Combustion synthesis can be performed in fine powders, liquids and gases. However, it is most commonly used for powder mixtures (loose or pelleted) and powder (pellet)-gas system.

Besides a number of advantages such as short production cycle, low processing cost, low energy requirement, simple production equipments, purity is sometimes reported as a major quality of combustion synthesis [64, 65]. This is due to the reason that heat generated as a result of exothermic reactions is sufficient to evaporate the low melting points impurities/volatile compounds. However, The main concern with this technique are that combustion synthesized materials often have considerable retained porosity [64], moreover it is difficult to fully control the degree of completion of a reaction.

Pawlowski [66] reported carbides (TiC, SiC), borides (TiB_2, LaB_6), silicides ($TiSi_2$, $MoSi_2$), aluminides (AlNi), titanites (TiNi), nitrides (NbN, Si_3N_4), hydrides (MgH_2, $ZrNiH_3$) and oxides (YBCO, $La_{0.8}Sr_{0.2}CrO_3$) compounds suitable for the SHS process.

Composite powder can be formed by adding a non-reactive powder to the initial mixture. For example to obtain a cermet of NiCr-TiC [67], a NiCr powder is added to the reacting precursors of Ti and C. Pawlowski [66] also reported that the composite powders produced with this method are porous and need a high temperature treatment such as the plasma spheroidization method [68] or post treatment of SHS powders using a high-power laser [69].

Self propagating high temperature synthesis (SHS) is used to develop magnesium aluminate spinel $TiAl/Ti_3Al$ interpenetrating phase composite [70], Al_2O_3/TiC [63], TiC/TiB_2 [71], ZrB_2/ZrN [72] ceramics composites, TiC/Al [65] and NiTi/TiC metal-matrix composite powders.

2.4. Die casting

This is a common and effective way of achieving high volume production of geometrically complex parts. It is used for the manufacture of parts in ferrous and non-ferrous alloys and has the advantage of achieving good surface finish with minimum scrap wastage. High production rate such as 200 parts per hour and batch sizes of about 300,000 parts are common in the die casting industry [73].

The die casting process is described by Shivpuri et.al. [73]. The process involves a die which consists of two halves called the cover die and the ejector. The die halves are closed together to make a die-cavity in which molten metal is injected with high pressure and velocity. The pressure and velocity with which molten metal is injected depends upon the size of the casting. Upon solidification, the desired shape is attained and later the die halves are opened to eject the cast part. For each casting cycle, the opened die halves are sprayed with water based lubricants and anti-solder compounds to facilitate the easy removal of the castings.

2.4.1. High pressure die casting process

Molten aluminium is poured into the shots sleeve and then injected into the die cavity by a plunger under pressure [74]. The melt temperature for the aluminium alloy is approximately 700 °C [75]. The cavity fill time is extremely quick, typically 0.1 second or less and the gate velocities range from 40-60 m/s but can be as high as 200 m/s [74]. A pressure of about 40 to 120 MPa is usually applied during solidification of

the metal. The purpose of the applied pressure is to reduce the amount of gas porosity, feed shrinkage porosity, and increase dimensional accuracy of the part. The die is usually internally cooled to increase the rate of solidification. After solidification the die opens and the casting is separated from the die by hydraulic ejector pins. The entire cycle time to produce a single casting may be 3-6 seconds but it may be 60-90 seconds in case of larger casting [74]. To facilitate the casting ejection, the die is usually sprayed with a water based lubricant at the beginning of every casting cycle. The process is summarised in fig. 2.3.

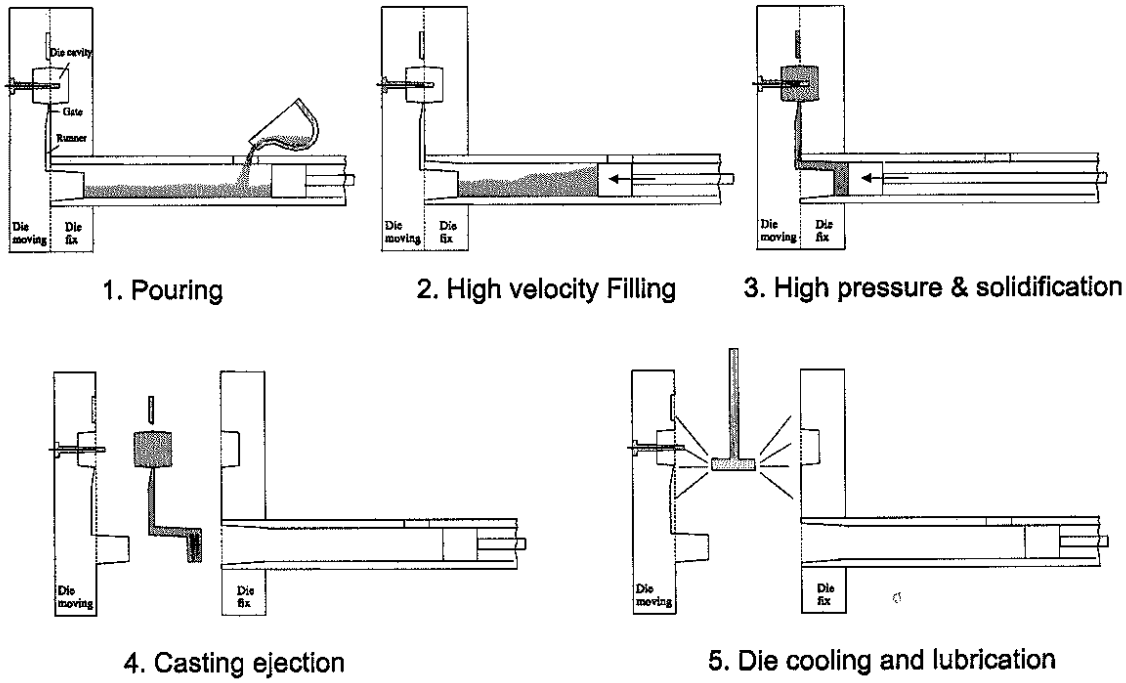

Figure 2.3: Stages of the die casting process [76].

The multiple reuses of a die (high production rate) and severe operating conditions such as high flow velocity of the melt and large die temperature gradients within a short of period, all limit the die life . A die life is usually described between 20,000 to over 250,000 parts depending upon the type of casting being produced [73]. Dies are expensive, the die cost being determined by the nature of the parts being produced and may cost more than US$100,000. For this reason die wear and failure is a matter of great concern to the die casting industries [77].

2.4.2. Modes of die failure

Die wear and failure involved a number of mechanisms. The most common modes of die failure are described by Shivpuri et al. [73] as;

- *Erosion or washout*

This occurs because of the high flow rate of molten aluminium inside the die cavity. The melt velocity may range between 20-60 m/s and can cause the steel surface to wash away. The wash out results in dimensional instability of the die and is commonly observed in the case of cores, pins, ribs and corners within a die. The regions need to be rebuilt in the case of severe wash out.

- *Heat checking (thermal cracking)*

During casting, injection of molten metals results in rapid heating of the die surface while the spraying of water base lubricants results in rapid quenching. Due to alternate heating and cooling cycles within a short span of time, the die surface is subjected to compression and tension respectively. As a result of thermal fatigue cracks appear on the die surface. The cracks are commonly called heat checks and result in poor surface finish and defective coatings. The cracks can propagate further with time and can cause gross failure of the die.

- *Soldering and corrosion*

Corrosion occurs because of a chemical reaction between the die material and Al melt. The reaction usually results in the formation of iron-aluminium compounds. Soldering takes place during solidification and results in sticking of the casting with the die surface and thus it not only makes casting ejection difficult but also causes damage to the die.

The wear phenomena are widely observed in AISI H13 die steel, the most commonly used die material. An understanding of die corrosion by aggressive molten aluminium attack is important and necessary for selecting a suitable coating for the H13 tool steel die.

2.5. Soldering

Soldering occurs when a molten metal develops a 'welds' with the die surface during the solidification process in a die casting operation. Soldering not only makes the casting ejection difficult but also damages die surfaces. It results in poor surface quality of the casting, requires a frequent die surface polishing and effects the process run time. Soldering is categorised into two types, based upon temperature; one that occurs at high temperature due to a chemical/metallurgical reaction between the molten aluminium alloy and the die, the other occurs at low temperature due to the mechanical interaction [78-80].

Soldering at high temperature occurs as a sequential effect of washout and chemical corrosion. Washout occurs when the molten aluminium alloy enters the die and destroys the protective film (coating or lubricant) on the die. During chemical corrosion, the molten aluminium reacts with the die surface. Iron in the die material dissolves into the melt whereas aluminium and other elements in the melt diffuse into the die. This forms a layer of intermetallics at the die surface. Under the right conditions, an aluminium-rich soldering layer may also form over the intermetallic layer [78, 79]. Yu et al. [81] have also shown that the molten aluminium alloys have a tendency to react with H13 tool and form intermetallic layers. At low temperature, the soldering results due to physical interlocking of molten aluminium with die without the formation of an intermetallic phase [82, 83].

Another classification of soldering, described by Tsuchiya et al. [83], is based on the surface appearance of the silvery casting alloy built up on the die. The two types of soldering based on appearance are film-like soldering and massive soldering. The film-like soldering is characterised as a built-up layer of solder with smooth surface finish and small sectional thickness [83]. Massive soldering is characterised by a built-up layer of solder with a rough surface and greater thickness [83].

It has been suggested that the interfacial intermetallic phases form first and thus cause the casting to adhere to the surface of the die [84]. However recent research work by Chen et al. [85] has indicated that casting alloy layers build up first on the die and subsequently the intermetallic phases form between the tool steel and the casting alloy built up layers.

2.5.1. Mechanism of soldering

Chemical corrosion and physical erosion are the main mechanisms of materials failure in molten aluminium [86]. In literature, two soldering mechanisms have been suggested. The first mechanism suggests that soldering occurs as a series of steps involving erosive wear, corrosive wear, dissolution of die steel and development of intermetallic phases [79]. Physical erosion results due to the high flow of the melt relative to the die surface, and becomes more severe when there are hard particles in the melt. However the research by Chen [87] showed that core pins subjected to the high melt impingement exhibit no erosive wear before the development of the soldered layer.

The second mechanism proposes that soldering is caused by corrosive wear due to the strong affinity of aluminium for iron in the die steel. During the die filling and solidification processes, the casting alloy reacts with the die steel and forms complex intermetallic compounds [85]. The iron from the steel diffuses into the aluminium melt resulting in the formation of intermediate layers. Intermetallic phases that form as a result of immersion of die steel samples into molten casting alloys have also been studied in an attempt to understand the soldering reaction. Shanker et al. [88] studied the interface reaction between the molten Al alloy and tool steel and reported soldering as a diffusional process (solid-liquid reaction) similar to the hot dip aluminizing of steel. However in a study reported by Chen and Jahedi [82] the soldering reaction in the die cavity occurs at a temperature below the liquidus temperature of the casting alloy and therefore most of the reaction occurs in the solid state. These researchers also reported that there is a possibility that soldering can occur initially without any formation of intermetallic phases. This stage is described as non reactive soldering or casting alloy build up. Tsuchiya et al. [83] also suggested that soldering can be a physical interlocking without the formation of an intermetallic phase.

The die life can be improved in a number of ways. The most common methods are, developing new die materials, improving die material heat-treatments, changing the die design, using better lubricants and applying appropriate coatings [73]

Surface engineering techniques that have been used to extend die life include surface modification of the die tool steel, such as nitriding [89-92], deposition of tribological coatings using PVD [93-106] and CVD [77, 107-112] that deposit wear resistant coatings onto the die tool steel, and duplex treatments that involve a die surface modification coupled with a wear resistant coating [113-120]. Hard coatings based on nitrides and carbides of transition metals (e.g CrN, CrC, TiAlN, TiB_2) have been used commonly to protect the steel surface from erosion and soldering of aluminium and improve resistance against thermal cracking.

2.6. Coating requirements for tool steel dies

The major requirements for a coating to be applied on tool steel dies for resistance against molten Al are described by Lin et al. [121] as follows:

(i) Non-wetting with liquid aluminium

(ii) Wear and oxidation resistance.

(iii) Ability to accommodate the thermal residual stresses induced due to heating and cooling cycles (good thermal shock resistance).

(iv) Adherence to the die material.

(v) Ability to delay the thermal fatigue cracking (heat checking).

Thus to achieve an optimum performance; adhesion, hardness, soldering behaviour, oxidation resistance and stress state have to be carefully optimized, before big and heavy dies can be coated.

A single layer coating alone cannot entirely fulfil the above requirements. This promotes a new concept of using multilayer or graded coatings so that each layer can serve a specific function such as, adhesion to the substrate, good tribological behaviour, corrosion resistance, good thermal shock resistance and non-wetability with the molten metal [122]. Based on this concept Lin et al. [121] proposed that an optimized, multilayer and graded coating architecture must be designed in which each layer has a specific purpose.

2.7. Coatings used for preventing soldering in Al-die casting dies

Suitable surface treatment can significantly improve the performance and lifetime of the tools used in the die casting [108, 123]. The most widely used techniques described in the literature for coating die casting dies against molten Al attack are physical vapour deposition (PVD), plasma assisted chemical vapour deposition (PACVD), Laser surface Engineering (LSE) [124, 125]. Chellapilla et al. [126] studied a number of potential coatings and concluded that physical vapour deposition (PVD), thermo-reactive diffusion (TRD) and chemical vapour deposition (CVD) have the potential to prevent soldering.

Chemical Vapour Deposition (CVD) is a coating deposition process in which a reactant gas mixture is passed in a high-temperature reactor to form a solid product in the form of a thin film at the substrate. The technique has an advantage that large and complex tools can be uniformly coated. However the high processing temperature (800-1000 °C) is the main concern with this technique. High processing temperatures (above the tempering temperature) can result in microstructural and dimensionional changes of the tool. The process thus requires a post-coating heat-treatment of the tools. It is not guaranteed that good dimensional stability can be maintained after a post-coating heat treatment. Therefore, CVD cannot be seen a promising coating method in the case of large and complex tools used in the Al die casting industry [108, 127]. However using a plasma-assisted chemical vapour deposition (PACVD) technique, the deposition temperature can be reduced to 300 °C [128]. The operating pressure for PACVD is in the range of several tens to hundreds of Pa [77] which allows the coating of big and heavy tools without rotation. However, PACVD coatings have more defects and lower density in comparison with the CVD coatings [128]. PACVD hard coatings containing nitrides and borides of titanium are well known for their high hardness, minimal difference in coefficient of thermal expansion between substrate and high corrosion stability against metal melts [129].

Lee et al. [130] used a plasma assisted chemical vapour deposition (PACVD) technique to deposit a titanium diboride TiB_2 coating on H13 tool steel. Different types of hard coatings TiN, Ti(C,N), Ti(B,N) and (Ti,Al)(C,N) produced by PACVD were tested in aluminium die casting applications by Hiem et al. [108] and results showed a significant increase in core life with no tendency of soldering for all types of

coatings. Duplex treatments consisting of plasma nitriding and PACVD hard coatings have proven to be successful in improving wear, fatigue and corrosion resistance and the load carrying capability of steel substrates [131, 132]. Duplex-PACVD coatings of Ti(B,N), TiB_2/TiN, Ti(B,N)/TiB_2 were studied by Klimek et al. [129] for aluminium and magnesium die casting applications. The Zr(B,C) and Zr(B,C,N) coatings were synthesized by means of DC-pulse-PACVD for applications in aluminium die casting [132].

A thermo reactive deposition technique is used to coat steels containing hard and wear resistant layers of carbides, nitrides, or carbonitrides. A coating containing carbide or nitride forming elements such as vanadium, niobium, tantalum, chromium, molybdenum, or tungsten is deposited on the steel. A dense, metallurgical bond develops at high temperature between the steel and deposited coating layer. Diffusion of carbon or nitrogen from the steel to the deposited coating layer results in carbide or nitride coatings at the substrate surface [133, 134]. TRD coatings, like CVD coatings require a high process temperature (1038 °C) which also involves a post-coating heat-treatment of the steel substrate due to the high process temperature.

In the PVD deposition technique, a coating material is evaporated under vacuum by various mechanisms (resistance heating, high-energy ionized gas bombardment, or electron gun) and the resulting vapour phase is transported to the substrate to form a coating. It is a line-of-sight process because the coating material is sputtered from a target and thus requires substrate rotation to obtain homogeneous and uniform coatings. However it is difficult to coat complex features such as undercuts, slits and cavities. Various metallic and ceramics coating can be applied using this method typically at a rate of a few millimetres or less per hour. The PVD coating process has been successful in a wider range of substrates and applications. This success is largely due to its lower process temperatures (93-400 °C) and average coating thicknesses of 2-5 µm. No post heat treatment of substrate is required after coating due to a low process temperature. All these characteristics make PVD coatings ideal for applications involving high speed steel and carbide cutting tools. The major disadvantages are high capital cost and low deposition rate. It is a line-of-sight technique which requires complex sample movement [135]. Moreover, it is difficult to coat forming tools (most commonly extrusion dies) with complex geometry such as cavities, slits or undercuts using this technique. [136]. Also the degree of adhesion of

the coating to the substrate is somewhat less than that for CVD, because the high processing temperature (800-1000 °C) used in thermal CVD allows some diffusion of the coating material into the substrate [137].

Most of the literature, describing PVD coatings is biased towards cutting tool applications. There is little information about their performance on tools used for high pressure die casting of aluminium alloys. To fully understand the mechanisms leading to their failure, these coatings should be extensively evaluated for a number of industrial applications. PVD coatings such as TiN, CrN and TiCN have been evaluated for their performance against molten aluminium soldering in high pressure die casting. The results of these studies showed that PVD coatings have a potential to act as a physical barrier against soldering [138]. Wang [139] studied the effects of TiN, TiAlN and CrN PVD coatings on a series of tool steels for resistance against molten aluminium corrosion and thermal cracking. The results of this study showed that all the coatings significantly improve the corrosion and erosion resistance of the tool steels in molten aluminium. However, a TiN coating was not found to last long because of its low oxidation temperature. Among all types of coated steel, only H19 tool steel showed significant reduction in heat checking.

To improve the properties of PVD coating further, a new approach is to replace the single layer coating with the multilayered one. In multilayer coatings, two or more different layers are alternatively deposited on the substrate. The multilayer structure improves the properties of the coating. In several investigations, it has been shown that ceramic multilayered coatings can exhibit an improved fracture resistance as compared with single layered ceramics coatings [140]. In addition multilayered coatings have also been shown to possess very high harnesses [141, 142] and excellent corrosion resistance [143].

Both conventional single and multi-layer coatings have been successful in improving the thermal fatigue resistance of steel dies used in die casting. However, Srivastava et al. [97] proposed a new concept of using a thermal barrier coating within a three layer coating architecture to improve the thermal fatigue resistance of die steel. The aim of using a thermal barrier coating was to reduce heat transfer and chemical diffusion to the die steel. Using this approach, a substrate with, an outer layer of thermal barrier coating (rare earth oxides), middle layer of TiAlN and an inner layer of Ti was tested

up to 4000 cycles in molten aluminium. The results of this study showed a significant improvement in the thermal fatigue resistance of the substrate compared with a substrate coated with a conventional multi-layer PVD coating

An investigation of AISI H13 tool steel, coated with TiN, CrN and a duplex coating (nitriding plus TiN) [144] resulted in increased thermal fatigue resistance. The duplex treatment (plasma nitriding/PVD coating) has also been used to improve the performance applications as coatings on dies and cores [114].

PVD coatings including TiN, CrN, (Ti,Al)N and TiB_2 were investigated on aluminium extrusion dies [145]. The most promising coatings to increase the die life were (Ti,Al)N and TiB_2. A central factor for this selection was the chemical inertness of the coatings. In another study of multilayered coatings [146], a combination of PVD TiN, Ti_2N, Ti(C,N) and (Ti,Al)N layers were deposited on M2 tool steel and their wear resistance studied. The resistance to sliding wear seems to be mainly affected by the coating hardness, where the (Ti,Al)N and Ti(C,N) based multi-layers showed the best results.

The Cathodic arc physical vapour deposition (CAPVD) technique is widely used to deposit hard coatings because of its many advantages such as high deposition rate and strong adhesion between the coating and substrate. The CAPVD process involves vaporization of material from a cathode target by using an electric arc. The vaporised material then condenses on a substrate to form a thin film. The process allows monolayer, multilayer, graded or alloy films to be deposited on a variety of substrates [147-149]. However, a major disadvantage with this process is generation of molten ‘macroparticles’ during coating deposition. These ‘macros’ usually create pin holes and bumps in the film [150].

A laser surface engineering technique has been used by Agarwal [125] and Shah et al. [124] to deposit TiB_2 and VC coatings respectively on AISAI steel. The results showed significant improvement in the corrosion resistance of steel to molten Al.

2.8. Ti-based alloys and composite powders for coating materials

The unique properties of titanium make it one of the most important industrial materials. This is because of its high strength, light-weight, excellent corrosion

resistance and biocompatibility which make it suitable for a number of applications. A number of titanium base alloys have been developed as structural materials for aerospace applications. The scope of these alloys is now expanding to other areas such as energy production, petrochemical, automobile, metallurgical, papermaking, medical, and food industries. Ti based alloys can operate at a moderately high temperatures (600 °C) which is far below the maximum service temperature (1100 °C) of Ni based alloys. This limits its use for higher temperature applications, for which Ti based intermetallics such as Ti_3Al, TiAl, and $TiAl_3$ are being developed [151-153]. However, low ductility at room temperature is the major obstacle to the use of Ti_3Al, TiAl and $TiAl_3$ as structural materials. Titanium aluminide surface coatings are considered to be another promising application for these intermetallic compounds [154-156].

There is a great interest in intermetallic matrix composites due to the reason that monolithic intermetallic alone can not satisfy the properties required for advance applications. One of the effective way to improve the wear resistance of intermetallic compounds is to obtain hard phase reinforced intermetallic matrix composites (IMCs), which are expected to possess high hardness and subsequently good wear resistance. However the processing of intermetallic matrix composites is a critical issue. A number of methods have been explored to fabricate such composites with either continuous or discontinuous reinforcements. The composite with discrete reinforcement provides less improvement in mechanical properties compared to the one with continuous reinforcement. Mechanical alloying provides an economical processing route for composite with discrete reinforcement whereas composite with continuous reinforcement are usually produce by SHS method.

Al_2O_3 is found to be a suitable reinforcement for improving the wear resistance of metal matrix composites (MMCs) due to its excellent chemical and thermal resistance and high hardness [23, 154, 155]. The high hardness of the titanium alloy intermetallics and composites make their application appropriate as wear resistant coating materials.

A suitable and economical coating method is an important consideration for potential coatings on die casting dies or other surfaces. Most die casting dies have complicated geometrical features such as cores, pins, ribs and corners. The methods widely used

for coatings such as physical vapour deposition (PVD), chemical vapour deposition (CVD), plasma–assisted chemical vapour deposition (PACVD) may not be effective in coating these complicated features. Some of the methods either take more time or need to be carried out at higher temperature which might alter the properties of the substrate materials. With these problems in mind, a thermally sprayed coating seems to be very promising as a method for coating a substrate material with complex geometry. The major advantages are summarised below;

(i) A wide variety of materials can be used to produce coatings.

(ii) Higher coating deposition rate

(iii) Coatings can be applied to substrates without significant heat input.

(iv) Worn or damaged coatings can be recoated without changing the properties or dimensions of parts.

The main disadvantages of thermally sprayed technique are the difficulty in attaining uniform, high quality and dense coatings. The line-of-sight nature can lead to non uniform coatings on complex shapes. However, the problem can be overcome with moving fixture design.

Thermal spraying is one of the advanced spraying techniques commonly used to spray metal/alloy, composite and ceramic powders. The powders can be deposited using advanced deposition techniques such as high velocity oxy-fuel (HVOF), plasma or flame spraying and cold spraying to produce coatings with high wear and corrosion resistance.

2.9. Thermally sprayed coatings

Thermal spraying is low cost method that applies thick coatings to improve the surface properties of a component. Coatings are used in a wide range of applications including automotive systems, boiler components, power generation equipment, chemical process equipment, aircraft engines, pulp and paper processing equipment, bridges, rollers and EAF electrodes in steel mills, concrete reinforcements, orthopaedics and dental, land-based and marine turbines, ships, etc. [157-159]. The applications of thermally sprayed coatings are varied but the largest categories are to

enhance the wear and/or corrosion resistance of a surface. A wide diversity of materials are used as thermal spray feedstock like metals, intermetallics, cermets, ceramics, glasses as well as polymers.

Thermal spraying technology has undergone remarkable development since its beginnings 80 years ago. It remains unchallenged as the most diverse of all coating processes with the capacity to deposit, at high rate, numerous metal, ceramic and polymeric materials in thickness from a few tens of microns to many millimetres. The techniques are complimentary, but not competitive, to thin film processes such as CVD/PVD. Generally such coatings have greater porosity than CVD or PVD coatings and thickness control is more difficult to achieve. PVD and CVD coatings are commonly known as thin films when their thickness is less than 10 μm. Thermal sprayings can deposit relatively thick coatings which vary with process parameters such as deposit time, temperature, nozzle length, and particle velocity.

Coating material in the form of powder, rod or wire is heated into a molten or semi molten state. The resultant heated particles are accelerated and directed towards a substrate surface either by process gases or atomization jets. The particles develop a bond with the substrate surface as a result of high impact. A continuous process results in a build up layer with a lamellar structure (fig. 2.4). The thin "splats" undergo very high cooling rates, typically in excess of 106 K/s for metals [160].

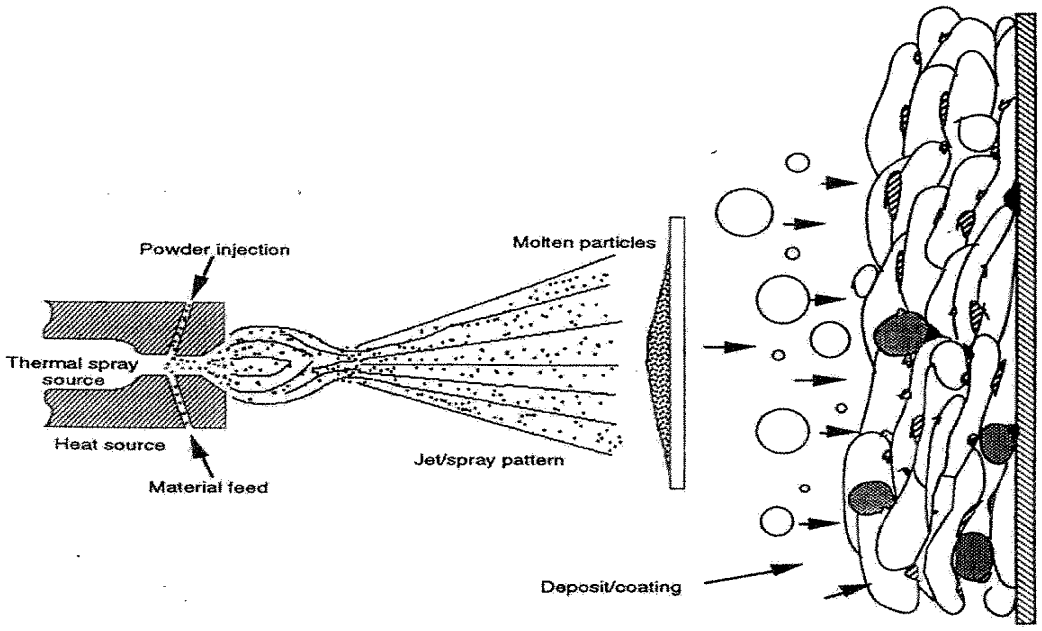

Figure 2.4: General thermal spray process [161].

Thermal spraying is a well-established coating technique in industries where large components are required for wear and corrosion resistance applications [66]. Cermet materials, such as WC-Co or Cr_3C_2-NiCr, are commonly used feedstock materials for a number of applications. The microstuctural refinement of these composite powders improves mechanical properties such as hardness and fracture toughness. The thermal spraying of the nanostructured composite powders leads to the formation of wear and corrosion resistant coatings along with low porosity. Several studies have investigated the grain growth of nanostructured powders during the spraying process [162-165].

2.9.1. Techniques

The thermal spray processes can be grouped into four broad categories (fig. 2.5).

- Combustion
- Plasma Spray
- Cold spray
- Wire Arc

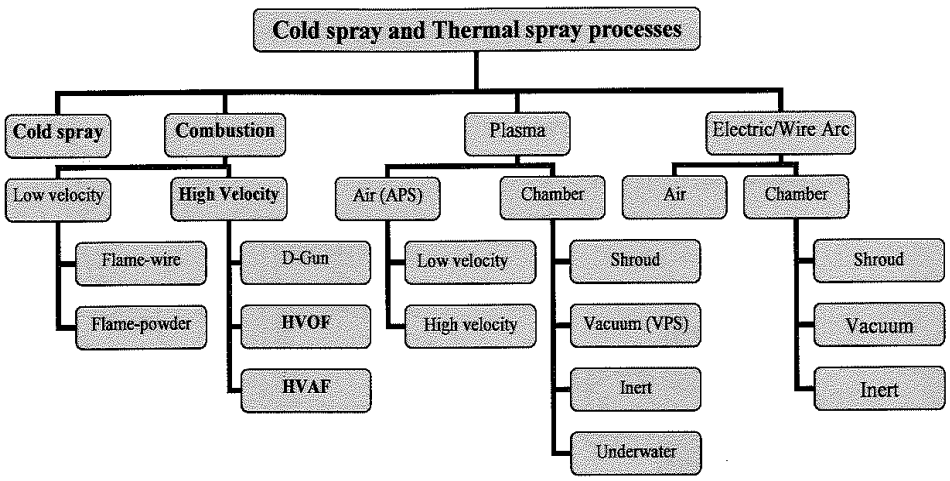

Figure 2.5: Thermal spray and cold spray processes [161].

The techniques differ from each other on the basis of their modes of heating, variation in temperature and velocity of the particles attained during spraying. A comparison of thermal spray processes is shown in table 2.1. Both HVAF and HVOF thermal spray processes are distinctive among the other thermal spray processes due to the combination of high particle velocities and relatively low gas temperature.

Table 2.1: Comparison of thermal spray [161, 166] and cold spray [167, 168] processes

Attribute	Cold spray	HVAF	HVOF	D-Gun	Flame Spray	Air Plasma	Wire Arc
Jet temperature (°C)	450-650	900-1500	1300-2000	5300	3300	15000	>25000
Particle temperature (°C)	350-450	800-1300	1200-1900	N/A	2200	>3500	>3500
Jet velocity (m/s)	400-1000	500-2000	500-2200	>1000	50-100	300-1000	50-100
Particle velocity (m/s)	400-1000	200-1000	200-1100	N/A	50-100	200-800	50-100
Bond strength (MPa)		>70	>70			>34	
Oxides	none	none	Moderate to dispersed	small	high	Moderate to coarse	Moderate to high

2.9.2. Detonation-gun spraying (D-Gun)

The detonation gun coating technique was introduced by Union Carbide in the mid 1950s [169]. It is the starting point for the development of high velocity flame spraying process.

The D-Gun (fig. 2.6) includes a long water cooled barrel with an ID of about 25 mm. A mixture of oxygen and acetylene is fed into the barrel together with a charge of the powder (5-60 µm). The gas is ignited, explodes and its detonation wave accelerates the powder. There are about 4-8 detonations per second. In order to avoid backfiring i.e. the explosion of the fuel gas supply, an inert gas such as nitrogen is used between the portions of exploding mixture. Nitrogen gas also purges the barrel.

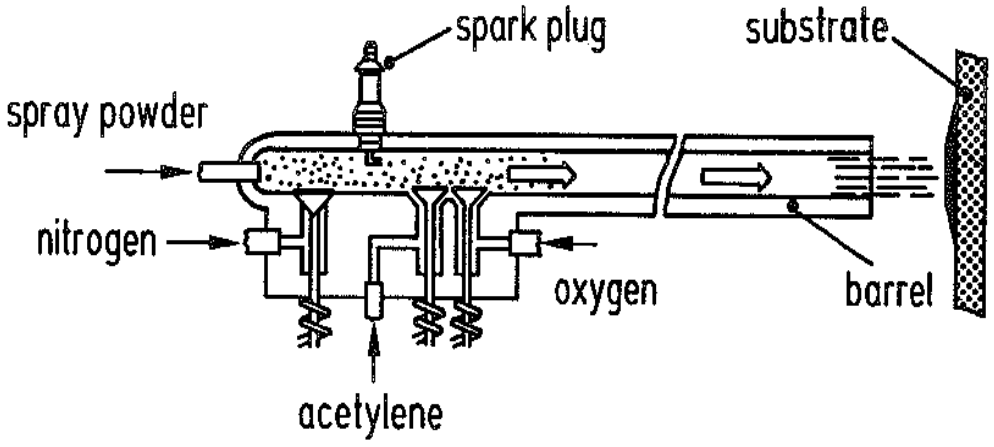

Figure 2.6: Schematics of the D-Gun process [128]

The maximum temperature is 4500 K and the detonation wave may attain a velocity of 2930 m/s [170] while the velocity of the particles reportedly reached 750 m/s and

1000 m/s in the super D-gun [171]. Kadyrov [172] reported velocities varying between 1000 m/s and 3000 m/s. The high velocities of the hot particles on impact with the substrate result in a build up of a very dense and strong coating.

The most used powders are composite with carbide reinforcements. Oliker et al. [173] studied the D-Gun spraying technique for mechanically alloyed Ti and Al elemental powders The porosity of coatings made by using a D-gun is very small, 0.5% for WC-Co coatings and about 2% for Al_2O_3 [174]. The tensile bond strengths were 83 and 70 MPa respectively. The thickness of the detonation gun-sprayed coatings does not exceed 300 µm [66].

The name D-Gun is a trademark and a proprietary process. There is only one supplier available.

2.9.3. Combustion (HVOF, HVAF)

The HVOF spray process was developed at the end of 1970s. Many authors, Bick and Jurgens [175] and Kreye et al. [176] agree that initial work was carried out at Thayer School of Engineering (Hanover, USA) and by Browning Engineering (USA). The principles of this technique are similar to the D-gun, except for a difference in the way a fuel medium is burned in oxygen. The burning is continuous for HVOF and repetitive for D-gun. At present, the HVOF is the fastest growing thermal spray process [158, 171].

The high velocity oxy-fuel (HVOF) and high velocity air fuel (HVAF) processes have some of the highest particle velocities at relatively low gas temperatures. The particle velocities result in high impact energies, thus ensuring excellent bond strength (70 MPa) and very low porosity levels (<1%) [66]. Low gas temperatures and short dwell times limit the maximum particle temperatures achievable, the spraying technique is less suitable for ceramics which have high melting points but is advantageous for cemented carbide and other materials with low melting points or materials prone to degradation at high temperatures. The most used powders are composites with carbide reinforcements and metal or alloys matrices. Typical thicknesses are in the range 100-300 µm. In particular, HVOF spraying has been established into a reliable technique to coat a great variety of metallic surfaces with hard, adherent and tribologically improved composite coatings [177].

The materials widely used for HVOF spraying are WC-Co, WC-CoCr, NiCr-Cr_3C_2 [178], TiC-FeCr, TiB_2-FeCr [179] and NiCr-TiB_2 [180]. Wang et al. [181] studied the bond strength of Ni and Co based composite coatings deposited by HVOF using WC-Co, SiC-Co, TiC-Co, TiC-Ni, Al_2O_3-Ni, W-Ni composite powders. Schorr et al. [182] characterised the FeCrAlY-Cr_3C_2 cermet coatings applied to low carbon steel substrate using a HVOF spray technique. Moreover the FeNiCo alloys i.e. Hastelloys, Stellites, Tribaloys and self fluxing Ni based alloys can be effectively deposited. The other common metals and alloys sprayed by a HVOF spraying technique include copper, nickel-aluminium, iron-chromium-molybdenum and cobalt-molybdenum-chromium.

The HVOF process combusts a hydrocarbon fuel and oxygen mixture under pressure in a water cooled chamber. Powders (5-45 µm) with a carrier gas are fed into the nozzle where the particles are carried with the confined high pressure combusting gases. The gun (fig. 2.7) is designed to achieve high gas flows with supersonic expansion. The gas exit velocities are so high (typically 1000 m/s) that multiple shock diamond shaped patterns are observed in the gas jet indicating that supersonic velocities have been attained [161]. The majority of HVOF systems use gaseous fuels such as ethylene, propane, propylene and natural gas. Liquid fuel kerosene is used in the HVOF torch JP-5000.

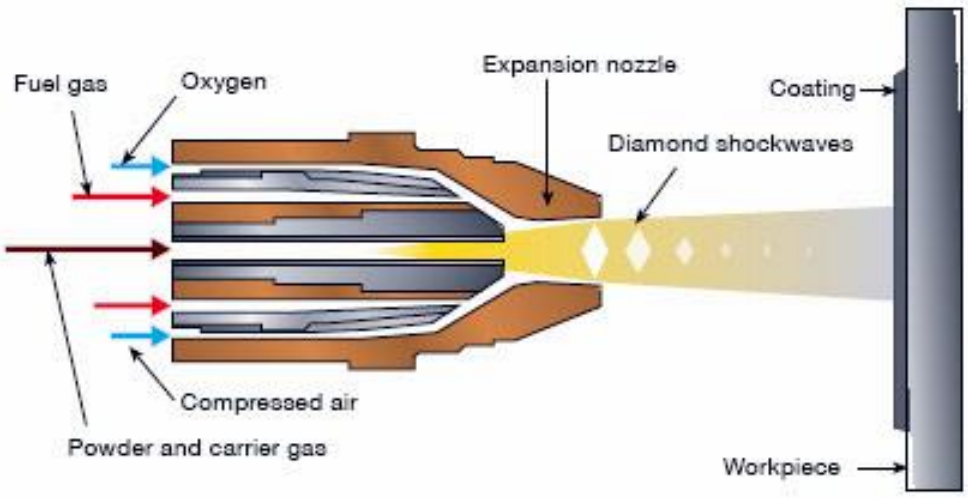

Figure 2.7: Schematic of an HVOF torch [183].

High velocity air fuel (HVAF) spraying is a recently developed technology for deposition of metallic and carbide-metal coatings of commercial powder materials

[184]. The HVAF process was originally developed as a cheaper alternative to the HVOF thermal spray process. It utilizes compressed air for combustion and generates considerably lower temperature than the HVOF process. Initial studies suggest that coatings sprayed with HVAF have the advantage of not exhibiting the oxidation or decarburization effects as observed in HVOF [185]. High quality coatings of 316L stainless steel, Zn-Al, Ni-Cr, CoCr-WC and WC-Co have been produced by using HVAF spraying system.

2.9.4. Plasma spraying

Plasma spraying involves the injection of particles, usually in the range 20-90 μm into a plasma jet with temperatures of up to 15000 K which causes a high degree of particle melting and velocities of up to 800 m/s which leads to improved deposition densities (> 95 %) and bond strength (> 34 MPa) compared with other techniques, such as flame and wire arc spray coatings. A high plasma temperature makes it possible to spray refractory materials such as oxides and high melting-point metals such as molybdenum.

The thickness of individual splats is typically in the range of 1-20 μm. The porosity of the air plasma spraying (APS) coatings is usually in the range 1-7 % and the thickness of the deposit varies between 300-1500 μm [66].

Traditionally plasma spraying has been used for corrosion and wear protection, thermal insulation or repair applications. However, recent developments in controlled atmosphere processes have extended its scope for other applications such as production of powder metallurgy (P/M) structures, composite metal structures, metal/ceramic matrix materials, superconducting oxide processing and near net shape manufacturing [186]. Plasma spraying is used widely for spraying ceramic coatings.

2.9.5. Cold spraying

Cold spray technology was initially developed in the mid 1980s in Russia [187]. In a cold spraying process, fine solid particles (generally 1-50 μm) are accelerated to velocities in a range between 500 and 1000 m/s using a carrier gas [168]. The solid particles undergo plastic deformation and bond to the surface, rapidly building up a layer of deposited material. Only the powders of materials that can deform plastically

can be sprayed by using cold spraying and therefore this technique is suitable for ductile metals and alloys. The f.c.c metals have good deformability; h.c.p metals have less deformability while b.c.c metals have the lowest deformability. Another indicator of sprayability is the melting point. A low value of T_m is beneficial for successful cold spraying [66]. On the other hand, materials that work harden under mechanical stress such as 317L or the alloy TiAl8V4 are difficult to spray.

Most metals and alloys such as Cu, Al, Ni, Ti , Ta , Ni-based alloys, aluminium alloys, iron-based amorphous alloy [188], steel [189] and nanostructured materials, can be deposited by cold spray [190, 191] and even cermets [192] such as Al-Al_2O_3 and ceramics [193] can be embedded into a substrate to form a thin layer coating in cold spray. In practice copper is the most popular material to cold spray.

2.9.6. Wire arc spraying

Wire-arc process is used for any metal that can be drawn into a wire. The thermal efficiency of the wire arc spraying is higher than that of all the thermal spray processes. This is due to reason that process involves direct heating of the electrode wire compared with other thermal spray processes which require indirect heating of the particles through heated gas jets. In wire-arc spraying, a pair of electrically conductive wires is melted by an electric arc. An arc temperature may reach 5800 °C with an arc current of 280 A .The molten metal is atomised by a high velocity air jet into fine droplets which are accelerated towards the substrate surface to form a coating. Molten metal particles formed of wires can reach velocities up to 150 m/s [194]. The process has a number of advantages such as high spray rates and low running cost. The main disadvantage is that the process is only suitable for electrically conductive wires.

2.10. References

1. Guindal, M.J.M., X. Turrillas, T. Hansen, and M.A. Rodriguez, *Time-resolved neutron diffraction study of Ti–TiC–Al_2O_3 composites obtained by SHS.* Journal of the European Ceramic Society, 2008. **28**: p. 2975-2982.

2. Zhang, X., C. Hong, J. Han, and H. Zhang, *Microstructure and mechanical properties of TiB_2/(Cu, Ni) interpenetrating phase composites.* Scripta Materialia, 2006. **55**(6): p. 565-568.

3. Wegner, L.D. and L.J. Gibson, *The mechanical behaviour of interpenetrating phase composites - I: modelling.* International Journal of Mechanical Sciences, 2000. **42**(5): p. 925-942.

4. Travitzky, N.A., *Effect of metal volume fraction on the mechanical properties of alumina/aluminum composites.* Journal of Materials Science, 2001. **36**(18): p. 4459-4463.

5. Clarke, D.R., *Interpenetrating phase composites.* Journal of American Ceramics Society, 1992. **75**(4): p. 739-749.

6. Kim, J.S., Y.S. Kwon, O.I. Lomovsky, M.A. Korchagin, V.I. Mali, and D.V. Dudina, *A synthetic route for metal-ceramic interpenetrating phase composites.* Materials Letters, 2006. **60**(29-30): p. 3723-3726.

7. Zhou, W., W. Hu, and D. L. Zhang, *Metal-matrix interpenetrating phase composite and its in-situ fracture observation.* Materials Letters, 1999. **40**: p. 156-160.

8. Goswami, R.N., S. Mitra, and S. Sarkar, *Experimental investigation on electrochemical grinding of alumina-aluminium interpenetrating phase composite.* International Journal of Advanced Manufacturing Technology, 2009. **40**: p. 729-741.

9. Zhou, W., W. Hu, and D. L. Zhang, *The study of the making of Metal Matrix interpenetrating phase composites.* Scripta Materialia, 1998. **39**(12): p. 1743-1748.

10. Han, C.Z., I.W.M. Brown, and D.L. Zhang, *Microstructure development and properties of alumina-Ti aluminide interpenetrating composites.* Current Applied Physics, 2006. **6**(3): p. 444-447.

11. Skirl, S., R. Krause, S.M. Wiederhorn, and J. Rodel, *Processing and mechanical properties of Al_2O_3/Ni_3Al composites with interpenetrating network microstructure.* Journal of the American Ceramic Society, 2001. **84**(9): p. 2034-2040.

12. Welham, N.J., P.E. Willis, and T. Kerr, *Mechanochemical formation of metal-ceramic composites.* Journal of the American Ceramic Society, 2000. **83**: p. 33-40.

13. Tomoshige, R., T. Goto, T. Matsushita, K. Imamura, A. Chiba, and M. Fujita, *High-temperature-shock compaction of ceramics/silicide composites produced by combustion synthesis.* Journal of Materials Processing Technology, 1999. **85**: p. 100-104.

14. Munir, Z.A. and U. Anselmi-Tamburini, *Self-propagating exothermic reactions: the synthesis of high-temperature materials by combustion. Materials Science Reports*, 1989. **7-8**: p. 277-365.

15. Merzhanov, A.G., *History and recent developments in SHS.* Ceramics International, 1995. **21**(5): p. 371-379.

16. Misra, A.K., *Reaction of Ti and Ti-Al alloys with alumina.* Metallurgical and Materials Transactions A, 1991. **22A**: p. 715-721.

17. Kelkar, G.P. and A.H. Carim, *Phase equilibria in the Ti-Al-O system at 945 °C and analysis of Ti/Al_2O_3 reactions.* Journal of the American Ceramic Society, 1997. **78**: p. 572-576.

18. Schicker, S., D.E. García, J. Bruhn, R. Janssen, and N. Claussen, *Reaction synthesized Al_2O_3-based intermetallic composites.* Acta Materialia, 1998. **46**(7): p. 2485-2492.

19. Horvitz, D., I. Gotman, E.Y. Gutmanas, and N. Claussen, *In situ processing of dense Al_2O_3-Ti aluminide interpenetrating phase composites.* Journal of the European Ceramic Society, 2002. **22**(6): p. 947-954.

20. Fan, R., B. Liu, J. Zhang, J. Bi, and Y. Yin, *Kinetic evaluation of combustion synthesis $3TiO_2 + 7Al \rightarrow 3TiAl + 2Al_2O_3$ using non-isothermal DSC method. Materials Chemistry and Physics*, 1995. **91**: p. 140-145.

21. Bruhn, J., S. Schicker, D.E. Garcia, R. Janssen, F. Wagner, and N. Claussen, *Novel reaction-based processing of co-continuous ceramic-metal composites.* Key Engineering Materials, 1997. **127-131**: p. 73-80.

22. García, D.E., S. Schicker, J. Bruhn, R. Janssen, and N. Claussen, *Processing and mechanical properties of pressureless-sintered niobium-alumina-matrix composites.* Journal of the American Ceramic Society, 1998. **81**(2): p. 429-432.

23. Gunther, R., T. Klassen, B. Dickau, F. Gärtner, A. Bartels, and R. Bormann, *Advanced alumina composites reinforced with titanium-based alloys.* Journal of the American Ceramic Society, 2001. **84**(7): p. 1509-1513.

24. Schicker, S., D.E. Garcia, J. Bruhn, R. Janssen, and N. Claussen, *Reaction processing of Al_2O_3 composites containing iron and iron aluminides.* Journal of the American Ceramic Society, 1997. **80**(9): p. 2294-2300.

25. Klassen, T., R. Gunther, B. Dickau, F. Gärtner, A. Bartels, R. Bormann, and H. Mecking, *Processing and properties of intermetallic/ceramic composites with interpenetrating microstructure.* Journal of the American Ceramic Society, 1998. **81**(9): p. 2504-2506.

26. Claussen, N., D.E. Garcia, and R. Janssen, *Reaction sintering of alumina-aluminide alloys (3A).* Journal of Materials Research, 1996. **11**(11): p. 2884-2888.

27. Pan, J., J.H. Li, H. Fukunaga, X.G. Ning, H.Q. Ye, Z.K. Yao, and D.M. Yang, *Microstructural study of the interface reaction between titania whiskers and aluminum.* Composites Science and Technology, 1997. **57**(3): p. 319-325.

28. Mattern, A., B. Huchler, D. Staudenecker, R. Oberacker, A. Nagel, and M.J. Hoffmann, *Preparation of interpenetrating ceramic-metal composites.* Journal of the European Ceramic Society, 2004. **24**(12): p. 3399-3408.

29. Travitzky, N., I. Gotman, and N. Claussen, *Alumina-Ti aluminide interpenetrating composites: microstructure and mechanical properties.* Materials Letters, 2003. **57**(22-23): p. 3422-3426.

30. Wagner, F., D.E. Garcia, A. Krupp, and N. Claussen, *Interpenetrating Al_2O_3-$TiAl_3$ alloys produced by reactive infiltration.* Journal of the European Ceramic Society, 1999. **19**: p. 2449-2453.

31. Prielipp, H., M. Knechtel, N. Claussen, S.S. K, H. Mullejans, M. Ruhle, and J. Rodel, *Strength and fracture toughness of aluminum/alumina composites with interpenetrating networks.* Materials Science and Engineering A, 1995. **197**(1): p. 19-30.

32. Saiz, E., S. Foppiano, W. Moberlychan, and A.P. Tomsia, *Synthesis and processing of ceramic-metal composites by reactive metal penetration.* Composites Part A: Applied Science and Manufacturing, 1999. **30**(4): p. 399-403.

33. Loehman, R.E., K. Ewsuk, and A.P. Tomsia, *Synthesis of AI_2O_3-Al composites by reactive metal penetration.* Journal of the American Ceramic Society, 1996. **79**(1): p. 27-32.

34. Tiegs, T.N., P.A. Menchhofer, K.P. Plucknett, P.F. Becher, C.B. Thomas, and P.K. Liaw, *Comparison of sintering behaviour and properties of aluminide-bonded ceramics.* Ceramic Engineering and Science Proceedings, 1998. **19**(3): p. 447-455.

35. Raddatz, O., G.A. Schneider, and N. Claussen, *Modelling of R-curve behaviour in ceramic/metal composites.* Acta Materialia, 1998. **46**(18): p. 6381-6395.

36. Lange, F.F., B.V. Velamakanni, and A.G. Evans, *Method for processing metal-reinforced ceramic composites.* Journal of the American Ceramic Society, 1990. **73**(2): p. 388-393.

37. Henager Jr., C.H. and J.L. Brimhalla, *Solid state displacement reaction synthesis of interpenetrating-phase Ni-Al/Al_2O_3 composites.* Scripta Metallurgica et Materialia. 1993. **29**(12): p. 1597-1602.

38. Tjong, S.C., K.F. Tam, and S.Q. Wu, *Thermal cycling characteristics of in-situ Al-based composites prepared by reactive hot pressing.* Composites Science and Technology, 2003. **63**(1): p. 89-97.

39. Skirl, S., M. Hoffman, K. Bowman, S. Wiederhorn, and J. Rödel, *Thermal expansion behaviour and macro-strain of Al_2O_3/Al composites with interpenetrating networks.* Acta Materialia, 1998. **46**(7): p. 2493-2499.

40. Park, H.S. and D.K. Kim, *Effect of silica surface dopants on the formation of alumina/aluminium composites by the directed metal oxidation of an aluminium alloy.* Journal of the American Ceramic Society, 2001. **84**(11): p. 2526-2530.

41. Antolin, S., A.S. Nagelberg, and D.K. Creber, *Formation of Al_2O_3/metal composites by the directed oxidation of molten aluminium-magnesium-silicon alloys: part I, microstructural development.* Journal of the American Ceramic Society, 2005. **75**(2): p. 447-454.

42. Rödel, J., H. Prielipp, N. Claussen, M. Sternitzke, K.B. Alexander, P.F. Becher, and J.H. Schneibel, *Ni_3Al/Al_2O_3 composites with interpenetrating networks.* Scripta Metallurgica et Materialia, 1995. **33**(5): p. 843-848.

43. Rankin, D.T., J.J. Stiglich, D.R. Petrak, and R. Ruh, *Hot-pressing and mechanical properties of Al_2O_3 with Mo-dispersed phase.* Journal of the American Ceramic Society, 2006. **54**(6): p. 277-281.

44. Sun, X. and J.A. Yeomans, *Microstructure and fracture toughness of nickel particle toughened alumina matrix composites.* Journal of Materials Science, 1996. **31**: p. 875-880.

45. Welham, N.J., *Mechanical activation of the solid-state reaction between Al and TiO_2.* Materials Science and Technology, 1998. **255**: p. 81-89.

46. Kamali, A., I. Nejad, M. Aboutalebi, and H. Razavizadeh, *Effect of ball milling on reaction between TiO_2 and Al.* Russian Journal of Non-Ferrous Metals, 2009. **50**(3): p. 246-249.

47. Ying, D.Y., D.L. Zhang, and M. Newby, *Solid-state reactions during heating mechanically milled Al/TiO_2 composite powders.* Metallurgical and Materials Transactions A, 2004. **35**(7): p. 2115-2125.

48. Feng, C.F. and L. Froyen, *Formation of Al_3Ti and Al_2O_3 from an Al-TiO_2 system for preparing in-situ aluminium matrix composites.* Composites Part A: Applied Science and Manufacturing, 2000. **31**(4): p. 385-390.

49. Gaus, S.P., M.P. Harmer, H.M. Chan, H.S. Caram, and N. Clasussen, *Alumina-aluminide alloys (3A) technology: Model development.* Journal of the American Ceramic Society, 2000. **83**(7): p. 1599-1605.

50. Zhang, D.L., Z.H. Cai, and G. Adam, *The mechanical milling of Al/TiO_2 composite powders.* JOM, 2004. **56**(2): p. 53-56.

51. Welham, N.J., *Mechanical activation of the formation of an alumina—titanium trialuminide composite.* Intermetallics, 1998. **6**(5): p. 363-368.

52. Klassen, T., M. Oehring, and R. Bormann, *Microscopic mechanisms of metastable phase formation during ball milling of intermetallic TiAl phases.* Acta Materialia, 1997. **45**(9): p. 3935-3948.

53. Zhang, D.L., J. Liang, and J. Wu, *Processing Ti_3Al-SiC nanocomposites using high energy mechanical milling.* Materials Science and Engineering A, 2004. **375-377**: p. 911-916.

54. Esteban, P.G., E. Gordo, and E.M. Ruiz-Navas, *Influence of High-energy milling and sintering cycle on obtaining TiAl from elemental Ti and Al powders.* Materials Science Forum, 2007. **534-536**: p. 813-816.

55. Kim, G.H., H.S. Kim, and D.-W. Kum, *Determination of titanium solubility in alpha-aluminium during high energy milling.* Scripta Materialia, 1996. **34**(3): p. 421-428.

56. Mao, S.X., N.A. McMinn, and N.Q. Wu, *Processing and mechanical behaviour of TiAl/NiAl intermetallic composites produced by cryogenic mechanical alloying.* Materials Science and Engineering A, 2003. **363**(1-2): p. 275-289.

57. Kong, L.B., J. Ma, W. Zhu, and O.K. Tan, *Preparation and characterisation of PLZT (8/65/35) ceramics via reaction sintering from ball milled powders.* Materials Letters, 2002. **52**(4-5): p. 378-387.

58. Murty, B.S. and S. Ranganathan, *Novel Materials synthesis by mechanical alloying.* International Materials Reviews, 1998. **43**(3): p. 101-141.

59. Benjamin, J.S. and T.E. Volin, *The mechanism of mechanical alloying.* Metallurgical and Materials Transactions B, 1974. **5**(8): p. 1929-1934.

60. Aikin, B.J.M. and T.H. Courtney, *The kinetics of composite particle formation during mechanical alloying.* Metallurgical and Materials Transaction A, 1993. **24**(3): p. 647-657.

61. Fogagnolo, J.B., F. Velasco, M.H. Robert, and J.M. Torralba, *Effect of Mechanical alloying on the morphology, microstructure and properties of aluminium matrix composite powders.* Materials Science and Engineering A, 2003. **342**: p. 131-143.

62. Davis, R.M. and C.C. Koch, *Mechanical alloying of brittle components: Silicon and germanium.* Scripta Metallurgica, 1987. **21**(3): p. 305-310.

63. Lee, J.H., S.K. Ko, and C.W. Won, *Sintering behaviour of Al_2O_3-TiC composite powder prepared by SHS process.* Materials Research Bulletin, 2001. **36**: p. 989-996.

64. Grebe, H.A., A. Advani, N.N. Thadhani, and T. Kottke, *Combustion synthesis and subsequent.* Metallurgical and Materials Transaction A, 1992. **23**(9): p. 2365-2372.

65. Choi, Y., M.E. Mullins, K. Wijayatilleke, and J.K. Lee, *Fabrication of metal matrix composites of TiC-Al through self-propagating synthesis reaction.* Metallurgical and Materials Transactions A, 1992. **23**(9): p. 2387-2392.

66. Pawlowski, L., *The Science and Engineering of thermal spray coatings*. Second Edition. 2008, UK: Willey.

67. Bertuli, C., R.W. Smith, and E. Shtessel, *Self propagating high-temperature synthesis (SHS) of ceramics and composite powders for thermal spray applications*. Advances in Inorganic Film Coatings, Ed. P. Vincenzini. 1995, Italy: Techna, Faenze. 131-140.

68. Ovcharenko, V.E. and O.P. Solonenko, *Physical peculiarities of plasma spheroidization of composite powders having a micro-disperse inner structure in thermal spraying: Current status and future trends*, Ed. A. Ohmori. 1995, Osaka, Japan: High Temperature Society of Japan. 1151-1156.

69. Tondu, S., T. Schnick, L. Pawlowski, B. Wielage, S. Steinhäuser, and L. Sabatier, *Laser glazing of FeCr-TiC composite coatings.* Surface and Coatings Technology, 2000. **123**(2-3): p. 247-251.

70. Horvitz, D. and I. Gotman, *Pressure-assisted SHS synthesis of $MgAl_2O_4$-TiAl in-situ composites with interpenetrating networks.* Acta Materialia, 2002. **50**(8): p. 1961-1971.

71. Yeh, C.L. and Y.L. Chen, *Combustion synthesis of TiC-TiB_2 composites.* Journal of Alloys and Compounds, 2008. **463**(1-2): p. 373-377.

72. Camurlu, H.E. and F. Maglia, *Synthesis of zirconium diboride–zirconium nitride composite powders by self-propagating high-temperature synthesis.* Journal of Materials Science, 2007. **42**(24): p. 10288-10295.

73. Shivpuri, R., Y.L. Chu, K. Venkatesan, J.R. Conrad, K. Sridharan, M. Shamim, and R.P. Fetherston, *An evaluation of metallic coatings for erosive wear resistance in die casting applications.* Wear, 1996. **192**(1-2): p. 49-55.

74. Barresi, J., Z. Chen, C.J. Davidson, M.T. Murray, T. Nguyen, D.H. Stjohn, and W.R. Thorpe, *Casting of aluminium alloy components.* Materials Forum, 1996. **20**: p. 53-70.

75. Persson, A., J. Bergström, C. Burman, and S. Hogmark, *Influence of deposition temperature and time during PVD coating of CrN on corrosive wear in liquid aluminium.* Surface and Coatings Technology, 2001. **146-147**: p. 42-47.

76. Chen, Z.W. and M.Z. Jahedi. *Metallurgy of soldering in high pressure die casting of Al-Si-Cu alloy*. In the Proc. of the *Biennial Materials Conference of the Institute of Materials Engineering*. 1998. University of Wollongong, Australia.

77. Mitterer, C., F. Holler, F. Ustel, and D. Heim, *Application of hard coatings in aluminium die casting - soldering, erosion and thermal fatigue behaviour.* Surface and Coatings Technology, 2000. **125**(1-3): p. 233-239.

78. Han, Q., E.A. Kenik, and S. Viswanathan, *Die soldering in aluminium die casting*. Light Metals, Ed. R.D. Peterson. 2000, Warrendale, PA: TMS. 765-770.

79. Chu, Y.L., P.S. Cheng, and R. Shivpuri, *Soldering phenomenon in aluminium die casting: possible causes and cures.* NADCA Transactions, 1993: p. 361-371.

80. Argo, D., R.J. BamhursL, and W. Wakington, *NADCA sponsored research: The causes of soldering in Zinc die casting.* NADCA Transaction, 1997: p. 77-82.

81. Yu, M., R. Shivpuri, and R.A. Rapp, *Effects of molten aluminium on H13 dies and coatings.* Journal of Materials Engineering and Performance, 1995. **4**(2): p. 175-181.

82. Chen, Z.W. and M.Z. Jahedi, *The effect of temperature on soldering and the sequence of formation of soldered layer during high pressure casting of Al-11Si-3Cu alloy.* International Journal of Cast Metals Research, 1998. **11**: p. 129-138.

83. Tsuchiya, T., H. Kawara, K. Hashimoto, H. Inagaki, and T. Arai. *Core pin failure in aluminium die casting and the effect of surface treatment*. In Proc. of the *19th International Die Casting Congress*. 1997. Minneapolis, Minnesota, USA.

84. Sundqvist, M. and S. Hogmark, *Effects of liquid aluminium on hot-work tool steel.* Tribology International, 1993. **26**(2): p. 129-134.

85. Chen, Z.W., M.Z. Jahedi, and J.A. Law. *Metallurgical phenomena in die/casting interfacial regions during high pressure die casting of aluminium alloy*. In Proc. of the *20th International Die Casting Congress*. 1999. Cleveland, Ohio, USA.

86. Yan, M. and Z. Fan, *Durability of materials in molten aluminium alloys.* Journal of Materials Science, 2001. **36**: p. 285-295.

87. Chen, Z.W. and M.Z. Jahedi, *Die erosion and its effect on soldering formation in high pressure die casting of aluminium alloys.* Materials & Design, 1999. **20**(6): p. 303-309.

88. Shankar, S. and D. Apelian, *Die soldering: Mechanism of the interface reaction between molten aluminium alloy and tool steel.* Metallurgical and Materials Transactions B, 2002. **33B**(3): p. 465-476.

89. Joshi, V., A. Srivastava, R. Shivpuri, and E. Rolinski, *Investigating ion nitriding for the reduction of dissolution and soldering in die-casting shot sleeves.* Surface and Coatings Technology, 2003. **163-164**: p. 668-673.

90. Molinari, A., M. Pellizzari, G. Straffelini, and M. Pirovano, *Corrosion behaviour of a surface-treated AISI H11 hot work tool steel in molten aluminium alloy.* Surface and Coatings Technology, 2000. **126**(1): p. 31-38.

91. Zagonel, L.F., C.A. Figueroa, J.R. Droppa, and F. Alvarez, *Influence of the process temperature on the steel microstructure and hardening in pulsed plasma nitriding.* Surface and Coatings Technology, 2006. **201**(1-2): p. 452-457.

92. Genel, K. and M. Demirkol, *A method to predict effective case depth in ion nitrided steels.* Surface and Coatings Technology, 2005. **195**(1): p. 116-120.

93. Joshi, V., K. Kulkarni, R. Shivpuri, R.S. Bhattacharya, S.J. Dikshit, and D. Bhat, *Dissolution and soldering behaviour of nitrided hot working steel with multilayer LAFAD PVD coatings.* Surface and Coatings Technology, 2001. **146-147**: p. 338-343.

94. Vetter, J., R. Knaup, H. Dweletzki, E. Schneider, and S. Vogler, *Hard coatings for lubrication reduction in metal forming.* Surface and Coatings Technology, 1996. **86-87**(Part 2): p. 739-747.

95. Wang, D.-Y., K.-W. Weng, C.-L. Chang, and W.-Y. Ho, *Synthesis of Cr_3C_2 coatings for tribological applications.* Surface and Coatings Technology, 1999. **120-121**: p. 622-628.

96. Lugscheider, E., C. Barimani, S. Guerreiro, and K. Bobzin, *Corrosion tests of PVD coatings with die lubricant used for Al high-pressure die-casting dies.* Surface and Coatings Technology, 1998. **108-109**(1-3): p. 408-412.

97. Srivastava, A., V. Joshi, R. Shivpuri, R. Bhattacharya, and S. Dixit, *A multilayer coating architecture to reduce heat checking of die surfaces.* Surface and Coatings Technology, 2003. **163-164**: p. 631-636.

98. Lugscheider, E., K. Bobzin, T. Hornig, and M. Maes, *Investigation of the residual stresses and mechanical properties of (Cr,Al)N arc PVD coatings used for semi-solid metal (SSM) forming dies.* Thin Solid Films, 2002. **420-421**: p. 318-323.

99. Rojo, A., J. Oseguera, O. Salas, and J.A. Acosta, *Process structure properties relationship during formation of CrN and AlN layers on H13 Steel.* Surface and Coatings Technology, 2008. **203**(3-4): p. 217-222.

100. Ho, W.-Y., D.-H. Huang, L.-T. Huang, C.-H. Hsu, and D.-Y. Wang, *Study of characteristics of Cr_2O_3/CrN duplex coatings for aluminium die casting applications.* Surface and Coatings Technology, 2004. **177-178**: p. 172-177.

101. Navinsek, B., P. Panjan, I. Urankar, P. Cvahte, and F. Gorenjak, *Improvement of hot-working processes with PVD coatings and duplex treatment.* Surface and Coatings Technology, 2001. **142-144**: p. 1148-1154.

102. Quaeyhaegens, C., M. Kerkhofs, L.M. Stals, and M. Van Stappen, *Promising developments for new applications.* Surface and Coatings Technology, 1996. **80**(1-2): p. 181-184.

103. Navinsek, B. and P. Panjan, *Novel applications of CrN (PVD) coatings deposited at 200 °C.* Surface and Coatings Technology, 1995. **74-75**(Part 2): p. 919-926.

104. Navinsek, B. and P. Panjan, *Oxidation resistance of PVD Cr, Cr-N and Cr-N-O hard coatings.* Surface and Coatings Technology, 1993. **59**(1-3): p. 244-248.

105. Knotek, O., F. Löffler, and B. Bosserhoff, *PVD coatings for die-casting moulds.* Surface and Coatings Technology, 1993. **62**(1-3): p. 630-634.

106. Loffler, F.H.W., *Systematic approach to improve the performance of PVD coatings for tool applications.* Surface and Coatings Technology, 1994. **68-69**: p. 729-740.

107. Heim, D. and R. Hochreiter, *TiAlN and TiAlCN deposition in an industrial PaCVD-plant.* Surface and Coatings Technology, 1998. **98**(1-3): p. 1553-1556.

108. Heim, D., F. Holler, and C. Mitterer, *Hard coatings produced by PACVD applied to aluminium die casting.* Surface and Coatings Technology, 1999. **116-119**: p. 530-536.

109. Mitterer, C., F. Holler, D. Reitberger, E. Badisch, M. Stoiber, C. Lugmair, R. Nöbauer, T. Müller, and R. Kullmer, *Industrial applications of PACVD hard coatings.* Surface and Coatings Technology, 2003. **163-164**: p. 716-722.

110. Mitterer, C., F. Holler, C. Lugmair, R. Nöbauer, R. Kullmer, and C. Teichert, *Optimization of plasma-assisted chemical vapour deposition hard coatings for their application in aluminium die-casting.* Surface and Coatings Technology, 2001. **142-144**: p. 1005-1011.

111. Pfohl, C., A. Gebauer-Teichmann, and K.T. Rie, *Application of wear-resistant PACVD coatings in aluminium diecasting: economical and ecological aspects.* Surface and Coatings Technology, 1999. **112**(1-3): p. 347-350.

112. Lux, B., R. Haubner, and C. Wohlrab, *Chemically vapour-deposited hard coatings: Applications and selection guidelines.* Surface and Coatings Technology, 1989. **38**(3): p. 267-280.

113. Sokovic, M., P. Panjan, and R. Kirn, *Possibilities of improvement of dies casting tools with duplex treatment.* Journal of Materials Processing Technology, 2004. **157-158**: p. 613-616.

114. Panjan, P., M. Cekada, R. Kirn, and M. Sokovic, *Improvement of die-casting tools with duplex treatment.* Surface and Coatings Technology, 2004. **180-181**: p. 561-565.

115. Smolik, J., M. Gulde, J. Walkowicz, and J. Suchanek, *Influence of the structure of the composite: nitrided layer/PVD coating on the durability of forging dies made of steel DIN-1.2367.* Surface and Coatings Technology, 2004. **180-181**: p. 506-511.

116. Klimek, K.S., H. Ahn, I. Seebach, M. Wang, and K.T. Rie, *Duplex process applied for die-casting and forging tools.* Surface and Coatings Technology, 2003. **174-175**: p. 677-680.

117. Smolik, J., J. Walkowicz, and J. Tacikowski, *Influence of the structure of the composite: nitrided layer/PVD coating on the durability of tools for hot working.* Surface and Coatings Technology, 2000. **125**(1-3): p. 134-140.

118. Bjork, T., R. Westergård, S. Hogmark, J. Bergström, and P. Hedenqvist, *Physical vapour deposition duplex coatings for aluminium extrusion dies.* Wear, 1999. **225-229**(Part 2): p. 1123-1130.

119. Bell, T., H. Dong, and Y. Sun, *Realising the potential of duplex surface engineering.* Tribology International, 1998. **31**(1-3): p. 127-137.

120. Pellizzari, M., A. Molinari, and G. Straffelini, *Thermal fatigue resistance of plasma duplex-treated tool steel.* Surface and Coatings Technology, 2001. **142-144**: p. 1109-1115.

121. Lin, J., S. Carrera, A.O. Kunrath, D. Zhong, S. Myers, B. Mishra, P. Ried, and J.J. Moore, *Design methodology for optimized die coatings: The case for aluminium pressure die-casting.* Surface and Coatings Technology, 2006. **201**(6): p. 2930-2941.

122. Salas, O., K. Kearns, S. Carrera, and J.J. Moore, *Tribological behaviour of candidate coatings for Al die casting dies.* Surface and Coatings Technology, 2003. **172**(2-3): p. 117-127.

123. Chou, Y.L., P. Cheng, and R. Shivpuri. *Study of erosive wear in die casting dies: surface treatments and coatings*. In Proc. of the *17th International Die Casting Congress and Exposition*. 1993. Cleveland: T93-073.

124. Shah, S.V. and N.B. Dahotre, *Laser surface-engineered vanadium carbide coating for extended die life.* Journal of Materials Processing Technology, 2002. **124**(1-2): p. 105-112.

125. Agarwal, A., *Laser surface engineering of composite titanium diboride coating on steel: synthesis and characterization, Ph.D. thesis*. 1999, University of Tennessee: Knoxville, TN.

126. Chellapilla, S., R.A. Shivpuri, and S. Balasubramaniam. In *Transaction of the 17th International Die Casting Congress*. 1997. *Minneapolis. NADCA*. T97-T101.

127. Haefer, R.A., *Oberfla¨chen-und Du¨nnschicht technologie.* Beschichten von Oberfla¨chen, 1987. **1**: p. 143-161.

128. Bunshah, R.F., *Handbook of hard coatings, deposition technologies, properties and applications*, Ed. R.F. Bunshah. 2001, New Jersey, USA: Noyes publications.

129. Klimek, K.S., A. Gebauer-Teichmann, P. Kaestner, and K.T. Rie, *Duplex-PACVD coating of surfaces for die casting tools.* Surface and Coatings Technology, 2007. **201**(9-11): p. 5628-5632.

130. Lee, S.H., K.H. Nam, S.C. Hong, and J.J. Lee, *Low temperature deposition of TiB_2 by inductively coupled plasma assisted CVD.* Surface and Coatings Technology, 2007. **201**(9-11): p. 5211-5215.

131. Mogensen, K.S., N.B. Thomsen, S.S. Eskildsen, C. Mathiasen, and J. Bøttiger, *A parametric study of the microstructural, mechanical and tribological properties of PACVD TiN coatings.* Surface and Coatings Technology, 1998. **99**(1-2): p. 140-146.

132. Rie, K.T., C. Pfohl, S.H. Lee, and C.S. Kang, *Development of zirconium and boron containing coatings for the application on aluminium die-casting tools by means of MO-PACVD.* Surface and Coatings Technology, 1997. **97**(1-3): p. 232-237.

133. Arai, T., *Thermoreactive deposition/diffusion process for surface hardening of steels*. ASM Handbook. Vol. 4. 1990, Ohio: ASM International, Ohio. 448-453.

134. Sen, U., *Wear properties of niobium carbide coatings performed by pack method on AISI 1040 steel.* Thin Solid Films, 2005. **483**(1-2): p. 152-157.

135. Jehn, H.A., *PVD and ECD-competition, alternative or combination?* Surface and Coatings Technology, 1999. **112**(1-3): p. 210-216.

136. Bjork, T., R. Westergård, and S. Hogmark, *Wear of surface treated dies for aluminium extrusion - a case study.* Wear, 2001. **249**(3-4): p. 316-323.

137. Eskildsen, S.S., C. Mathiasen, and M. Foss, *Plasma CVD: process capabilities and economic aspects.* Surface and Coatings Technology, 1999. **116-119**: p. 18-24.

138. Gulizia, S., M.Z. Jahedi, and E.D. Doyle, *Performance evaluation of PVD coatings for high pressure die casting.* Surface and Coatings Technology, 2001. **140**(3): p. 200-205.

139. Wang, Y., *A study of PVD coatings and die materials for extended die-casting die life.* Surface and Coatings Technology, 1997. **94-95**: p. 60-63.

140. Larsson, M., P. Hollman, P. Hedenqvist, S. Hogmark, U. Wahlström, and L. Hultman, *Deposition and microstructure of PVD TiN-NbN multilayered coatings by combined reactive electron beam evaporation and DC sputtering.* Surface and Coatings Technology, 1996. **86-87**(Part 1): p. 351-356.

141. Chu, X., S.A. Barnett, M.S. Wong, and W.D. Sproul, *Reactive unbalanced magnetron sputter deposition of polycrystalline TiN/NbN superlattice coatings.* Surface and Coatings Technology, 1993. **57**(1): p. 13-18.

142. Huang, Y. and H.W. Zhang, *The role of metal plasticity and interfacial strength in the cracking of metal/ceramic laminates.* Acta Metallurgica et Materialia, 1995. **43**(4): p. 1523-1530.

143. Herranen, M., U. Wiklund, J.O. Carlsson, and S. Hogmark, *Corrosion behaviour of Ti/TiN multilayer coated tool steel.* Surface and Coatings Technology, 1998. **99**(1-2): p. 191-196.

144. Starling, C.M.D. and J.R.T. Branco, *Thermal fatigue of hot work tool steel with hard coatings.* Thin Solid Films, 1997. **308-309**: p. 436-442.

145. Bjork, T., M. Berger, R. Westergård, S. Hogmark, and J. Bergström, *New physical vapour deposition coatings applied to extrusion dies.* Surface and Coatings Technology, 2001. **146-147**: p. 33-41.

146. Imbeni, V., C. Martini, E. Lanzoni, G. Poli, and I.M. Hutchings, *Tribological behaviour of multi-layered PVD nitride coatings.* Wear, 2001. **251**(1-12): p. 997-1002.

147. Ali, M., E. Hamzah, I.A. Qazi, and M.R.M. Toff, *Effect of cathodic arc PVD parameters on roughness of TiN coating on steel substrate.* Current Applied Physics, 2010. **10**(2): p. 471-474.

148. Birol, Y. and D. Isler, *Response to thermal cycling of CAPVD (Al, Cr)N-coated hot work tool steel.* Surface and Coatings Technology, 2010. **205**(2): p. 275-280

149. Isler, D., Y. Birol, and M. Urgen, *PVD coated hot worked tool steels for tooling applications in semi-solid processing of steel.* The International Journal of Materials Forming, 2010. **3**(1): p. 744-750.

150. Mattox, D.M., *The foundations of vacuum coating technology*. 2003, Norwick, New York: Noyes Publications/William Andrew publishing.

151. Li, Z.W., W. Gao, D.Y. Ying, and D.L. Zhang, *Improved oxidation resistance of Ti with a thermal sprayed $Ti_3Al(O)$-Al_2O_3 composite coating.* Scripta Materialia, 2003. **48**(12): p. 1649-1653.

152. Froes FH, C. Suryanarayana, and and D.J. Elieze, *Synthesis, properties and applications of titanium aluminides.* Journal of Materials Science, 1992. **27**(19): p. 5113-5140.

153. Sauthoff, G., *Intermetallics*. 1995, Germany: Weinheim: VCH.

154. Matsubara, T., T. Shibutani, K. Uenishi, and K.F. Kobayashi, *Fabrication of thick intermetallic compound Al_3Ti Layer on Ti substrate by reactive-pulsed electric current sintering.* Intermetallics, 2000. **8**: p. 815-822.

155. DePoorter, G.L., T.K. Brog, and M.J. Readey, *ASM handbooks online, Structural Ceramics*. Vol. 2. 2002, OH, USA: ASM International.

156. Peters, M., J. Kumpfert, C.H. Ward, and C. Leyens, *Titanium and titanium alloys: fundamentals and applications*, ed. C. Leyens and M. Peters. 2003: Wiley-VCH Verlag GmbH.

157. Chawla, V., B.S. Sidhu, D. Puri, and S. Prakash, *Performance of plasma sprayed nanostructured and conventional coatings.* Journal of Australian Ceramic Society, 2008. **44**(2): p. 56-62.

158. Turunen, E., T. Varis, T.E. Gustafsson, J. KesKinen, P. Lintunen, T. Falt, R. Nowak, and S.P. Hannula, *Process optimization for naostructured HVOF thermally sprayed Al_2O_3- based ceramic coatings.* Key Engineering Materials, 2006. **317-318**: p. 545-548.

159. Haman, J.D., J.J. Boulware, L.C. Lucas, and D.E. Cramer, *High- velocity oxyfuel thermal spray coatings for biomedical applications.* Journal of Thermal Spray Technology, 1995. **4**(2): p. 179-184.

160. Knight, R. and R.W. Smith, *Spray forming of materials, powder metal technologies and applications*. *ASM Hand book*. Vol. 7. 1998: ASM International.

161. Smith, R.W., *Equipment and Theory- A Lesson from thermal spray technology course 51, lesson/test 2*. ASM International. 1992, Material Park, OH- USA.

162. Stenberg, T.H., K.J. Niemi, P.M.J. Vuoristo, J.E. Vuorinen, T.A. Mantyla and T.J. Tiainen, *Effect of powder manufacturing method, particle size and binder content on the properties of TiC-Ni composite coatings.* In Proc. of the *International Thermal Spray Conference ITSC'95*. 1995. Kobe, Japan: High Temperature Society of Japan.

163. Schlump, W., J. Willbrand, and H. Grewe, *Properties of nano-crystalline composite material produced by high-energy milling.* Metall, 1994. **48**(1): p. 34-39.

164. Usmani, S., S.Sampath, D. Huock, and D.Lee, *Effect of carbide grain size on the sliding and abrasive wear behaviour of thermally sprayed WC-Co coatings.* Tribology Transactions, 1997. **40**: p. 470-478.

165. Eigen, N., F. Gärtner, T. Klassen, E. Aust, R. Bormann, and H. Kreye, *Microstructures and properties of nanostructured thermal sprayed coatings using high-energy milled cermet powders.* Surface and Coatings Technology, 2005. **195**(2-3): p. 344-357.

166. Browning, J.A., *Hypervelocity impact fusion- A technical note.* Journal of Thermal Spray Technology, 1992. **1**(4): p. 289-292.

167. Assadi, H., F. Gartner, T. Stoltenhoff, and H. Kreye, *Bonding mechanism in cold gas spraying.* Acta Materialia, 2003. **51**: p. 4379-4394.

168. Grujicic, M., C.L. Zhao, C. Tong, W.S. Derosset, and D. Helfritch, *Analysis of the impact velocity of powder particles in the cold-gas dynamic-spray process.* Materials Science and Engineering A, 2004. **368**(1-2): p. 222-230.

169. Poorman, R.M., H.B. Sargent, and H. Lamprey, *Method and apparatus utilising detonation wave for spraying and other purposes*. 1955: US Patent 2714533.

170. Smith, R.G., *The basic principles of detonation spraying in Science and Technology of surface coatings*, ed. B.N. Chapman and J.C. Anderson. 1974, London, UK: Academic press.

171. Irving, B., R. Knight, and R.W. Smith, *The HVOF Process - the hottest topic in the thermal spray industry.* Welding Journal, 1993. **72**(7): p. 25-30.

172. Kadyrov, E. and V. Kadyrov, *Gas dynamical parameters of detonation powder spraying.* Journal of Thermal Spray Technology, 1995. **4**: p. 280-286.

173. Oliker, V.E., V.L. Sirovatka, I.I. Timofeeva, T.Y. Gridasova, and Y.F. Hrechyshkin, *Formation of detonation coatings based on titanium aluminide alloys and aluminium titanate ceramic sprayed from mechanically alloyed powders Ti-Al.* Surface and Coatings Technology, 2006. **200**(11): p. 3573-3581.

174. Tucker, R.C., *Plasma and detonation gun deposition techniques and coating properties, in deposition technology for films and coatings*, Ed. R.F. Bunshah. 1982, Park Ridge, NJ, USA: Noyes. 454-489.

175. Bick, H. and W. Jurgens. *Advanced high velocity thermal spraying of metallic and ceramic powders*. In Proc. of the *10th International Thermal Spray Conference*. 1983. Dusseldorf, Germany: DVS.

176. Kreye, H., D. Fandrich, H.H. Muller, and G. Reiners, *Microstructure and bond strength of WC-Co coatings deposited by hypersonic flame spraying, advances in thermal spraying*. 1986: Pergamon Press. 121-128.

177. Dorfman, M., J. DeFalco, and J. Karthikeyan. *Tungsten carbide-cobalt coatings for industrial applications*. In Proc. of the *First International Thermal Spray 2000 Conference*. 2000. Montreal, Canada, 471-478.

178. Harvey, D., *The tough truth-wear resistant coatings using high velocity Oxyfuel.* Industrial Lubrication and Tribology, 1996. **48**(2): p. 11-16.

179. Jones, M., A.J. Horlock, P.H. Shipway, D.G. McCartney, and J.V. Wood, *A comparison of the abrasive wear behaviour of HVOF sprayed titanium carbide- and titanium boride- based cermet coatings.* Wear, 2001. **251**(1-12): p. 1009-1016.

180. Horlock, A.J., D.G. Mccartney, P.H. Shipway, and J.V. Wood, *Thermally sprayed Ni(Cr)-TiB_2 coatings using powder produced by self-propagating high temperature synthesis: microstructure and abrasive wear behaviour.* Materials Science & Engineering-A, 2002. **336**(1-2): p. 88-98.

181. Wang, Y.Y., C.J. Li, and A. Ohmori, *Examination of factors influencing the bond strength of high velocity oxy-fuel sprayed coatings.* Surface and Coatings Technology, 2006. **200**(9): p. 2923-2928.

182. Schorr, B.S., K.J. Stein, and A.R. Marder, *Characterization of thermal spray coatings.* Materials Characterisation, 1999. **42**(2-3): p. 93-100.

183. http://www.sulzermetco.com/desktopdefault.aspx/tabid-2008//3390_read-5302/.

184. Verstak, A. and V. Baranovski. *Activated combustion HVAF coatings for protection against wear and high temperature corrosion*. In Proc. of the *2003 International Thermal Spray Conference*. 2003. Orlando, Florida, USA: ASM International

185. Jacobs, L., M.M. Hyland, and M.D. Bonte, *Comparative study of WC-cermet coatings sprayed via HVOF and HVAF processes.* Journal of Thermal Spray Technology, 1998. **7**(2): p. 213-218.

186. Smith, R. and D. Apelian, *Thermal plasma materials processing - applications and opportunities.* Plasma Chemistry and Plasma Processing, 1989. **9**(1): p. 135s-165s.

187. Alkhimov, A.P., A.N. Papyrin, V.F. Dosarev, N.I. Nestorovich, and M.M. Shuspanov, *Gas dynamic spraying method for applying a coating*. 1994: US 5,302,414.

188. Ajdelsztajn, L., E.J. Lavernia, B. Jodoin, P. Richer, and E. Sansoucy, *Cold gas dynamic spraying of iron-base amorphous alloy.* Journal of Thermal Spray Technology, 2006. **15**(4): p. 495-500.

189. Borchers, C., T. Schmidt, F. Gärtner, and H. Kreye, *High strain rate deformation microstructures of stainless steel 316L by cold spraying and explosive powder compaction.* Applied Physics A, 2008. **90**(3): p. 517-526.

190. Alkhimov, A.P., V.F. Kosarev, and A.N. Papyrin, *A method of cold gas dynamic deposition.* Doklady Akademii nauk SSSR, 1990. **318**(5): p. 1062-1065.

191. Stoltenhoff, T., H. Kreye, H.J. Richter, and H. Assadi. *Optimisation of the cold spray process*. In Proc. of the *2001 Thermal Spray Conference: New Surfaces for a New Millennium*. 2001. Materials Park, OH: ASM International.

192. Karthikeyan, J., C.M. Kay, J. Lindemann and R.S. Lima, *Cold sprayed nanostructured WC-Co*. In Proc. of *Thermal Spray Conference*: New Surfaces for a New Millennium. 2001. Materials Park, OH: ASM International.

193. Yang, G.J., F. Han, and C.J. Li. In the Proc. of the *Fifth International Seminar and Sixth China National Thermal Spraying Conference*. 2002. Anshan, China.

194. Rudzki, G.J., *Surface finishing systems*. 1983, Teddington, UK: Finishing Publication Ltd.

This page is intentionally left blank

Chapter 3

Experimental Procedures

This chapter describes the experimental methodologies and materials used in this research work. In particular, a description is provided for the production of composite powders, coating deposition and performance evaluation, friction and wear testing and sample characterisation.

3.1 Powder production

3.1.1 Production of Al/TiO_2 composite powders by high energy mechanical milling

The starting materials used were commercially available TiO_2 (Anatase, 99% purity) with a particle size ranging from 5 to 50 μm and commercially available pure aluminium powder (99.5% purity) with an average particle size of 40 μm. Two types of composite powders were produced using high energy milling.

3.1.1.a Powder A

The Al and TiO_2 ratio was determined according to the following nominal ratio with 5wt% surplus aluminium:

$$3TiO_2 + 4Al \longrightarrow 3Ti + 2Al_2O_3 \quad \text{Eq. 3.1}$$

3.1.1.b Powder B

The Al and TiO_2 ratio was determined according to the following nominal ratio with 5 wt% surplus aluminium:

$$3TiO_2 + 7Al \longrightarrow 3TiAl + 2Al_2O_3 \quad \text{Eq. 3.2}$$

The reaction products in these eqs. are not Ti or pure TiAl intermetallic compound. The Ti phase usually contains some aluminium and oxygen in solid solution, while the TiAl phase has a certain amount of oxygen interstitial. An extra 5 wt% aluminium was added to the above mixtures to compensate the loss of aluminium during milling and to compensate for the impurity presence in the starting Al powder.

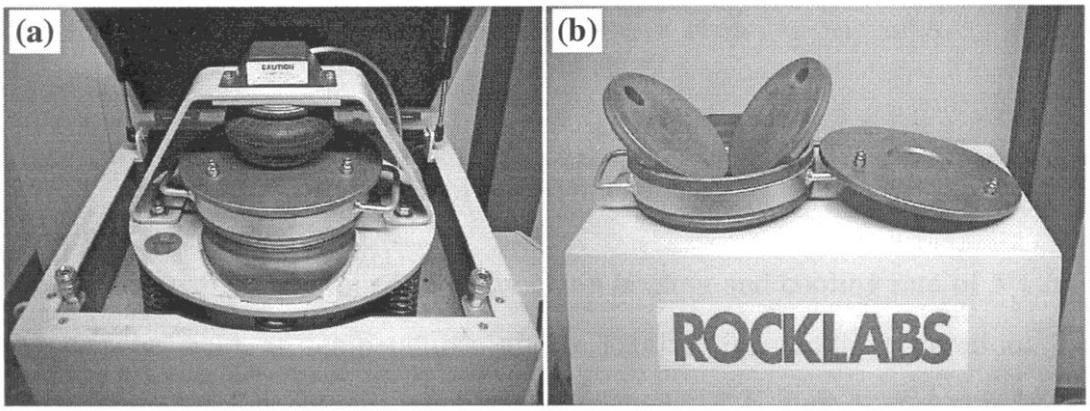

Figure 3.1: (a) High energy discus mill, (b) milling vial and discs

The powders were mechanically milled in a high energy mechanical mill (Rocklabs, New Zealand) under argon atmosphere (fig. 3.1). A process control agent (PCA), isopropyl alcohol, was added up to 3 wt% into each batch before milling to prevent the powder sticking to the vial walls and the discs. Each batch of powder was milled for 4 hours.

The effect of disc to powder weight ratio (DPR) on the degree of intermixing was studied using 300 g of powder A (Eq. 3.1) using Al and TiO_2 starting powders with a molar ratio of 3:4. Three different disc to powder weight ratios (DPRs) of 4.5:1, 13:1 and 22:1 were used, with a milling time of four hours for each. The optimized results of this study were used to produce Powder A and powder B, using 500 g of initially charged mixture of TiO_2 and Al with molar ratios of 3:4 and 3:7 respectively, with an disc to powder ratio (DPR) of 13.2:1. The as milled powders were stabilized in a glove box under argon atmosphere.

3.1.1.c Disc to powder weight ratios (DPRs)

Disc to powder weight ratio determines the intensity of milling. It affects the degree of mixing and refinement of starting powders. The higher the disc to powder weight ratio (DPR), the lower will be the milling time.

Disc to powder weight ratio = Weight of the milling media (discs/balls)/powder weight

The details of various disc to powder weight ratios (DPRs) used for powder A and B are shown in table 3.1.

Table 3.1: Disc to powder weight ratios (DPRs)

Powder Type	**Powder Weight**	**Milling Media**			**Disc to Powder weight Ratio (DPR)**
		Type	**Size (mm)**	**Weight (g)**	
Powder A	300	2 large discs	195 each	6600	22:1
		2 small discs	164 each	3900	13:1
		15 steel balls	Diameter: 14	1334	4.5:1
	500	2 large discs	195 each	6600	13.2:1
Powder B	500	2 large discs	195 each	6600	13.2:1

3.1.2 Combustion reacted powders

As-milled Al/TiO_2 composite powders, which were produced with molar ratios of 3:4 and 3:7 using high energy milling, were thermally reacted by a self propagating high temperature synthesis (SHS) technique to produce Ti(Al,O)/A_2O_3 and TiAl(O)/Al_2O_3 feedstocks for thermal spraying. The combustion reactions were performed inside a glove box (fig. 3.2) under argon atmosphere (with oxygen < 200 ppm) using a graphite crucible. The combustion reactions (fig. 3.2) were triggered by an electrically heated external source (Ni-Cr coil) connected to a low voltage power supply.

The combustion reacted powder A ($Ti(Al,O)/A_2O_3$) was produced using a disc to powder weight ratio (DPR) of 22:1 and 300 g of an initially charged mixture of TiO_2 and Al with molar ratios of 3:4. This was mechanically milled for 2 minutes in a discuss mill and the feedstock was then thermally sprayed at Triple R Engineering Ltd., Palmerstone North, New Zealand.

Figure 3.2: Combustion reaction experimental set up

Two batches of combustion reacted powder A ($Ti(Al,O)/A_2O_3$) and powder B ($TiAl(O)/Al_2O_3$), were produced using a disc to powder weight ratio (DPR) of 13.2:1 and 500 g of an initially charged mixture of TiO_2 and Al with molar ratios of 3:4 and 3:7 respectively. Each batch of the combustion reacted powder was mechanically milled in a ball mill using three steel balls (25.40 mm diameter) for different intervals of 15 minutes, depending upon the characteristics of the combustion reacted powder. The feedstock powders were processed further to control their flowability through the spray gun nozzle. The feedstock powders A and B were then used for thermal spraying at Holster Engineering, Tokoroa, New Zealand.

3.1.2.a Powder flowability control

After each interval of 15 minutes, the combustion reacted powder batches (produced from 500 g of an initially charged mixture of TiO_2 and Al) were classified using a

combination of sieves of sizes 75 µm and 125 µm. The powder fractions with size < 75 µm and 75 µm < size < 125 µm were collected separately and checked for their flowabilty (ASTM B 213) using a flow meter. Powder fraction with size > 125 µm was subjected to further milling. The powder classification process was continued until the whole batch was subdivided into two fractions. One fraction with size < 75 µm and the other with 75 µm <size < 125 µm. The smaller fraction with 75 µm < size < 125 µm was found suitable for thermal spraying due to its good flowability, whereas the larger fraction with size < 75 µm had poor flowability and therefore was subjected to agglomeration using 2% PVA (polyvinyl alcohol) binder. After agglomeration, the powder had good flowability in the size range of < 106 µm. The agglomerated powder fraction of size < 106 µm was mixed with the un-agglomerated powder 75 µm < size < 125 µm fraction. The over all flowability of the feedstock powders A (Ti(Al,O)/A_2O_3) and B (TiAl(O)/Al_2O_3) was measured using a flow meter to ASTM B 213 standard.

3.1.2.b Feedstocks particle size evaluation

The particle size distributions of the un-agglomerated feedstock fractions (75 µm < size < 125 µm) and (size < 75 µm) of powders A and B were measured using a Malvern Mastersizer Laser Particle Size Analyzer. The particle size distributions of the PVA-agglomerated feedstock fractions were measured using SEM images only due to the problem of PVA dissociation in water (used as a particles carrier) in the particle size analyzer.

3.2 Substrate preparations

The substrate material used in the test specimens was a AISI H13 hot work tool steel (DIN 1.2344 EFS), with the nominal chemical composition (wt%) 0.4% C, 1.0% Si, 5.3% Cr, 1.4% Mo, 1.0% V and Fe balance. Prior to coating, the steel was hardened and double tempered to a nominal hardness of 48-50 HRC. Heat-treatment of the specimen was carried out at Heat-Treatments Ltd., Auckland. The hardened steel substrates were grit blasted using alumina (36 grit) with an air pressure of 0.17 MPa prior to coating application. The surface roughness of the grit blasted samples was measured using a T1000A roughness profiler (MTF, Harbin, China).

Steel substrates of three different shapes/dimensions were used for coating application for various tests. The choice of a coupon shape is according to the requirement for a particular test.

1 Cylindrical coupons of 63 mm length and 20 mm diameter for immersion tests.

2 Bar coupons of dimensions 125 × 10 × 10 mm for thermal shock resistance tests.

3 Circular discs of 70 mm diameter for wear and friction tests.

3.3 Coating deposition (HVOF thermal spraying)

The combustion reacted powders were used as a feedstock for thermal spraying using a high velocity oxygen fuel (HVOF) method (fig. 3.3) on a heat-treated, grit blasted H13 tool steel substrate. More detail of thermal spray conditions/parameters is given in chapter four. A single and double layer coating that consisted of an intermediate layer of pure Ti and an outer layer of Ti(Al,O)/Al_2O_3 or TiAl(O)/Al_2O composite were produced for various tests. A Ti under layer/bond coat was produced by thermal spraying of either hydride and dehydrate Ti powder or atomized Ti powder (-100 mesh).

Figure 3.3: HVOF thermal spraying of composite powder feedstock

The composite coating details are given in table 3.2.

Table 3.2: Composite coating references with their feedstock and performance evaluation details

Coatings	Powder feedstock	PVA agglomeration	As-milled powder (TiO_2/Al)	HVOF spraying performed at	Types of Ti under layer	Performance evaluation	Industrial trial
A1	Ti(Al,O)/Al_2O_3	No PVA	300 g	Triple R Engineering Ltd.	Atomized Ti	Thermal shock	-
A2		2% PVA	500 g	Holster Engineering Ltd.	HDH Ti	Liquid metal corrosion resistance (immersion test), thermal shock resistance, wear resistance	Dummy block used in Al extrusion
B2	TiAl(O)/Al_2O_3	2%PVA	500 g	Holster Engineering Ltd	HDH Ti	Liquid metal corrosion resistance (immersion test), thermal shock resistance, wear resistance	-

The surface roughness of the as-sprayed composite coatings was measured using a T1000A roughness profiler (MTF, Harbin, China). Coating thickness was measured using optical microscopy and SEM images.

3.4 Micro-hardness measurements

The micro-hardness of the coating surface was measured using a Leco LM-700 micro-indenter with a load of 100 g and dwell time of 20 s. At least 15 surface harness readings/measurements were recorded in case of each coating. The coating surface was polished gently using 4000 grit SiC paper and followed by polishing with alumina suspension (0.3 µm agglomerated alpha alumina). Because of the fine structure in the interpenetrating composites with a separation distance between phases of about 3 µm, a hardness for individual phases was not measured.

3.5 Coating performance in molten aluminium

3.5.1 Aluminium alloy composition

The aluminium alloy used in the tests was C601 alloy with a nominal chemical composition, Al, 7% Si, 0.34% Mg and a small amount of strontium for modification. Composite coatings referred to as A2 (Ti(Al,O)/Al_2O_3) and B2 (TiAl(O)/Al_2O_3) were used for a performance evaluation in molten Al.

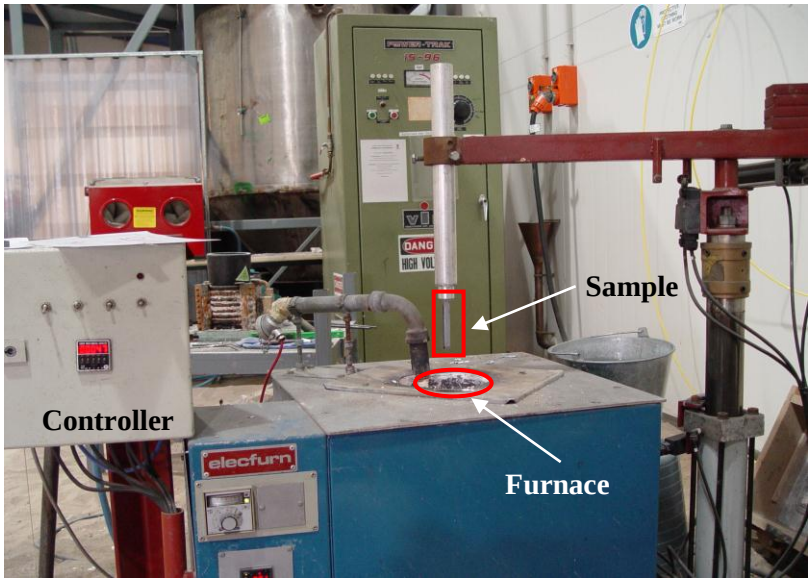

Figure 3.4: Immersion and thermal shock tests experimental set up

A test apparatus (fig. 3.4) designed at Glucina Smelting Ltd., Auckland was used to perform immersion and thermal shock resistance tests. The test apparatus consists of;

- An electrical furnace with a thermocouple to maintain the molten aluminium temperature.
- A removable sample holder with single and multiple specimen holding capacity.
- A pneumatic system to support alternating heating in molten Al and cooling in water.
- An automatic controller, for regulating the holding time in molten Al, movement speed and for displaying the number of cycles.
- A bath with water.

3.5.2 Immersion test

For Al soldering evaluation, coated and uncoated cylindrical coupons were dipped for different time intervals into the static molten Al melt at a temperature of 710 ± 10 °C followed by air cooling. For each given time interval a set of three cylindrical coupons (two with different types of coatings and one uncoated) were immersed into the molten aluminium at the same time using a sample holder. The nature of the Al soldering to the coated and uncoated samples (cross-sections) was assessed using scanning electron microscopy (SEM).

The dissolution of the coatings/wash out in molten aluminium was evaluated by determining the weight loss of the coated coupons dipped into molten aluminium for various time intervals. The coupons were kept overnight in an oven at a temperature 70 °C and weighed carefully prior to molten Al immersion. The weighing was carried out with accuracy to the nearest 0.0001 g. During an immersion test, the coated and uncoated samples were immersed into molten aluminium at 700 ± 10 °C for different time intervals. The samples were then removed from the melt and air cooled. The Al layer soldered to the samples was removed by using warm (50 °C - 60 °C) 20% NaOH solution. The weight loss of the coupons was determined from the difference in weight before immersion in molten aluminium and after soldered aluminium removal using NaOH solution. The weight loss per unit area of test coupons was used to report the degree of wash out.

3.5.3 Thermal shock resistance tests

Thermal shock tests were performed using the test apparatus (fig. 3.4) which enabled controlled cycling of test coupons between molten aluminium and water. Coated coupons (square bar) were dipped into the molten aluminium furnace which was kept at a temperature of 700 ± 10 °C and then quenched into the water. Three faces of each coupon were coated while one face was left uncoated for the comparison purpose. Coupons of different types of coatings were tested at the same time using a sample holder. For each thermal shock cycle, a specimen was held above the molten metal for 6 seconds and then dipped into molten Al for 30 seconds, lifted out over the water bath and immersed into water for 10 sec. After every 100 cycles, the sample was removed from the holder and the surfaces of the coupons were examined for Al

soldering and an evaluation of surface spallation. The composite coatings and areas of cracking/spallation on the surface and from cross-sections were analyzed using scanning electron microscopy.

3.6 Wear and friction testing

Pin on disc Test

The friction and wear tests were carried out using an MG-2000 high temperature Pin on Disc Tribometer (Beilun Corp.) (fig. 3.5) for both high temperature testing without lubrication and room temperature testing under dry and lubricating conditions. The wear performance of the composite coating was assessed using a spherical ended alumina pin (10 mm diameter), a flat ended high speed steel pin (5 mm diameter) and a spherical ended hardened steel pin (10 mm diameter) as counter bodies at a load of 20 N with a sliding speed of 0.5 m/s. The pin was rubbed against the rotating coated H13 disc (70 mm diameter).

Figure 3.5: MG-2000 high temperature Pin on Disc Tribometer

The surface roughness of both the uncoated H13 tool steel and coating were measured at two different positions before conducting the wear test using a T1000A roughness profiler (MTF, Harbin, China) (fig. 3.6). The frictional movements were continuously recorded by a computer. The samples were cleaned by ethanol after each wear test and the wear rate of the coating (where a spherical ended alumina pin was used as a counter body) was measured from the depth of the wear track by using a profiler/surface texture measuring perthometer (S3P, Germany) (fig. 3.7).

Figure 3.6: T1000A roughness profiler

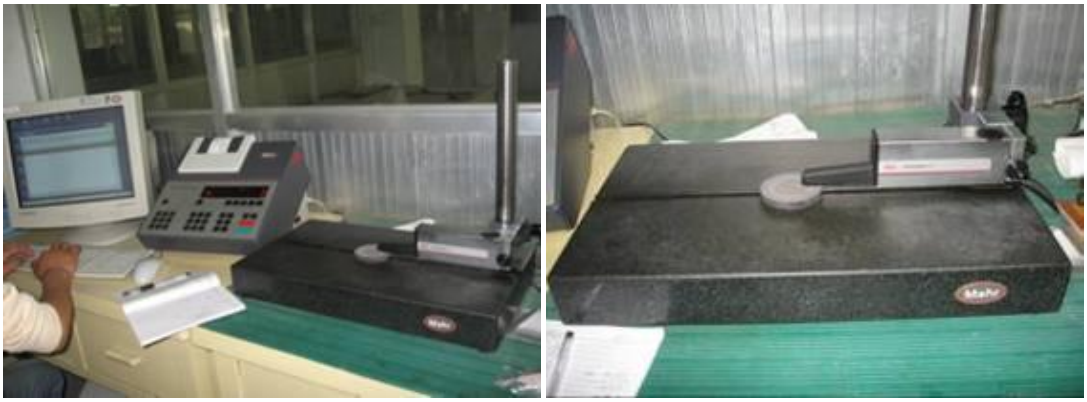

Figure 3.7: Profiler/surface texture measuring equipment

For each wear track, two readings were recorded to calculate the average wear track depth. Friction test data was used to estimate the friction coefficient and average life of the coating under a given condition. The specific wear rate of the coating was assessed both at high temperature and room temperature.

3.7 Microstructure characterisation

3.7.1 Sample preparation

Coated samples (cross-sections) were cut by using a diamond blade under water lubricant. The powder and coated samples (cross-sections) were embedded in Epoxy resin and hardened for 24 hours. The mounted specimens were ground using 320, 600,

1000, 2000 and 4000 grit SiC papers, followed by polishing using an alumina suspension (0.3µm agglomerated alpha alumina).

3.7.2 Scanning Electron Microscopy (SEM) and Energy Dispersive X-ray analysis (EDX)

Microstructure characterisation of as-milled and combustion reacted powders/feedstocks and thermally sprayed coatings were carried out using an Hitachi S-4000 scanning electron microscopy, at an operating voltage of 20KV. Energy Dispersive X-ray analysis (EDX) was carried out using a Kevex microanalyser attachment.

3.7.3 X-Ray Diffractometry (XRD)

X-ray diffraction analysis (XRD) was performed to determine the phase constituents in both powder and coating samples using an X'pert diffractometer (Philips, the Netherlands) with Cu Kα radiation. The XRD patterns were obtained using a 0.02° step size averaging for 5 seconds per increment, with voltage of 40 KV and a current of 40 mA.

3.7.4 Differential Thermal Analysis (DTA)

Differential thermal analysis (DTA) was conducted to evaluate the progress of the mechanical alloying/reaction in as-milled and combustion reacted powders using a simultaneous SDT 2960 analyzer under flowing argon at a rate of 150 ml/sec. The heating rate was set at 20 °C/min rate from room temperature to 1000 °C following by cooling to 200 °C.

Chapter 4

Powder Processing and Characterisation

4.1. Introduction

The solid state reactions between Al and TiO_2 have been studied widely over the past ten years [1, 2] The reactions consist of the reduction of TiO_2 by Al in an inert atmosphere to form dense, interpenetrating in-situ metal matrix composites (MMCs) and intermetallic matrix composites. The rate of reaction between TiO_2 and Al can be enhanced by reducing the size of initially milled powders using a ball mill or discus mill. Thus a combination of high energy mechanical milling and heat treatment or sintering can be used to produce in situ metal matrix composites (MMCs) and intermetallic matrix composite (IMCs) powders with favourable microstructure. These composites are considered as low price materials for high temperature applications. Self propagating high temperature synthesis (SHS) is also known as combustion synthesis or thermal explosion. This process has been [3] recognised as a very promising technique for materials processing at low cost. Zhang et.al [4] successfully used high energy mechanical milling and combustion reaction to produce a range of valuable TiO_2 and Al composites.

This chapter covers processing and characterisation of composite powders produced by the high energy milling of a mixture of Al and TiO_2 powders (using two different molar ratios) followed by a thermal reaction process. Powder characterisation was carried out because an understanding of the changes that occur from powder to coating as a result of thermal spraying are important. Moreover, coating performance is strongly dependent on the coating microstructure, which in turn is dependent on the characteristics of the starting powder from which the coating is formed. Although the coating microstructure is often very different to that of the powder, due to processes that occur during spraying and rapid solidification of the splats, the characteristics of

the powder feedstock have a strong influence on the coating microstructures so they should be characterised very carefully.

4.2. Production of Al/TiO_2 composite powders

The powders studied had two compositions:

Powder A: The Al/ TiO_2 ratio was determined according to reaction:

$$3TiO_2 + 4Al \longrightarrow 3Ti(Al,O) + 2Al_2O_3 \quad \text{Eq. 4.1}$$

Powder B: The Al/ TiO_2 ratio was determined according to reaction:

$$3TiO_2 + 7Al \longrightarrow 3TiAl(O) + 2Al_2O_3 \quad \text{Eq. 4.2}$$

The reaction products in the above are not pure Ti and TiAl intermetallic compound. The Ti phase usually contains some aluminium and oxygen in solid solution, while the TiAl phase has certain amount of oxygen interstitial.

To produce the composite powders a high degree of intermixing between the Al and TiO_2 starting materials is necessary. The degree of intermixing is largely dependent upon the milling parameters such as milling time and disc to powder weight ratio (DPR). The effect of milling time and the powder charge and their effects on the microstructure evaluation using a discus mill was reported by Liu et.al [5]. The study showed that longer milling times and smaller starting powder charges, gives more homogenous mixing and a finer microstructure. It is further reported that the reaction between TiO_2 and Al during subsequent heat-treatment is influenced by the milling condition. Liu et.al [6] further studied the effect of self sustained reactions in an TiO_2/Al composite powder (eq.4.1) produced by high energy mechanical milling. It is reported that a fine homogenous TiO_2/Al composite structure produced by a longer milling time resulted in fine/equilibrium phases after the reaction. The previous studies suggested that a time of six hours milling with 1% of PCA (process control agent) is sufficient to produce a homogenous intermixed TiO_2/Al composite powder (eq.4.1) and a subsequent fine combustion reacted powder.

The effect of various milling times on the degree of intermixing of Al and TiO_2 using powder A (Eq. 4.1) was also investigated in a separate study [7,8]. The study reported

a reaction between as-milled powders after six hours milling and suggested a milling time of four hours with 3% of PCA is sufficient to produce a homogenously intermixed TiO_2/Al composite powder. However, a reaction between the milled powders is not reported in previous studies by Liu et.al [5,6]. Based on previous results it looks as though an increased amount of PCA has a significant effect by increasing the degree of intermixing. A previous study did not involve an optimisation of milling conditions for TiO_2/Al powders based on eq.4.2. Therefore the current study selected four hours of milling time and 3wt% PCA to produce the composite powders.

Further, the effect of disc to powder weight ratio (DPR) using three different milling intensities (larger discs, smaller discs and steel balls) was investigated on the degree of intermixing using 300 g of powder A (Eq. 4.1) consisting of Al and TiO_2 starting powders with a molar ratio of 3:4. The optimised results of this study was used to produce Powder A and powder B using 500 g of an initially charged mixture of TiO_2 and Al with molar ratios of 3:4 and 3:7 respectively.

As-milled Al/TiO_2 composite powders, which were produced by using molar ratios of 3:4 and 3:7 using high energy milling, were thermally reacted by a self propagating high temperature synthesis (SHS) to produce Ti(Al,O)/A_2O_3 and TiAl(O)/Al_2O_3 based feedstocks for thermal spraying.

4.3. Results and discussion

4.3.1. Powder characteristics

The powder characterisations in the current study are based on the evaluation of the degree of intermixing of the starting powders to produce composite powders, chemical and phase compositional analysis (SEM, EDAX XRD analysis), thermal behaviour of the composite powders (DTA analysis), morphological studies of the combustion reacted powders or feedstocks and evaluation of their flowability for thermal spraying.

4.3.2. As-milled powder characterisations

4.3.2a Powder A

Figure 4.1 shows a comparison of the shapes and microstructures of the powder particles in the as-milled powders with the three different DPRs.

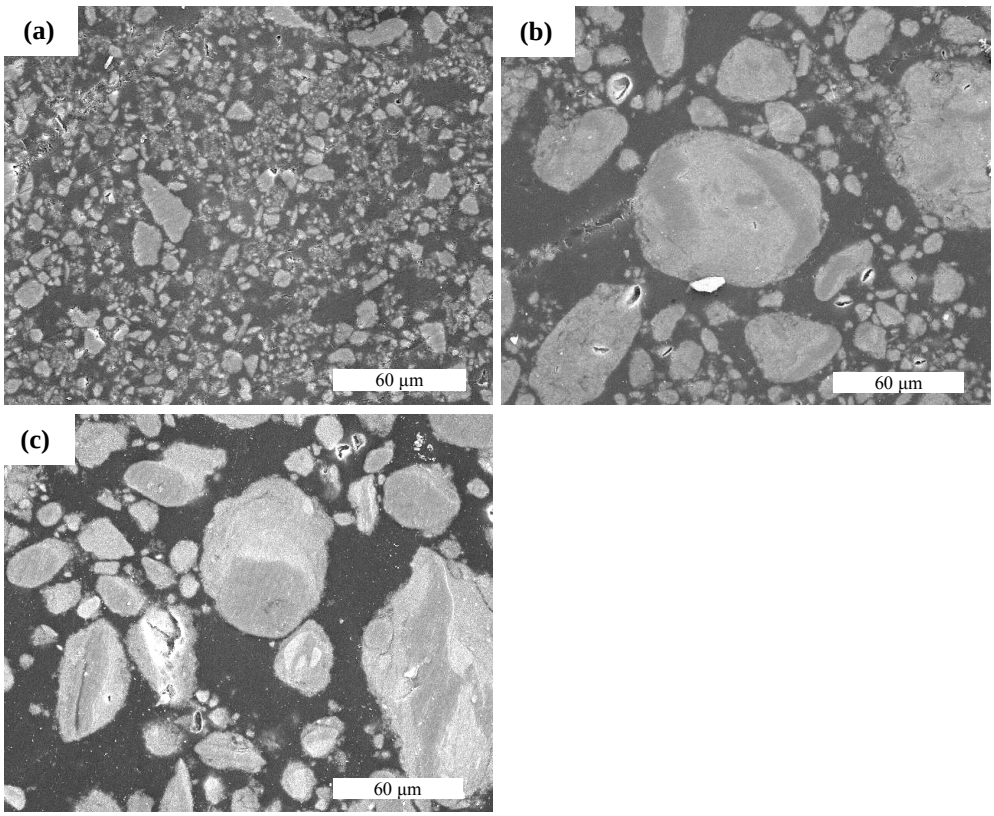

Figure 4.1: SEM micrographs of mechanically milled composite powder A (produced using 300 g mixture of TiO_2 and Al) after 4 hour milling with disc to powder weight ratios (DPRs) of (a) 22:1 (b) 13:1 (c) 4.5:1

It is clear that the powder made with disc to powder weight ratio (DPR) of 22:1 (using larger discs) exhibited a high level of mechanical mixing with a refined particle size(Fig. 4.1a). Powder with a DPR ratio of 13:1 (using smaller disc) also resulted mechanically well mix powder with a fine particle size; however some big and not very well mixed particles were also observed (fig. 4.1b). Powder made with a lower ratio of 4.5:1 (fig. 4.1c) by using steel balls showed little mixing with a coarse particle size, which means that this ratio is not enough to develop a good level of mixing between the two powders. At least two samples of each DRP were used for Energy dispersive X-ray analysis (EDAX) to examine the composition and homogeneity of

the powder after discus milling. The phase constituents were examined using X-ray diffraction analysis (XRD).

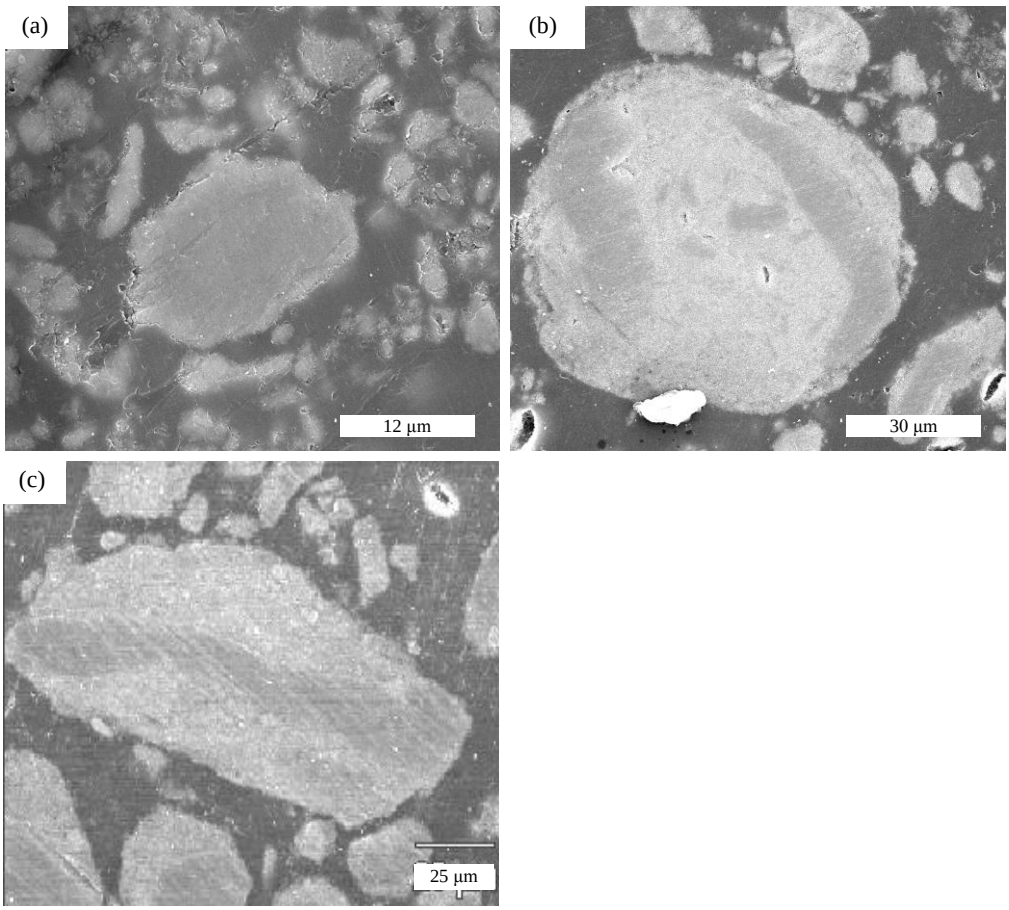

Figure 4.2: SEM micrographs of mechanically milled composite powder A (produced using 300 g mixture of TiO_2 and Al) particles after 4 hour milling with disc to powder weight ratios (DPRs) (a) 22:1, (b) 13:1 and (c) 4.5:1

Figure 4.2 shows the degree of homogeneity of the composite powder particles produced with disc to powder weight ratios (DPRs) 22:1, 13:1 and 4.5:1 The results show that with increased disc to powder weight ratio (DPR) to 22:1 (fig. 4.2a) there is good mixing between Al and TiO_2 and boundaries between TiO_2 and Al can not be clearly seen. The composite powders which were milled with DPRs 13:1 and 4.5:1 are more inhomogeneous with dark and bright phases within the particles (fig. 4.2b, c). The EDAX analysis of the dark and bright phases showed that the darker area mainly contains aluminium and the lighter area contains Ti, Al and a high concentration of oxygen.

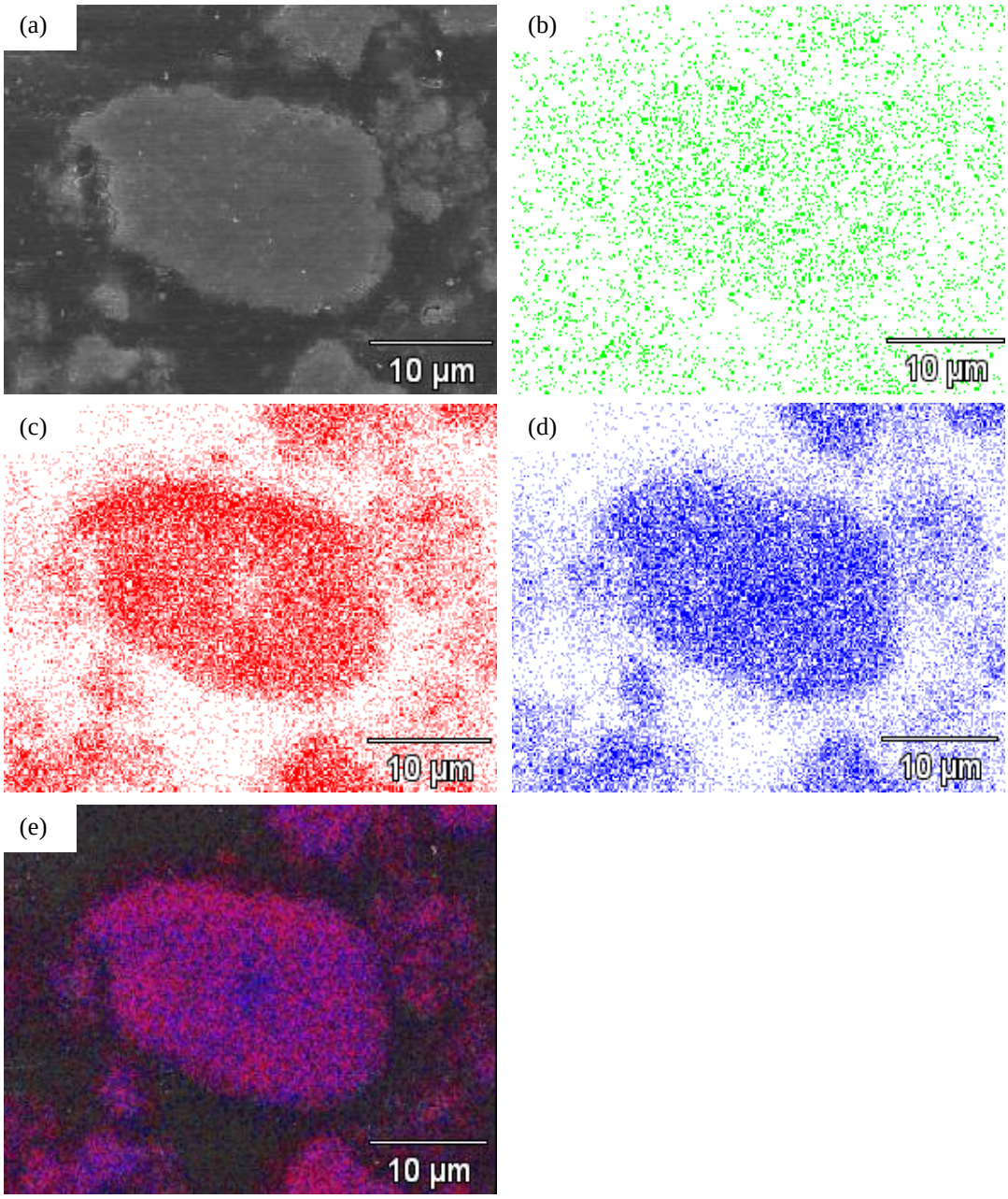

Figure 4.3: (a) SEM micrograph of powder A (produced using a 300 g mixture of TiO_2 and Al) and elemental maps of (b) oxygen (c) aluminium, (d) titanium and (e) titanium and aluminium overlay on powder A prepared with a with DPR of 22:1

The degree of homogeneity of composite powders milled with DPRs 22:1 and 4.5:1 is further confirmed by the elemental mapping of Al, Ti and oxygen within the particles (fig. 4.3 and fig. 4.4). The composite powder which was milled DPR 22:1 clearly shows a higher degree of homogeneity. The as milled powder with DPR 4.5:1 shows that the milling intensity using steel balls is not enough to produce composite powder structure. However, the elemental maps of as milled powders with DPR 13:1 showed

mostly a composite structure within the particles; however a few areas within the particles were also observed where the aluminium distribution was in-homogenous.

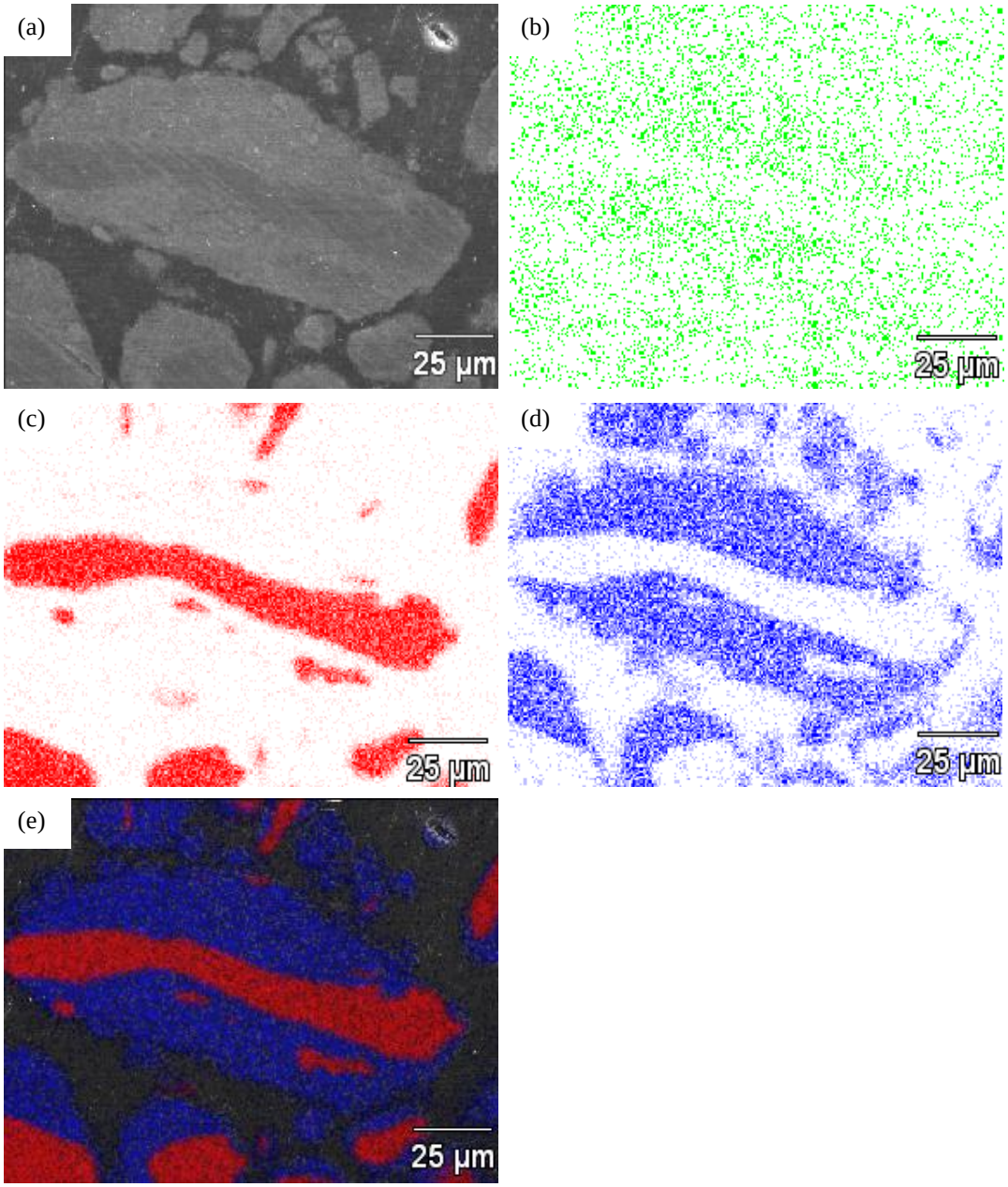

Figure 4.4: (a) SEM micrograph of powder A(produced using 300 g mixture of TiO_2 and Al) and elemental maps of (b) oxygen (c) aluminium (d) titanium and (e) titanium and aluminium overlay on powder A prepared with a DPR of 4.5:1

Figure 4.5 shows the XRD spectra of the as-milled powders (Al and TiO_2) with three different DPRs. The results show that no chemical reaction has occurred between the Al and TiO_2 after 4 hours milling.

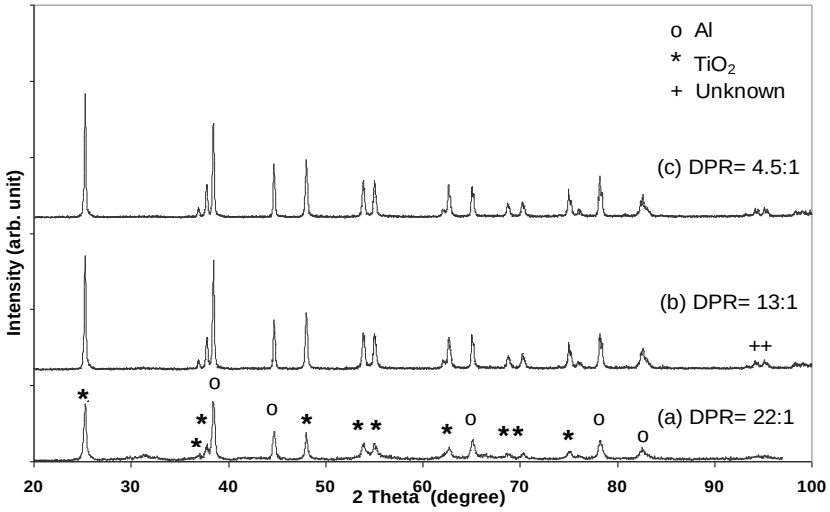

Figure 4.5: XRD patterns of as-milled composite powder A (produced using 300 g mixture of TiO_2 and Al) with DPRs of (a) 22:1(b) 13:1(c) 4.5:1

A large disc to powder weight ratio (DPR) imparts more impact energy to the powder, which in turn causes more internal energy/internal strain and a finer grain size. This was confirmed by the broadened and overlapped peaks observed in XRD patterns obtained from the samples milled with different DPRs as shown in fig. 4.5. The only phases shown by the XRD pattern were Al and TiO_2 phases, suggesting that the chemical reaction between Al and TiO_2 did not occur to any significant extent during milling. The XRD patterns of the as-milled powder also showed some unknown peaks of very low intensity and these peaks are most likely from the impurities in the starting powders. Similar peaks were also reported as unknown in an earlier study [8] using a similar powder composition.

The effect on the degree of intermixing when milling a larger amount of powder was also investigated. The degree of intermixing was evaluated for 500 g of as-milled powder (using larger discs) with disc to powder weight ratio of 13.2:1 and a milling time of four hours. The results (fig. 4.6) show that the increased amount of powder from 300 g to 500 g, there was not a significant difference in the degree of intermixing of Al and TiO_2, only a few particles showed a low level of mixing but generally the powder remained homogenous. An XRD pattern (fig. 4.7) from a sample of the 500 g batch of as-milled powder after 4 hours milling time using a DPR of 13.2:1, is the same as that for the 300 g of powder (fig. 4.5a). This also indicates that the increased amount of powder does not significantly affect the phase constituents of

the as-milled powder A. The as-milled powder A had a mean particle size of 14.4 µm and a particle size range of 1 µm to 100 µm.

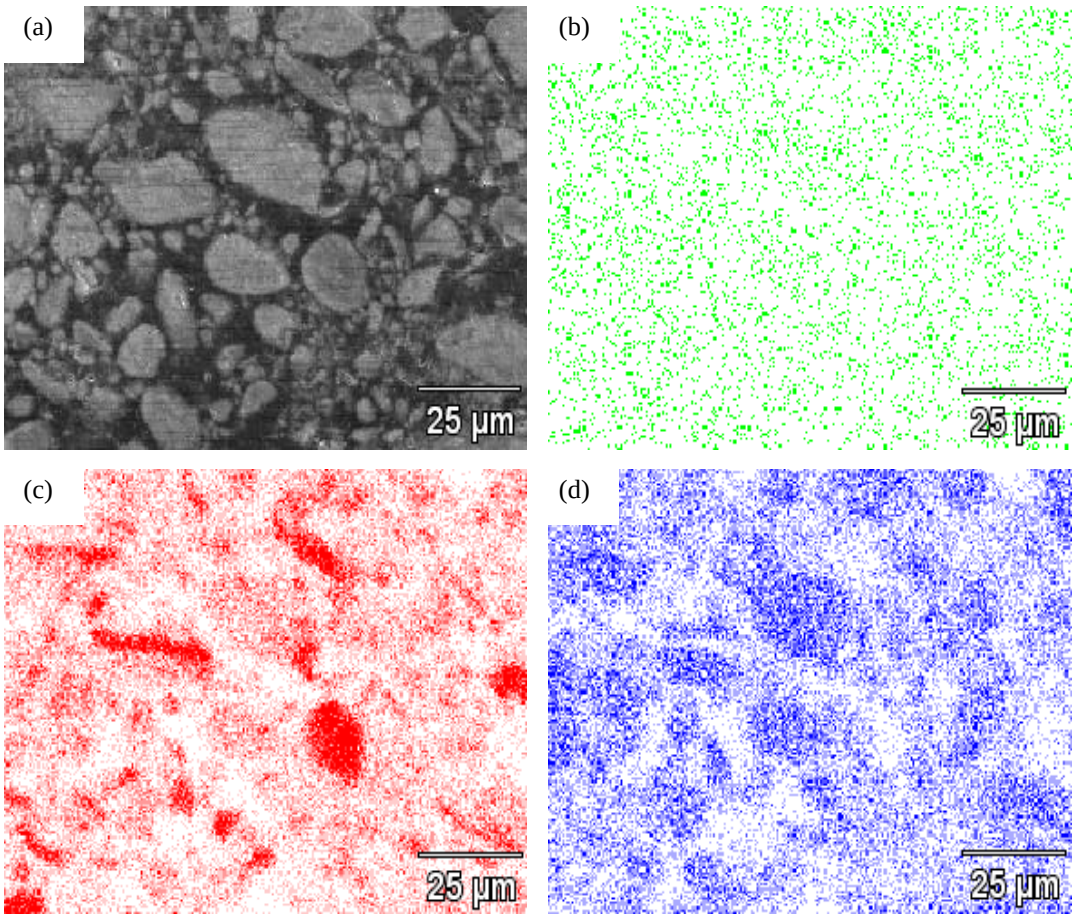

Figure 4.6: (a) SEM micrograph of mechanically milled composite powder A (produced using 500 g mixture of TiO_2 and Al) after 4 hour milling with a DPR of 13.2:1 with elemental maps of (b) oxygen (c) aluminium and (d) titanium

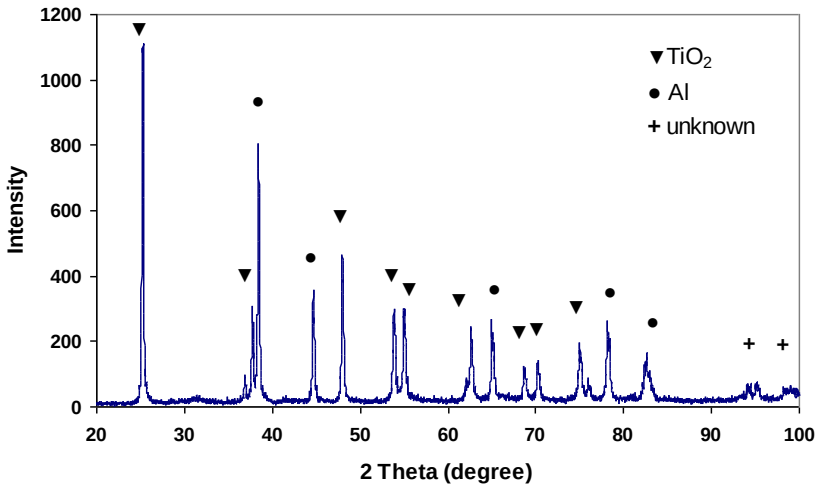

Figure 4.7: XRD pattern of as-milled composite powder A (produced using 500 g mixture of TiO_2 and Al) with DPR 13.2:1 after 4 hours of milling

4.3.2b Powder B

Based on the investigations already described, on the effect of various milling times and milling intensities (DPRs) on the degree of intermixing of Al and TiO_2 using powder A, four hours of milling time and DPR 13.2:1 (larger discs size) were selected to produce 500 g of powder B.

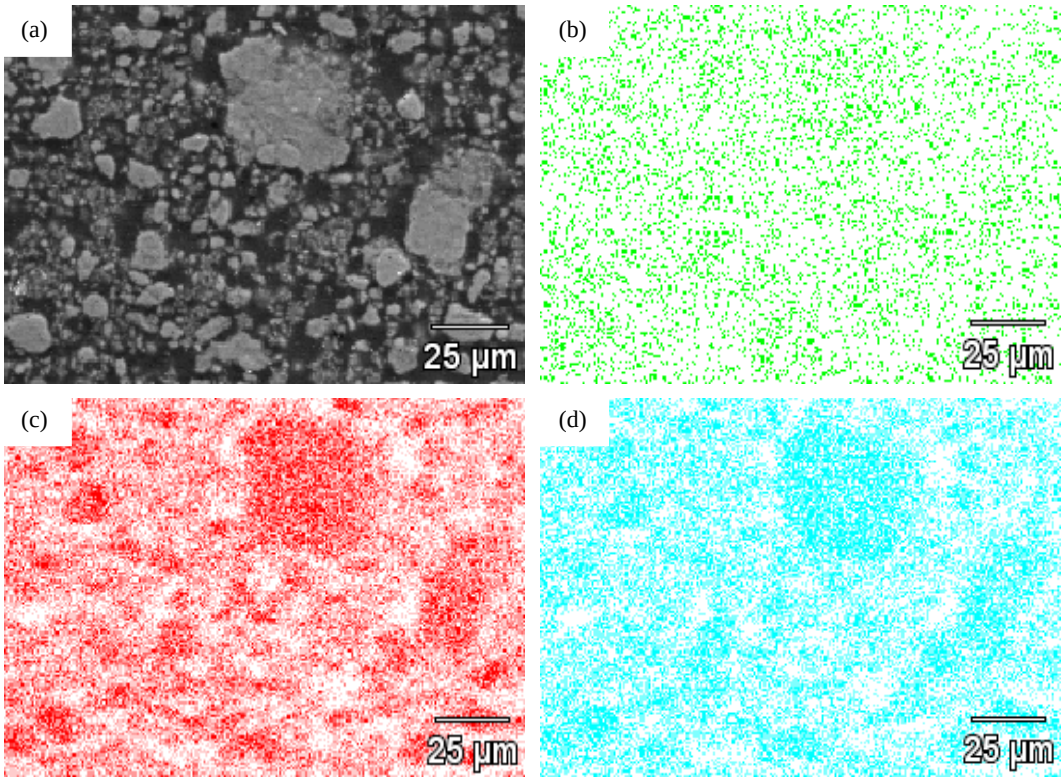

Figure 4.8: (a) SEM micrograph of mechanically milled composite powder B (produced using a 500 g mixture of TiO_2 and Al) after 4 hours milling with a DPR of 13.2:1 with elemental maps of (b) oxygen, (c) aluminium and (d) titanium

Figure 4.8 shows a micrograph (fig. 4.8a) of the cross section of powder B produced after 4 hour discus milling with a DPR of 13.2:1 along with the elemental maps of oxygen, aluminium and titanium (figs. 4.8 b, c, d). The as-milled powder exhibited a high level of intermixing and fine particle size after 4 hours milling. However some larger but well mixed particles were also present in the as-milled powder B. Figure 4.9 shows that the larger particles in the composite powder are the result of agglomeration of fine particles. The composite structure of the powder particles is homogenous and the boundary between Al and TiO_2 can not be seen clearly. The as-

milled powder B had a mean particle size of 19 µm and a particle size range of 1µm to 700 µm. The larger size is most likely recorded as a result of agglomeration.

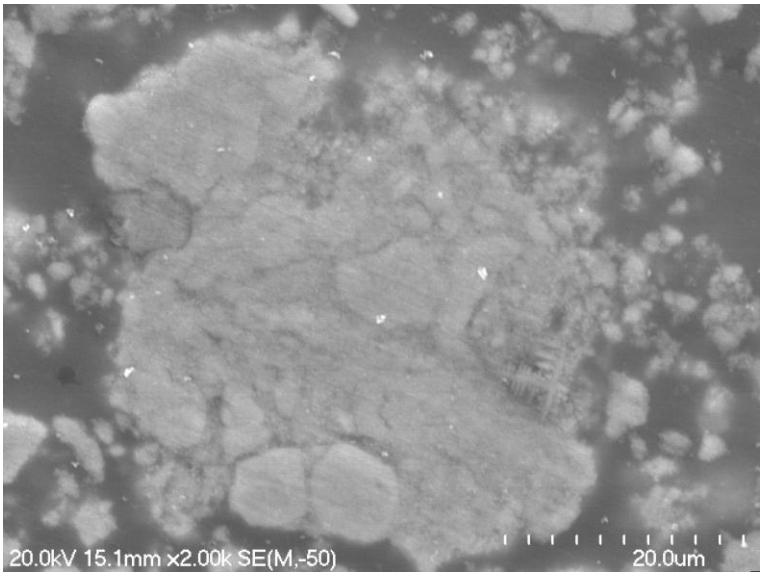

Figure 4.9: SEM micrograph of mechanically milled composite powder B after 4 hour milling with DPR 13.2:1

Figure 4.10 shows the XRD pattern of the powder B after four hours milling time with a DPR of 13.2:1. The only phases observed in the XRD were Al and TiO_2 this suggests that after 4 hours milling no chemical reaction has occurred between Al and TiO_2. EDAX analysis shows that the particles mainly contain Al, Ti and O.

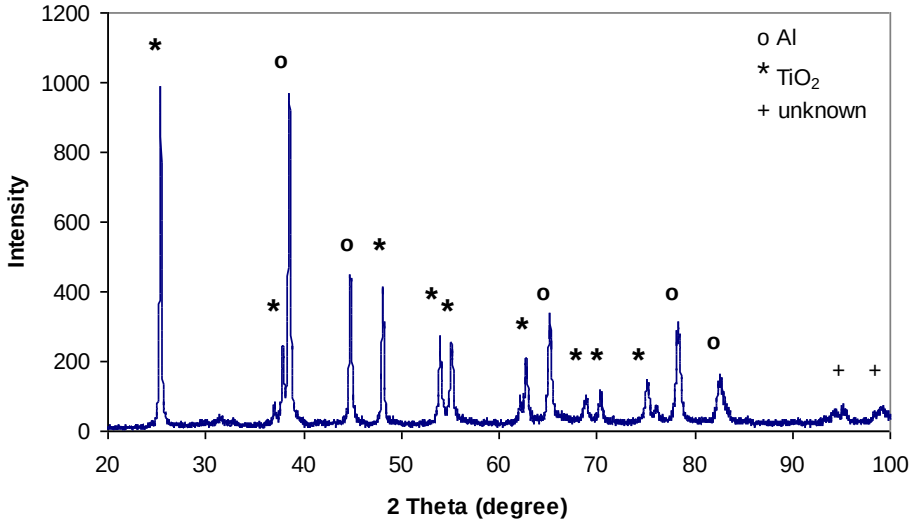

Figure 4.10: XRD pattern of as-milled composite powder B (produced using 500 g mixture of TiO_2 and Al) after four hour milling time with DPR 13.2:1

4.3.3. Thermal analysis of the as-milled powders

4.3.3a Powder A

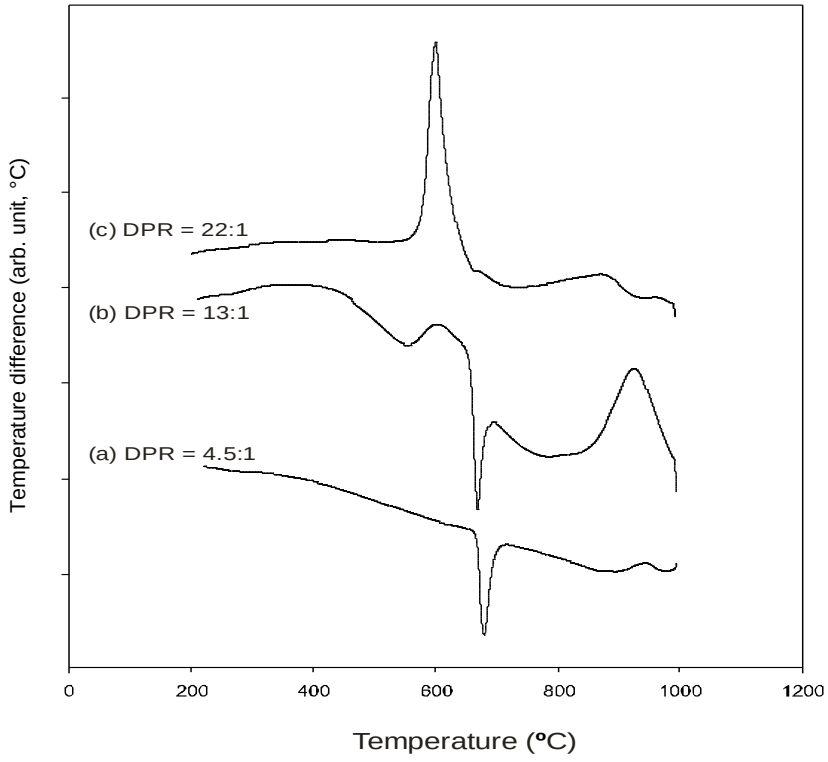

Figure 4.11: DTA traces of as-milled powder A (produced using a 300 g mixture of TiO_2 and Al) with DPRs of (a) 4.5:1(b) 13:1(c) 22:1

The DTA traces of the as-milled powder produced using DPRs of 13:1 and 4.5:1 showed an endothermic peak with a peak temperature of about 665 ºC (fig. 4.11). The position of the peak suggests that it is caused by Al melting, with the higher DPR of 13:1 showing a slightly lower melting temperature. The DTA traces also show exothermic peaks. Their intensity and position depends upon the DPR. In the case of a DPR of 22:1, two exothermic peaks are observed. The first exothermic peak is stronger with an onset temperature of about 560 °C and with a peak temperature of about 602 ºC, while the second peak becomes weaker with an onset temperature of about 765 °C with peak temperature 880 °C. The first exothermic peak at about 602ºC in this study is much lower than the one reported by Liu et al. [6] and Zhang et al. [4]. The lowering of first exothermic peak in this study is due to the increased level of mixing between the starting powder mixture (amount of charged powder was only 300gm). However the peak values (onset temp and peak temp.) were found to be

similar to those from another study by Whelham [1]. The homogeneity of the elements/starting powder is the most important factor in the enhancement of the reaction. A further, lowering of the temperature mainly resulted because of an increase in interfacial area and shortening of diffusional path length between the starting powders. In the case of 13:1, the first exothermic peak is weaker with an onset temperature 563 °C with a peak temperature 604 °C while the second peak in stronger with an onset temperature of about 833 ºC and a peak temperature of about 930 °C. In the case of 4.5:1, the only exothermic peak was found at an onset temperature of about 903 ºC. As the milling intensity increases, there is a peak shift from 903 ºC to 765 °C for the second exothermic peak.

Previous work from Ying et al. [2] has reported that no reaction occurs between mechanically milled Al and TiO_2 during heating at temperature 500 °C. At 700 °C the formation of Al_3Ti is reported suggesting that the first exothermic event in the DTA traces (fig. 4.11) is due the reaction between Al and TiO_2, forming Al_3Ti. The reaction between Al_3Ti and TiO_2 is reported to complete from 1000 °C-1200 °C with the formation Al_2O_3, Ti rich phase, Ti_3Al and TiO suggesting that the second exothermic reaction in DTA traces is due to the formation of these phases. Ying et.al [2] reported that the formation of TiO is likely caused by the surface oxidation of Ti- rich metallic phases during heating at higher temperature.

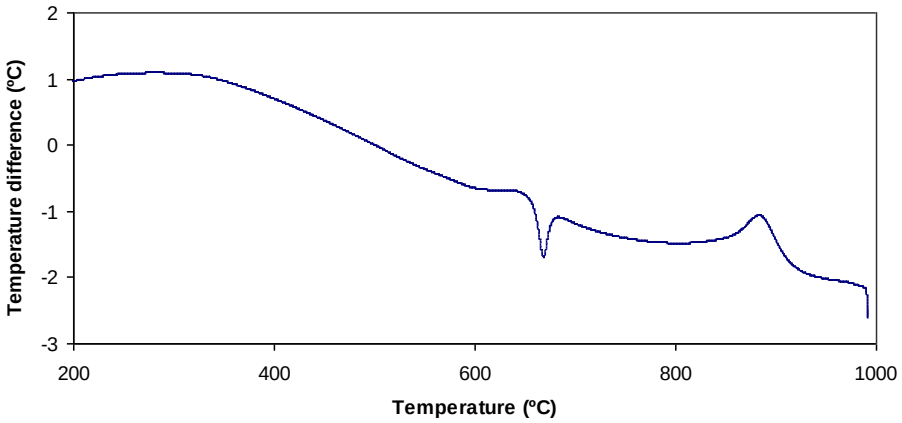

Figure 4.12: DTA traces of as-milled powder A (produced using 500 g mixture of TiO_2 and Al) after four hours of milling with DPR 13.2:1

Increasing the amount of milled powder A from 300 g to 500 g brings a change in the DTA curve of powder A milled with a DPR of 13.2:1 (fig. 4.12). This shows the

appearance of an endothermic peak at a temperature of about 670 ºC and two similar exothermic peaks with different intensities and positions compared with the DTA curve for 300 g of milled powder A with a DPR of 22:1 (fig. 4.11c). The position of the endothermic peak at 670 ºC suggests that it is caused by the melting of aluminium. The first exothermic peak with an onset at about 609 ºC is relatively weak. This is overlapped by a strong endothermic peak. The second exothermic peak is stronger with an onset of about 831 ºC and a peak temperature of about 888 ºC. The first exothermic reaction is caused by the formation of Al_3Ti as a result of a reaction between TiO_2 and Al while the second exothermic reaction is caused by a reaction between Al_3Ti and TiO_2 forming Al_2O_3 , Ti rich phases, Ti_3Al and TiO.

4.3.3b Powder B

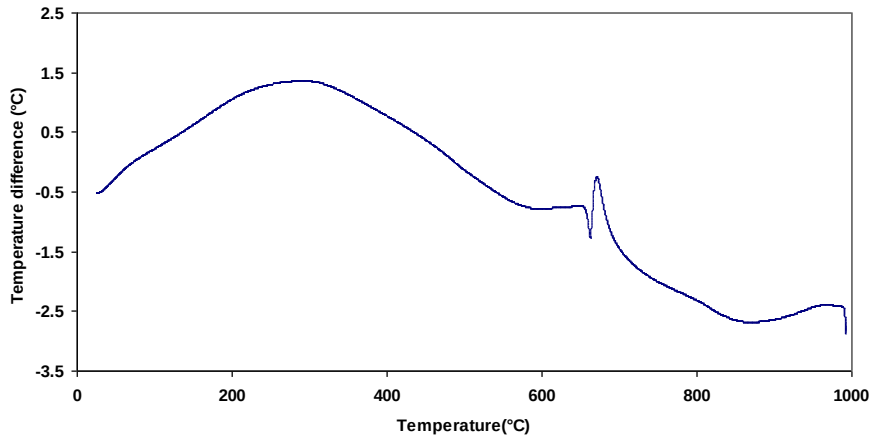

Figure 4.13: DTA traces of as-milled powder B (produced using 500 g mixture of TiO_2 and Al) after 4 hours milling with DPR 13.2:1

Figure 4.13 shows the DTA trace of the powder B after four hours milling with DPR 13.2:1. The DTA curve shows an endothermic peak with a peak temperature about 663 °C. The position of the endothermic peak suggests that it is caused by the melting of aluminium. An exothermic peak with an onset temperature of about 600 °C and a peak temperature of about 673 °C is overlapped with the endothermic peak. Kamali et al. [9] also reported an exothermic peak at 693 °C in the DTA trace of powder ball milled for 5 hours, with the formation of TiAl-Al_2O_3 as a result of single step reaction. This suggests that the exothermic peak in the DTA trace of powder B is due to the formation TiAl and Al_2O_3 phases.

The above thermal analyses are very useful in describing the nature of reactions/phases resulting during controlled/ uniform heating of the as-milled powders. In this study, a self-propagating high temperature synthesis (SHS)/ combustion reaction is used to react the as-milled powders which involves uncontrolled heating. In this case, the above discussed DTA curves (under controlled powder heating) will not be suitable to depict the nature of the various phases formed in combustion reacted powder. However, this study is helpful for understanding powder behaviour under controlled heating.

4.3.4. Characterisation of the combustion reacted powders

4.3.4a Powder A

Figure 4.14 shows the cross sections of the combustion reacted powder particles which were produced from 300 g of as-milled powder after 4 hours milling using DPRs 22:1 and 13:1. The batch milled with a DPR of 4.5:1 failed to react due to poor mixing between Al and TiO_2 powders.

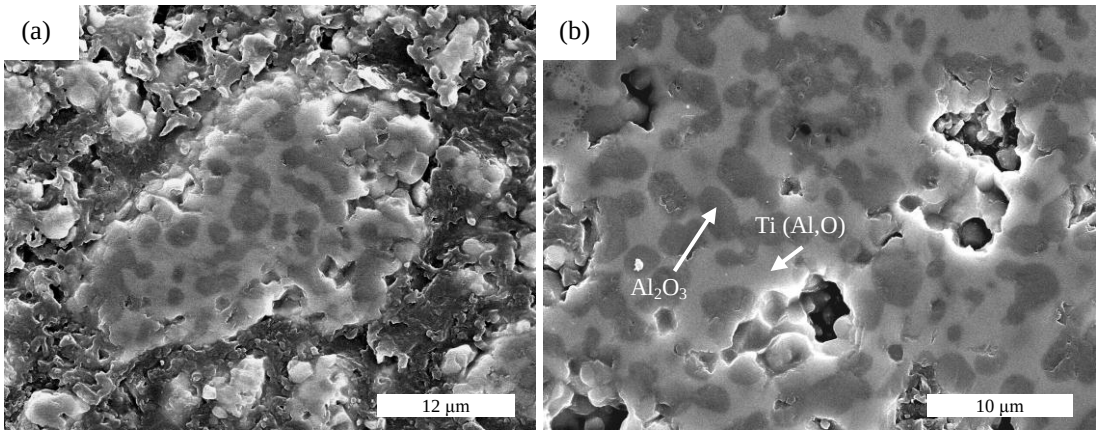

Figure 4.14: SEM micrographs of the combustion reacted composite powder A (produced using a 300 g mixture of TiO_2 and Al) after 4 hours milling with DPRs (a) 22:1 (b) 13:1

An XRD analysis (fig. 4.15) of the reacted powders with DPR 13:1 and 22:1 showed that there are three types of phases, a dominant Al_2O_3 phase, a Ti phase and TiO. This was further confirmed from EDAX analyses (table 4.1) which shows that the dark area contains a very high atomic percentage of oxygen and aluminium with considerable atomic percentage of titanium. It is therefore likely to contain oxide phases of Al_2O_3 and TiO. The atomic percentage of Ti in the dark area is higher in the case of a reacted powder produced with a DPR of 22:1 than one produced with a DPR

of 13:1. The increase in Ti concentration is most likely due to a higher level of intermixing in the powder with a DPR of 22:1. The darker phase revealed a particle size of 1-4 µm in both types of powders. The light area in these powders contains a high percentage of Ti with Al and oxygen. It is therefore likely to be Ti(Al,O), a Ti phase with dissolved Al and oxygen. It was also noted that these two major phases form a continuous and homogenous interpenetrating network throughout the feedstock powder. Based upon the XRD and EDAX analysis of the combustion reacted powders after milling with DPRs of 22:1 and 13:1, it was found that the powders consisted predominantly of the metallic phase Ti(Al,O) and a ceramic phase Al_2O_3 with some TiO.

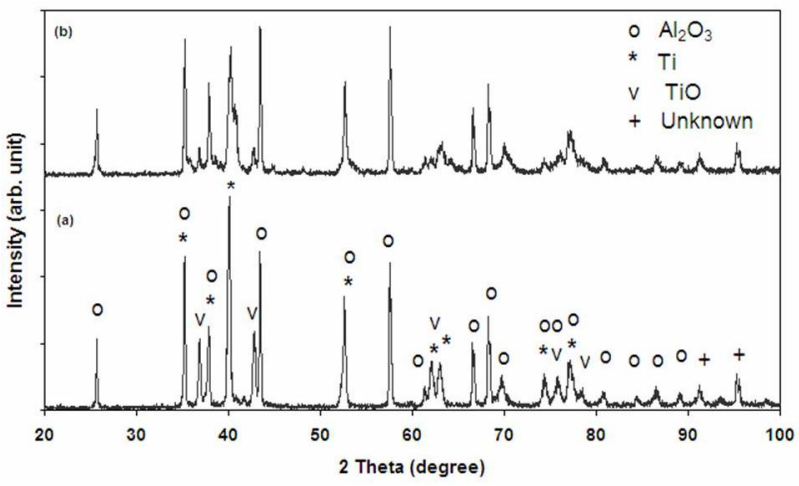

Figure 4.15: XRD patterns of combustion reacted powder A produced from 300 g of as milled powder with DPRs of (a) 22:1 (b) 13:1

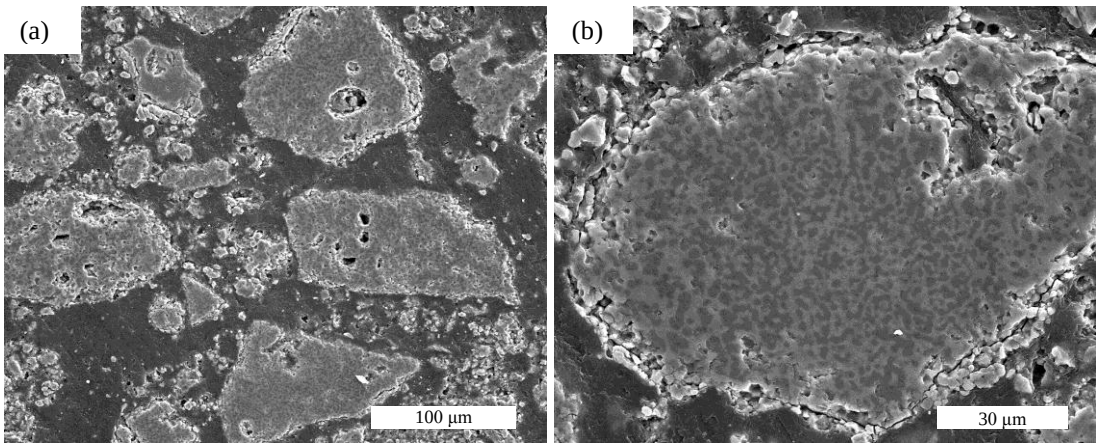

Figure 4.16: SEM micrographs of the cross section of the combustion reacted powder A produced from 500 g of as-milled powder with DPR 13.2:1 after 4 hours milling (a) multiple particles and (b) single particle

Figure 4.16 shows the combustion reacted powder A which was produced from 500 g of as-milled powder after four hours of milling with a DPR of 13.2:1. The combustion reacted powder has a continuous interpenetrating network of dark and bright phases with a similar composition to the 300 g batch milled powder. Moreover, a darker phase also revealed a particle size of 1-4 µm The XRD pattern (fig. 4.17) from combustion reacted powder A, produced from 500 g of as-milled powder with a DPR of 13.2:1, also confirmed the presence of Ti, Al_2O_3 and TiO phases. Based upon the XRD and EDAX analysis of the combustion reacted powders after milling with DPR 13.2:1, it was found that the powders consisted predominantly of the metallic phase Ti(Al,O) and a ceramic phase Al_2O_3 with some TiO.

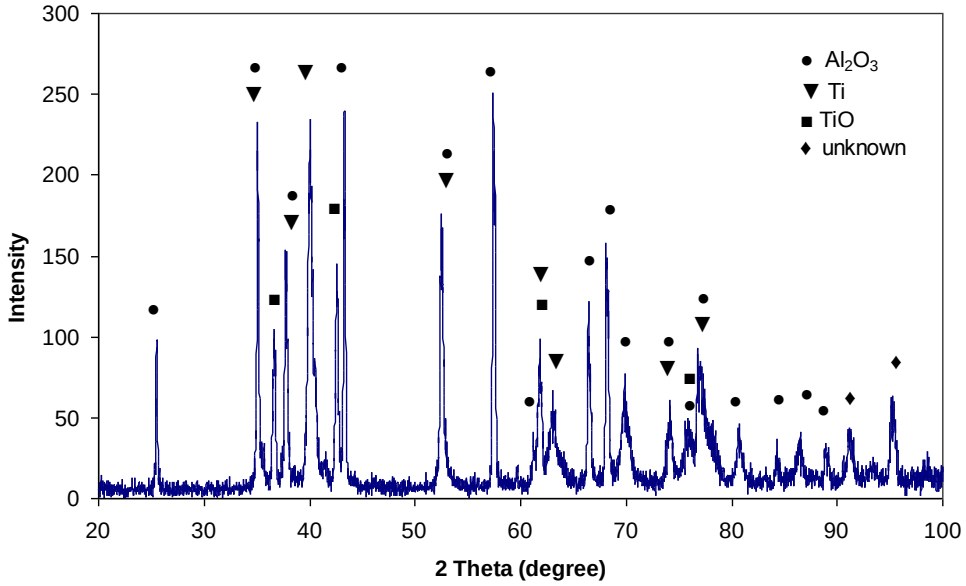

Figure 4.17: XRD pattern of combustion reacted powder A produced from 500 g of as-milled powder with DPR 13.2:1

This also confirms that an increase in the amount of as-milled powder A from 300 g to 500 g (DPR 13.2:1, 4 hrs milling) followed by a combustion reaction did not effect the types of phases formed.

4.3.4b Powder B

Figure 4.18 shows the SEM micrographs of the combustion reacted powder B particles with two dominant phases a brighter phase and a darker phase. Within the particles the darker and brighter phases are mostly interpenetrated expect for few regions where the brighter phase is continuous with few particles of the darker phase

and thus creating a non-homogenous structure. The non-homogenous structure is most likely due to a lesser degree of intermixing between the starting powders or due to processing temperature (SHS) conditions.

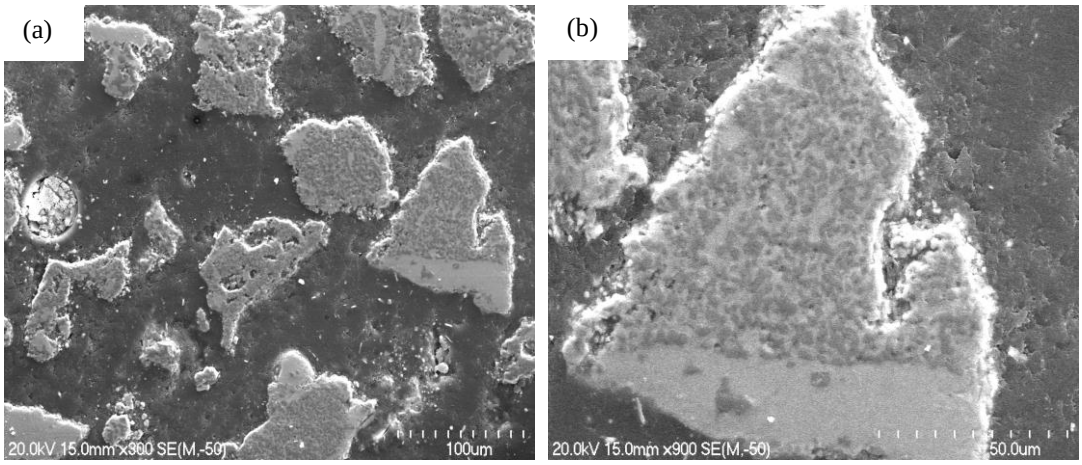

Figure 4.18: SEM micrographs of the cross section of the of combustion reacted powder B particles produced from 500 g of as-milled powder with DPR 13.2:1 after 4 hours milling (a) multiple particles and (b) single particle

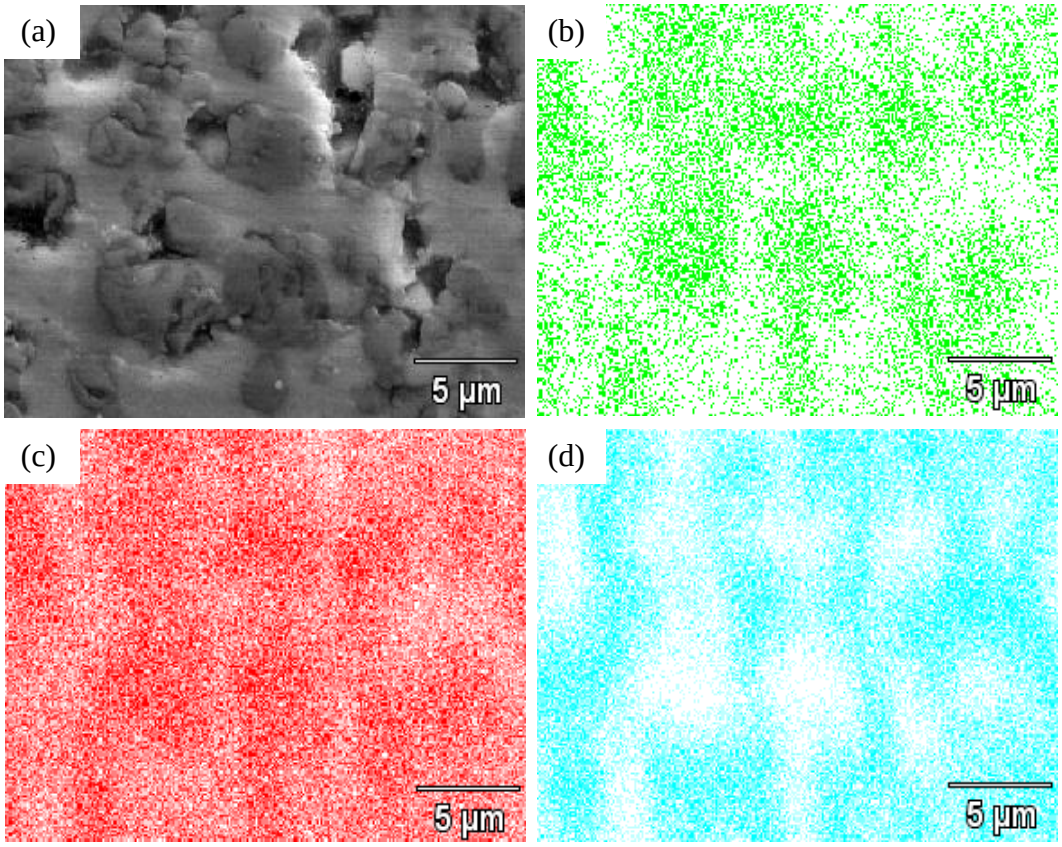

Figure 4.19: Elemental maps of combustion reacted powder B (a) SEM micrograph and elemental maps of (b) oxygen (c) aluminium and (d) titanium

The elemental maps (fig. 4.19) and EDAX analysis (fig. 4.20a) of the combustion reacted powder B show that the lighter phase had a high percentage of Ti and a low percentage of Al while the darker phase had a high percentage of aluminium and oxygen with a very low percentage of titanium. This suggests that the darker phase is Al_2O_3 and the lighter phase is a metallic phase consisting of titanium aluminide based intermetallic compounds. The darker phase also revealed a particle size of 1-4 µm

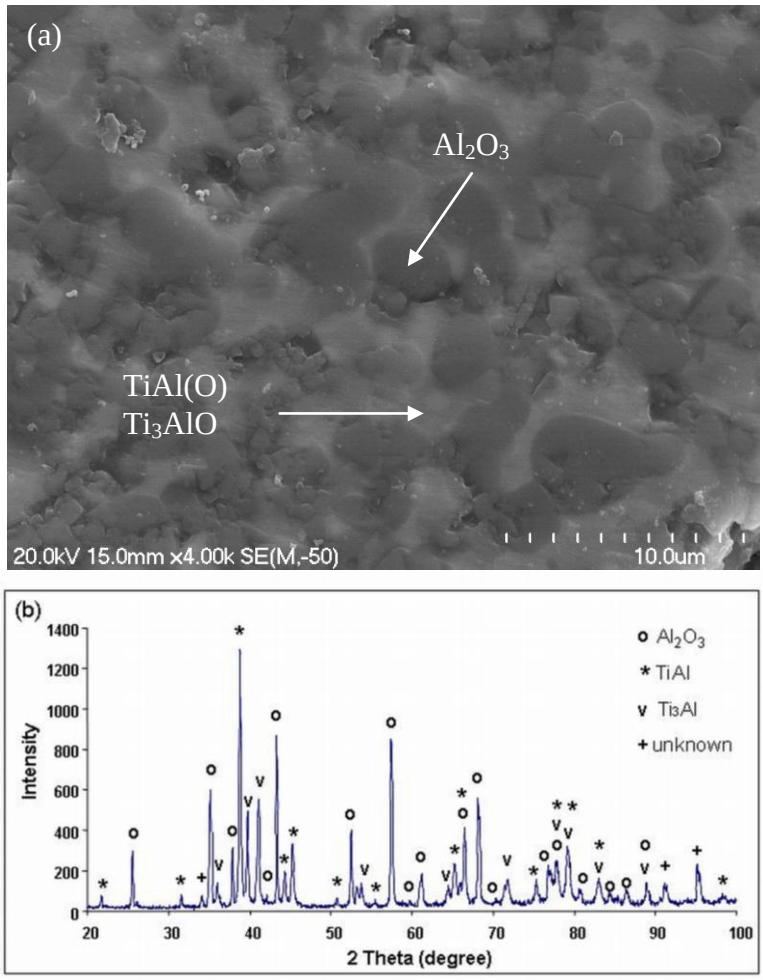

Figure 4.20: (a) SEM micrograph of the combustion reacted composite powder B and (b) an XRD pattern of the combustion reacted powder produced from 500 g of as-milled powder with a DPR of 13.2:1

The XRD analysis (fig. 4.20b) of the reacted powder shows that there are three types of phases in the structure, a dominant Al_2O_3 phase and metallic phases TiAl, and Ti_3Al. The formation of a Ti-rich aluminide (Ti_3Al) indicates that there was not enough Al for the formation of TiAl. This is possibly due to the loss of some Al, which sticks to the walls of the milling bowl (due to a lower amount of PCA), and

also due to some in- homogenous mixing between the starting powders after 4 hours milling time. Combing the XRD and of EDAX analysis results it is fairly certain that the lighter phase is metallic and consists of TiAl(O) and $Ti_3Al(O)$ whereas the darker area is Al_2O_3. EDAX analysis also confirmed that the lighter areas where the interpenetrating phase was absent (a non-homogenous structure) mainly consists of TiAl/Ti_3Al with low amount of oxygen (0.00at%-3.39at%).

Based on the EDAX analysis, the major phases present in each type of feedstock powders are tabulated in table 4.1. EDAX analysis tabulation is based on an average value of three readings for each phase. The standard deviation of the data was also taken into account.

Table 4.1: EDAX analysis of various phases of combustion reacted powders

Feed stock powder	As-milled powder weight (gm)	Disc to powder weight ratio (DPR)	Visible phases	Elements (At%)			Major phases present
				O	Al	Ti	
A	300	22:1 (larger discs)	Dark/particle	32.18 ± 2.89	37.38 ± 5.00	30.43 ± 7.89	Al_2O_3/TiO
			Light with O	24.50 ± 4.66	20.78 ± 10.69	54.69 ± 15.35	Ti(Al,O)/Ti(O)/Ti_3Al(O)
	300	13:1 (smaller discs)	Dark/particle	57.21 ± 3.27	23.66 ± 6.78	19.12 ± 4.23	Al_2O_3/TiO
			Light with O	29.45 ± 12.52	15.28 ± 7.86	55.26 ± 18.04	Ti(Al,O)/Ti_3Al(O)/Ti(O)
			Light with low O	3.47 ± 3.81	14.89 ± 0.74	81.63 ± 4.56	Ti_3Al(O)/Ti(O)
	500	13.2:1 (larger discs)	Dark/particle	59.82 ± 5.42	32.00 ± 4.84	8.18 ± 4.20	Al_2O_3/ TiO
			Light with O	23.49 ± 13.26	22.67 ± 0.88	53.84 ± 12.46	Ti(Al,O)/Ti_3Al(O)/Ti(O)
B	500	13.2:1 (larger discs)	Dark/particle	54.86 ± 0.40	44.29 ± 3.30	0.84 ± 2.14	Al_2O_3 with small amount of TiO
			Light with O	39.36 ± 5.67	38.75 ± 2.84	21.88 ± 3.21	TiAl (O)/Ti(O)
			Light with low O	0.00 ± 2.40	43.11 ± 1.28	56.88 ± 1.12	TiAl (O)/ Ti_3Al (O)

4.3.5. Thermal analysis of the combustion reacted powders

4.3.5a Powder A

Figure 4.21 shows that there is no peak after heating the powders up to 1000 °C, which is an indication that the combustion reaction was complete and there was no composite powder left un-reacted. A DTA trace of the combustion reacted powder produced from a 500 g batch of as-milled powder also gave a similar result, confirming that no powder was left un-reacted after the combustion reaction.

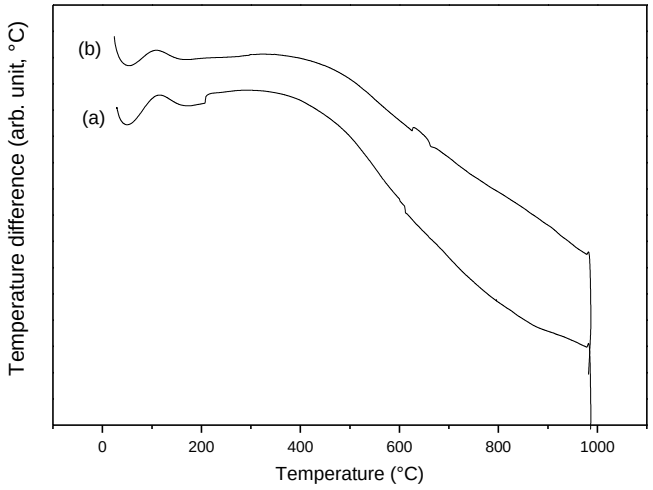

Figure 4.21: DTA traces of the combustion reacted powder A produced from 300 g of as-milled powder with DPRs of (a) 22:1 and (b) 13:1

4.3.5b Powder B

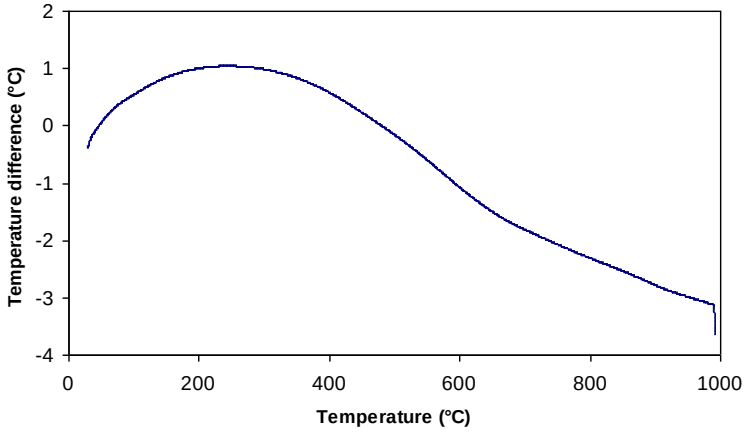

Figure 4.22: DTA traces of combustion reacted powder B produced from 500 g of as-milled powder with DPR 13.2:1 after 4 hours milling

Figure 4.22 shows the DTA traces of the combustion reacted powder B produced from 500 g of as-milled powder with a DPR of 13.2:1 after 4 hours milling. This result also confirmed that there is no peak after heating the powder up to 1000 °C, which is also an indication that the combustion reaction was complete and that there was no powder left un-reacted.

4.3.6. Morphology, size distribution and flowability of combustion reacted powders

4.3.6a Powder A

Figure 4.23: Macrograph of the combustion reacted powder A (produced from 500 g of as-milled powder with DPR 22:1) before ball milling

Figure 4.23 shows the macrograph of combustion reacted powder A (produced from 500 g of as-milled powder with DPR 13.2:1) before ball milling. These large lumps of powder were crushed by ball milling to prepare the feedstock for thermal spraying with good flowability. Figure 4.24 shows the SEM images of the particle morphology of the fine feed (< 75 µm) which resulted after 15 minutes of ball milling. Powder with this size and morphology was unable to flow through a flowmeter. The surface texture and shape of the particles is clear from the SEM images. In general particles are seen to be angular with rough surfaces which contributed towards the poor flowability. The particle size distributions of the fine feed was < 75 µm after 15 min of ball milling and the distributions in figure 4.25 show that the particle size ranged

from 0.9 µm to 125 µm. The median particle diameter of the fine feed is about 30.9 µm. The fine feed comprises about 90% of the particles with a size less than 72 µm and 10% of the particles are less than 10 µm. The very fine particles of less than 10 µm were largely responsible for the poor flowability of this feedstock powder.

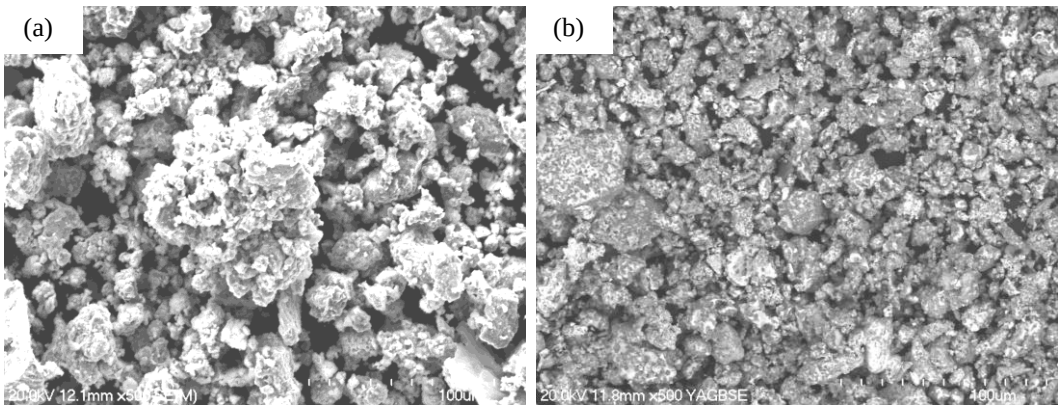

Figure 4.24: Particle morphology of combustion reacted ball milled powder A (produced from 500 g of as-milled powder with DPR 13.2:1) with fine feed (< 75 µm) (a) SEM micrograph (b) Back scattered image

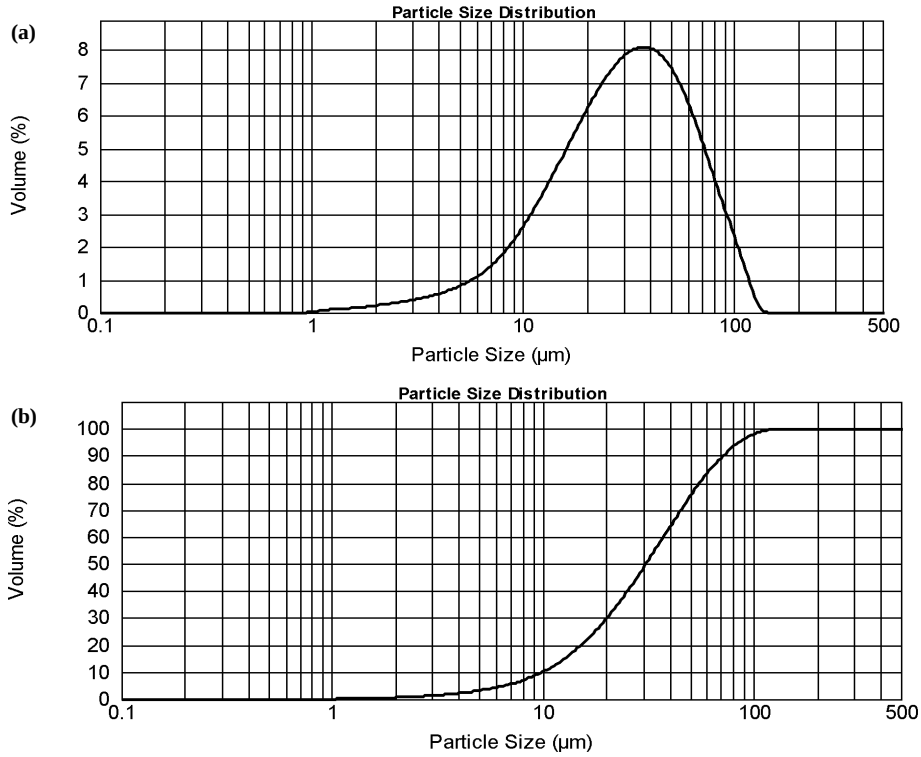

Figure 4.25: Particle size distributions (a) frequency (b) cumulative of powder A fine feed < 75 µm after 15 min ball milling

Figure 4.26 shows the SEM back scattered micrograph of the particle morphology of the fine feed < 75 µm after agglomeration and sieving to < 106 µm. Agglomeration resulted in an increase in the effective size of the particles. The fine angular particles before agglomeration (fig. 4.24) were turned into nearly spherical particles which improved their flowability. Due to the use of a water soluble binder PVA (polyvinyl alcohol) for agglomeration, it was not possible to determine the particle size of this feed using a size analyzer.

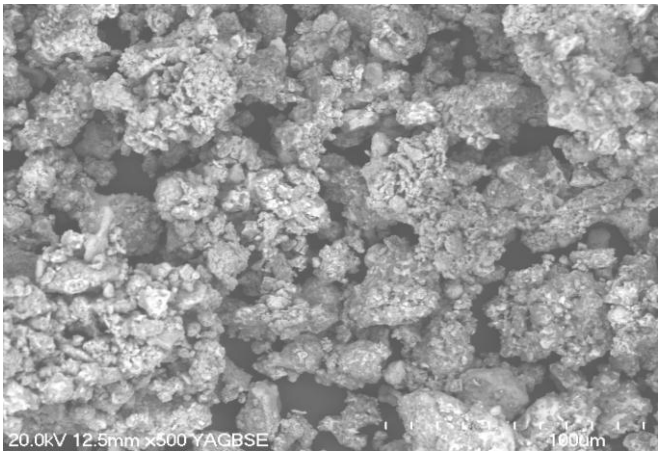

Figure 4.26: Particle morphology of combustion reacted powder A fine feed (< 75 µm) after agglomeration with 2%PVA and sieving to < 106 µm

Figure 4.27 shows the particle morphology of the combustion reacted and ball milled coarse feed (125 µm > size > 75 µm) after 15 min milling. This had good flowability. The coarse feed consists of two types of particles, irregularly shaped and with smooth surfaces while the others are irregularly shaped with rough surfaces.

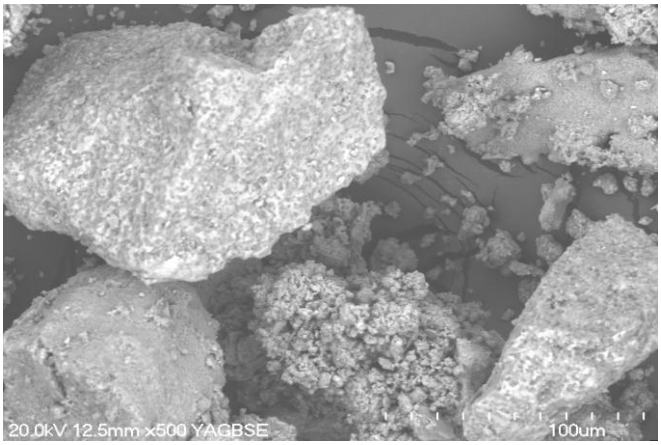

Figure 4.27: Particle morphology of combustion reacted powder A coarse feed (125 µm > size > 75 µm) after 15 min ball milling

Figure 4.28 shows the particle size distributions of the coarse feed (125 µm > size > 75 µm) after 15 min of ball milling. The very fine particles are in the range of about 0.98 µm to 6.0 µm while the coarse particles are in the range of 52 µm to 198 µm. The median particle diameter of the coarse feed is about 119 µm. The coarse feed mainly consists of about 90% of the particles less than 172 µm and 10% of the particles less than about 82 µm. The fine particles within the coarse feed might have resulted from the separation of fine particles which were entrapped within the rough particles surfaces.

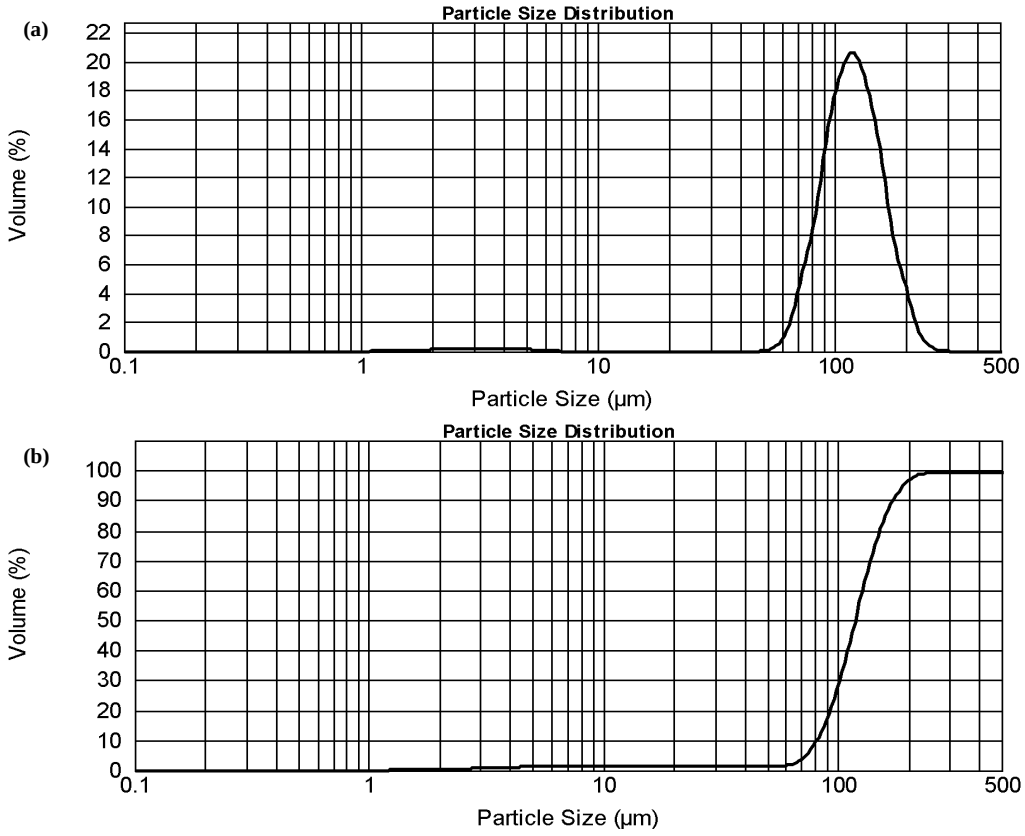

Figure 4.28: Particles size distributions (a) frequency and (b) cumulative of powder A coarse feed 125 µm > size > 75 µm after 15 min ball milling

Figure 4.29 shows the morphology of the combustion reacted powder A (feedstock) for thermal spraying which had good flowability. The feedstock largely consists of fine agglomerated particles with rough surfaces along with coarse particles with smooth or rough surfaces. The feedstock powder size range could not be measured using a particle size analyzer because the binder used to agglomerate the powder is water soluble. However SEM analysis (fig.4.30) indicates that the size range of powder is generally less than 50 µm with a few particles between 50 µm and 100 µm.

The average flowability of the powder A feedstock based on ASTM standard B213-03 [10] was 50 g/109 s.

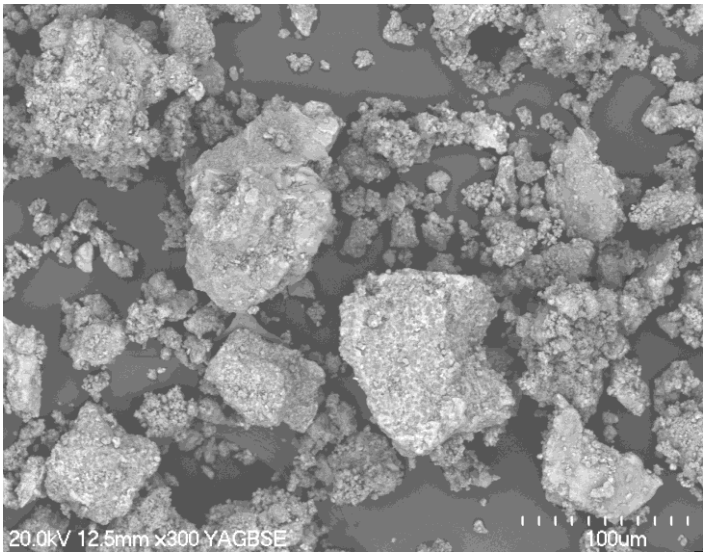

Figure 4.29: Particle morphology of combustion reacted powder A (feedstock) for thermal spraying

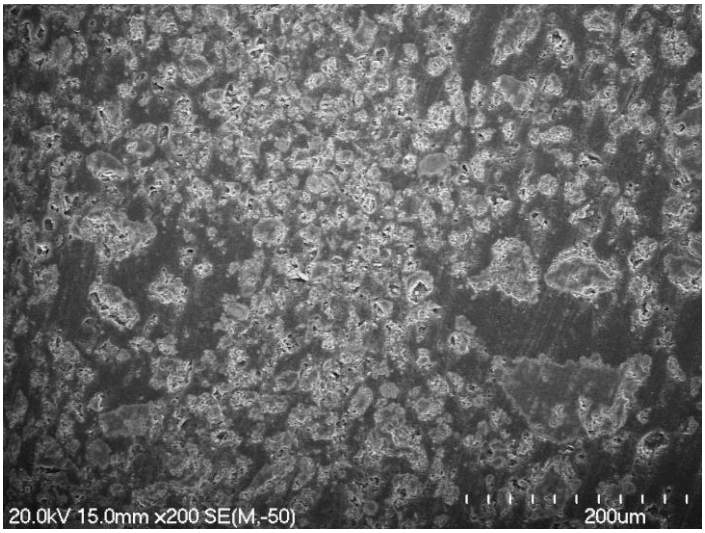

Figure 4.30: Combustion reacted powder A (feedstock) for thermal spraying

4.3.6b Powder B

Figure 4.31 shows a macrograph of combustion reacted powder B (produced from 500 g of as-milled powder with DPR 13.2:1) before ball milling in the porous form with small granules. The combustion reacted powder was subjected to crushing using ball milling to prepare the feedstock for thermal spraying with good flowability.

Figure 4.31: Macrograph of the combustion reacted powder B (produced from 500 g of as-milled powder with DPR 13.2:1) before ball milling

Figure 4.32 shows the SEM images of the particle morphology for the fine feed (< 75 µm) after 15 min of ball milling. This powder was unable to flow through the flowmeter. In general most of the particles are seen to be angular with rough surfaces and this is likely to have contributed towards poor flowability. The particle size distributions (fig. 4.33) of the fine feed (< 75 µm) after 15 min of ball milling ranged from 0.7 µm to 150 µm with a median particle diameter of about 45 µm. The fine feed consists of 10% of the particles with size less than 10 µm which is also responsible for the poor flowability.

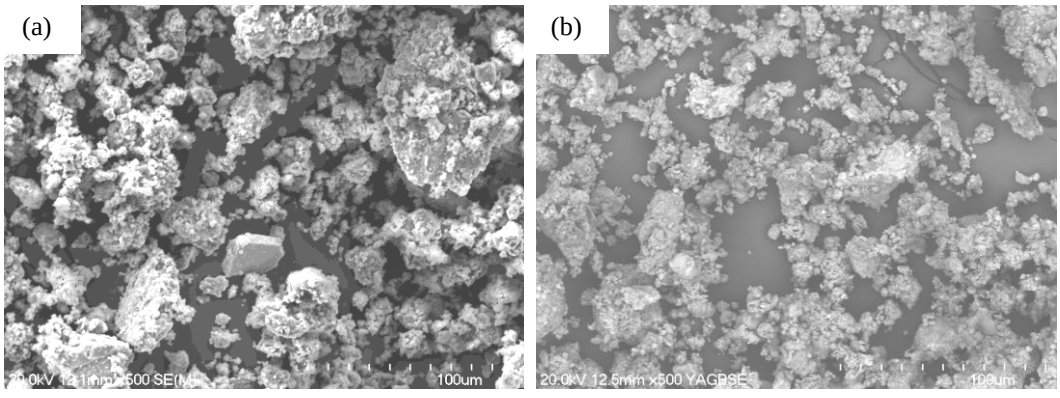

Figure 4.32: Particle morphology of combustion reacted and ball milled fine powder B (produced from 500 g of as-milled powder with DPR 13.2:1) with fine feed (< 75 µm) (a) SEM micrograph (b) Back scattered image

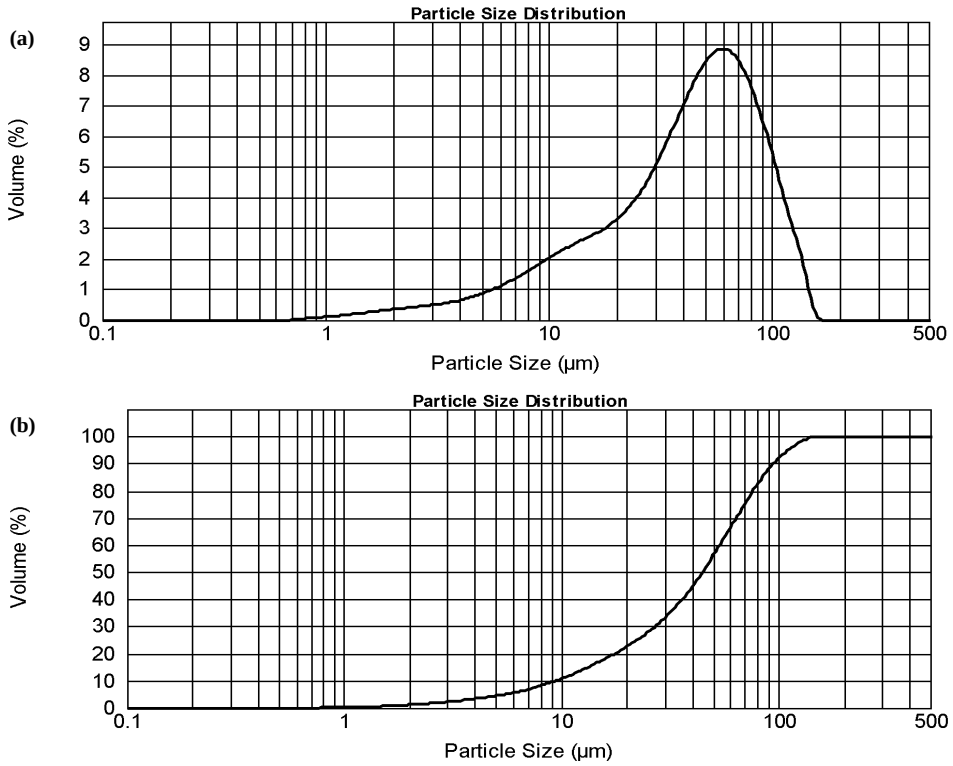

Figure 4.33: Particle size distributions (a) frequency (b) cumulative of powder B fine feed < 75 µm after 15 min ball milling

Figure 4.34 shows an SEM back scattered micrograph of the particle morphology of the fine feed < 75 µm after agglomeration and sieving to <106 µm . Agglomeration resulted as an increase in the size of the particles. The fine angular particles before agglomeration (fig. 4.32b) were turned into a more spherical shape which improved the flowability. Due to the use of a water soluble binder PVA (polyvinyl alcohol) for agglomeration, it was not possible to determine the particle size of this feed using a particle size analyzer.

Figure 4.35 shows the particle morphology for the coarse feed (125 µm > size > 75 µm) component of combustion reacted powder after 15 min ball milling. This showed good flowabity through the flowmeter. The coarse feed consists mostly of particles with irregular shape and smooth surfaces. Figure 4.36 shows the particle size distributions for the coarse feed component of (125 µm > size > 75 µm) powder B after 15 min of ball milling The particles are in the range 50 µm to 250 µm. The median particle diameter of the coarse feed is about 120 µm. The coarse feed powder particle size distribution has approximately 90% of the particles less than about 171 µm and 10% of the particles less than 84 µm. The very fine particles, less than 10 µm

were not observed in the coarse feed of Powder B due to the smooth surfaces of the particles which restricted the tendency for the fine particles to become entrapped.

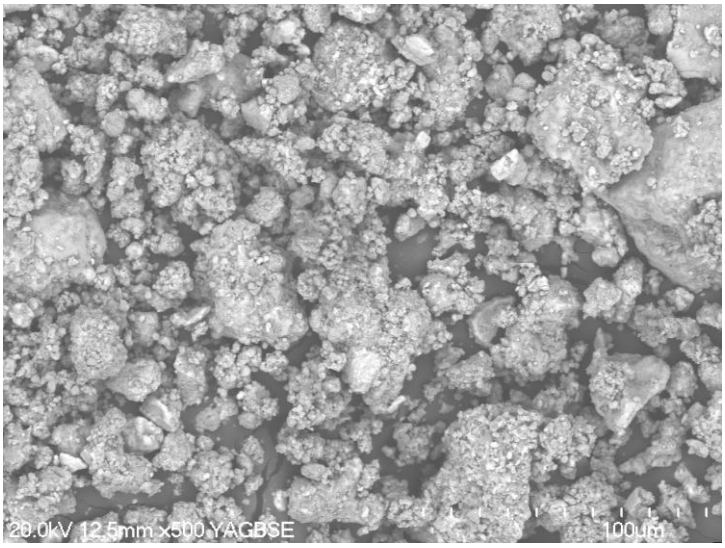

Figure 4.34: Particle morphology of combustion reacted powder B fine feed (< 75 µm) after agglomeration with 2% PVA and sieving to < 106 µm

Figure 4.35: Particle morphology of combustion reacted powder B coarse feed (125 µm > size > 75 µm) after 15 min ball milling

Figure 4.37 shows the morphology of the combustion reacted powder B (feedstock) to be used for thermal spraying. This morphology had good flowability. The feedstock largely consists of fine agglomerated particles with rough surfaces along with coarse particles with smooth or rough surfaces. The size of the feedstock powder B from the SEM measurements (fig.4.38) shows that most of the particles are less 50 µm but the

amount of powder particles in the range of 50 µm to 100 µm is larger than for powder A. The average flowability of the powder B feedstock based on ASTM standard B213-03 was 50 g/104 s [10].

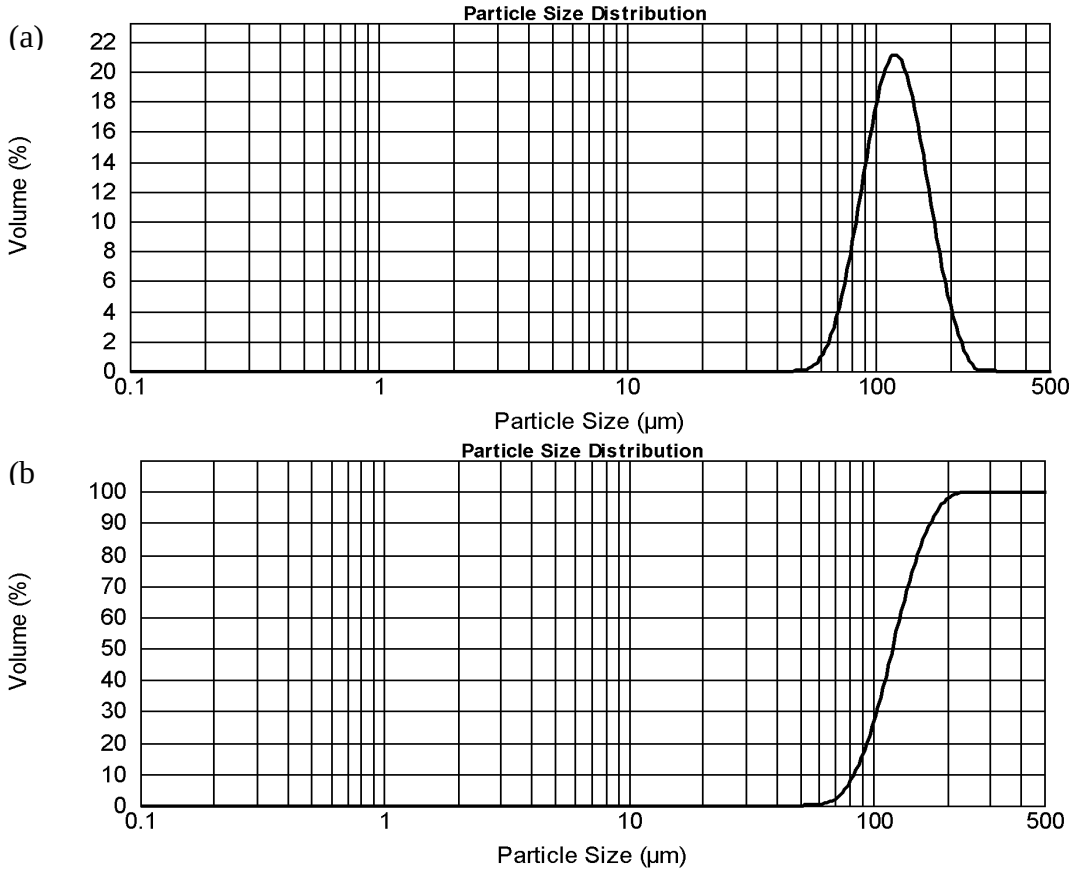

Figure 4.36: Particle size distributions (a) frequency and (b) cumulative of powder B coarse feed 125 µm > size > 75 µm after 15 min ball milling.

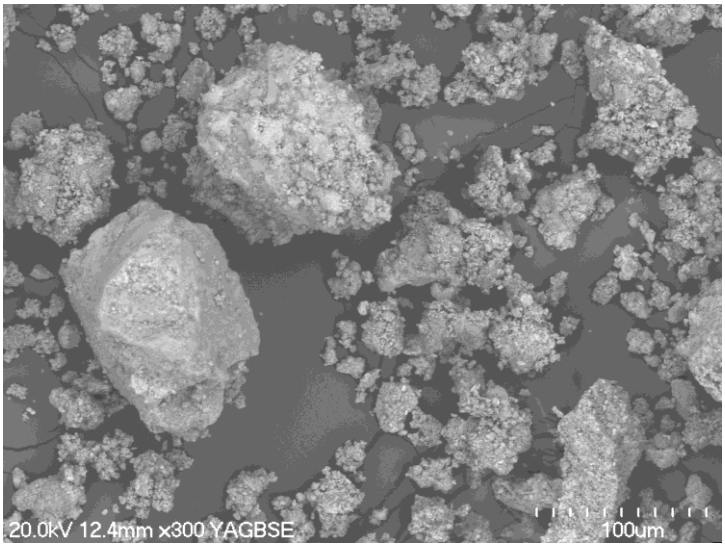

Figure 4.37: Particle morphology of combustion reacted powder B (feedstock) for thermal spraying

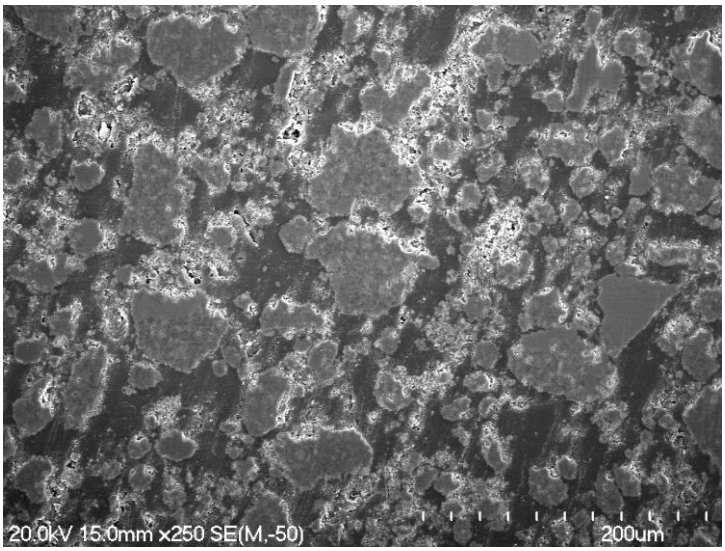

Figure 4.38: Combustion reacted powder B (feedstock) for thermal spraying

4.4. Summary

- Two batches of composite powders were produced using two different molar ratios of TiO_2 and Al. On the basis of the investigations on the effect of disc to powder ratios (DPRs), a ratio of 13.2:1 and a milling time of 4 hours were selected to produce two batches of homogenously intermixed composite powders of TiO_2 and Al. The SEM and XRD results of the as-milled powders showed that there was no reaction occurring after 4 hours of milling time. The composite powders were completely homogenous and boundaries between TiO_2 and Al particles cannot be clearly seen.

- A self propagation high temperature synthesis of the as-milled powder resulted in $Ti(Al,O)/Al_2O_3$ and $TiAl(O)/Al_2O_3$ based interpenetrated phase composites. The XRD analysis of the combustion reacted powders/interpenetrated phase composites confirmed the presence of a Ti based metallic phase and an Al_2O_3 based ceramic phase. The Ti based metallic and Al_2O_3 based ceramic phases were continuous and exhibited an interpenetrated network. However, in powder B powder particles showed a few areas where interpenetrating phases were absent creating a non-homogenous structure. Thermal analyses of the combustion reacted powders showed that the combustion reaction was complete.

- The combustion reacted powders were further processed to produce feedstocks, with good flowability, for thermal spraying. The fine feeds resulting from the ball

milling of combustion reacted powders were separated from the coarse feeds and treated with an organic binder consisting of 2% PVA (polyvinyl alcohol) to produce agglomerated particles with good flowability. Feedstocks of composite powders with good flowability and suitability for thermal spraying were successfully produced.

4.5. References

1. Welham, N.J., *Mechanical activation of the solid-state reaction between Al and TiO_2.* Materials Science and Technology, 1998. **255**: 81-89.

2. Ying., D.Y., D.L. Zhang and M. Newby, *Solid-state reactions during heating mechanically milled Al/TiO_2 composite powders.* Metallurgical and Materials Transactions A, 2004. **35**(7): 2115-2125.

3. Bartuli, C., R.W. Smith and E. Shtessel, *SHS powders for thermal spray applications.* Ceramics International, 1997. **23**(1): 61-68.

4. Zhang, D. L., Z. H. Cai, and G. Adam, *The mechanical milling of Al/TiO_2 composite powders.* JOM, 2004. **56**(2): p. 53-56.

5. Liu, Z. G., S. Raynova, and D. L. Zhang, *Investigation of a discus- milling process using powder mixture of Al and Ti.* Metallurgical and Materials Transactions A, 2006. **37A**(1): p. 225-233.

6. Liu, Z., S. Raynova, D. Zhang, and B. Gabbitas, *Study on the self sustained reactions in an Al–TiO_2 composite powder produced by high-energy mechanical milling.* Materials Science and Engineering A, 2007. **A449-451**: p. 1107-1110.

7. Zheng, L., *The characterisation of titanium alloy composite powder coatings produced by thermal spraying*. 2005, ME thesis, The University of Waikato, Hamilton. p. 54.

8. Cao, P., B. Gabbitas, L. Zheng, and D. L. Zhang, *Fabrication of Ti(Al,O)-Al_2O_3 of powder feedstock for thermal spraying and evaluation of composite coating. Materials Science Forum*, 2006. **534-536**: p. 421-424.

9. Kamali, A.R. and J. Fahim, *Mechanically activated alumina-thermic reduction of titanium dioxide.* International Journal of Self-Propagating High-Temperature Synthesis, 2009. **18**(1): 7-10.

10. *ASTM Test Method B 213-97, Standard test method for flow rate of metal powders*. Annual Book of ASTM Standards. Vol. 02.05. 1998, West Conshohocken, PA: American Society for the Testing of Materials.

Chapter 5

Microstructure and Characterisation of Ti(Al,O)/Al_2O_3 and TiAl(O)/Al_2O_3 Composite Coatings

5.1. Introduction

Thermal sprayed coatings are characterised by a layered microstructure consisting of many individual deposits. The deposition processes is a thermo-mechanical process involving continuous bombardment of the substrate with fully or partly melted or solid particles. Solid particles are not desirable because these particles rebound easily or remain weakly connected to the rest of the coating. This results in the poor mechanical properties of the coating. The molten particles deform, become lamellae and solidify into columnar or fine-grained equiaxial crystals. The lamellae have two principle morphologies, pancake and flower. The solidification and deformation processes occur more or less simultaneously, however deformation stops when particles become solidified. The deposition process results in a unique lamellar microstructure consisting of deformed splats, oxide inclusion, voids/porosities and un-melted particles.

In this research, a study of a coating surface and its cross-section was carried out to characterise the deposits. Composite coating characterisation was also helpful in understanding the changes that occur from powder to coating as a result of thermal spraying. The study of microstructure of the composite coatings in this work was also very important due its strong influence on the performance of the coatings. The characterisation work includes as-sprayed coating analysis (using XRD, SEM), microstructure evaluation, thickness and hardness measurements.

5.2. Feedstocks for thermal spraying

Two types of composite powders containing different Ti based metallic phases with Al_2O_3 ceramic phase were used as feedstock to produce HVOF composite coatings A (A1, A2) and B2. Composite coating references with their feedstock details are explained further in table 5.1.

Table 5.1: Composite coating references with their feedstock details

Coatings	Powder feedstock	PVA agglomeration	As-milled powder (TiO_2/Al) (g)
A1	Ti(Al,O)/Al_2O_3	No PVA	300
A2		2% PVA	500
B2	TiAl/Al_2O_3	2% PVA	500

5.2.1. Spraying parameters

HVOF spraying conditions for coatings produced at Triple R Engineering Ltd., Palmerston North to make coating A1 from the feedstock powder produced from 300 g of as-milled powder is shown in table 5.2.

Table 5.2: HVOF spraying parameters at Triple R Engineering Ltd.

Equipment Model	JETKote-II
Powder feed rate	2.44 unit
Carrier gas	N_2 (85%)
Fuel Gas	Propane C_3H_8 (82%)
O_2	42%

HVOF spraying conditions for coatings produced at Holster Engineering Co. Ltd., Tokoroa to produce coatings A2 and B2 from feedstock powders each produced from 500 g of as-milled powder are given in table 5.3.

Table 5.3: HVOF spraying parameters at Holster Engineering Co. Ltd.

Gun type	GMA Microjet	
Spraying parameters	Pressure (MPa)	Flow rate (l/min)
Oxygen pressure	0.69	42
Fuel pressure (propane)	0.35	24
Carrier gas pressure (N2)	0.69	38
Powder feed screw		110 rpm
Stand off distance		76-100 mm
Number of passes for Ti (bond coat)		2
Number of passes for composite coatings		6

5.2.2. Substrate condition

Heat treated H13 tool steel was grit blasted using Al_2O_3 (36 grit) at an air pressure of 0.17 MPa and this gave a surface roughness (Ra) of 5.20 µm.

5.3. Results and discussion

5.3.1. Surface topography

The surface topography of the HVOF sprayed coatings A2 and B2 produced from feedstock powders Ti(Al,O)/Al_2O_3 and TiAl(O)/Al_2O_3 respectively was studied using SEM. Both of the HVOF sprayed coatings had similar surface topography although feedstock powders of different composition were used to form different coatings. Figure 5.1 shows the overall surface topography of the as-sprayed composite coating A2 on H13 tool steel which is typical of coating A1 and B2 as well.

Coating A2 was composed of well deposited flat areas and sloping areas. The flat areas (marked by a solid rectangle) derive from the impact of molten particles with the substrate. The surface morphology of the coating indicates that the particles were in a fully molten state when they transferred to the substrate, as no powder particle features were observed on the coating surface. The size of the splats originating from the impact of superheated particles varies due to the different particle sizes in the powder feedstock. The sloping areas (marked by a dashed rectangle) originate from a pile up of splats and the debris resulting from the splashed splats.

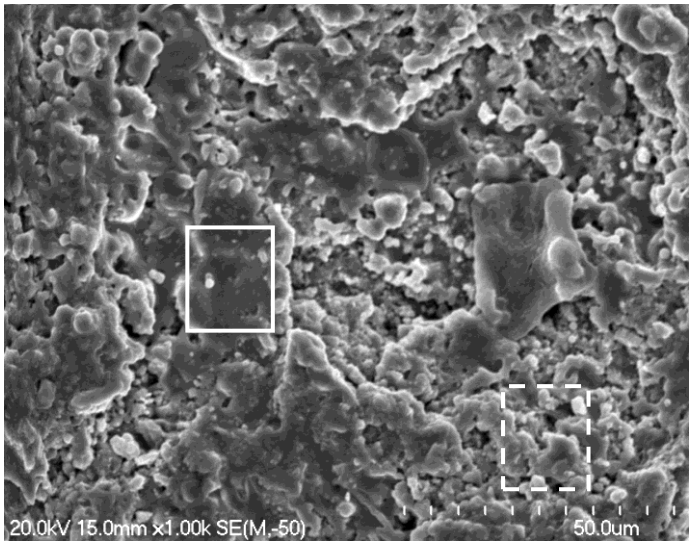

Figure 5.1: SEM surface topography of as-sprayed coating A2

Figure 5.2 shows a high magnification image of the flat area of coating A2 with intra-splat micro cracks and porosities. The splashes of fine debris particles can also be seen due to the impact of molten particles. The intra-splat micro cracks most likely resulted from the residual shrinkage or thermal stresses, due to the difference of thermal expansion coefficient of various phases present in the coating. The high magnification image of the slope area of coating B2 with marked porosity is shown in fig. 5.3 whereas the intra-splat cracks, intra splat porosities and splashes of fine debris are shown in fig. 5.4. The porosities in both types of coatings A2 and B2 are generally less than 3µm. Powder made by a self propagating high temperature reaction (SHS) generally contains porosity. After thermal spraying, this porosity persists as intra-splat porosity (fig 5.2).

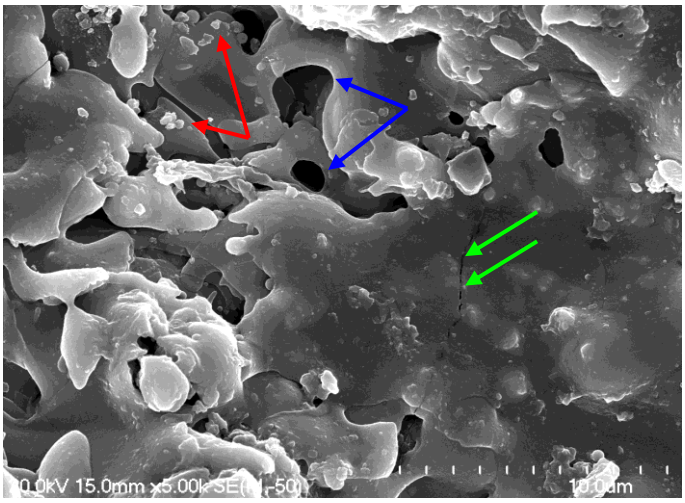

Figure 5.2: SEM surface topography of flat area of as-sprayed coating A2 with intra-splat cracks (green arrows), intra-splats porosities (blue arrows) and splashes of fine debris (red arrows)

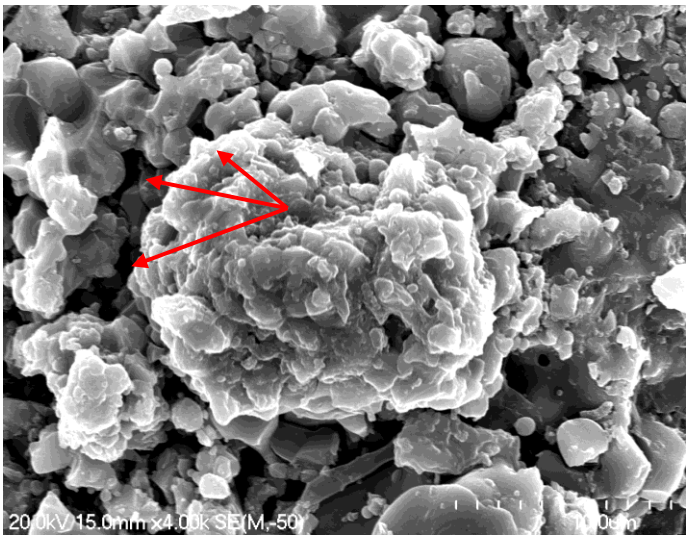

Figure 5.3: Surface topography of as-sprayed coating B2. Slope area with porosities indicated by arrows

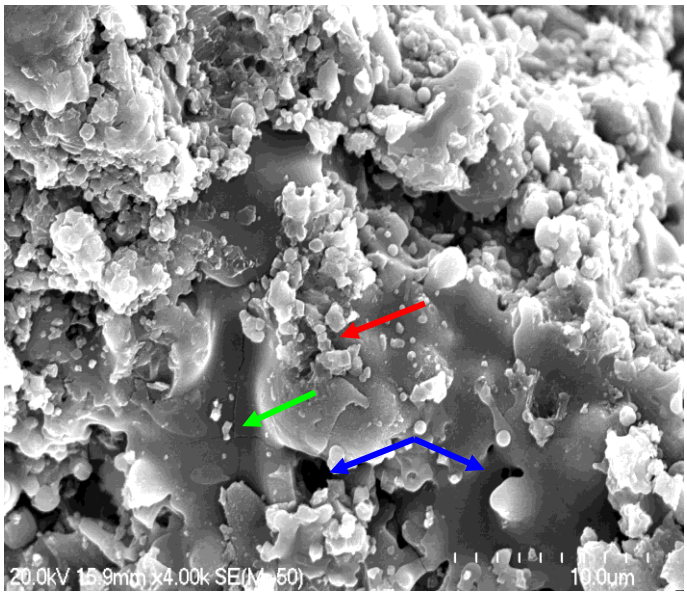

Figure 5.4: SEM surface topography of as-sprayed coating B2 with intra-splat cracks (green arrow), intra-splats porosities (blue arrows) and splashes of fine debris (red arrow)

The average surface roughness (Ra) of the coating A2 and B2 was about 5.56 µm and 8.05 µm respectively. The surface roughness of the as sprayed composite coatings is comparable with the surface roughness of as sprayed (HVOF) NiCrBSi (Ra 6.8 µm) and Cr_3C_2-Ni (Ra 5.15 µm) composite coatings for elevated temperature applications [1, 2]. The roughness also depends on the initial powder particle size, where large sized particles (semi-molten form) produce rough surfaces compared to fine powder deposits. The larger powder particles in the feedstock used for thermal spaying of

coating B2, compared with coating A2, is also responsible for the higher surface roughness of this coating. Moreover, the higher surface roughness of coating B2 is possibly due to the presence of more splashes consisting of fine debris particles which were cast out from the splats (fig. 5.4) in this coating.

5.3.2. Surface analysis of the composite coatings

Surface analysis of the composite coatings was carried out using EDAX elemental mapping. Elemental mapping was done over the outer surfaces of the coatings to analyze the compositional homogeneity. This is an important factor to understand the corrosion behaviour the coating in molten aluminium.

A surface SEM image and associate chemical composition mapping for titanium, aluminium and oxygen in coating A2 is shown in fig. 5.5. This shows a more uniform titanium distribution within the interpenetrating phase network and areas where the aluminium and oxygen distribution appears to be less homogenous. However, the interpenetrating oxides are continuous.

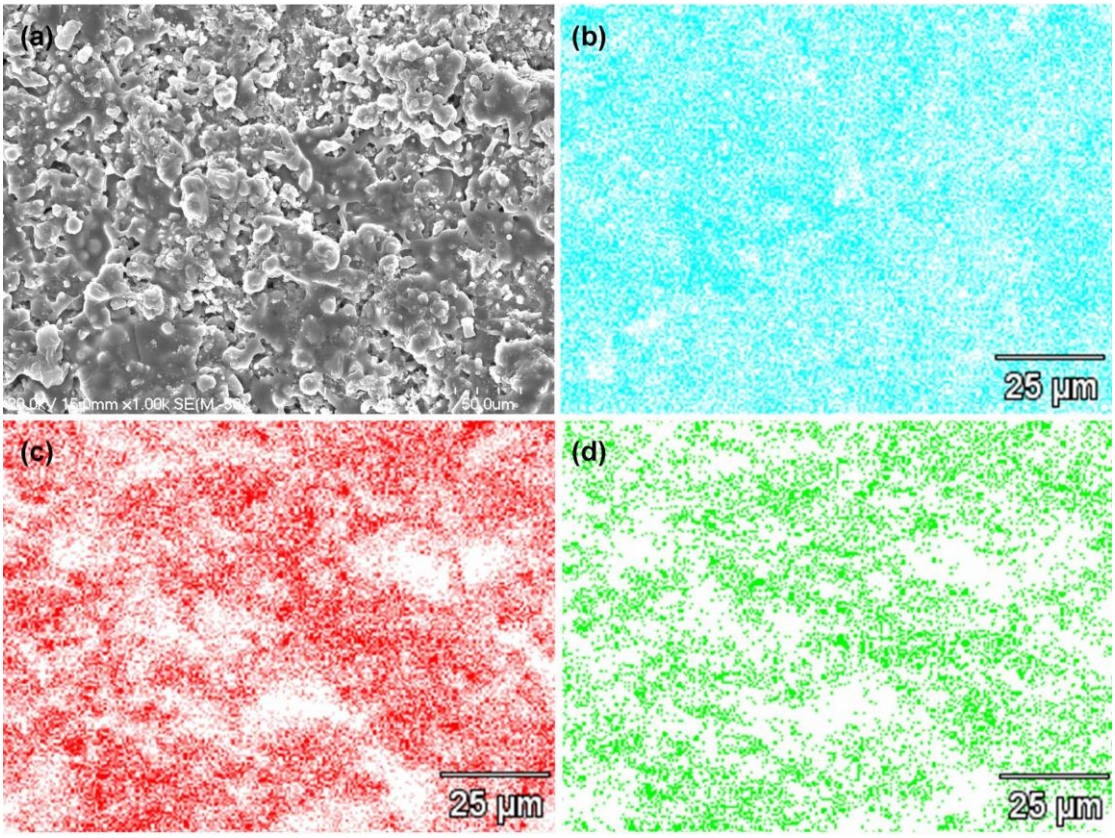

Figure 5.5: (a) SEM micrograph of the surface coating A2 and; (b-d) elemental maps of titanium, aluminium and oxygen respectively

A surface SEM image and associated chemical composition mapping for titanium, aluminium and oxygen in coating B2 is shown in fig. 5.6. The SEM image shows that the titanium matrix is homogenous, as in coating A2 but there is less homogeneity of the interpenetrating oxide network.

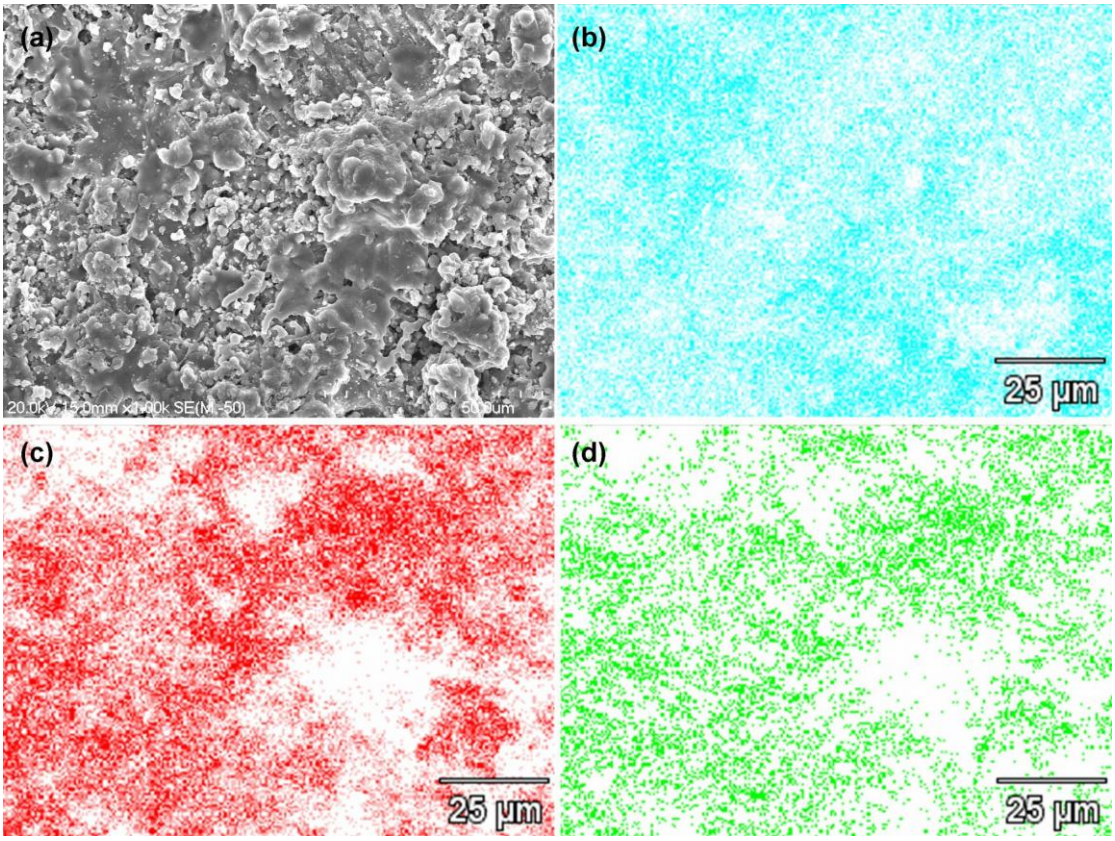

Figure 5.6: (a) SEM micrograph of the surface coating B2 and; (b-d) elemental maps of titanium, aluminium and oxygen respectively

5.3.3. Coating microstructure (cross sectional study)

Figure 5.7 shows the cross-sectional microstructure of the double layer coating A1 produced from 300 g of as-milled powder (DPR 22:1) without agglomeration of the feedstock with PVA. The dark area with visible voids is the Ti (Al,O)/Al_2O_3 composite coating while the light area is the Ti coating (undercoat). The reason for applying a Ti undercoat is to enable good adhesion of the composite coating with the substrate. The composite coating produced from this feedstock was mostly patchy and thin as shown in fig. 5.7a and the bulk of the coating was Ti only. The non uniformity of the coating was due to the poor flowability of the very fine (average particle size 12 µm) composite powder through the spray gun. The Ti coating (undercoat) which was produced using atomized Ti powder was also non-uniform (fig. 5.7b) due to variation

in the size of the atomized powder particles and this factor further contributed towards the non-uniformity of the composite coating (topcoat). The average thickness of single layer coatings was about 6 µm to 30 µm, whereas the average thickness of the double layer coating, Ti/Ti(Al,O)/Al_2O_3, was 75 µm to 113 µm.

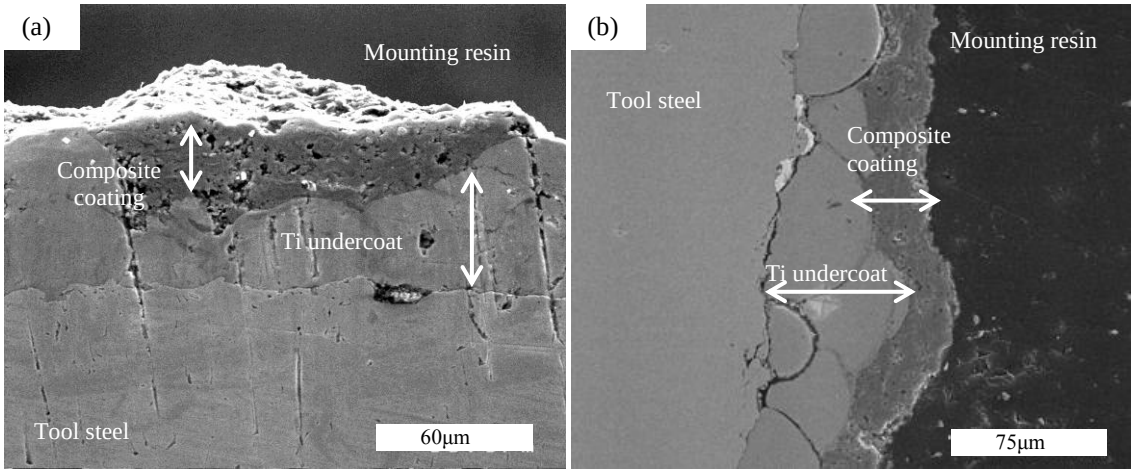

Figure 5.7: SEM micrographs of Ti/Ti(Al,O)/Al_2O_3, a double layer coating A1 on H13 tool steel produced from 300 g of as-milled powder (DPR 22:1) without agglomeration of the feedstock with PVA (a) a patchy porous coating (b) coating on a non-uniform Ti undercoat

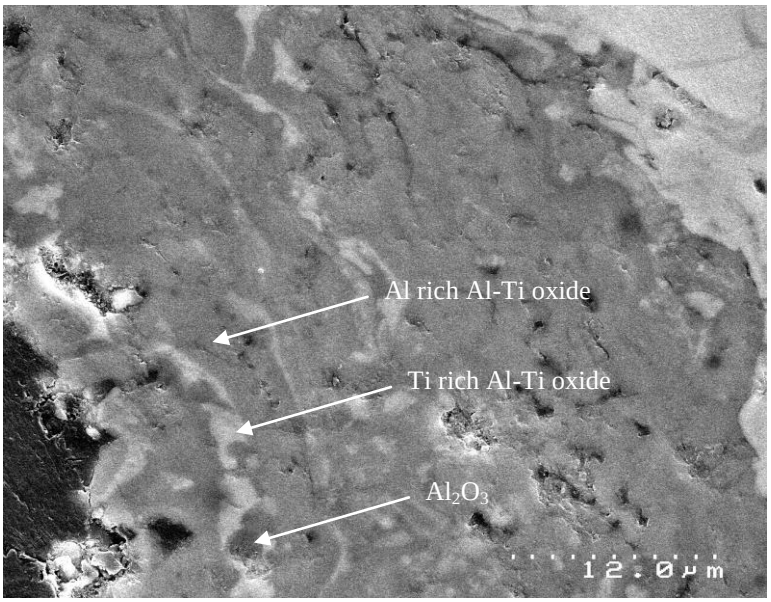

Figure 5.8: SEM micrograph of cross section of composite coating A1 with various phases present. The dark area is Al rich Al-Ti oxide and the bright area is Ti rich Al-Ti oxide and the particles are alumina

The composite coating mainly consisted of a bright phase (Ti rich Al-Ti oxide), a dark phase (Al rich Al-Ti oxide) and a few dispersed dark alumina particles (fig. 5.8). The

micro hardness of the composite coating surface varied from HV 726 to HV 2960 with an average value of HV 1453.

The micrographs of the cross sections of the coating A2 and B2 produced from 500 g of as-milled powder (DPR 13.2:1) and with agglomeration of the feedstock with PVA is shown in fig. 5.9a and fig. 5.9b respectively. The coatings produced from the agglomerated feedstocks were continuous with an average thickness of the double layer coating of 15-25 µm in the case of B2 and 20-35 µm for A2 under the same spraying condition. The difference in the coating thicknesses under similar spraying conditions is likely due to the difference in the deposition efficiency of the respective feedstock powders. The lower deposition efficiency of coating B2 was most likely caused by a large mean particle size after agglomeration of feedstock powder resulting in a greater chance of powder being deflected from the substrate due to incomplete melting. The thickness of the HDH (hydride-dehydride) Ti under coat was about 2-6 µm. The composite coating A2 (fig. 5.10a) exhibits a characteristic layered structure typical of thermal spray coatings and has good bonding with the substrate. It is composed mainly of three phases, a bright phase Ti(Al,O), a dark phase (Al rich Al-Ti oxide) and a dispersion of dark round alumina particles measuring about 1-6 µm (fig. 5.10b). The back scattered cross sectional images of coating B2 (fig. 5.11a, b) confirm the presence of two phases, a dark lamella phase (alumina) and a bright lamella phase (TiAl(O), $Ti_3Al(O)$). Vicker's micro-harness measurements on the surface of the composite coating A2, using 100g load and 20 secs dwell time gave surface harness values ranging between HV 700 to HV 3500. The surface of the composite coating B2, under similar conditions, was similar to that of coating A2, varying from HV 800 to HV 3000. Because of the fine structure in the interpenetrating composites (fig.5.10b and fig.5.11b), with a separation distance between phases of about 3 µm, a hardness for individual phases was not measured. The indent size, typically 7 µm, for the higher hardness regions was much larger than the separation distance between individual phases.

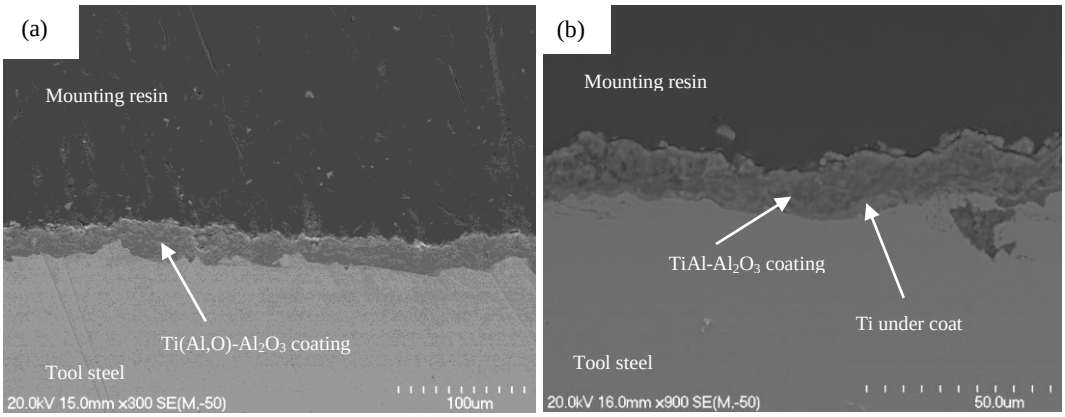

Figure 5.9: SEM micrographs of a double layer coating cross section produced from 500 g of as-milled powder (DPR 13.2:1) and agglomeration of feedstock with PVA. (a) Ti/ Ti (Al,O)/Al_2O_3 composite coating A2 (b) Ti/TiAl/Al_2O_3 composite coating B2

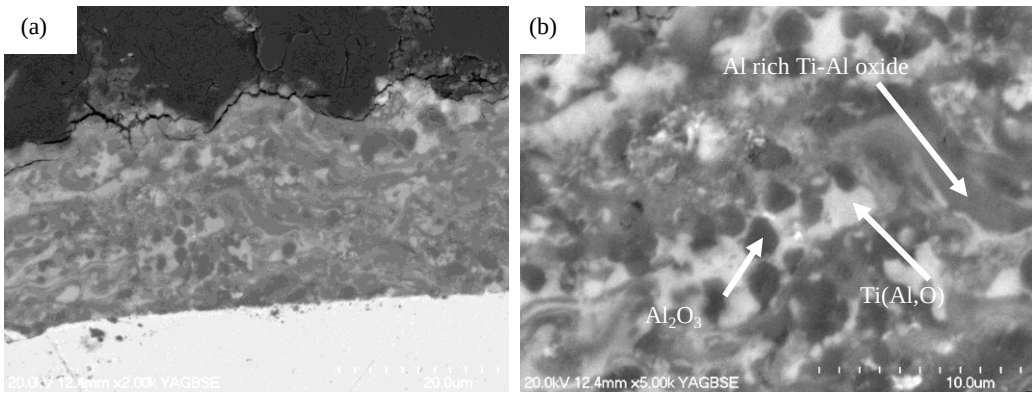

Figure 5.10: Backscattered cross-sectional images of composite coating A2 produced from 500 g of as-milled powder (DPR 13.2:1) and agglomeration of feed stock with PVA (a) coating cross-section and (b) high magnification cross-section

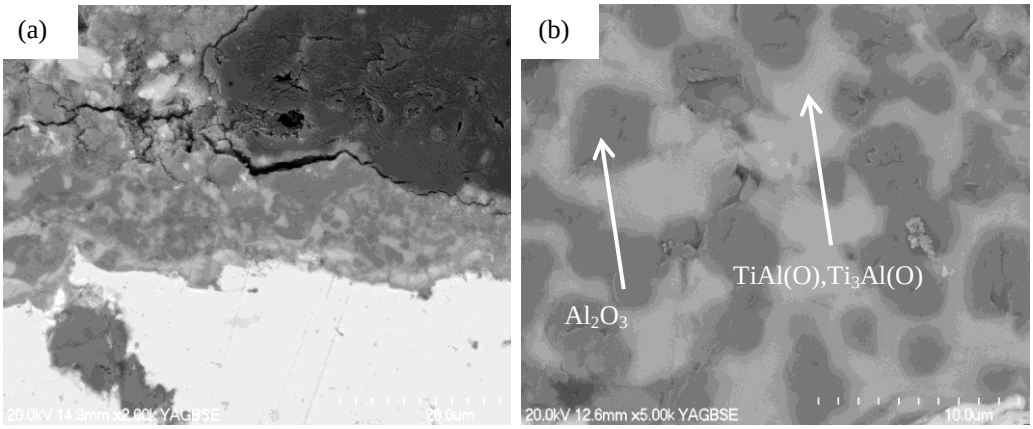

Figure 5.11: Backscattered cross-sectional images of coating B2 produced from 500 g of as-milled powder (DPR 13.2:1) and agglomeration of feedstock with PVA, (a) coating cross-section, (b) high magnification cross-section

5.3.4. Phase identification with XRD and EDAX

The XRD analysis of the single layered as-sprayed composite coatings was carried out to identify the major phases present within the coatings. The coating XRD spectrums were also compared with the relevant feedstock powder to describe the changes that happened as a result of thermal spraying. SEM was used to study the microstructure of the coating. EDAX analysis involves the characterisation of the three main phases within the coating microstructure visible under the SEM, the dark lamellae phase, light lamella phase and a phase consisting of dark particles.

Figure 5.12 shows the XRD spectrum of coating A1 along with its feedstock powder. It can be seen that the feedstock powder produced without PVA agglomeration mainly contains Al_2O_3, Ti, and TiO phases. The presence of the similar phases is also confirmed in the feedstock powder used with PVA agglomeration to produce coating A2 (fig. 5.13). It is clear from the results that there is no effect on the types of the phases produced in the composite coatings A1 and A2 using feedstocks powders produced from 300 g and 500 g as-milled powders. However PVA agglomeration of the feedstock powder did affect the degree of uniformity and the thickness of the coating on the substrate. The composite coating A1 is patchy and porous (5.7a) due to the poor flowability of feedstock through the spray gun. However, for the feedstock produced from 500 g of as-milled powder with PVA agglomeration, a continuous, and uniform composite coating A2 resulted on the tool steel substrate (fig. 5.9a).

In both types of coatings A1 and A2, new peaks which match with $(Al_mTi_n)O_x$ and likely to be $(Al_2Ti)O_5$ have been identified. Therefore, it is likely that these phases were formed due to high temperature reactions of the molten particles in flight during the spraying process. Lu et al. [4] reported that Ti and Al_2O_3 can react at relatively low temperature (500 °C) to form a Ti_3Al intermetallic. Heffelfinger et al. [5] also reported the formation of a Ti_3Al intermetallic at 900 °C in a Ti/Al_2O_3 metal matrix composite. Zalar et al. [3] studied the interfacial reactions in Al_2O_3/Ti, Al_2O_3/Ti_3Al and Al_2O_3/TiAl bi-layers up to 700 °C and reported that an Al_2O_3/Ti interface showed a higher reactivity compared to an Al_2O_3/Ti_3Al interface. With decomposition of alumina, an oxygen solid solution in Ti and the formation of Ti_3Al were observed in these bi-layers. No reaction was found in the Al_2O_3/TiAl interface even after heating till 700 °C. The interface reactions between the gamma TiAl and Al_2O_3 reinforcement

was also studied by Shih et al. [4]. The results of this study showed that there is no reaction product, even after thermally exposing for up to 124 hours at temperature of 1175 °C.

The constitution of the coatings was also analysed using EDAX and found to consist of alumina and titanium/ aluminium oxides. Formation of Ti_3Al was not indicated by XRD analysis in coating A1 and A2. However EDAX analysis of these coatings suggested the formation of Ti_3Al phase.

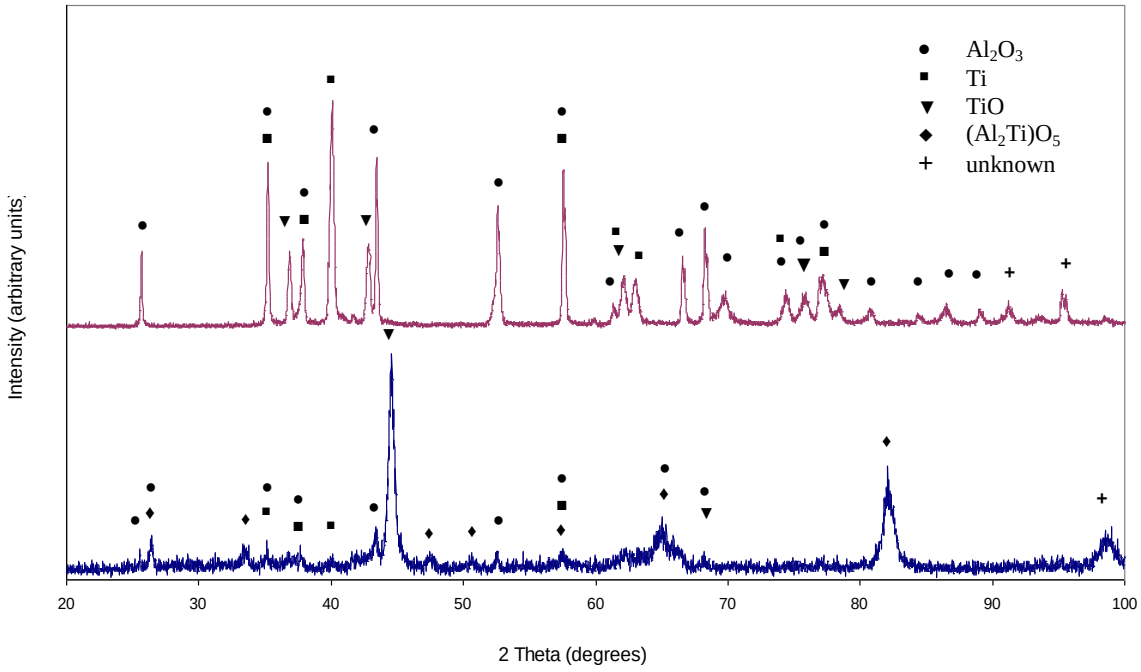

Figure 5.12: XRD pattern of coating A1 (bottom) and its feedstock powder (top) produced from 300 g of as-milled powder.

From the EDAX analysis, it was observed that the dark phase in both types of coatings A1 (fig. 5.8) and A2 (fig. 5.10b) contain a high atomic percentage of oxygen along with Ti and Al. In the dark phase the Al atomic percentage is higher than the Ti and hence it is likely to contain Al rich Al-Ti oxide likely to be $(Al_2Ti)O_5$ as indicated in the XRD spectrum (figs. 5.12 & 5.13). The light phase in both coatings contains a high atomic percentage of Ti with a little oxygen and Al suggesting that Al and oxygen are present in the form of dissolved elements. This metallic phase with the presence of dissolved Al and oxygen can be renamed as Ti(Al,O) in these coatings. The dark particular phase within both coating microstructures is identified as likely to be Al_2O_3 since the EDAX results showed that this phase predominantly contains Al

and oxygen at similar atomic percentages. Some TiO may also be present within the alumina particles, as a low amount of Ti has also been detected by EDAX analysis.

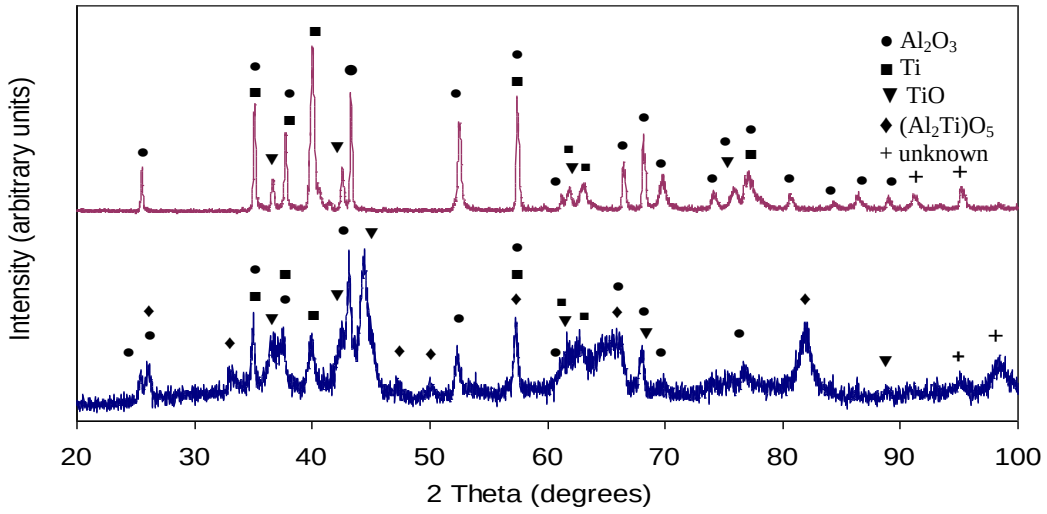

Figure 5.13: XRD pattern of single layer (without Ti bond coat) coating A2 (bottom) and its feedstock powder (top) produced from 500 g of as-milled powder.

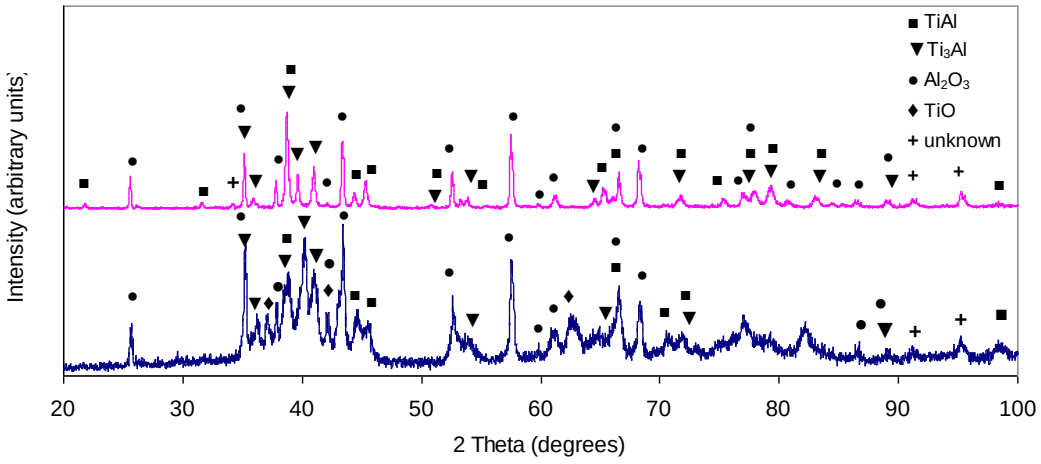

Figure 5.14: XRD pattern of single layer (without Ti bond coat) coating B2 (bottom) and its feedstock powder (top) produced from 500 g of as-milled powder.

Figure 5.14 shows the XRD spectrums of coating B2 along with its feedstock powder produced from 500 g of as-milled powder. The XRD analysis of the PVA agglomerated feedstock powder of coating B2 showed that it predominantly contains TiAl, Ti_3Al and Al_2O_3. The XRD analysis of the coating shows that all the three phases which were present in the feedstock powder were also retained in the coating B2 after thermal spraying, however new peaks of TiO were also identified by the XRD analysis. EDAX analysis of the coating (fig. 5.11b) suggested that the dark

lamellae/particle phase consists of Al_2O_3, while the bright lamellae phase was identified as a metallic phase, consisting of $Ti_3Al(O)$, TiAl(O). Hung [7] reported the presence of three phases, dark and light lamella phases with a dispersion of Al_2O_3 particles in a separate study on similar coatings. The XRD peaks for the coating in fig. 5.14 are broader than those for the feedstock powders, suggesting that the coating is more amorphous.

It was not possible to pinpoint the exact locations of specifics phases identified from XRD analysis with EDAX using SEM. However the proportion of different elements by EDAX analysis provided some help to generalise the location of the oxide and metallic phases within the coating's microstructure. Based upon the XRD analysis and EDAX analysis, the major phases present in each type of coatings are tabulated in table 5.6. EDAX analysis tabulation is based on an average value of three readings for each phase. The standard deviation of the data was also taken into account.

Table 5.4: Elements detected from the three phases visible under SEM using EDAX analysis

Coating	Visible Phases	Element (At%)			Major Phases Present
		O	Al	Ti	
A1	Dark	36.70 ± 5.60	33.89 ± 1.66	29.39 ± 4.74	Al rich Al-Ti oxide likely$(Al_2Ti)O_5$ or Al_2O_3/TiO
	Light with O	24.46 ± 5.78	23.32 ± 6.40	52.32 ± 4.49	Ti rich Al-Ti oxide Ti(Al,O)/Ti(O)/$Ti_3Al(O)$
	Light without O	0.00 ± 0.00	25.16 ± 10.69	74.84 ± 10.69	Ti_3Al
	Particle	37.33 ± 3.36	56.03 ± 8.08	6.63 ± 7.09	Al_2O_3 with small amount of TiO
A2	Dark	38.19 ± 1.93	41.01 ± 0.47	20.79 ± 2.28	Al rich Al-Ti oxide likely $(Al_2Ti)O_5$ or Al_2O_3/TiO
	Light with oxygen	17.92 ± 7.52	19.65 ± 6.25	62.43 ± 6.49	Ti(Al,O)/Ti(O)/$Ti_3Al(O)$
	Particle	52.01 ± 4.06	47.54 ± 4.38	0.44 ± 0.33	Al_2O_3 with small amount of TiO
B2	Dark or particle	54.47 ± 0.75	43.88 ± 0.24	1.65 ± 0.79	Al_2O_3 with small amount of TiO
	Light with low O	6.74 ± 2.51	43.38 ± 1.93	49.87 ± 3.89	Ti(O)/TiAl(O)/$Ti_3Al(O)$
	Light with O	38.12 ± 3.25	25.88 ± 3.12	35.98 ± 5.99	TiO/ Ti-rich Ti-Al Oxide

5.4. Summary

Two types of composite coatings A (A1, A2) and B2 were successfully deposited by HVOF spraying on to H13 tool steel. SEM observation of the as sprayed coatings and

cross sectional images confirmed that the particles were in the fully molten/semi-molten state during transfer onto the substrate; no original powder features were identified.

It is clear from the results that there is no effect on the types of phases produced in the composite coatings A1 and A2 using feedstock powders produced from 300 g and 500 g as-milled powders respectively. However PVA agglomeration of the feedstock powder did affect the uniformity and thickness of the coating on the substrate.

The lower temperature of the HVOF spray process resulted in coatings similar to the original composition of their respective starting feedstock powders. However, some new phases were also formed in both types of coating due to reactions of the molten particles in flight during the spraying process.

Based upon the EDAX analysis, the dark lamella phase in the coatings A1 and A2 was confirmed to be composed of oxide phases, as a high concentration of oxygen was observed in both types of coating. The light lamellae phase in these coatings is metallic with no or low oxygen concentration which is likely to exist as dissolved oxygen in the metallic phase. The dark phase was identified as un-melted/re-solidified Al_2O_3 particles due to their shape and similar atomic percentages of Al and oxygen with very little Ti.

EDAX analysis of the coating B2 suggested that the dispersed particle phase consists of Al_2O_3 with a small amount of TiO, while the bright lamellae phase was identified as a metallic phase, consisting of Ti_3Al(O), TiAl(O). The presence of a dark lamella phase was not observed in this type of coating and is most likely due to the greater thermal stability of the TiAl phase with alumina compared with Ti_3Al and Ti.

5.5. References

1. Miguel, J.M., J.M. Guilemany and S. Vizcaino, *Tribological study of NiCrBSi coating obtained by different processes.* Tribology International, 2003. **36**: 181-187.

2. Yin, B., G. Liu, H. Zhou, J. Chen and F. Yan, *Sliding wear behaviour of HVOF-sprayed Cr_3C_2-NiCr/CeO_2 composite coatings at elevated temperature up to 800 °C.* Tribology Letters, 2010. **37**(2): 463-475.

3. Zalar, A., B.M.M. Baretzky, S. Hofmann, M. Ruhle and P. Panjan, *Interfacial reactions in Al_2O_3/Ti, Al_2O_3/Ti_3Al and Al_2O_3/TiAl bilayers.* Thin Solid Films, 1999. **352**(1-2): 151-155.

4. Lu, Y.C., S.L. Sass, Q. Bai, D.L. Kohlstedt and W.W. Gerberich, *The influence of interfacial reactions on the fracture toughness of Ti-Al_2O_3 interfaces.* Acta Metallurgica et Materialia, 1995. **43**(1): 31-41.

5. Heffelfinger, J.R., R.R. Kieschke and C.B. Carter, *Characterisation and microanalysis of interfacial reactions in metal-matrix composite system.* Journal of Microscopy, 1997. **185**: 217-224.

6. Shih, D.S. and R.A. Amato, *Interface reaction between gamma TiAl alloys and reinforcements.* Scripta Metallurgica et Materialia, 1990. **24**: 2053-2058.

7. Hung, J.H., Y.L. Chiu and J. Liang, *Reciprocating wear properties of thermal sprayed titanium aluminide-alumina composite coatings.* Surface and Coatings Technology, 2008. **202**(22-23): 5599-5602.

Chapter 6

The Performance of Ti(Al,O)/Al_2O_3 and TiAl/Al_2O_3 Composite Coatings in Molten Aluminium

6.1. Introduction

The durability of materials, especially those metallic materials exposed to molten aluminium is an important consideration for a number of engineering applications in the aluminium processing industry because aluminium melt can react with nearly all metals and metal oxides. Important examples are die casting dies, dummy blocks used in Al extrusion and molten aluminium handling and container materials. Accelerated dissolution (washout), thermal cracking and soldering of die casting dies are major problems in the aluminium die casting industry. An understanding of the causes of die corrosion by aggressive molten aluminium attack is important and necessary for selecting a coating for the protection of H13 tool steel. The performance of a number of coatings was evaluated against molten aluminium attack for their possible applications in Al high pressure die casting dies. The details of these coatings have already been discussed in chapter 2.

The main objective of this work is to evaluate the performance of Ti(Al,O)/Al_2O_3 (A2, A1) and TiAl/Al_2O_3 (B2) composite coatings on a H13 tool steel substrate against molten aluminium attack. In this study, an effort has been made to develop Ti based Ti(Al,O)/Al_2O_3 and TiAl/Al_2O_3 composite coatings on AISI H13 tool steel using the HVOF thermal spraying technique. We chose to investigate the potential of composite coatings made from feedstock powders of composition Ti(Al,O)/Al_2O_3 and TiAl(O)/Al_2O_3 because the ceramic phase Al_2O_3 has excellent high temperature

properties and is not wetted by molten aluminium below 1000 °C [1], while the metallic Ti phase can be used as a binder enabling good adhesion to the substrate. It also acts to accommodate the difference in thermal expansion between tool steel and alumina. In addition, Ti appears to be more inert to molten aluminium than iron [2]. The important aspect of this work is to identify the suitability of these coatings to protect die-casting dies or dummy blocks used in the Al extrusion process from attack by molten aluminium.

For a material to be used in contact with molten Al it has to possess good corrosion and erosion resistance, high temperature oxidation resistance, thermal shock resistance and good strength and toughness.

The oxidation resistance of the coating is also one of the important aspects to be considered when designing any particular coating for die-casting dies. The oxidation kinetics of Ti(Al,O)/Al_2O_3, TiAl/Al_2O_3 were reported by Zhang [3] at 700 °C for 400 hours in air on a pure titanium substrate. The results of this study showed that the oxide scale that formed on top of the coating was very well bonded to the coating, providing enhanced protection to the base material from further oxidation. Liang [4] studied the reaction kinetics of Ti(Al,O)/Al_2O_3, TiAl/Al_2O_3 and Ti_3Al/ Al_2O_3 coatings at 800 °C and reported that for all these coatings the oxidation kinetics essentially followed a parabolic law, indicating protective oxidation. The Ti(Al,O)/Al_2O_3 coating showed the lowest mass gain while the Ti_3Al/Al_2O_3 coating showed the highest mass gain, with oxidation products at 800 °C in these coatings reported to be TiO_2 and Al_2O_3.

The promising results of Ti based composite coatings for high temperature oxidation resistance, initiated an extension of the work on these coatings to investigate their performance against attack by molten aluminium and their possible application as a coating on aluminium die casting dies and dummy blocks used in aluminium extrusion. This made the evaluation of the performance of the coatings against a molten aluminium environment very important.

It is reported in the literature that an immersion test/dip test is suitable for assessing coating performance as part of coating selection and development for die casting and extrusion applications [5]. In the present study, an immersion test in liquid aluminium

was designed to study the physical nature of the attack on the coating and substrate and to evaluate the weight loss of coated samples with time (reaction kinetics). This step is very important for preliminary screening of the coating for further and more extensive testing. The immersion tests used in this study provided the soldering evaluation of the composite coatings when an Al (601) melt comes into contact with coated and uncoated H13 tool steel specimens. Thermal shock resistance is also very important for applications where extreme temperature cycling occurs. Adequate thermal-shock resistance in protective coatings, i.e., the capacity to withstand without fracture, the stresses which develop during temperature changes, is an important consideration in the development of a protective coating, designed for applications in the Al processing industry. It is stated that in addition to the thermo-elastic stresses which develop during thermal shock, the coatings undergo additional stresses due to the differences in the thermal expansion coefficients between the coatings and the base. The stresses cannot be avoided because it is not possible to have two different materials with the same coefficients of thermal expansion over a wide temperature range [6]. Because of the thermal expansion mismatch between the coating and substrate, cracking and coating spalling can occur under thermal and mechanical loading. Surface cracking is one of the major failure mechanisms that significantly affect coating life. In this study, the Ti(Al,O)/Al_2O_3 and TiAl/Al_2O_3 composite coatings were evaluated for their resistance to thermal shock as a result of thermal cycling, in which coated steel samples were repeatedly held for half an hour at 700 ± 10 °C in molten aluminium, followed by a water quench. The number of cycles to failure of the composite coatings during thermal shock experiments gives an indication of their thermally cycled life time.

For the industrial trials of the coatings, a dummy block (made of hot worked H13 tool steel) used in an aluminium extrusion process at Fletcher Aluminium, Auckland was tested as an industrial application of the coating. The role of a dummy block is critical in extrusion because when extrusion begins, the ram and stem push the dummy block through the container. This extrudes the softened alloy through the die. The sticking of aluminium onto the dummy block is a serious problem, especially when using the softer alloys, and with larger billets. Boron nitride lubricants are most commonly used to address this problem. The main aim of these trials was to evaluate the performance

of the coating under actual working conditions such as under high pressure and temperature.

A Ti(Al,O)/Al_2O_3 (A2) composite coating was selected for the industrial trial because of its excellent oxidation resistance, high stability against molten aluminium attack and lower weight loss per unit area in an immersion test compared with a TiAl/Al_2O_3 (B2) composite coating. There are a number of advantages to using a Ti(Al,O)/Al_2O_3 (A2) composite coating for a dummy block used in Al extrusion. Firstly, it is a potentially cheaper way of solving a problem caused by Al sticking and soldering to a dummy block, as both the coating production and coating application methods are not costly. Secondly, the worn dummy block can be recoated easily in contrast with the other most commonly applied coating techniques such as PVD. Lastly, a Ti(Al,O)/Al_2O_3 coating has an advantage of not being attacked by the concentrated NaOH during the dummy block cleaning process. There are cases reported of PVD nitride coatings being attacked by caustic solution used for Al removal.

6.2. Results and discussion

6.2.1. Aluminium soldering and corrosion resistance of composite coatings on a H13 tool steel in a molten Aluminium alloy

To understand the nature of Al attack and soldering of composite coatings applied to H13 tool steel, coated specimens were dipped for 1, 3, 6, 22 and 38 hours into molten Al alloy (601) at 700 ± 10 °C followed by air cooling. Cylindrical coupons (63 mm high, 20 mm diameter) were used for an immersion test using a test rig presented in chapter three (fig. 3.4).

The samples were then examined to evaluate the nature and reaction kinetics of the attack. In order to compare the performance of coated and uncoated specimens to Al attack, uncoated H13 tool steel specimens were also dipped into molten aluminium under similar immersion test conditions. Two cross-sectional samples were cut from a single coupon (coated and uncoated) at different positions (within a dipping height of 38mm).

6.2.1a. Soldering/corrosion resistance of a tool steel (H13) substrate to a molten Aluminium alloy

Figure 6.1 shows the photographs of the uncoated H13 coupons as they appeared straight out of the Al melt after various immersion times. A visual inspection of all the coupons confirmed that Al was firmly soldered or strongly bonded with the steel after dipping into the molten aluminium. An uncoated coupon of H13 tool steel after 22 hours immersion (fig. 6.1c) showed severe Al soldering to the sample. Increasing the immersion time to 38 hours gave an interesting result (fig. 6.1d). The uncoated sample was severely eroded due to extensive corrosive attack from the molten Al. This accelerated dissolution and continuous metal loss most likely derived from a detachment of the intermetallic layer, resulting in a significant decrease in diameter.

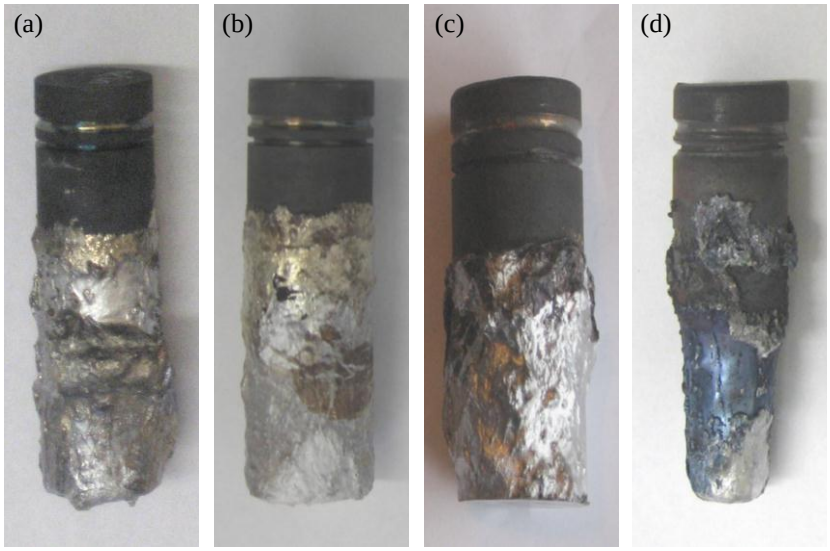

Figure 6.1: Photographs of uncoated H13 tool steel coupons after (a) one hour (b) six hours (c) 22 hours and (d) 38 hours immersion into molten aluminium at 700 °C

There are various definitions of soldering given in the literature. In high pressure die casting (HPDC) industry the term soldering is used to describe a reaction which originates between die and the casting alloy. As a result of soldering the solidified alloy can stick to the die [7]. The chemical reaction between the casting alloy and steel results in the formation of intermetallic phases. Chen et al. [8] referred to this type of soldering as “reactive soldering” or metallurgical soldering in which an intermetallic phase is produced as a result of a solid state reaction between previously formed soldered layers (containing only casting alloy build up) and the tool steel

during subsequent casting cycles. Usually a high metallurgical bond strength results from the formation of these intermetallic layers between the casting and die surface. Some researchers have suggested that soldering can also occur without any formation of intermetallic phases. They name this stage of soldering "non reactive soldering" or casting alloy build up or mechanical soldering [7, 8]. The mechanical keying is caused by molten aluminium entering into die surface defects, such as machining marks, cracks, pits, and holes. Based upon the literature, soldering can therefore be explained in terms of the strong bonding which exists between casting and die surfaces. A chemical or metallurgical reaction, mechanical interlocking or keying, physical adhesion and diffusion phenomena all contribute to strong bonding.

It is not possible to describe the exact nature of the soldering as reactive or non reactive just by visual inspection of the general appearance of the aluminium coated specimens after removal from the molten aluminium, as shown in fig. 6.1. To assess the exact nature of the aluminium soldering, SEM work was carried out on the circular cross-section samples. Figure 6.2 shows aluminium soldering to a steel substrate along with the nature of the attack after various time intervals. An examination of the cross section of the samples after 1 hour, 3 hours 6 hours and 22 hours immersion in molten Al revealed that an intermetallic layer/reaction zone had grown under the built-up layer and had grown completely along the steel interface, fig. 6.2. The formation of an iron-aluminium intermetallic/reaction zone (up to hundreds of microns thick), formed between the steel substrate and molten aluminium has also been reported by other researchers [2, 9-13]. A significant amount of research has been conducted on the nature of these intermetallics [14]. The intermediate zone is reported to consist of successive layers of iron aluminides, typically consisting of two intermetallic layers, namely, $FeAl_3$ directly adjacent to the aluminium alloy and Fe_2Al_5 adjacent to the steel substrate. $FeAl_2$ has also been reported to form between the steel substrate and Fe_2Al_5 intermetallic phase for H13 and H21 tool steels, submerged in liquid A380 alloy [2, 15, 16].

High magnification micrographs (figs. 6.2b, d, g) of the reaction zone between H13 tool steel and molten aluminium alloy after 1, 3 and 22 hours shows that the two different layers of intermetallic were formed. One layer was thin and compact and the other was thick and porous. The formation of similar types of layers is also described

by Yan et al. [9] in the case of H21 tool steel submerged in an A380 Al melt. The immersion test results revealed that after one hour immersion in molten aluminium, a thin compact layer of thickness of about 8-12 μm formed next to the H13 steel and a thick porous layer, with a thickness of about 130 μm, formed next to the aluminium alloy with the solidified casting alloy above this layer.

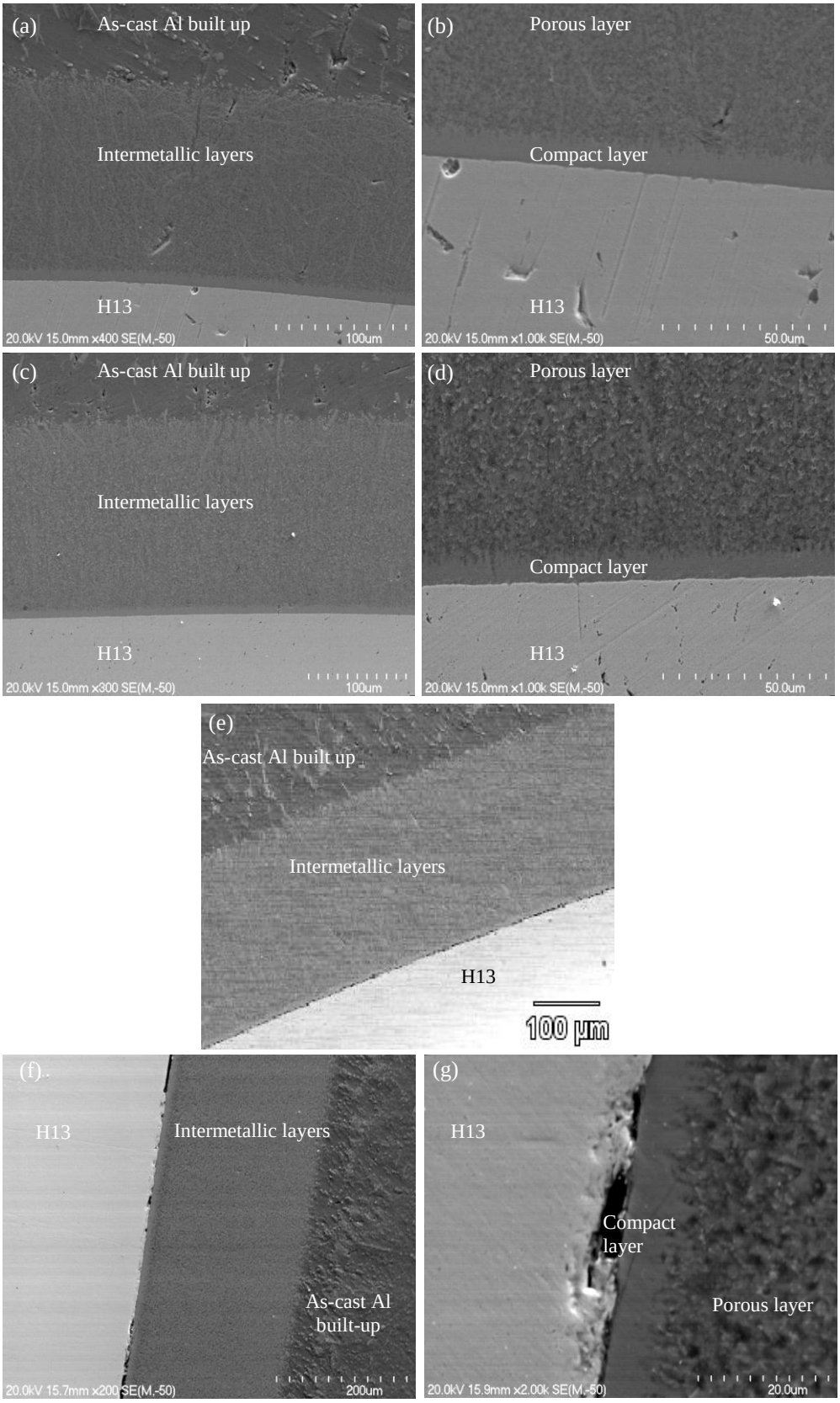

Figure 6.2: SEM micrographs of aluminium soldering to the steel substrate along with the generalized attack morphology of the reaction zone between steel and molten Al alloy after (a, b) one hour (c, d) three hours (e) six hours and (f, g) 22 hours immersion (cross-sections)

The thickness of the thin compact layer remained almost unchanged at about 8-12 µm for all immersion time intervals; however the thickness of the thick porous layer increased with increased dipping time up to six hours immersion in molten aluminium. With an increased dipping time of 22 hours, the thickness of the porous layer remained the same (at about 240 µm) as that for six hours immersion. However, after 22 hours immersion clear gaps appear between the compact layer and steel substrate in some areas (fig. 6.2g). This is evidence of the intermetallic detachment process. Yan [9] described a continuous increase in the thickness of the porous layer in an H21 steel after immersing into an A380 molten alloy for 9 hours. The thicknesses of the intermetallic layers after different immersion times are listed in table 6.1.

Table 6.1: Thickness of intermetallics layers with immersion time

Immersion time (hours)	Thickness of compact thin layer (µm)	Thickness of porous thick layer (µm)
1	8-12	130
3	8-12	170
6	8-12	240
22	8-12	240

An EDAX analysis (four measurements) of the thin and thick layers listed in table 6.2. indicates that these layers most likely consist of Fe-Al intermetallic compounds respectively. The errors in the EDAX analysis results are calculated by considering the standard deviation of four separate measurements.

Table 6.2: Composition of intermetallic layers by EDAX analysis

Intermetallic layers	**Al** **At%**	**Fe** **At%**	**Possible intermetallics**
Compact thin layer	77.44 ± 0.71	22.56 ± 0.71	Fe_2Al_5 with H21 and H11 steel [2, 15]
Thick porous layer	86.22 ± 1.23	13.78 ± 1.23	Al rich Al-Fe intermetallic $FeAl_2$, Fe_2Al_5 with H11 [15], Fe_3Al with H21 steel and A380 melt [2]

X-ray mappings of the steel (fig. 6.3) after three hours immersion in molten Al clearly confirmed that a reaction zone consisting of Fe and Al intermetallics formed between the built up casting alloy layer and the steel substrate.

In the literature, casting alloy build up and the formation of intermetallic phases are described as contributing factors towards Al soldering in tool steel dies. Chu et al. [17] reported that under the right conditions an Al rich soldering layer may form over the intermetallic layer. It has been suggested that the interfacial intermetallic phases form first and then cause the casting alloy to adhere to the steel surface [11]. However recent work by Chen et al. [18] suggests that firstly layers of the casting alloy build on the die and subsequently interfacial phases nucleate between the tool steel die and the casting alloy layer. Han et al. [19] reported that the formation of an interlocked structure consisting of an aluminium–rich phase and an intermetallic phase between the die and the casting alloy, is responsible for joining the casting to the die. According to this, it is the existence of the aluminium-rich phase in conjunction with and situated in between the intermetallic phase that plays the role of glue, joining the casting to the die.

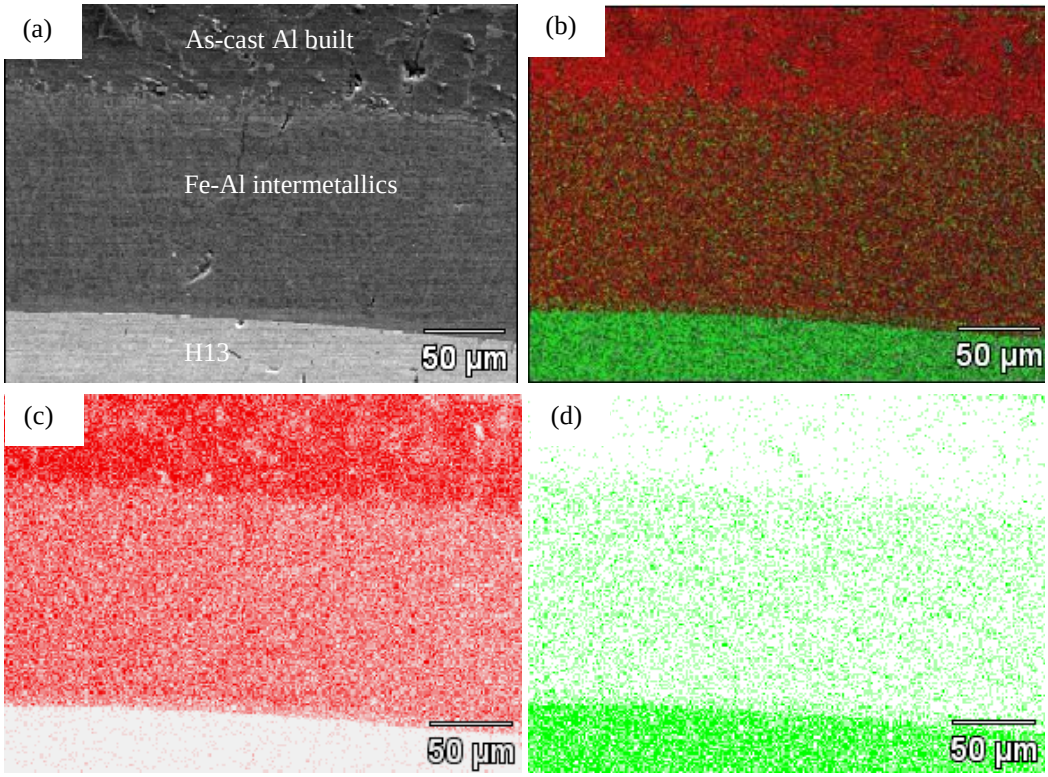

Figure 6.3: Elemental mapping of H13 samples after three hours immersion in molten aluminium. (a) SEM micrograph (b) Al and Fe maps overlay on SEM image (c) elemental map of aluminium and (d) elemental map of Iron

Metallographic analysis of the cross-sections of uncoated steel specimens confirmed that the nature of soldering in the case of uncoated H13 steel is entirely "reactive" as a reaction had taken place between the aluminium alloy and an H13 tool steel. This resulted in the formation of intermetallic compounds and is consistent with the results of Yu et al. [12].

6.2.1b. Soldering/corrosion resistance of a composite coating (A2) Ti(Al,O)/Al_2O_3 to molten Aluminium alloy

The soldering evaluation of an HVOF sprayed Ti(Al,O)/Al_2O_3 (A2) composite coating on H13 tool steel (as-sprayed) was carried out with molten Al for various time intervals. The role of carbon pick up (from the combustion fuel during thermal spraying on the as-sprayed coating was not taken into account during soldering evaluation with molten Al due to the weak reactivity of the Al with carbon below 1000 °C [20]. Figure 6.4 shows the as-sprayed coated coupon (fig. 6.4a) along with SEM micrographs showing the surface morphology prior to immersion in molten

aluminium. The as-sprayed coating clearly indicates a high level of roughness as expected in an HVOF thermally sprayed coating (fig. 6.4b). The average surface roughness of the coating was about Ra 5.56 µm. A high magnification micrograph (fig. 6.4c) of the as-sprayed composite coating clearly indicates the presence of intra-splat cracks, intra-splat porosities and fine debris.

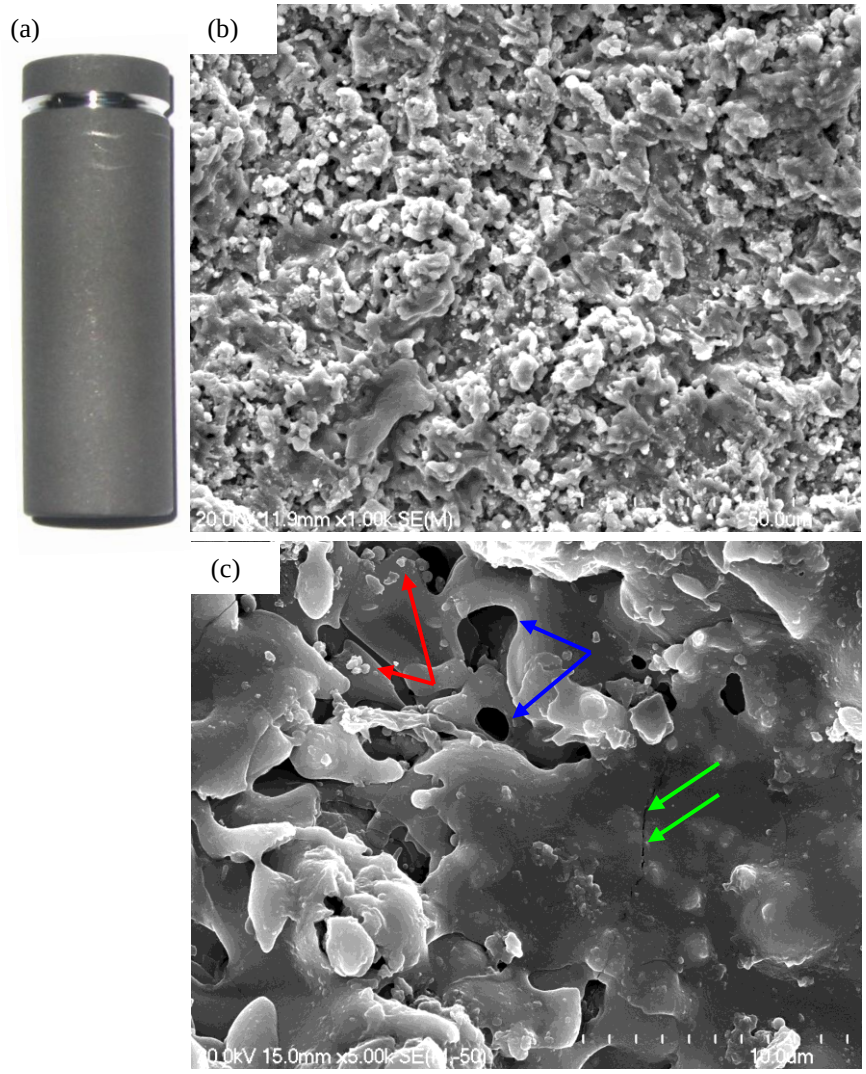

Figure 6.4: (a) Photograph of Ti (Al,O)/Al_2O_3 HVOF coated coupon before immersion in molten Al (b) as-sprayed coating morphology (c) intra-splat cracks (green arrows), intra splats porosities (blue arrows) and splashes of fine debris (red arrows) in as sprayed coating

Photographs of the coated coupons immersed into the molten aluminium at 700 ± 10 °C after 1, 3, 6, 22 and 38 hours are shown in fig. 6.5. After removal from the melt it was observed that, all the HVOF coated samples had to a greater or lesser degree some aluminium attached to the coatings. This is commonly described in literature as casting alloy build up. The casting alloy build up was compressed in some places on

the coupons while in others it was pulled away or absent from the surface (marked by rings). This is more clearly confirmed in the case of the coated coupon after 22 hours (fig. 6.5d) and 38 hours (fig. 6.5f) immersion in the molten aluminium where the previously attached and solidified Al was pulled away from the bottom ends of the coupons. The areas on the cylindrical coupons where aluminium strongly adhered to the coating could be the result of mechanical interlocking of aluminium with the coating due to its high surface roughness, or as a result of a chemical reaction between the as cast alloy and the steel/coating.

The Al layer formed on the coupon immersed for 22 hours (fig. 6.5e) was easily chipped off (unaided) when cross sectional samples (for microscopic analysis) were cut from the coupon. This is an indication of weak bonding or adherence between as cast aluminium and the coating. The removal of the as cast aluminium layer from this coupon revealed that the coating was fairly stable, even after 22 hours immersion in molten Al. However, in the case of uncoated H13 tool steel (fig. 6.1c) immersed into molten Al for the same time, cross-section samples showed that the aluminium had strongly adhered to the steel. This was due to the metallurgical/chemical nature of its bonding (due to the formation of Fe-Al intermetallic phases) with the casting Al alloy (fig. 6.2f). In the literature [21, 22] the high surface roughness of the coating is described as one of the contributory factors towards higher Al soldering and corrosion. Guliza et al. [22] described an increase in the amount of soldering on TiN PVD coated pins with increased surface roughness of the core pins/substrate (Ra increased from 0.17µm-to 0.59 µm). Coatings growing on rough surfaces feature high defect density and the corrosion initiates at the defects sites. The level of surface roughness of the H13 substrate (Ra 5.56) involved in this study is considerably higher compared with the substrate used in a TiN PVD coating. The high surface roughness of the substrate is required by the thermal spraying method for better coating adhesion. The high surface roughness of the substrate in this study definitely played a significant role in increasing the defect density of the coating surfaces and these defects lead to more cast alloy build up. The weak bonding between as cast aluminium and the composite coating (A2) is likely due to the mechanical interlocking as a result of high coating surface roughness (Ra 5.56 µm).

(a) (b) (c) (d) (e) (f)

Figure 6.5: Photographs of Ti(Al,O)/Al_2O_3 coated coupons after (a) one (b) three (c) six (d, e) 22 and (f) 38 hours immersion into molten aluminium at 700 °C

After 38 hours immersion in molten Al the coated coupon (fig. 6.5f) shows little attack from the molten Al compared with the uncoated H13 tool steel coupon (fig. 6.1d) which was immersed for a similar length of time. The dimensional stability of the coated coupon is evidence of coating stability and protection conferred to the steel substrate underneath. However the presence of some metallic macro-particles on the coupon indicates the possibility of some molten Al attack.

For a clearer understanding of the nature of the soldering with a Ti(Al,O)/Al_2O_3 composite coating (A2), whether it is reactive/chemical or non reactive/mechanical, cross-sectional samples were studied using SEM.

An SEM image (fig. 6.6) of a coated coupon after one hour immersion into molten Al shows an area of the coating where cast alloy build up is strongly adhered to the coating. This is likely due to the mechanical interlocking between the coating and aluminium as no chemical reaction was observed at the interface between the coating and aluminium.

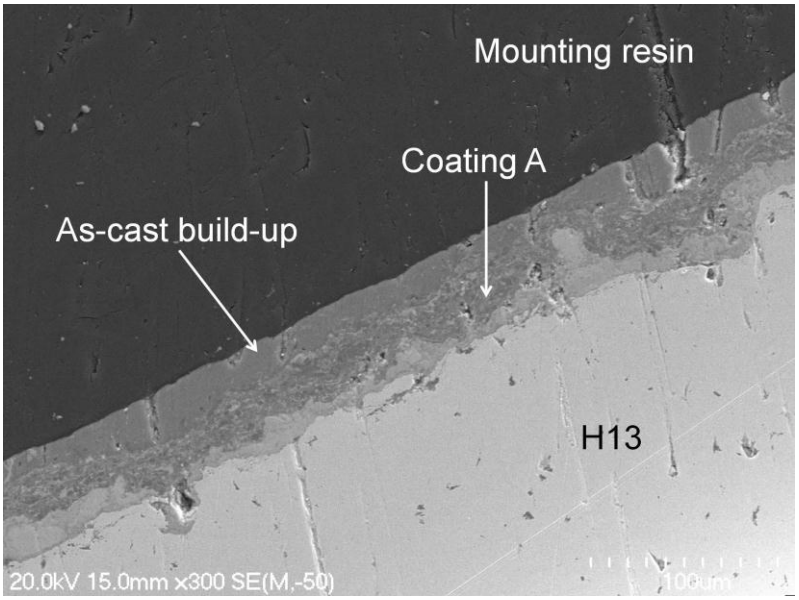

Figure 6.6: Cross-Sectional image of composite coating A2 after one hour immersion in molten Al

The cross-section micrographs of the Ti(Al,O)/Al_2O_3 (A2) coated coupon prior to the immersion test confirmed the presence of a continuous coating (fig. 6.7a) of thickness of about 20-35 µm on the substrate surface. The variation in coating thickness (fig. 6.7b) is a consequence of using a manual spraying technique (HVOF).

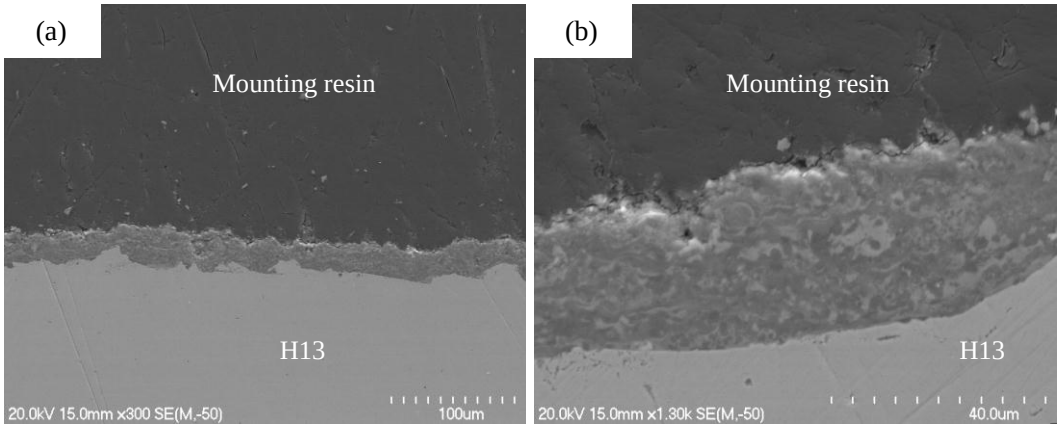

Figure 6.7: Cross-sectional images of coating (A2) prior to an immersion test; (a) coating continuity (b) thickness variations

Figures 6.8, 6.9, 6.10, 6.11 and 6.12 show the micro-structural features in a Ti(Al,O)/Al_2O_3 (A2) composite coating, sprayed onto a Ti bonding coat, after 1, 3, 6, 22 and 38 hours immersion in molten Al at 700 ± 10 °C. The cross-sectional micrographs clearly demonstrate the nature of molten Al attack with the composite coating. Localized attack was observed on the composite coating after immersion in

molten Al, for all exposure times. However; most of the coating was completely unaffected by the liquid aluminium exposure.

The cross sectional images of the coated coupons after one, three and six hours immersion (figs. 6.8, 6.9, 6.10) in molten aluminium show that a small amount of cast aluminium alloy had built up on the coating surface with a gap between the Al and the surface. This cast alloy build up is similar to that reported in the literature for PVD TiN, CrN and TiCN coatings [22]. The gap which separates the cast aluminium alloy from the coating is an indication that the coating is not wetted by molten aluminium. This is also a desirable condition for die casting coatings. When samples (figs. 6.5e, f) for cross-section examination were cut from the coupons, the adhered Al fell away. This is a good indication that the coating is not wetted by molten Al (figs. 6.11a, 6.12a).

Figures 6.8b, 6.9b, 6.10b, 6.11b, 6.12b show the nature of the attack and the morphology of corrosion pits for different exposure times to molten aluminium. Hemispherical pits with diameters substantially larger than the thickness of the coating were observed after 1, 3, 6 and 22 hours immersion. However the appearance of the soldering changed from localized hemispherical pitting to a more continuous deposit after 38 hours immersion.

The process of pit nucleation involved the formation of Fe-Al intermetallic compounds due to the inter-diffusion and reaction between the steel substrate and molten aluminium. The attack is likely to concentrate on an existing pit once the pit nucleates. Aharonov et al. [21] have suggested that the stress associated with a volume increase due to the formation of intermetallic compounds causes the coating to peel from the steel and thereby exposing the steel substrate to further corrosion. The change in soldering behaviour from hemispherical attack to a more continuous layer after 38 hour immersion (fig. 6.12b) is due to peeling of the coating as result of localized attack on the steel substrate and consequently Al solders to the steel.

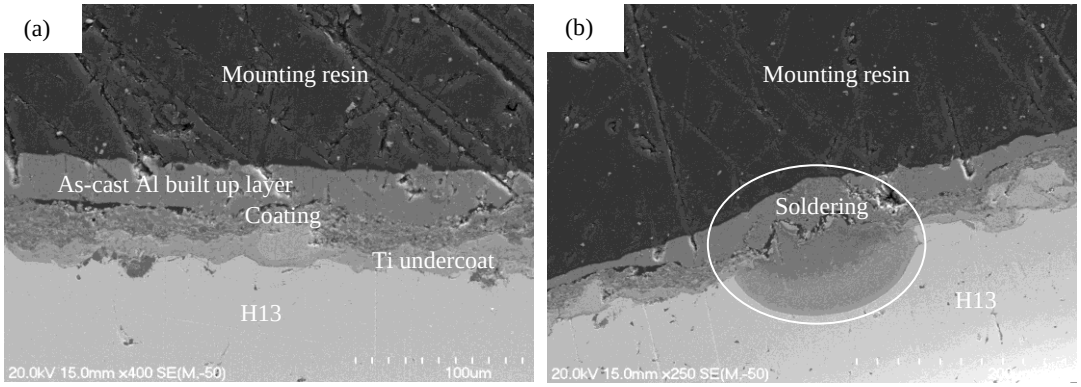

Figure 6.8: Cross-sectional images of composite coating (A2) after one hour immersion in molten Al (a) un-attacked coating (b) Al soldering with steel/attacked region

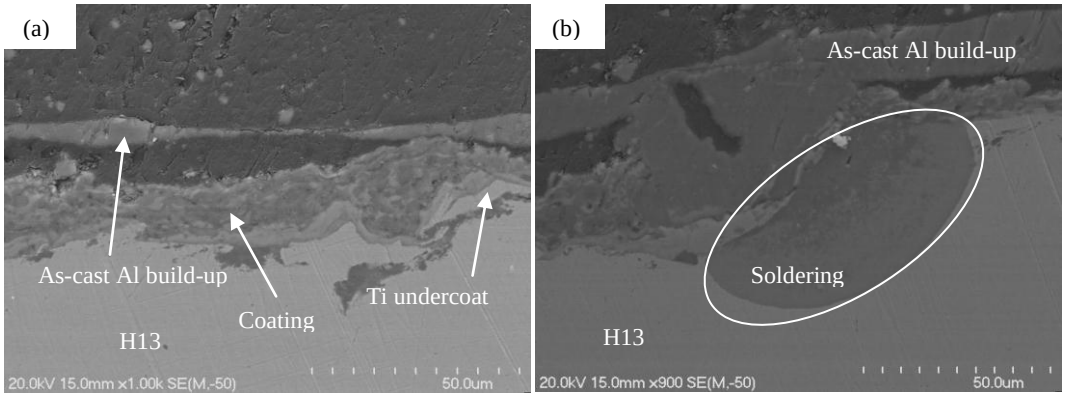

Figure 6.9: Cross-sectional images of composite coating (A2) after three hours immersion in molten Al (a) un-attacked coating(b) Al soldering to steel/attacked region

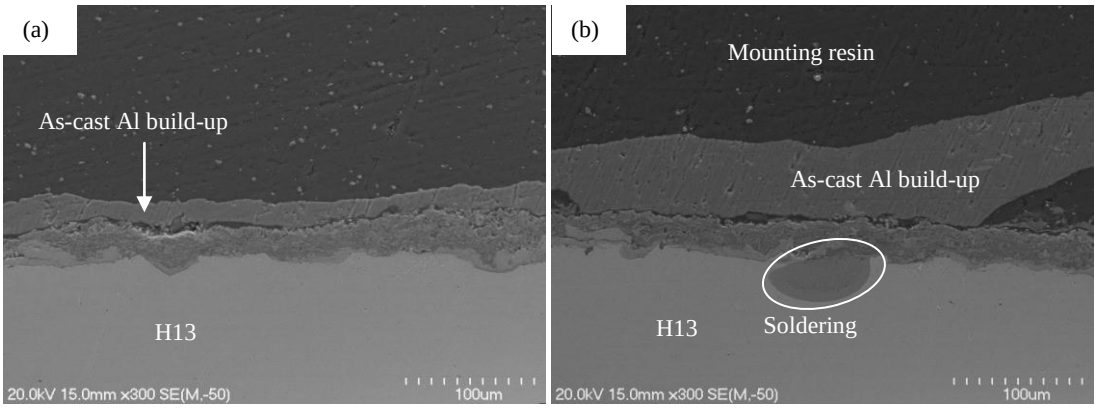

Figure 6.10: Cross-sectional images of composite coating (A2) after six hours immersion in molten Al (a) un-attacked region (b) Al soldering to steel/attacked region

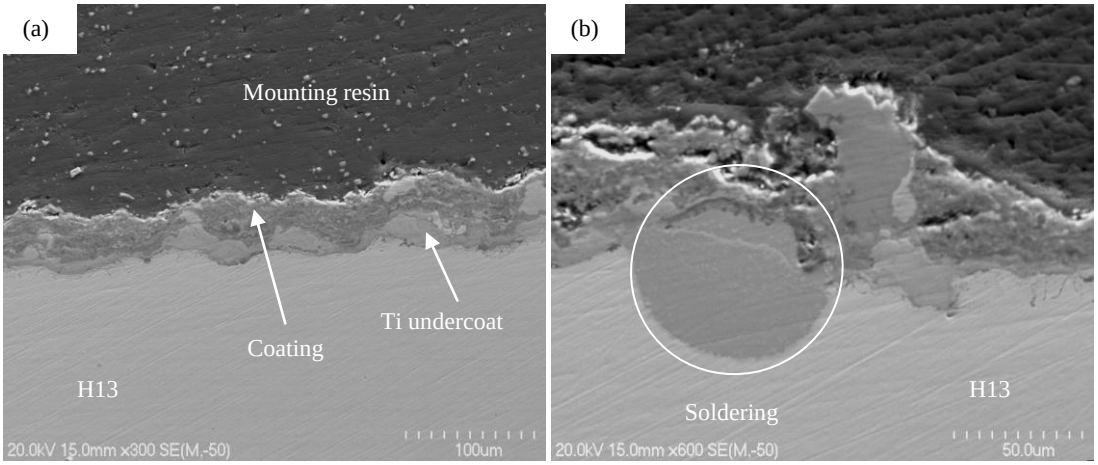

Figure 6.11: Cross-sectional images of composite coating (A2) after 22 hours immersion in molten Al (a) un-attacked region (b) Al soldering to steel/attacked region

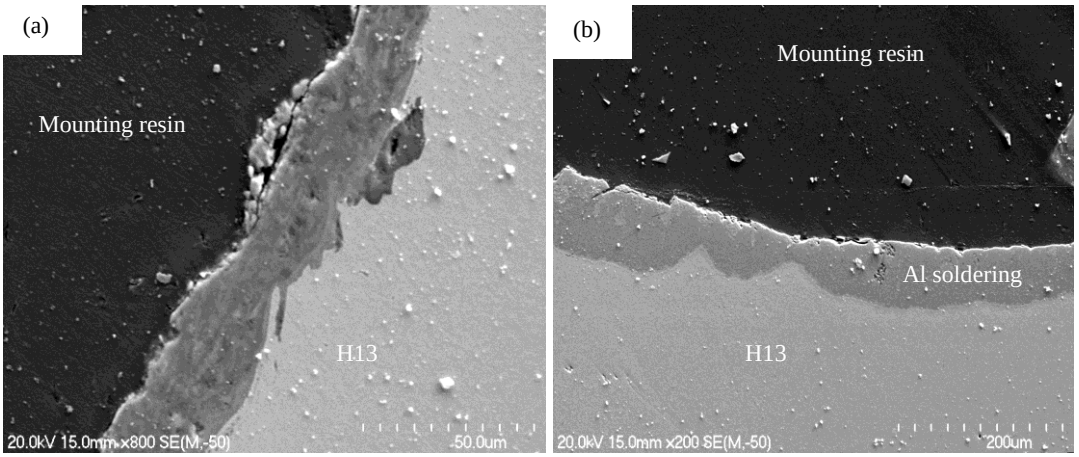

Figure 6.12: Cross-sectional images of coating (A2) after 38 hours immersion in molten Al (a) un attacked region (b) Al soldering with steel/attacked region

It is likely that molten Al penetrates through the coating defects and reacts with the steel substrate, and fractures the composite coating. Similar findings have been reported by other researchers [23, 24] for Cr_2O_3/CrN, CrN/TiN coatings for aluminium die casting applications. X ray mapping was performed to assess whether Al penetration through the coating plays any role in the observed corrosion. It is very clear from the X-ray mappings (fig. 6.13) that Al penetrated through the coating and attacks the steel substrate, resulting in the formation of Fe-Al intermetallics.

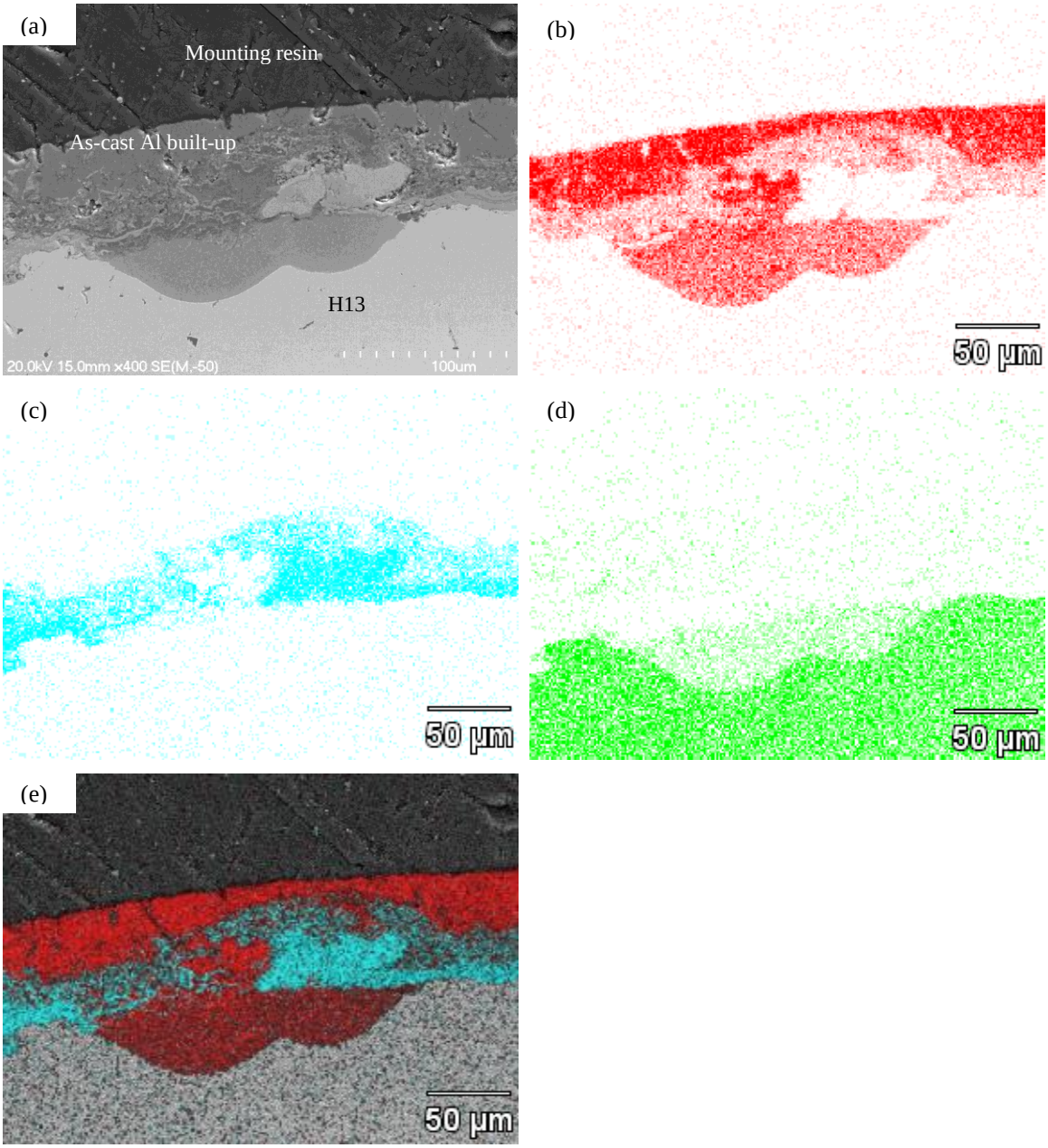

Figure 6.13: (a) SEM micrograph of Al soldering after one hour immersion in Al with elemental maps of (b) Al, (c) Ti, (d) Fe and (e) Ti, Al maps overlay on SEM image

This is possible if there are voids in the coating which allows Al penetration. Local coating defects, such as porosity and micro cracks are most likely the contributing factors causing aluminium penetration into the coating. Furthermore, in a few samples there were some un-melted Ti particles in the primary Ti coating layer. Poor bonding of these particles at the interface of steel substrate and composite coating was also found. Poorly bonded Ti particles together with other coating defects seem to be the major reason for the localised nature of attack on H13 tool steel.

An SEM image of a cross-section of the composite coating with an Al soldered region (hemispherical pit), after 6 hours immersion in molten Al, is shown in fig. 6.14. The image shows that in the Al soldered region there are three distinct zones. An outer zone consisting mainly of solidified aluminium (as-cast Al build up), an intermediate porous zone with variable thickness (max thickness of about 50 µm) adjacent to the as-cast aluminium, consisting of Al (85.53 at%) and Fe (14.47 at%) and an inner compact zone with a thickness smaller than the intermediate zone (max thickness of about 36 µm) with Al (69.56 at%) and Fe (30.44 at%).

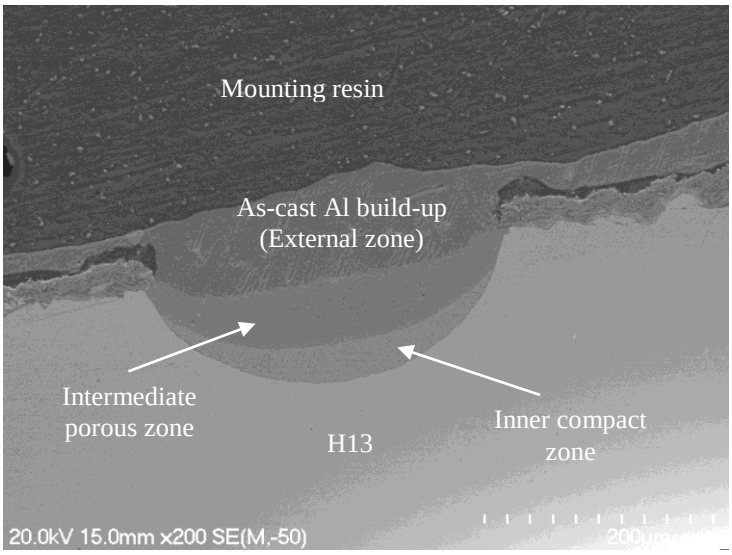

Figure 6.14: Cross-sectional image of composite coating (A2) with Al soldered region (hemispherical pit) after six hours immersion in molten Al

A non uniform coating thickness may be a reason for such localized attack on the steel substrate. Areas where the coating is thinner are the locations where coating defects are likely to be more easily attacked by the molten aluminium than defect free thicker areas. Aharonov et al. [21] reported that a better surface finish and thicker coatings yield better corrosion protection in molten aluminium. Corrosive wear in liquid aluminium may be affected by other factors such as a reaction between the coating and molten Al.

EDAX analysis (table 6.3) of various phases in the coating after six hours immersion in molten aluminium (fig. 6.15) confirmed that the constitution of these phases did not change considerably. The elemental concentrations of particle and light phase after six hours immersion are almost comparable with their concentrations prior to immersion

in aluminium (table 5.6). However a darker phase, after six hours immersion, shows some change in elemental concentration. An increase in oxygen and decrease in Al concentration was observed within this phase after six hours immersion in aluminium. This suggests that the coating is fairly stable in molten aluminium.

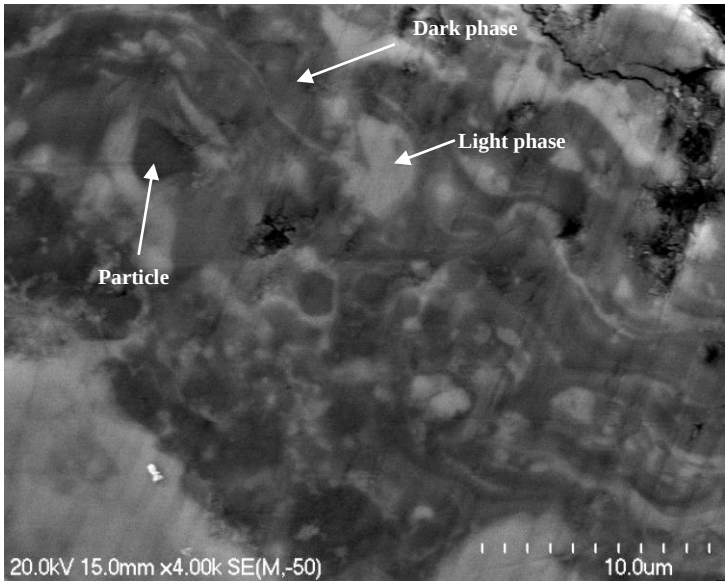

Figure 6.15: Composite coating (A2) phases after six hour immersion in molten aluminium

Table 6.3: EDAX analysis (at.%) of Ti(Al,O)/Al_2O_3 coating after six hours immersion in molten aluminium

Phases	O (at%)	Al (at%)	Ti (at%)	Possible phases
Light phase	20.99	16.52	62.48	Ti(Al,O)/Ti(O)/Ti_3Al(O)
Particle	55.72	41.34	2.93	Al_2O_3 with small amount of TiO
Dark phase	54.78	25.06	20.15	Al rich Al-Ti oxide likely $(Al_2Ti)O_5$ or Al_2O_3/TiO

The coating stability after longer immersion times of 22 hours and 38 hours is also an indication that the coating did not react with molten aluminium.

There is evidence from the literature that Ti(Al,O) and alumina phases in the coating are highly stable and resistant to molten aluminium attack. Ti has very low solubility (0.2% at 700 °C) in molten aluminium whereas alumina is not wetted by molten aluminium below 1000 °C [1, 25].

6.2.1c. Soldering/corrosion resistance of a composite coating (B2) $TiAl/Al_2O_3$ in molten Aluminium alloy

A similar study to that described above for a $Ti(Al,O)/Al_2O_3$ in-situ composite was carried out for H13 tool steel coupons coated with a composite coating $TiAl/Al_2O_3$ (B2). To study the nature of Al attack/soldering with the composite coating $TiAl/Al_2O_3$ (B2), the coated samples were immersed in molten Al at 700 ± 10 °C for 1, 3, 6, 22 and 38 hours.

Fig. 6.16a shows the coated coupon prior to molten aluminium immersion tests. The composite coating exhibits a high level of surface roughness (fig. 6.16b) with an average value of about Ra 8.02. The as-sprayed coating clearly indicates (fig. 6.16c) the presence of intra-splat cracks, intra-splat porosities and fine debris.

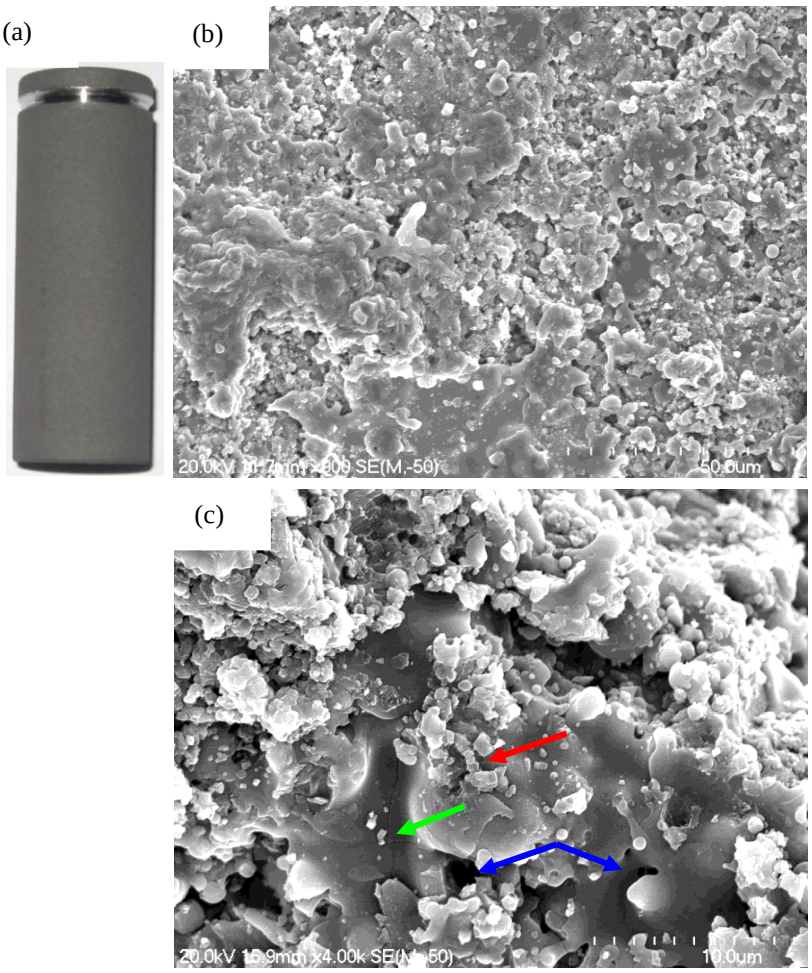

Figure 6.16: (a) Photograph of $TiAl/Al_2O_3$ coated coupon before immersion test (b) as-sprayed coating morphology (c) intra-splat cracks (green arrow), intra-splat porosities (blue arrows) and splashes of fine debris (red arrow) in the as-sprayed coating

Figure 6.17 shows images of the $TiAl/Al_2O_3$ coated coupons after immersion in molten aluminium at 700 ± 10 °C for various time intervals. On removing coupons from the melt it was noticed that an Al layer had built up (as-cast alloy build up) on all the coupons. The built up Al layer, which was firmly attached to the cylindrical coupons, was likely caused by the high surface roughness (Ra 8.02) of the as sprayed coating. For the coupon immersed for 22 hours, the Al layer was easily detached from the coated coupon (fig. 6.17d) while cutting cross sectional specimens from this coupon for metallographic examination. As in the case of the $Ti(Al,O)/Al_2O_3$ coating this is most likely due to the weak bonding (mechanical interlocking) between the coating surface and the as-cast metal. However, coated coupons showed a few places with Al soldered to the coating. The coupon immersed for 38 hours showed little Al build up because a large portion of the built up layer became detached during air cooling after removal from the melt. However the presence of some metallic macro-particles on the bottom surface indicated a degree of molten Al attack on the coating. The coupon showed little Al attack and more dimensional stability compared with the uncoated H13 coupon immersed into the molten aluminium for the same time (fig. 6.1d).

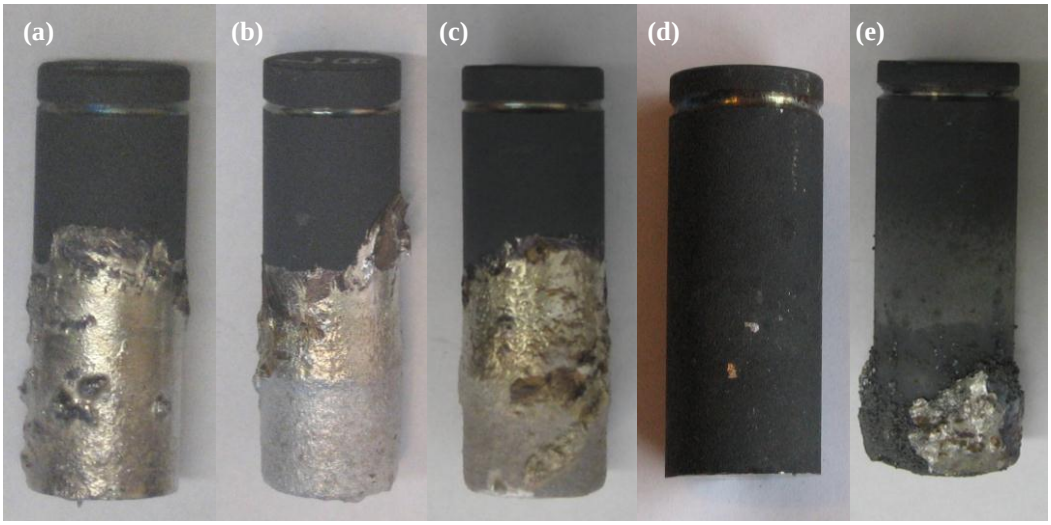

Figure 6.17: Photographs of coated coupons after (a) one (b) three (d) six (d) 22 and (e) 38 hours immersion in molten aluminium at 700 °C

A cross section of the coated coupons prior to the immersion test (fig. 6.18) confirmed that the coating was continuous around the section with a thickness of about 15-25 µm. Under the same spraying parameters the thickness of the coating was less than

that of the A2 coating (20-35 µm) and the surface roughness was higher than that for coating A2. The possible reasons for the variation in coating thicknesses and surface roughness under similar spraying parameters have been discussed in chapter 5.

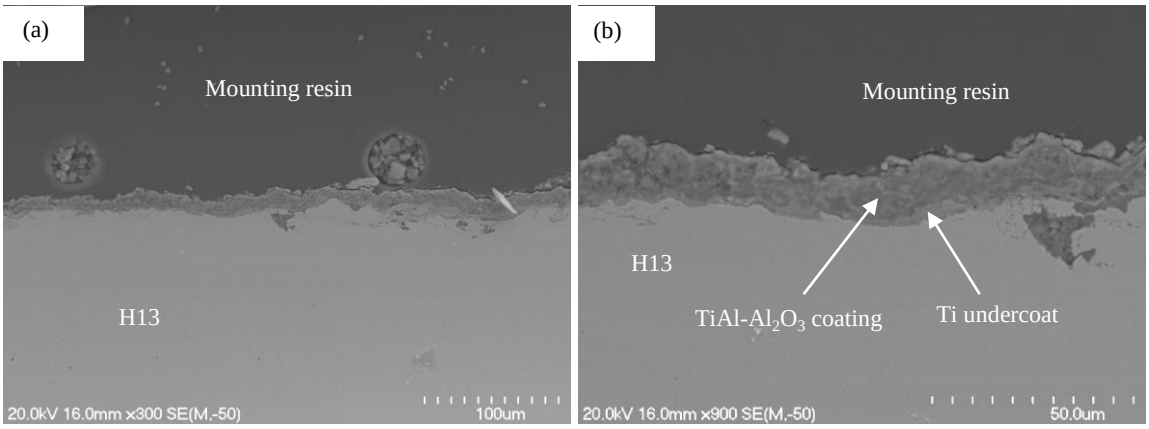

Figure 6.18: Cross-sectional images of coating (B2) prior immersion test (a) coating continuity (b) thickness variations

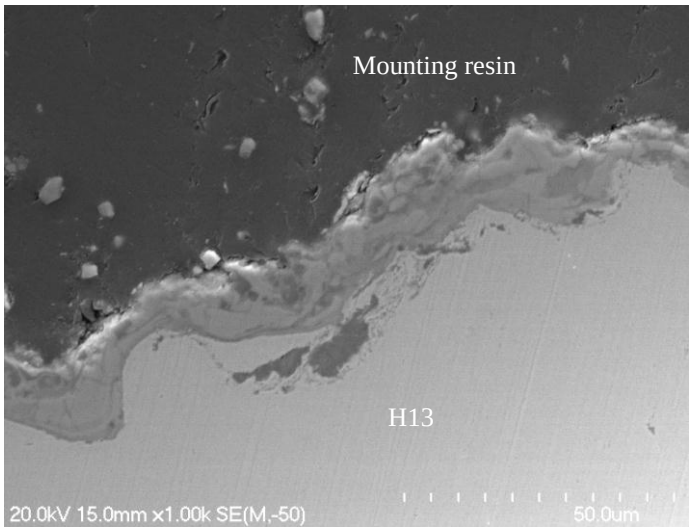

Figure 6.19: Cross-sectional image of composite coating (B2) after one hour immersion in molten Al

Figure 6.19 shows a cross section image of the composite coating B2 with a Ti undercoat after one hour immersion in molten aluminium. A thin patchy composite coating (topcoat) can be seen over the Ti under coat. The patchy appearance of the composite coating (topcoat) over the Ti undercoat can be seen more clearly with the X-ray elemental mapping (fig. 6.20). The thin and patchy coating over the Ti undercoat is an indication that the coating was most likely attacked by molten aluminium. The attack results in removal/dissolution of the coating while leaving the

Ti undercoat un-attacked. The low solubility of Ti in liquid aluminium plays an important role in the stability of the Ti undercoat.

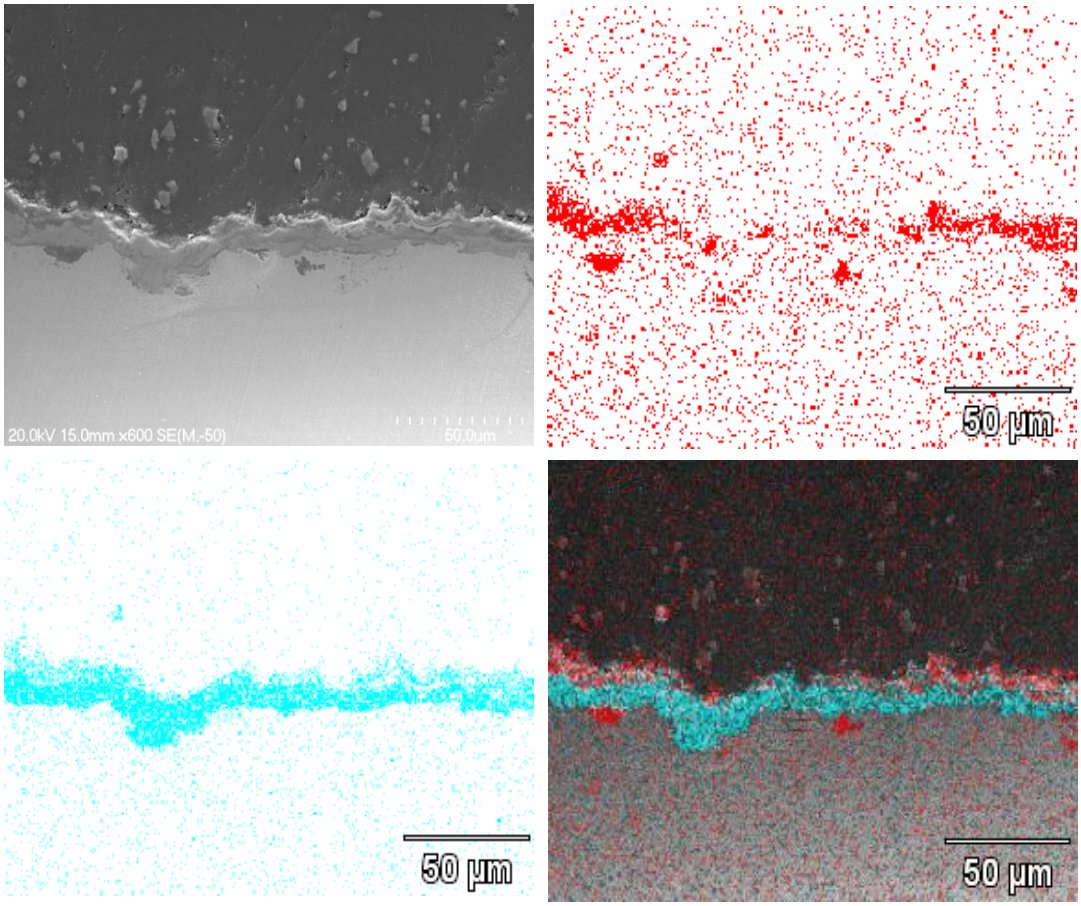

Figure 6.20: Elemental mapping of composite coating (B2) after one hour immersion in molten Al (a) SEM image (b) elemental map of Al (b) elemental map of Ti (c) Ti and Al maps overlay on SEM image

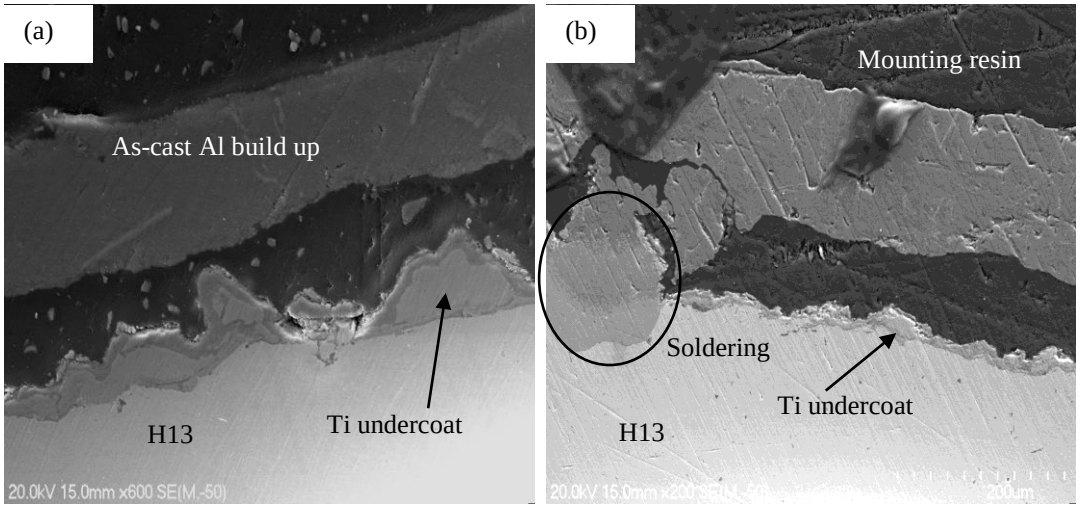

Figure 6.21: Cross-sectional images of composite coating (B2) after three hour immersion in molten Al (a) Ti undercoat without topcoat (b) Al soldered region/attacked region

After 3 hours immersion in molten aluminium, the coated coupon was entirely attacked by molten aluminium as no composite coating (topcoat) was observed over the Ti undercoat (fig. 6.21a). A localized hemispherical pit on the H13 steel substrate (fig. 6.21b) can be seen through the Ti undercoat as a result of molten Al attack after three hours immersion.

The coated coupon after one and three hours immersion did not provide the exact nature of molten aluminium attack/soldering with the $TiAl/Al_2O_3$ composite coating B2 (topcoat), due to possible removal/dissolution of the composite coating as a result of some reaction taking place. However, the nature of the aluminium soldering with the composite coating (topcoat) is much clearer after six hours immersion into molten aluminium (fig. 6.22). It was noticeable that this coated coupon had a considerably higher coating thickness, between 70-130 µm with an average thickness of about 120 µm, which is about six times higher than the coating thickness of the coupons used for one and three hours immersion. This thicker coating was helpful for providing clear evidence of aluminium penetration into the coating B2 (topcoat). The thinner coatings were unable to provide such information. After six hour immersion in molten aluminium (fig. 6.22) the coated coupon showed some attack on certain areas of the coating cross section while the other areas remained unaffected by the attack. The Al penetration in to the coating is likely to have occurred because of defects above or below the area from which the cross-section was taken. A small amount of cast aluminium alloy was built up on the composite coating surface with a gap in between. This is similar to the observation made for of composite coating A2.

Figure 6.23 clearly describes the different levels of Al penetration or Al attack with composite coating B2. After six hours immersion in molten Al, cross-sections of coated samples showed initial, intermediate and a complete Al weld with the coating. Moreover, the presence of very fine pin holes was also identified within the coating. The nature of attack was further confirmed using X-ray elemental mapping and EDAX analysis of the soldered region.

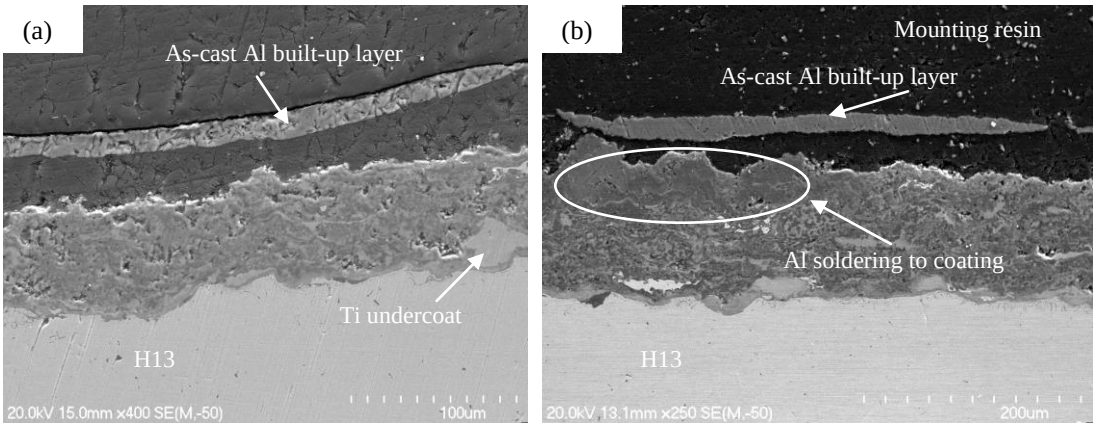

Figure 6.22: Cross-sectional images of composite coating (B2) after six hours immersion in molten Al (a) un-attacked region (b) Al penetration/attacked region

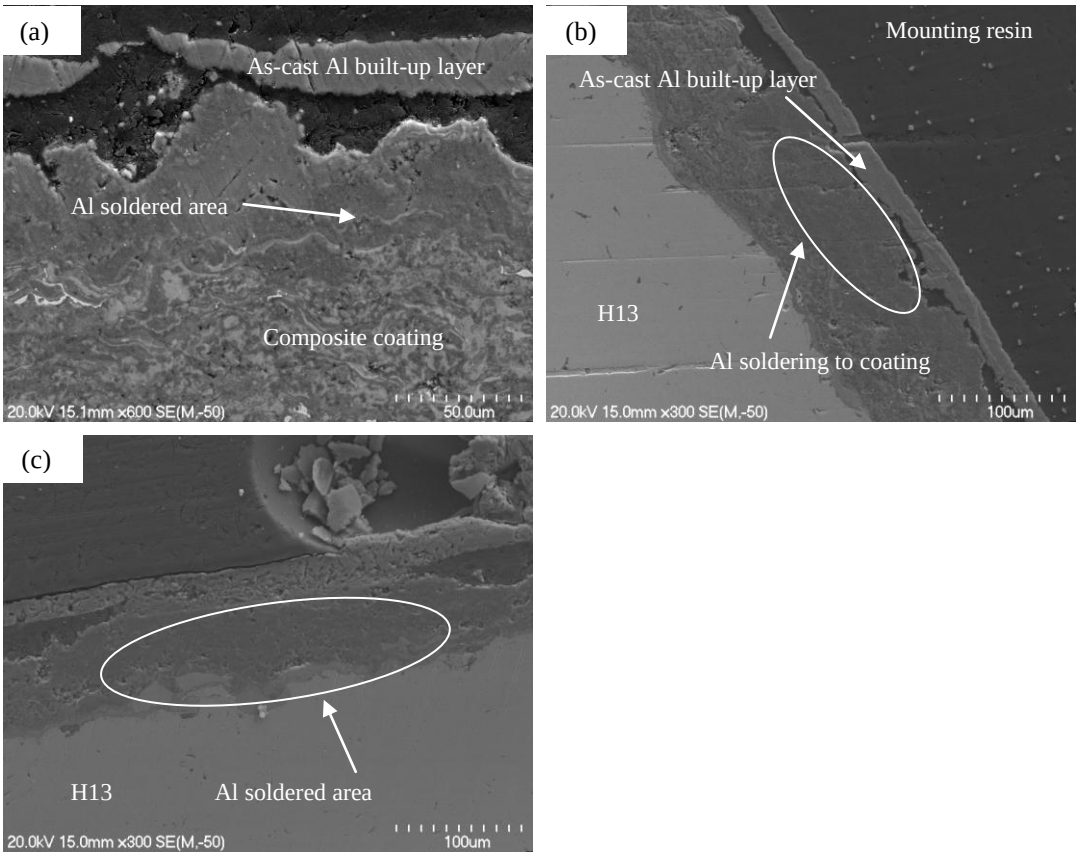

Figure 6.23: Different levels of Al penetration /attack with composite coating B2 after six hours immersion (a) initial (b) intermediate (c) complete Al weld

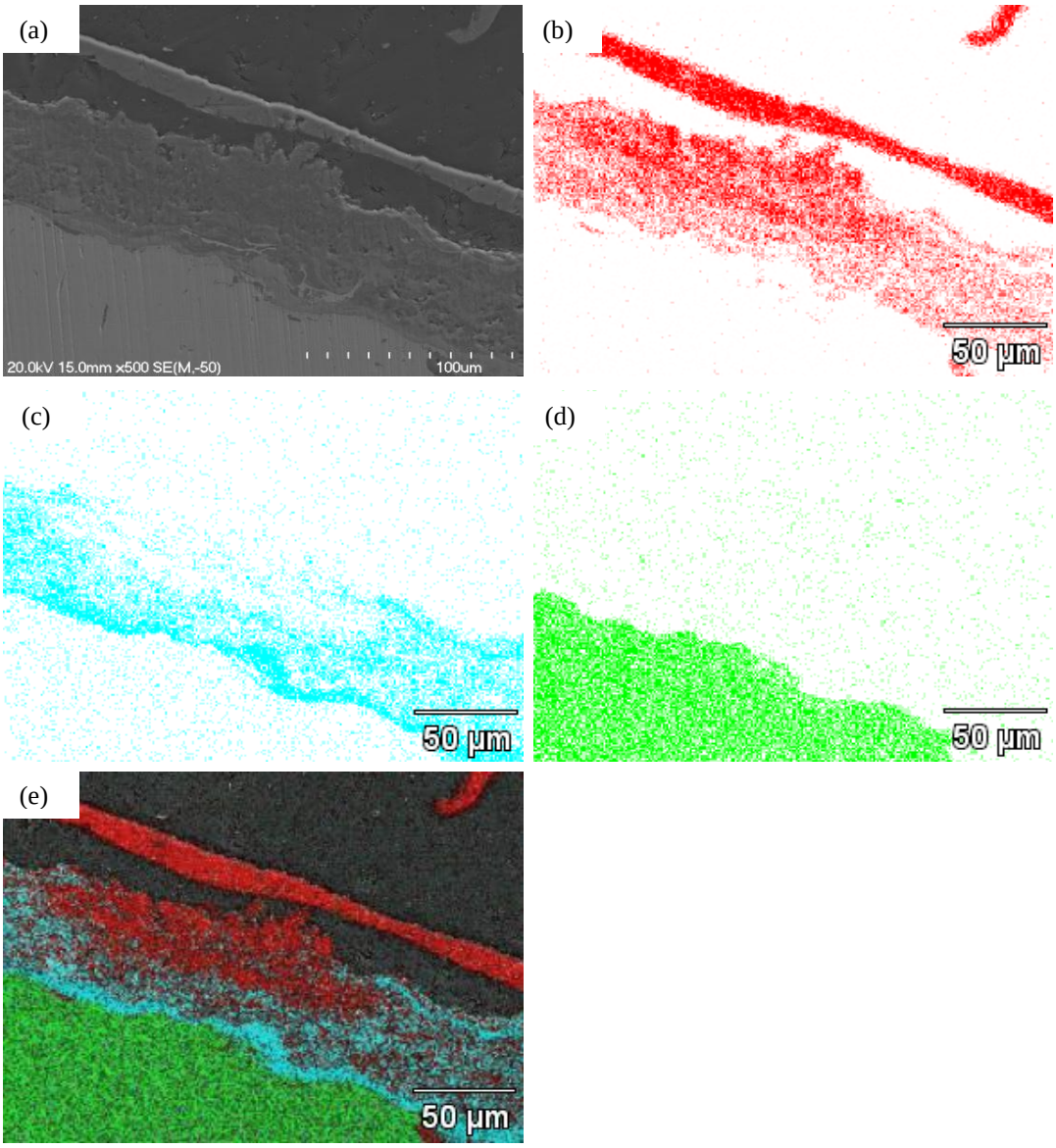

Figure 6.24: X-rays elemental mapping of the solder region after six hours immersion in molten Al. (a) SEM image and elemental maps of (b) Al (c) Ti (d) Fe (e) Al, Ti, Fe maps overlay on SEM image

Elemental mapping (fig. 6.24) clearly indicates that Al has penetrated into the coating. Local coating defects (porosity, micro-cracks as indicated in fig. 6.16c) and a possible coating reaction with the molten Al seem to be contributory factors leading to aluminium soldering The EDAX analysis of the Al soldered area in fig. 6.25 is shown in table 6.4.

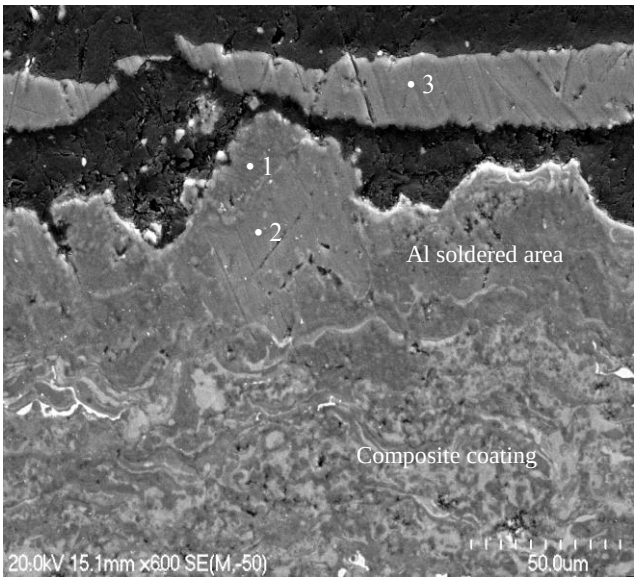

Figure 6.25: Al soldered region

Table 6.4: EDAX analysis of the Al soldered areas in TiAl/ Al_2O_3 coating

Phases	O At%	Al At%	Ti At%	Nature of soldered Area
1	34.40	54.80	10.80	Al-rich Al-Ti oxide
2	6.23	92.28	1.50	Soldered Al
3	6.18	93.68	0.15	As-cast Al built up layer

The microstructure of composite coating B2 after six hour immersion (fig. 6.26) clearly indicates the presence of corrosion pits which are likely due to molten aluminium attack. The corrosion pits are the potential sites for aluminium penetration into the coating.

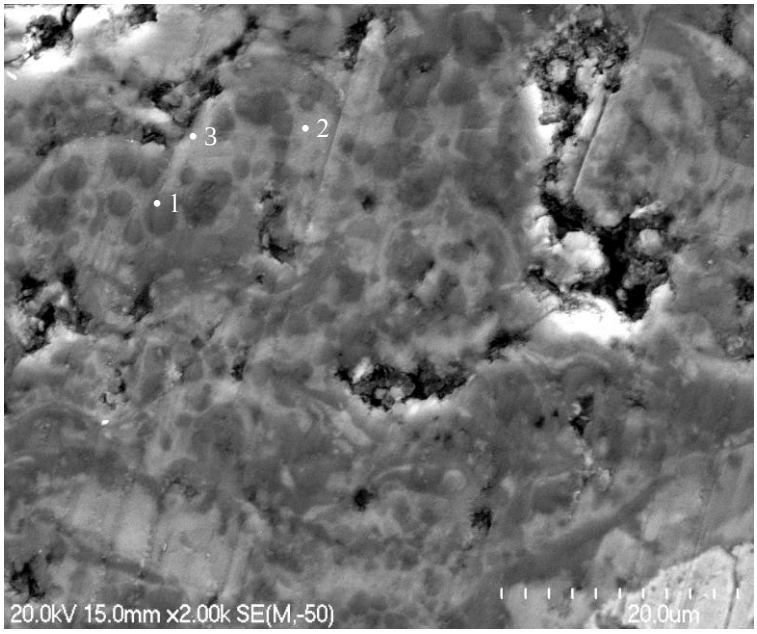

Figure 6.26: The composite coating B2 after six hours immersion in molten aluminium

The EDAX analysis shown in table 6.5 indicates that after six hours immersion in molten aluminium there are small changes in the coating constitution. The alumina particles in the coating showed an increase in titanium concentration, whereas the initial high oxygen concentration of 38.12 at% as observed in the metallic phase (light phase) of the as-sprayed coating was not present in the coating after 6 hours immersion in molten aluminium.

Table 6.5: EDAX analysis of composite coating B2 after six hours immersion in molten Al

Points	**Phase**	**O (At%)**	**Al (At%)**	**Ti (At%)**	**Nature of phase**
1	Particle	48.07	41.33	10.60	Al_2O_3 with TiO
2	Light phase	10.95	44.70	44.35	Ti(O)/TiAl(O)/Ti_3Al(O)
3	Light phase	21.87	34.31	43.82	Ti(O)/TiAl(O)/Ti_3Al(O)

It is very likely that the metallic matrix (TiAl/Ti_3Al) of the composite coating B2 is attacked by molten aluminium. Alumina is a highly stable phase constituent in the coating. It is resistant to attack by molten aluminium and is not wetable by molten aluminium below 1000 °C.

Lou [26] studied the corrosion resistance of TiAl in molten aluminium (6082). After 4 hours exposure at 670-680 °C, corrosion pits and intermetallic $TiAl_2$ formed on the TiAl surface, the latter due to the diffusion of aluminium and titanium. The presence of corrosion pits in the coating microstructure after six hour immersion can be linked with the attack of molten Al on the TiAl phase.

The SEM micrographs of the cross section of the coated sample after 22 hours exposure to molten aluminium are shown in fig. 6.27. A patchy composite coating $TiAl/Al_2O_3$ (topcoat) can be seen over the Ti undercoat even after 22 hours immersion in molten Al. The topcoat ($TiAl/Al_2O_3$) is likely to have been attacked by the molten aluminium, which resulted in its dissolution. Moreover the coated sample showed a few locations with aluminium soldering (fig. 6.27b).

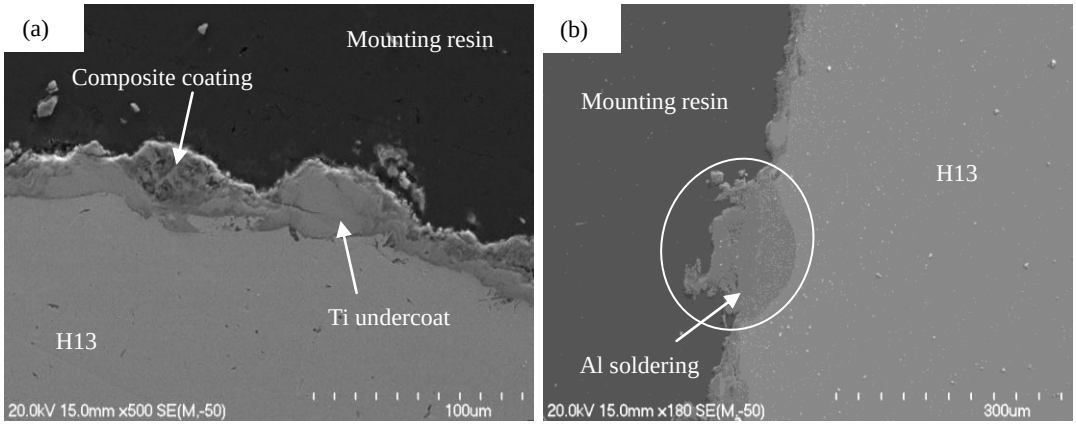

Figure 6.27: Cross-sectional images of composite coating (B2) after 22 hours immersion in molten Al (a) patch coating (b) Al soldering to steel/attacked region.

After 38 hours immersion in molten aluminium, the steel substrate was left with the Ti undercoat only (fig 6.28a). The severity of Al soldering increased after 38 hours immersion as indicated in fig. 6.28b. Moreover, the nature of soldering changed from discrete hemispherical adhesions to a continuous film. This is due to the peeling of the coating as a result of localized attacks on the steel leading to Al soldering to the steel.

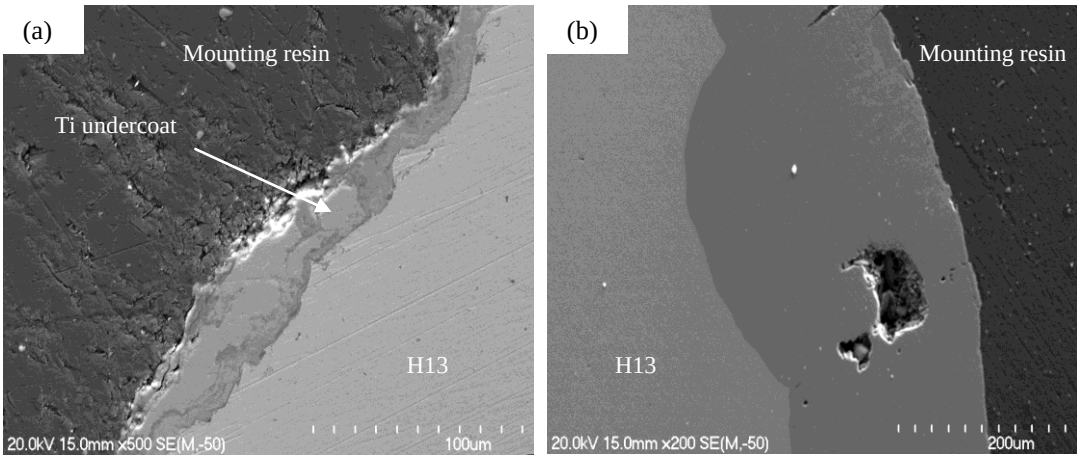

Figure 6.28: Cross-sectional images of composite coating (B2) after 38 hours immersion in molten Al (a) Ti undercoat (b) Al soldering to steel/attacked region

6.2.2. Coatings dissolution/washout evaluation

The dissolution of coatings in molten aluminium was evaluated by determining the weight loss of the coated coupons dipped into molten aluminium for various time intervals. During an immersion test, the coated samples were immersed for ½, 1, 2, 3, 4, 5 and 6 hours into molten aluminium held at 700 ± 10 °C. In order to compare the weight loss of the coated samples with that for uncoated H13 steel, the latter samples were immersed into molten Al for one, three and six hours only. The samples were then removed from the melt and air cooled. The Al layer soldered to the samples was removed by using a 20% NaOH solution. The weight loss per unit area of test coupons was used to report the degree of wash out.

The weight loss of the coupons was determined from the difference in weight before immersion in molten aluminium and after soldered aluminium removal using 20% NaOH solution. The weight loss was normalised and plotted as weight loss per unit surface area against immersion time. The same method was used by other investigators [26-29] to evaluate weight loss caused by exposure to molten aluminium.

Figure 6.29 shows a graph of weight loss of the coated (with coating A2) and uncoated H13 coupons as a function of time. In general observation of coating thickness before and after immersion in molten aluminium showed that there was little change. Because of such smaller weight losses and non-uniform coating

thickness, it was difficult to measure coating dissolution rate from measurements on specimen cross-sections. However, since all the aluminium was removed after NaOH solution, weight loss is attributed to minor changed in coating thickness and localised substrate attack, caused by aluminium penetration through coating defects.

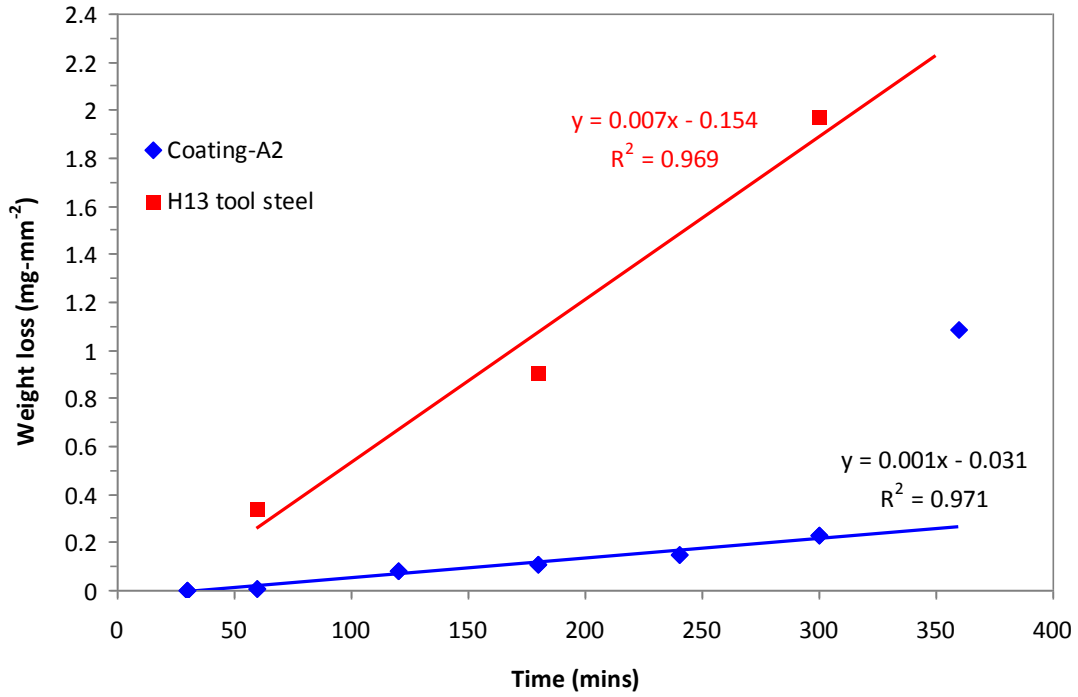

Figure 6.29: Weight loss as a function of time for (a) Ti (Al,O)/Al_2O_3 composite coating (A2) and H13 steel after the immersion test in molten aluminium

Steel samples with coating A2 show a significant reduction in weight loss compared with the uncoated H13 tool steel, so there is a significant improvement in performance using a Ti(Al,O)/Al_2O_3 composite coating A2. The improvement in performance of the coated samples is particularly noticeable up to about 300 minutes exposure to molten aluminium. The weight loss for 360 minutes is not taken into account in the linear trend line calculations. The possible reason for the significant rise in weight loss at 360 minutes is possibly due to the presence of a higher defect density within this coated coupon. A repeated test for this particular time interval (360 min) showed a considerable decrease in weight loss (0.13mg mm^{-2}) for this interval as well.

Figure 6.30 shows an SEM image of coating A2 after 5 hours immersion into molten aluminium and after soldered aluminium removal using NaOH. The image clearly indicates that the coating is fairly stable after 5 hours immersion into molten Al.

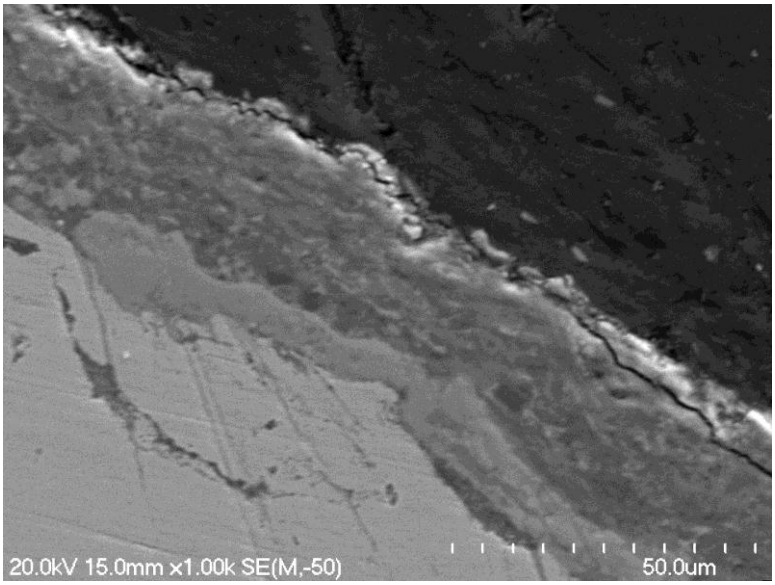

Figure 6.30: SEM image of coating A2 after 5 hours immersion into molten aluminium and after soldered aluminium removal using 20% NaOH solution.

In another study [30] to evaluate the performance of a vanadium carbide coating in molten aluminium at 680 °C, the weight loss per unit area of the coating was significantly higher than that measured in this study. For example, after 250 minutes exposure to molten aluminium, the weight loss was reported to be 9.5 mg/mm^2 for a surface engineered vanadium carbide coating on H13 tool steel but in this study using the Ti(Al,O)/Al_2O_3 composite coating, the weight loss after 250 minutes was 0.17 mg/mm^2. However the weight loss was comparable with a CrN PVD (5 µm thickness) coating i.e approx. 0.25 mg mg/mm^2 on H13 tool after dipping for 300 minutes into A380 melt at 710 °C [21].

The reduced weight loss in the case of the Ti(Al,O)/Al_2O_3 composite coating can be attributed to its high resistance to molten aluminium attack. No reaction has been found to occur between the coating and the molten aluminium where attack on the steel substrate has occurred. It is believed that molten Al diffuses through the coating defects and reacts with the steel substrate causing the composite coatings to break away.

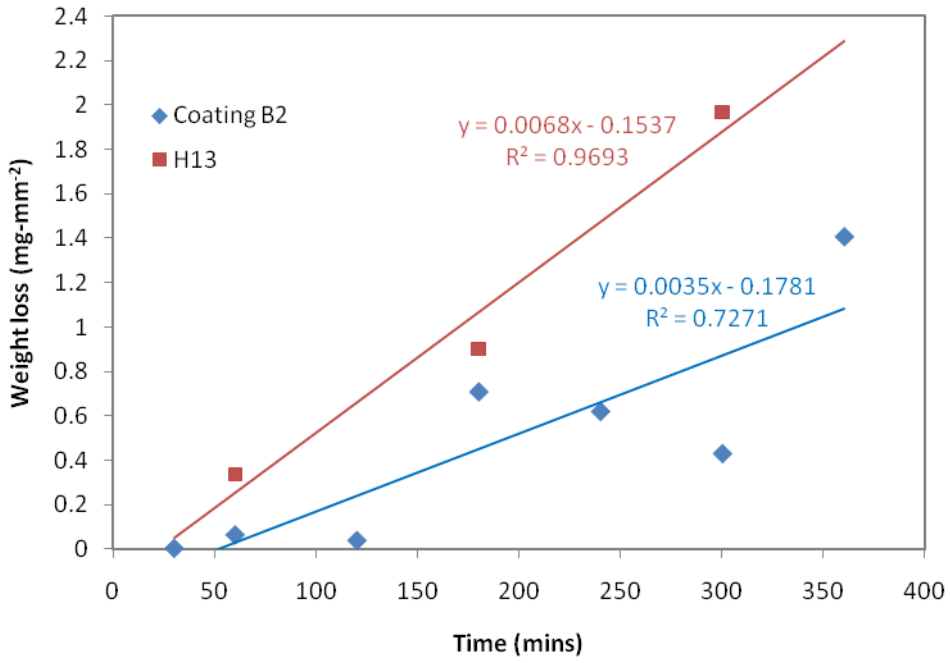

Figure 6.31: Weight loss as a function of time for TiAl/Al_2O_3 composite coating (B2) and H13 tool steel in the immersion test in molten aluminium.

The weight loss versus time results of TiAl/Al_2O_3 composite coating (B2) and uncoated H13 are shown in fig. 6.31. Under similar test conditions the steel coated with TiAl/Al_2O_3 composite material showed an increased weight loss (increased dissolution or wash out) compared with the steel coated with the Ti(Al,O)/Al_2O_3 composite coating. For example, the weight loss per unit area after 250 minutes exposure in molten aluminium in the case of TiAl/Al_2O_3 coated steel was found to be 0.65 mg/mm^2 which is about 3.8 times higher than that reported in case of Ti(Al,O)/Al_2O_3 composite coated steel for a similar exposure time The increased weight loss in the TiAl/Al_2O_3 coated steel can be explained to be as a consequence of molten aluminium attack on the coating leading to coating dissolution. Moreover, the variable/non uniform thickness of this coating would have had a pronounced effect on the extent of the molten aluminium attack in this coating and consequently on its dissolution rate. The high degree of data fluctuation in the weight loss per unit area of the TiAl/Al_2O_3 composite coating B2 after increasing immersion times can be linked with the variations in coating quality and thickness among the various samples used for the immersion tests.

An SEM image of coating B2 (fig. 6.32) after 5 hours immersion into molten aluminium and after soldered aluminium removal using NaOH shows a non-uniform, thin coating compared with coating A2 (fig 6.30).

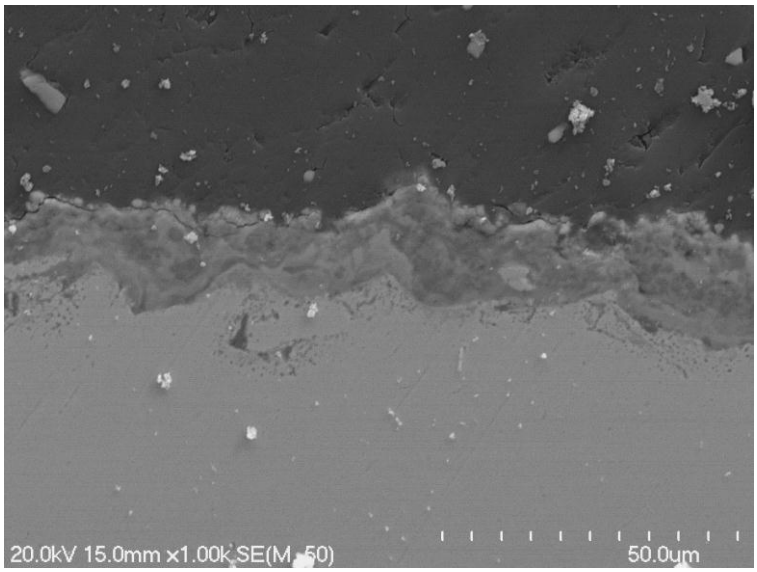

Figure 6.32: SEM image of coating B2 after 5hours immersion into molten aluminium and after soldered aluminium removal using 20% NaOH solution.

Aharonov et al. [21] studied the effect of coating thickness on the weight loss of PVD CrN coating in an Al melt and reported a decrease in coating weight loss with increased coating thickness.

6.2.3. Thermal shock resistance of composite coatings in molten Al

Thermal shock resistance of the composite coatings (A2, B2, A1) was investigated by subjecting the coated coupons to 400 cycles consisting of a holding time of 30 seconds in molten aluminium (700 ± 10 °C) for each cycle followed by quenching into water. The as-cast aluminium built up layer on all the coupons, which formed during immersion in molten aluminium, was automatically chipped off during quenching into water. The surfaces of the coupons were visually examined after every hundred cycles for Al soldering and an evaluation of surface spallation.

6.2.3a. Ti(Al,O)/Al_2O_3 composite coatings (A2)

Figure 6.33 shows the macrographs Ti(Al,O)/Al_2O_3 coated coupons after various thermal cycles. The coating was applied over an HDH Ti undercoat and for each cycle

a coupon was held for 30 second in molten Al and then water quenched. It is evident that after 400 cycles, there was no visible soldering on to the coating, however coating spallation occurred at the bottom edges of the coupon. The uncoated coupon, after 400 cycles, showed considerable spalling with a little Al sticking at the edges.

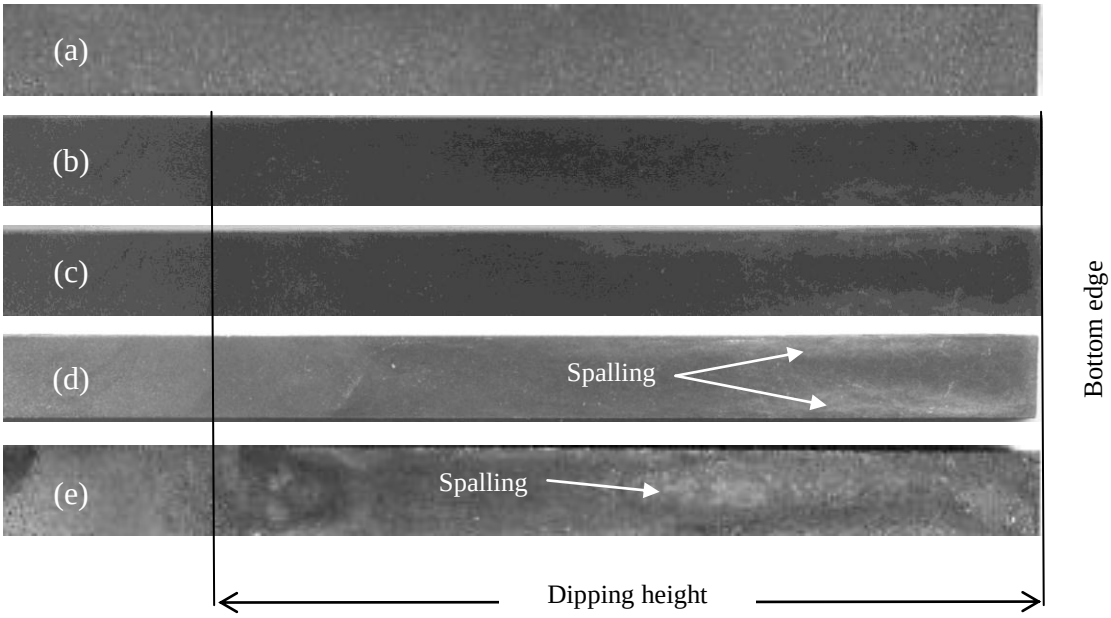

Figure 6.33: Macrographs of Ti/Ti(Al, O)/Al_2O_3 (A2) coated coupons after (a) zero (b) 200 (c) 300 (d) 400 cycles and (e) uncoated H13 coupon after 400 cycles

Figure 6.34 shows the surface morphology of the Ti (Al,O)/Al_2O_3 (A2) coating after 400 cycles. Surface cracks could originate from internal flaws in the topcoat or from surface flaws such as porosity and micro-cracks formed during deposition.

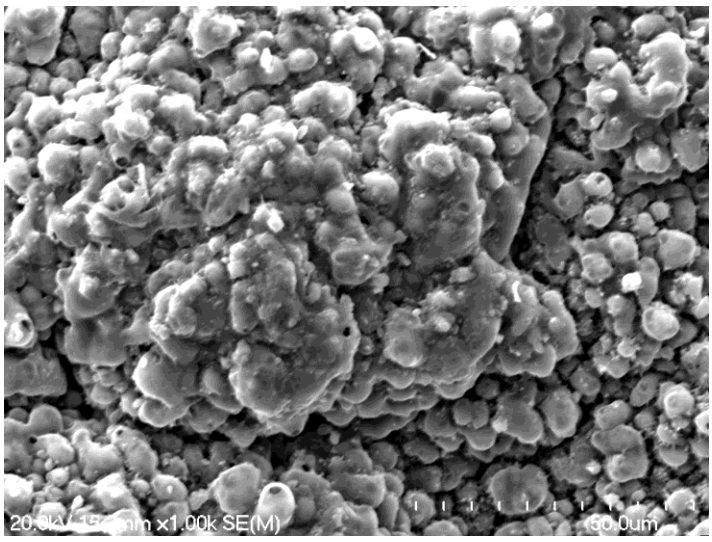

Figure 6.34: Surface morphology of the composite coating Ti(Al,O)/Al_2O_3 (A2) after 400 cycles

Figure 6.35 shows that coating failure occurred because of long horizontal cracks within the topcoat. The formation and growth of the horizontal cracks eventually lead to delamination, and a loss of structural integrity of this coating. No vertical cracks i.e. cracks normal to the coating interface were observed within the coating's cross-section. The presence of intra-splat cracks or horizontal cracks in the coating during thermal cycling could be as a result of lower bonding between the splats (not in fully molten state) or a lower deposition efficiency of the composite powder [31].

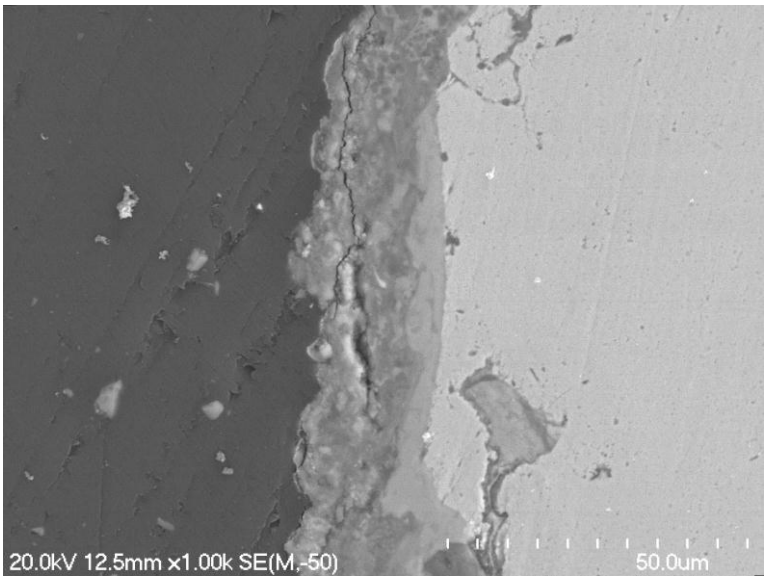

Figure 6.35: Composite coating Ti(Al,O)/Al_2O_3 (A2) after 400 cycles with crack morphology

6.2.3b. TiAl/Al_2O_3 composite coatings (B2)

Figure 6.36 shows the macrographs of the TiAl/Al_2O coated coupons. For each steel coupon the coating was applied on top of an HDH Ti undercoat. Coupons were given up to 500 thermal cycles with a 30 second holding time in molten aluminium, followed by water quenching for each cycle. From the macrographs, it is evident that coating failure occurred at the bottom edges of the coupons after 400 cycles. No Al soldering was observed on the coated surfaces even after 500 cycles. This indicates poor wetability of the coating by molten Al. The uncoated coupon, after 500 cycles, showed considerable spalling.

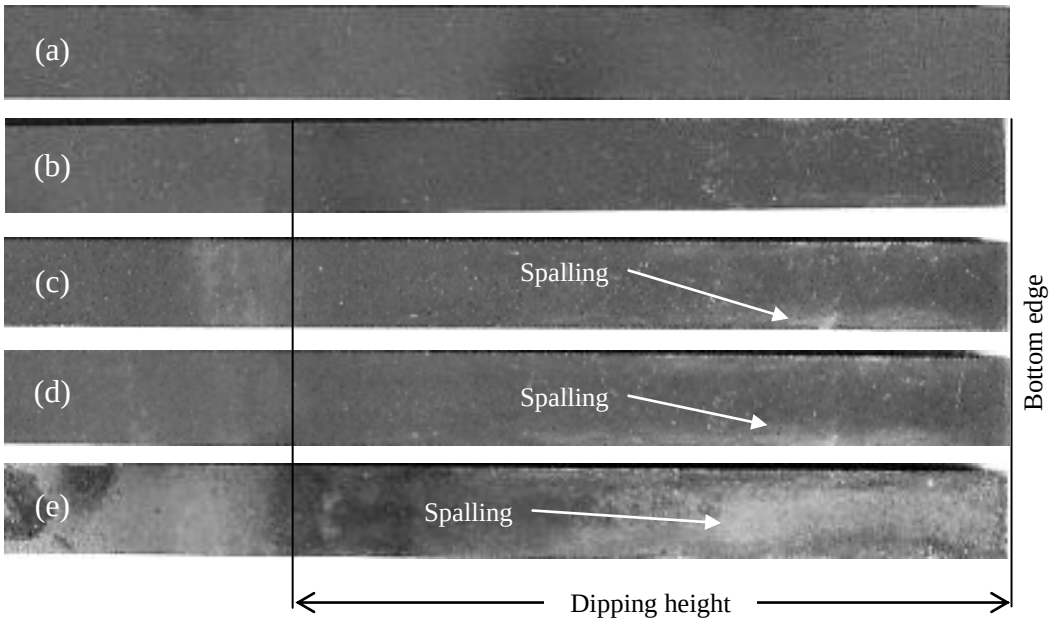

Figure 6.36: Macrographs Ti/TiAl/Al_2O_3 (B2) coated coupons after (a) zero (b) 200 (c) 400 (d) 500 cycles and (d) uncoated H13 coupon after 500 cycles.

XRD analysis (fig. 6.37) of the coating prior to and after thermal cycling suggests that the coating was fairly stable, even after 500 cycles in molten aluminium and mainly consisting of Al_2O_3, TiAl, Ti_3Al and TiO.

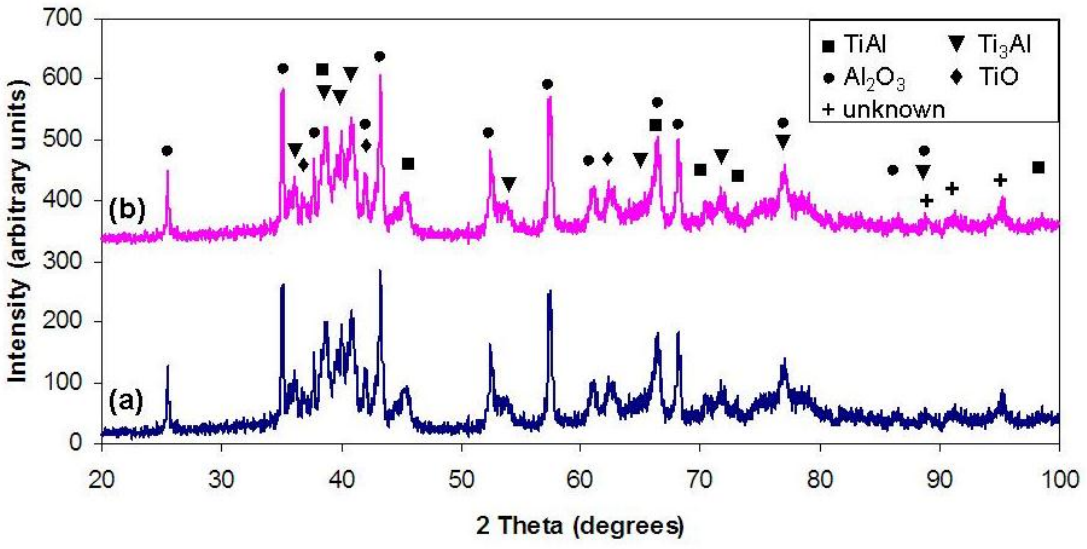

Figure 6.37: XRD patterns of coating (a) prior to and (b) after thermal cycling testing

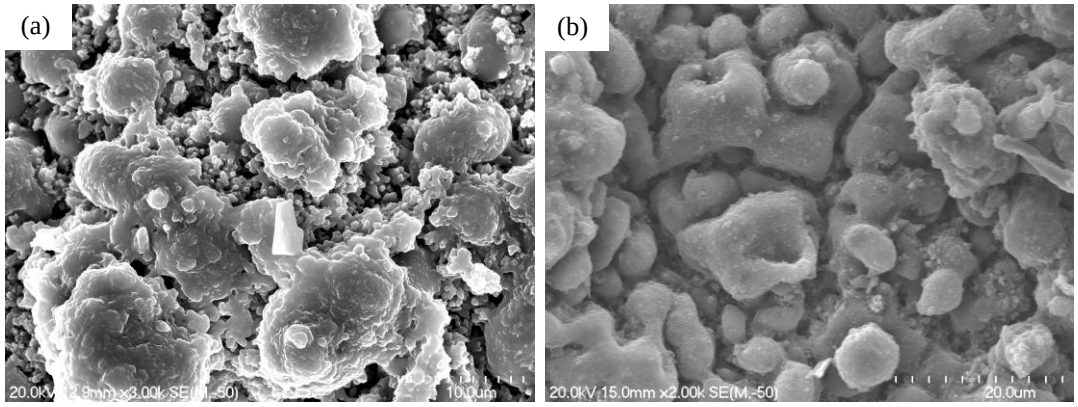

Figure 6.38: (a) Surface morphology of the composite coating TiAl/Al_2O_3 (B2) after 500 cycles, (b) surface cracks

Figure 6.38 shows the surface morphology and surface cracks in the TiAl/Al_2O_3 (B2) coating after 500 cycles. The presence of surface cracks (fig. 6.38b) after thermal cycling is likely due to the difference in thermal expansion coefficients of various phases present in the coating.

SEM micrographs (fig. 6.39) of the composite coating TiAl/Al_2O_3 (B2) cross-section after 500 cycles show three types of cracks, horizontal cracks (fig. 6.39a), vertical cracks (fig. 6.39b) and interfacial cracks (fig. 6.39c). The horizontal cracks were found directly below the vertical cracks. The extent of the horizontal cracks and interfacial cracks covered the entire coating examined. The formation and growth of the horizontal cracks eventually lead to delamination, of this coating. The obvious horizontal cracks at the interface of the Ti bond coat and topcoat are more detrimental to its thermal shock resistance.

Alumina is thermodynamically stable in TiAl, and its coefficient of thermal expansion (CTE) closely matches that for TiAl [32]. High interface stability and a high compatibility of thermal expansion coefficient of Al_2O_3 with TiAl alloys is also reported by Dixon et al. [33]. The CTE of TiAl/Al_2O_3 based upon the data reported [34] is about 9.9×10^{-6} °C^{-1} [35] but the value is closer to the CTE of Al_2O_3 (8.8×10^{-6} °C^{-1}) and TiO_2 (7.3×10^{-6} °C^{-1}) but much lower than H13 tool steel (12×10^{-6} °C^{-1}) [36, 37]. The difference in the CTEs of the TiAl/Al_2O_3 composite coating and tool steel is a possible reason for failure of this coating.

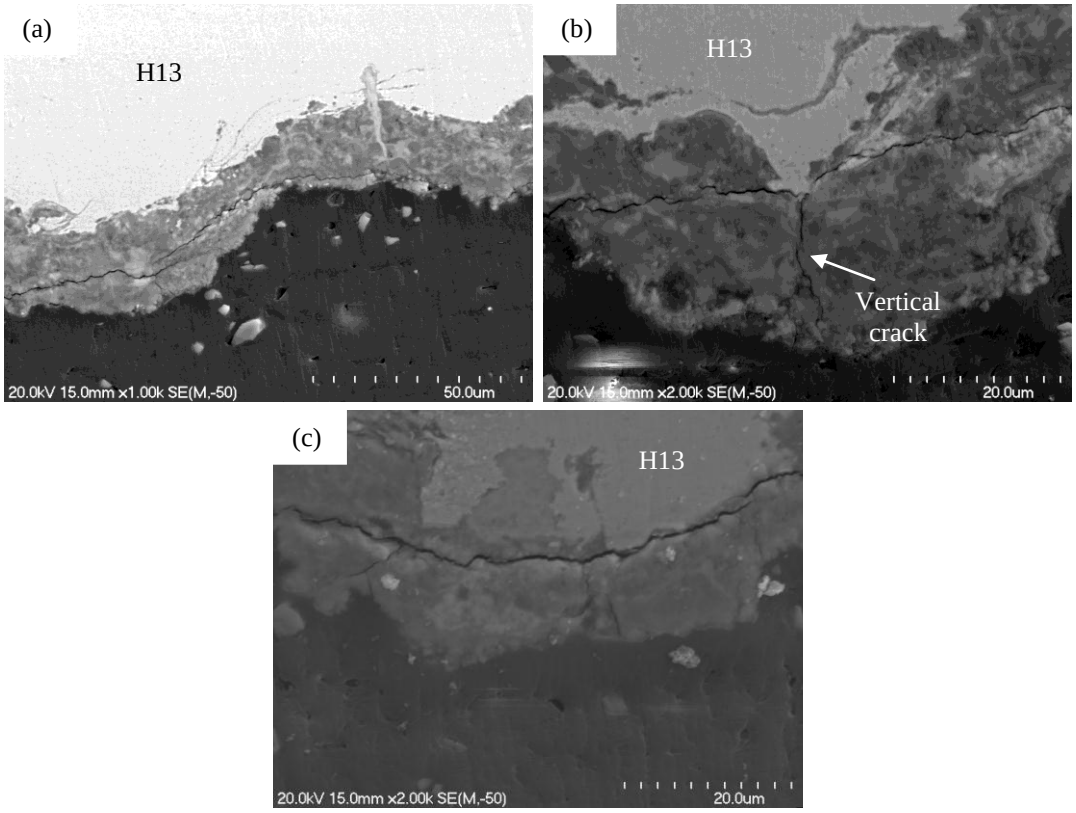

Figure 6.39: Composite coating $TiAl/Al_2O_3$ (B2) cross-section after 500 cycles with cracks morphologies; (a) horizontal, (b) vertical and (c) interfacial

In surface engineering a combination of substrate treatment leading to a hardness increase (gas nitriding) and an appropriate coating is described as a 'duplex process'. A nitriding treatment allows the synthesis of a specific nitride compound on a tool steel. Surface duplex treatment has also been used to improve the performance of the coatings on dies and cores [38]. In this study an attempt was made to further improve the thermal shock resistance of the composite coatings (A2, B2) using a duplex treatment (nitrided steel + coating). The attempt remained unsuccessful due to the poor efficiency of $Ti(Al,O)/Al_2O_3$ and $TiAl/Al_2O_3$ composite powders to deposit on nitrided H13 tool steel.

6.2.3c. $Ti(Al,O)/Al_2O_3$ composite coatings (A1)

The thermal cycling test for a $Ti(Al,O)/Al_2O_3$ (A1) composite coating with an atomized Ti under coat revealed that after 200 cycles with a holding time of one second in molten Al during each cycle, there was no evidence of spallation or any significant adherence of aluminium to the coated surface. After 400 cycles, with a holding time of 30 seconds per cycle in molten aluminium, the coated surface showed

a few aluminium spots adhering to the surface but no surface spallation (fig. 6.40a). A single layered Ti(Al,O)/Al_2O_3 composite coating A1 (without a Ti undercoat) on H13 tool steel also showed slight Al soldering and no spallation after 400 cycles. However, the uncoated coupon showed surface spallation and surface aluminium soldering after 400 cycles (fig. 6.40b). The ringed areas in fig. 6.40 show aluminium sticking to the coated and uncoated surfaces whereas the pointed arrows show the surface spallation.

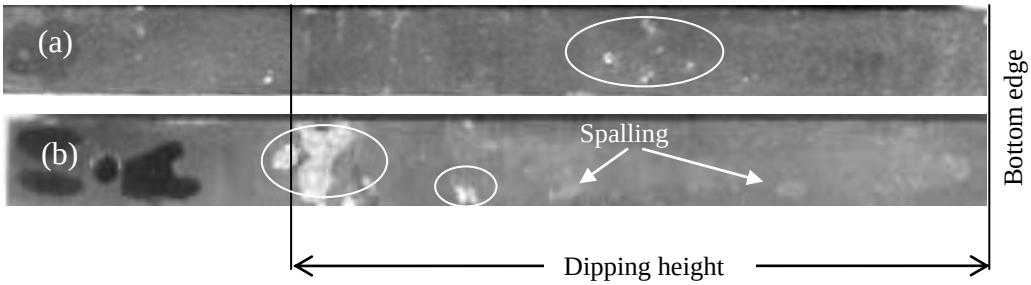

Figure 6.40: Macrographs of the Ti(Al,O)/Al_2O_3 (A1) coated coupons after (a) 400 cycles and (b) uncoated H13 steel after 400 cycles with a 30 second holding in molten Al.

EDAX data from an SEM evaluation of the areas where aluminium had soldered onto the uncoated steel substrate, showed that the aluminium had reacted with the steel to form an iron-aluminium intermetallic containing a high level of oxygen (fig. 6.41). Similar findings have been reported by other workers [2, 9]. The coating was examined in those areas where small amounts of aluminium appeared to stick to the composite coating. A typical area is shown in fig. 6.42. A careful examination showed that the aluminium did not react with the coating and that the apparent sticking was caused by a reaction with the Ti coating in those places where the composite coating was very thin or completely absent.

The reaction between the aluminium and titanium, shown in fig. 6.43, was observed after 200 cycles (with one second holding for each cycle) in molten Al. An EDAX analysis has shown various at% ratios of titanium and aluminium which indicate the presence of Ti-Al intermetallics. The solubility of titanium in liquid aluminium is not very high (0.2 % at 700 °C in pure liquid Al) [2] so that the liquid aluminium becomes quickly saturated with titanium solute. Sujata et al. [39] have found that $TiAl_3$ has the minimum free energy of formation and should therefore be the intermediate phase below 1200 °C. No evidence of $TiAl_3$ was found in this study. The presence of Ti-Al intermetallics was not observed around the Ti coating after 400

cycles (with 30 second holding in molten Al for each cycle). This was probably due to the removal of these brittle phases during further thermal cycling.

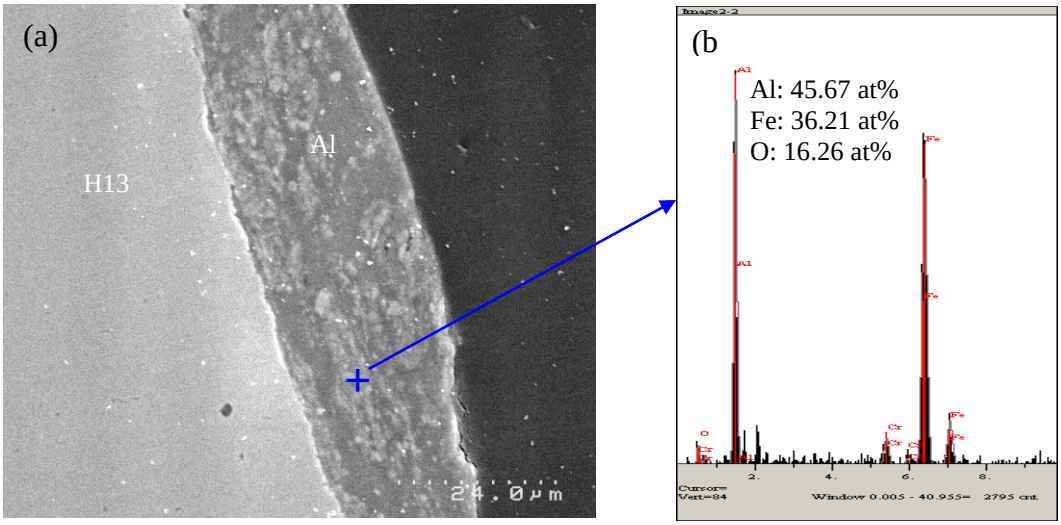

Figure 6.41: (a) SEM micrograph of aluminium soldering to the steel substrate after 400 cycles, (b) EDAX analysis showing formation of iron aluminide

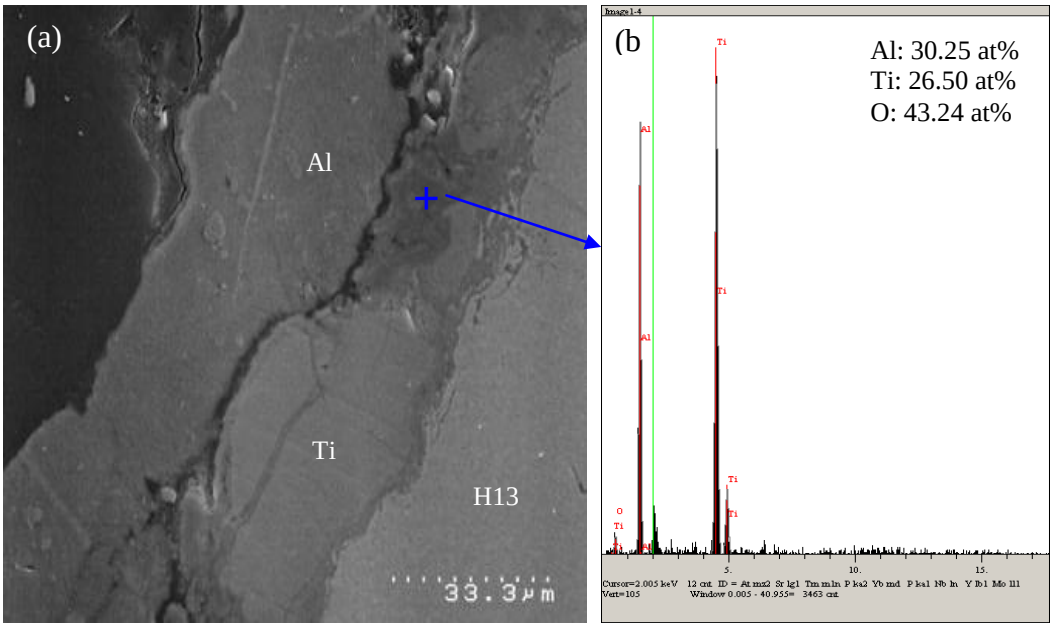

Figure 6.42: (a) SEM micrograph of aluminium sticking to the coating after 400 cycles (b) EDAX analysis

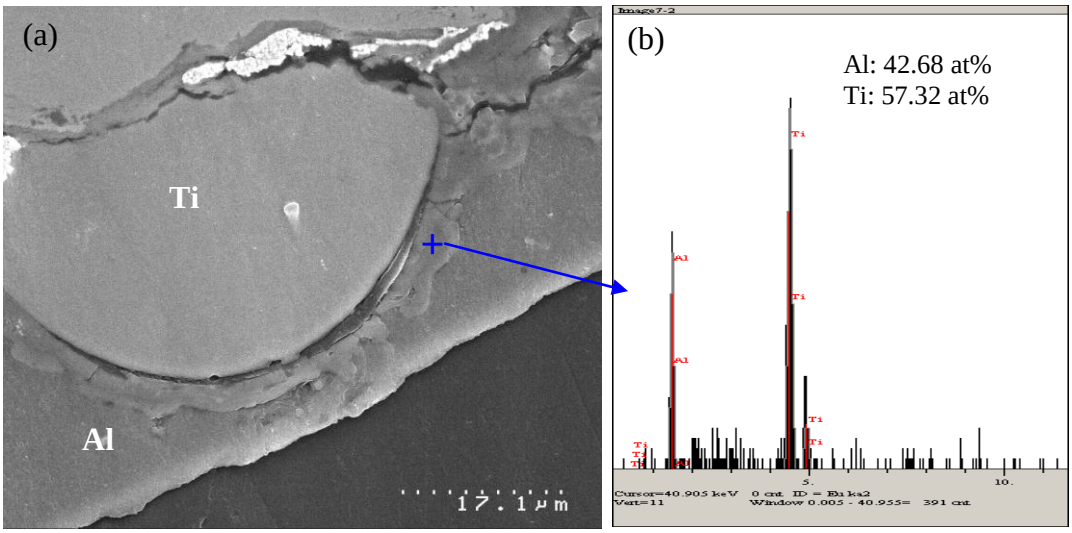

Figure 6.43: (a) SEM micrograph of aluminium reaction with the titanium after 200 cycles (b) EDAX analysis showing Ti-Al intermetallics

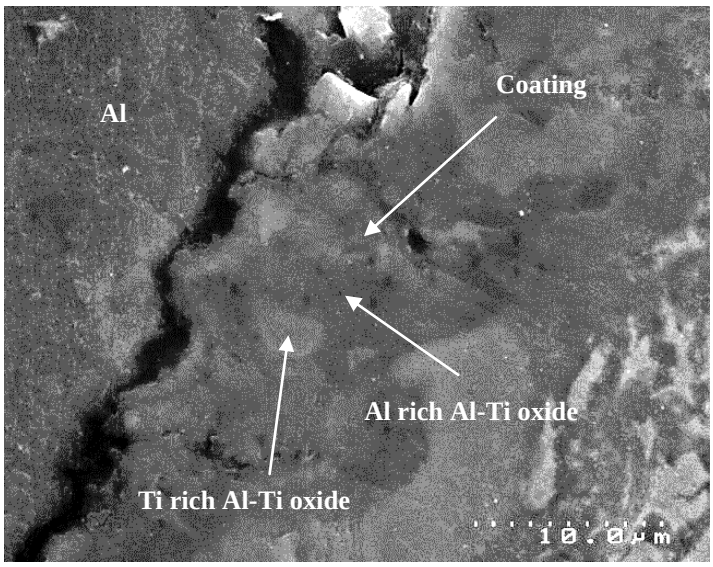

Figure 6.44: SEM micrograph of a double layer Ti/Ti(Al,O)/Al_2O_3 coating after 400 cycles of thermal cycling test in molten Al. Dark area is Al rich Al-Ti oxide and the light area is Ti rich Al-Ti oxide

An EDAX analysis of the coating prior to thermal cycling confirms the presence of Ti and Al rich Al-Ti oxides (ref chapter 5). After 400 thermal cycles in molten Al, the coating was assessed again using EDAX. The EDAX analysis of the coating after thermal cycling (fig. 6.44) confirms that the nature of the phases did not change. Moreover XRD analysis (fig. 6.45) shows that the coating mainly consists of Al_2O_3, Ti or Al-Ti oxides, which suggests that the coating was fairly stable.

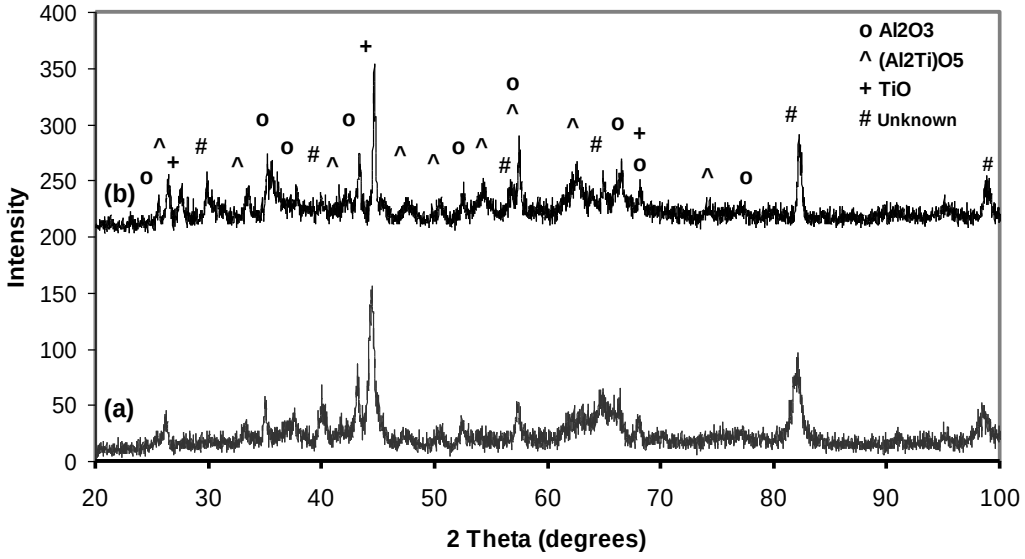

Figure 6.45: XRD patterns of single layer coating (a) prior to and (b) after thermal cycling testing

The thermal cycling life time of the composite coatings is listed in table 6.6.

Table 6.6: The thermal shock resistance of coatings on H13 tool steel

Coatings coding	Coatings Topcoat	Feedstock condition	Ti under coat/bond coat	No of thermal shocks (cycles)	Holding time in molten Al (Seconds)	Al soldering to coated surfaces after 400 cycles	Thermal shock life (cycles)
A2	$Ti(Al,O)/Al_2O_3$	Powder agglomeration with binder	HDH	400	30	no	400
A1	$Ti(Al,O)/Al_2O_3$	No powder agglomeration	Atomized Ti	200	1	Few Al spots	No failure
				400	30		
B2	$TiAl/Al_2O_3$	Powder agglomeration with binder	HDH	500		no	400

Coupons with $Ti(Al,O)/Al_2O_3$ (A2) and $TiAl/Al_2O_3$ (B2) composite coatings and an HDH Ti intermediate layer showed similar thermal shock life of 400 cycles under similar thermal cycling conditions. Both types of coating showed no Al sticking to the coating after 400 cycles. The formation and growth of the horizontal cracks eventually lead to delamination, of these coating. A $Ti(Al,O)/Al_2O_3$ (A1) composite coating with a Ti intermediate layer did not show any failure until 400 cycles. However, after 400 cycles, the $Ti(Al,O)/Al_2O_3$ (A1) coated surface showed a few aluminium spots

adhering to the surface but no surface spalling. One of the possible reasons for the good thermal shock resistance of the Ti(Al,O)/Al_2O_3 (A1) coating compared to the other composite coatings, Ti(Al,O)/Al_2O_3 (A2) and TiAl/Al_2O_3 (B2), is due to the possible good bonding between the splats (fully molten) due to the fine feedstock (without PVA agglomeration) with an average particles size of about 12.5 µm.

The thermal shock resistance of a coating depends on a number of factors, such as the thermal conductivity of the coating material, the difference in the thermal expansion coefficient between the coating and substrate. A material with higher thermal conductivity, in general, possesses a better resistance to thermal shock because of its tendency to reduce interior temperature gradients and to reduce thermal stress [40]. In the absence of thermal conductivity information of the composite coatings, it is difficult to compare the failure among the composite coatings. The difference in the thermal expansion coefficient between a coating and substrate is also described as one of the major causes of coating failure during thermal cycling testing [41]. The CTE of the composite coatings needs to be determined for a clear evaluation of the degree of mismatch of CTE between a coating and H13 tool steel.

6.2.4. Industrial trial of a Ti(Al,O)/Al_2O_3 composite coating (A2) on a dummy block used in aluminium extrusion

To improve the life time of a dummy block and to reduce the adherence of aluminium, a dummy block was coated with a double layer Ti/Ti(Al,O)/Al_2O_3 (A2) coating, a decision which was based upon its good corrosion resistance against molten Al attack over Ti/TiAl/Al_2O_3 (B2). The Ti (Al,O)/Al_2O_3 coating was evaluated for 61 hours of operation and a comparison was made with an uncoated dummy block for aluminium soldering and wear resistance over a similar service duration.

In the normal industrial operation, a dummy block needs to be visually inspected daily for aluminium build up on its face and land. Once a week, the dummy block is removed from the press, it is visually inspected for wear and cleaned in caustic soda solution and subsequently ground/polished.

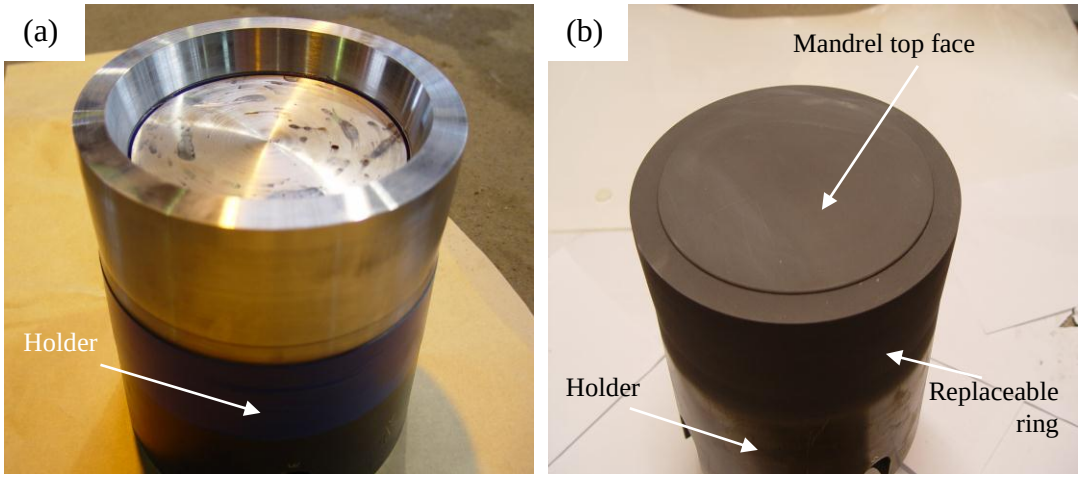

Figure 6.46: Photographs of dummy blocks used in aluminum extrusion before operation (a) uncoated (b) coated

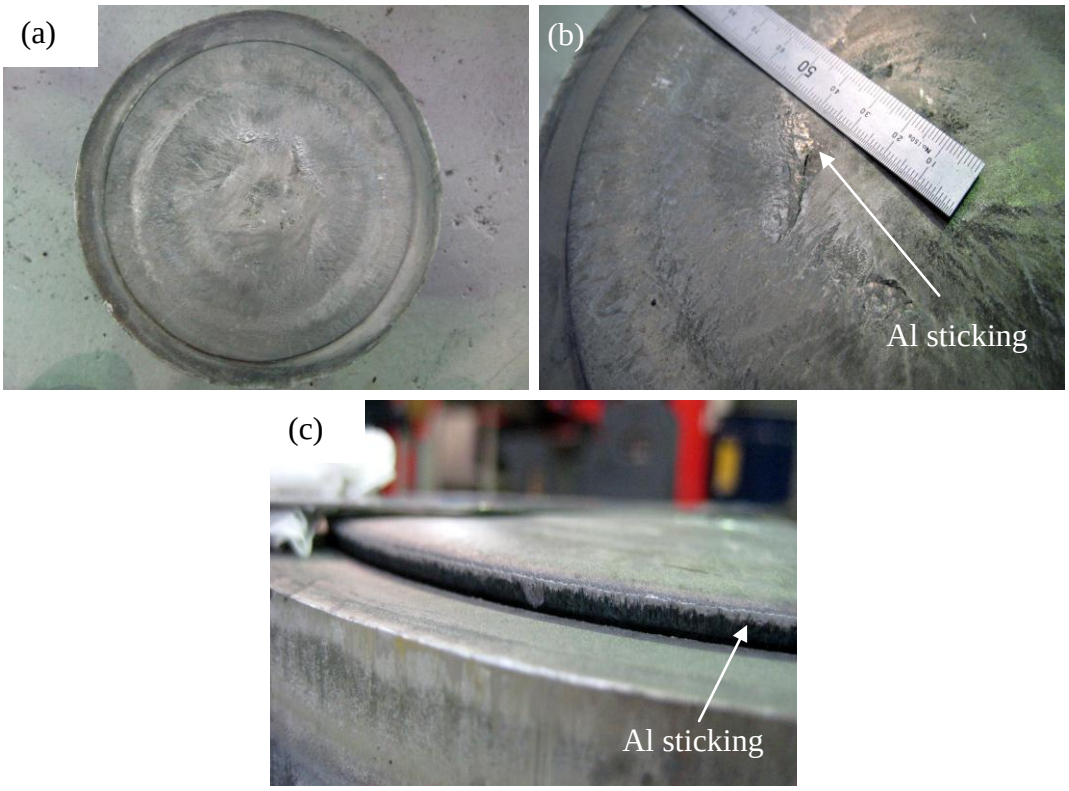

Figure 6.47: Photographs of the coated dummy block after eight hours of operations showing Al build up (a) overall surface appearance (b) the face (c) inside the lip

Figure 6.46 shows the uncoated and coated dummy block before operation. Figure 6.47 shows photographs of the dummy block after 8 hours of operation. It is clear that the face and inside lip of the dummy block has some aluminium build up. The aluminium build up is most likely due to localized coating failure at the centre and at the edges.

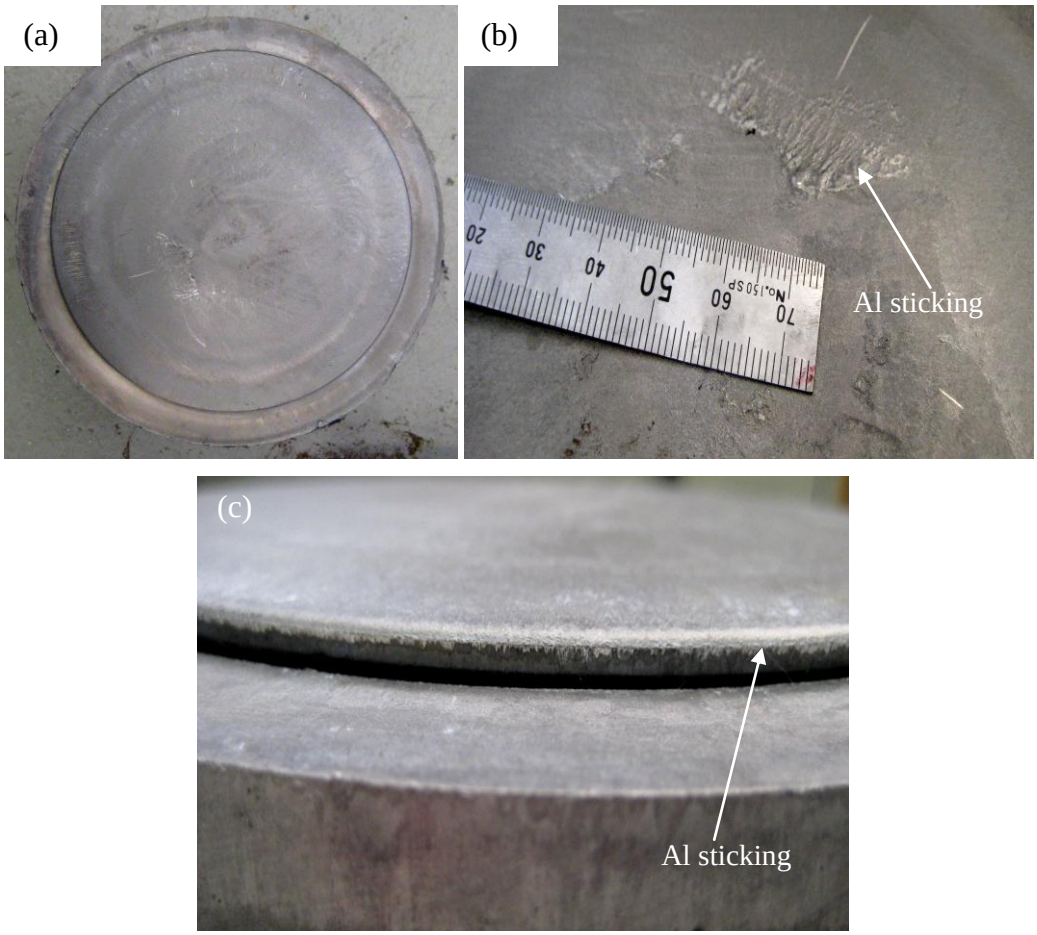

Figure 6.48: Photographs of the coated dummy block after 16 hours of operation showing Al build up (a) over all surface appearance (b) face (c) inside the lip

After 16 hours of operation (fig. 6.48) the amount of aluminium sticking to the face remained the same as for 8 hours operation. The Al build up on the face was reported to be similar to that after normal operation using an uncoated boron nitride lubricated dummy for a similar duration. However the Al build-up was slightly less for the other areas.

Figure 6.49 shows the degree of Al build-up on the uncoated dummy block after 60 hours of operation. The Al build-up is quite considerable at the lips and wall of the replaceable ring compared with that at the front face of the mandrel. These areas are important for the successful operation of a dummy block.

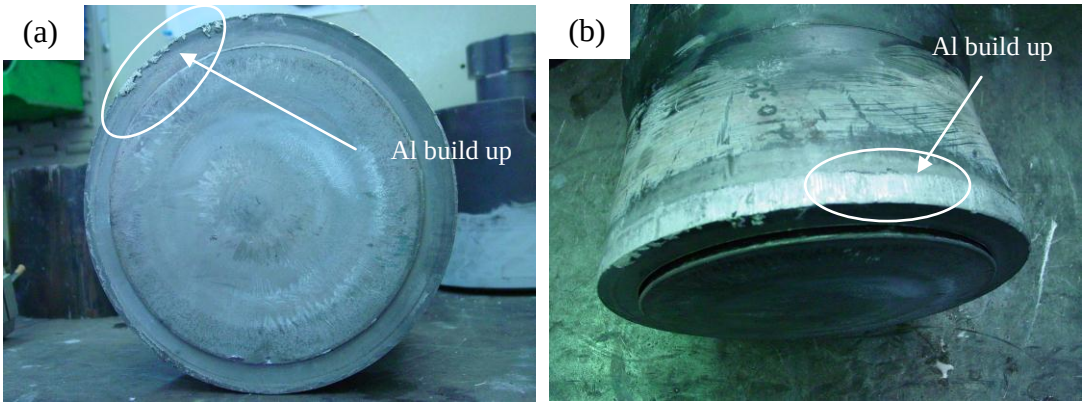

Figure 6.49: Photographs of uncoated dummy block after 60 hours of operation with Al-build up and without NaOH cleaning (a) front face view with Al build up at the lips (b) Al build up at the replacing ring

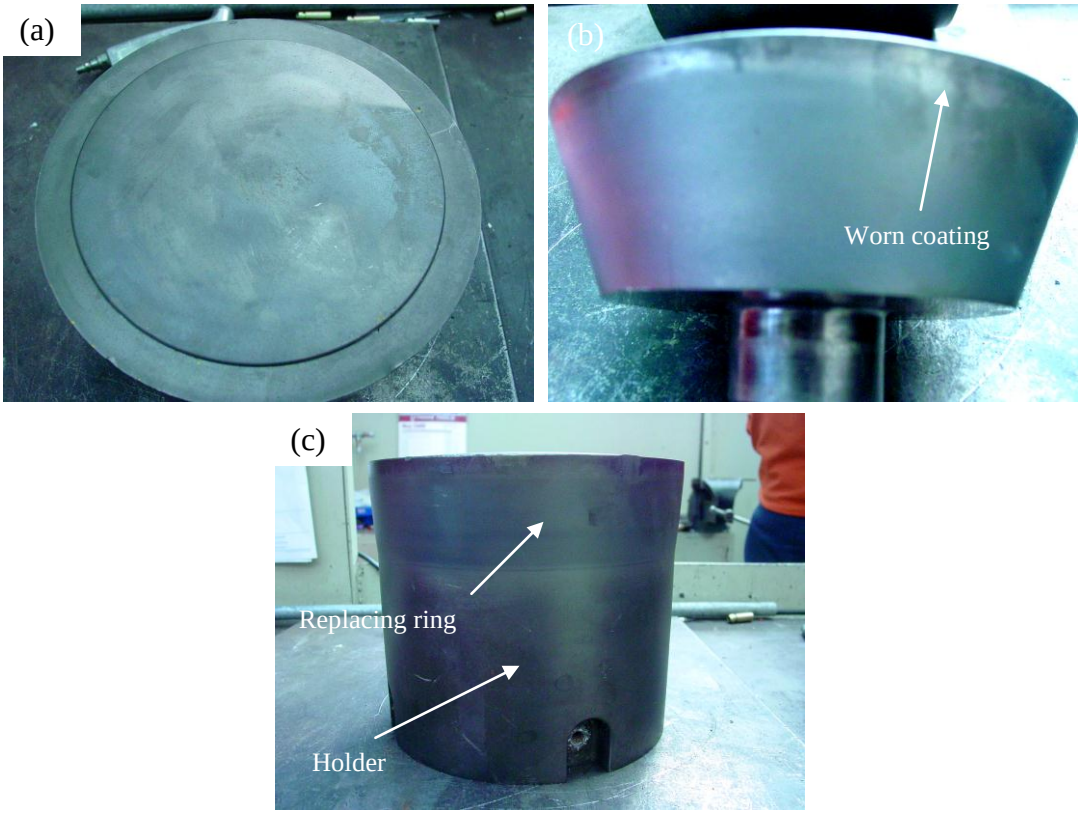

Figure 6.50: Photographs of the coated dummy block after 61 hours operation and after cleaning with NaOH (a) top surface view (b) mandrel side view and (c) replaceable ring with holder (side view)

Photographs of the coated surfaces after 61 hours of operation and after concentrated NaOH treatment (surface cleaning) shown are in fig. 6.50. It was observed that after 60 hours of operation, the coating remained mostly intact with the steel surface;

however it was partially worn at a few locations (top side wall of the mandrel). It also confirmed that the coating was not attacked by conc. NaOH solution during the cleaning operation. It was reported by Fletcher aluminium that the coating on dummy blocks coated with a PVD nitride coating is attacked by conc. NaOH during cleaning.

After 61 hours service the degree of wear to the coated and uncoated mandrel was visually observed. Figure 6.51 shows a photograph of the coated and uncoated mandrel. It is clear that after 61 hours of operation, the coated surface showed no sign of wear tracks compared with the uncoated mandrel surface. This is evidence that the coating successfully improves the wear resistance of the uncoated tool steel.

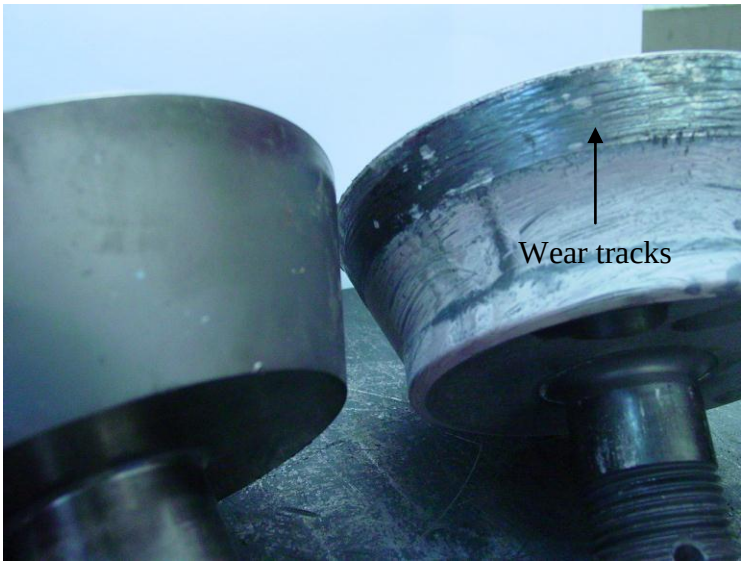

Figure 6.51: Wear comparison of coated (left) and un-coated (right) mandrel of the dummy block after 61 hours operation

This industrial trial of the composite coating revealed that the coating was successful in controlling the sticking of aluminium to some extent. The composite coating showed high wear resistance with a localized type of failure at certain areas during its operation. It is possible to recoat, easily and quickly, the partially worn coating areas due to the flexible nature of HVOF spraying in comparison with the PVD technique commonly used for such applications. Moreover, the quality of the coating can be improved further by modification to the powder spraying technique (process automation) to produce a thick and uniform coating.

6.3. Summary

The nature of Al soldering with a composite coated and uncoated tool steel was studied.

It was found that composite coatings delay molten Al attack on H13 tool steel. The coatings block, partially block or delay contact between the aluminium melt and H13 steel, but does not change the mechanism of aluminium attack on H13 tool steel. Unlike the uncoated steel substrate that was generally attacked, the composite coatings were locally attacked regardless of the type of coating.

The high surface roughness of the as-sprayed coatings, a non uniform coating thickness, especially the thinner coating areas and inhomogeneous composite coating microstructure were the most significant contributory factors leading to aluminium soldering and corrosion.

The local attack in coatings caused hemispherical pits on the steel substrate due to the local breakage of the sprayed coating. The diameter of the pits was significantly larger than the thickness of the coatings.

The soldering tests showed that a Ti(Al,O)/Al_2O_3 (A2) composite coating did not react with molten aluminium. This work suggests that Ti (Al,O) metallic binder is more resistance to attack by molten aluminium than the intermetallic TiAl binder because it already has aluminium in solid solution. The localized nature of the attack in this coating was due to the liquid aluminium penetrating through coating defects and its reaction with the tool steel substrate, an intermetallic phase formation occurred along with volume expansion due to diffusion of aluminium. The local coating detachment was due to the volume expansion below the defect.

No reaction between molten aluminium and a Ti(Al,O)/Al_2O_3 (A2) composite coating was identified, the phase constituents of the coating were found to be the same after immersion in molten aluminium. This is an indication that the coating is fairly stable in molten aluminium.

In a TiAl/Al_2O_3 composite coating, an inhomogeneous composite coating microstructure is responsible for molten Al-attack. The coating was found to be

attacked by molten aluminium as a result of a reaction between the coating and molten aluminium. The metallic phase TiAl in the composite coating is believed to be attacked by the molten Al. The presence of corrosion pits support the penetration of molten Al through the coatings.

It has been found that a Ti(Al,O)/Al_2O_3 (A2) composite coating is a better protective coating than the TiAl/Al_2O_3 (B2) composite coating due its stability against molten aluminium attack. Furthermore the extremely low weight loss of Ti(Al,O)/Al_2O_3 composite coating per unit area in the immersion test also confirmed its good resistance to molten aluminium.

The positive and encouraging results indicate that the application of a Ti(Al,O)/Al_2O_3 (A2) composite coating to an extrusion dummy block, to counter the effect of aluminium soldering, is attractive.

A Ti(Al,O)/Al_2O_3 coating (A1) on a hardened H13 steel showed better thermal shock resistance than a Ti(Al,O)/Al_2O_3 and TiAl/Al_2O_3 coatings (A2, B2) under similar test conditions. The thermal shock life of both Ti(Al,O)/Al_2O_3 and TiAl/Al_2O_3 coatings (A2, B2) were the same. The formation and growth of horizontal cracks eventually lead to delamination of these coatings.

Using a duplex treatment, a further improvement to the thermal shock resistance of the composite coatings remained unsuccessful due to the poor deposition characteristics of composite powders on nitrided steel substrates.

Successful trials of a Ti(Al,O)/Al_2O_3 composite coated dummy block revealed that the coating has a potential as an industrial coating. This coating showed good wear resistance with only localized coating failure.

Despite the local coating failure and aluminium soldering as a result of aluminium attack, the worn areas of the dummy block can be recoated easily and economically by using an HVOF spraying technique compared with a PVD technique, which is commonly used to protect H13 tool steel against molten aluminium attack.

Industrial trials confirmed that the coating remained unattacked/inert against concentrated NaOH attack during cleaning operations, which is a considerable advantage compared with PVD nitride coatings used for similar applications.

6.4. References

1. Yeomans, J.A., *Studies of ceramics-liquid metal reaction interfaces.* Journal of Materials Science, 1990. **25**(5): 2312-2320.

2. Yan, M. and Z. Fan, *Durability of materials in molten aluminum alloys.* Journal of Materials Science, 2001. **36**: 285-295.

3. Zhang, D., *Titanium based materials technology (NERF Report) in UOWX9909*. 2001-2002.

4. Liang, J., *Application of Titanium based composite powders in producing high performance coatings*, Internal Report, The University of Auckland, 1-19.

5. Persson, A., J. Bergstrom, C. Burman and S. Hogmark, *Influence of deposition temperature and time during PVD coating of CrN on corrosive wear in liquid aluminium.* Surface and Coatings Technology, 2001. **146-147**: 42-47.

6. Zhuravlev, G.I., L.V. Rudenko, G.A. Kudryavtseva and L.I. Venzel, *Thermal shock resistance of glass ceramics coatings.* Glass and Ceramics, 1984. **41**(7): 293-296.

7. Chen, Z.W. and M.Z. Jahedi, *The effect of temperature on soldering and the sequence of formation of soldered layer during high pressure casting of Al-11Si-3Cu alloy.* International Journal of Cast Metals Research, 1998. **11**: 129-138.

8. Chen, Z.W., *Formation and progression of die soldering during high pressure die casting.* Materials Science and Engineering A, 2005. **397**(1-2): 356-369.

9. Yan, M. and Z. Fan, *The erosion of H21 tool steel in molten A380 alloy.* Journal of Materials Science, 2000. **35**(7): 1661-1667.

10. Mitterer, C., F. Holler, F. Ustel and D. Heim, *Application of hard coatings in aluminium die casting - soldering, erosion and thermal fatigue behaviour.* Surface and Coatings Technology, 2000. **125**(1-3): 233-239.

11. Sundqvist, M. and S. Hogmark, *Effects of liquid aluminium on hot-work tool steel.* Tribology International, 1993. **26**(2): 129-134.

12. Yu, M., R. Shivpuri and R.A. Rapp, *Effects of molten aluminium on H13 dies and coatings.* Journal of Materials Engineering and Performance, 1995. **4**(2): 175-181.

13. Yan, M. and Z. Fan, *Investigation of the interaction between H21 steels and molten Al-alloys.* Journal of Materials Science, 2000. **35**: 1661-1667.

14. Shankar, S. and D. Apelian, *Die soldering: mechanism of the interface reaction between molten aluminium alloy and tool steel.* Metallurgical and Materials Transactions, 2002. **33B**(3): 465-476.

15. Molinari, A., M. Pellizzari, G. Straffelini and M. Pirovano, *Corrosion behaviour of a surface-treated AISI H11 hot work tool steel in molten aluminium alloy.* Surface and Coatings Technology, 2000. **126**(1): 31-38.

16. Mogensen, K.S., N.B. Thomsen, S.S. Eskildsen, C. Mathiasen and J. Bottiger, *A parametric study of the microstructural, mechanical and tribological properties of PACVD TiN coatings.* Surface and Coatings Technology, 1998. **99**(1-2): 140-146.

17. Chu, Y., P. Cheng and R. Shivpuri. *Soldering phenomena in aluminium die casting: possible causes and cures*. In Transactions of the 17th International die casting congress. 1993. Cleveland, Ohio, USA: North America Die Casting Association.

18. Chen, Z.W., M.Z. Jahedi and J.A. Law. *Metallurgical phenomena in die/casting interfacial regions during high pressure die casting of aluminium alloy*. In Transactions of the 20th International die casting congress. 1999. Cleveland, Ohio, USA: North America Die Casting Association.

19. Han, Q., E.A. Kenik and S. Viswanathan, *Die soldering in aluminium die casting*. In Proc. of the Light Metals 2000, Warrendale, PA: TMS. 765-770.

20. Eustathopoulos, N., J.C. Joud, P. Derse and J.M. Hicter, *The wetting of carbon by Al and Al alloys.* Journal of Materials Science, 1974. **9**(8): 1233-1242.

21. Aharonov, R.R., S. Chellapilla, B. Janoss, R. Shivpuri and A. Lakare, *An investigation of the corrosion of H13 coated with CrN in molten aluminium alloys: Effect of steel surface preparation and coating thickness*. In *Transactions of the 20th International Die Casting Congress*. 1999. Cleveland, Ohio, USA: North America Die Casting Association.

22. Gulizia, S., M.Z. Jahedi and E.D. Doyle, *Performance evaluation of PVD coatings for high pressure die casting.* Surface and Coatings Technology, 2001. **140**(3): 200-205.

23. Ho, W.Y., D.H. Huang, L.T. Huang, C.H. Hsu and D.Y. Wang, *Study of characteristics of Cr_2O_3/CrN duplex coatings for aluminium die casting applications.* Surface and Coatings Technology, 2004. **177-178**: 172-177.

24. Lin, C.S., C.S. Ke and H. Peng, *Corrosion of CrN and CrN/TiN coated heat-resistant steels in molten A356 aluminum alloy.* Surface and Coatings Technology, 2001. **146-147**: 168-174.

25. Sangghaleh, A. and M. Halali, *An investigation on the wetting of polycrystalline alumina by aluminium.* Journal of Material Processing Technology, 2008. **197**(1-3): 156-160.

26. Lou, D.C., O.M. Akselsen, M.I. Onsoien, J.K. Solberg and J. Berget, *Surface modification of steel and cast iron to improve corrosion resistance in molten aluminium.* Surface and Coatings Technology, 2006. **200**(18-19): 5282-5288.

27. Joshi, V., K. Kulkarni, R. Shivpuri, R.S. Bhattacharya, S.J. Dikshit and D. Bhat, *Dissolution and soldering behaviour of nitrided hot working steel with multilayer LAFAD PVD coatings.* Surface and Coatings Technology, 2001. **146-147**: 338-343.

28. Shivpuri, R., Y.L. Chu, K. Venkatesan, J.R. Conrad, K. Sridharan, M. Shamim and R.P. Fetherston, *An evaluation of metallic coatings for erosive wear resistance in die casting applications.* Wear, 1996. **192**(1-2): 49-55.

29. Swapnil, V.S. and B.D. Narendra, *Laser surface engineered vanadium carbide coating for extended die life.* Journal of Materials Processing Technology, 2002. **124**: 105-112.

30. Shah, S.V. and N.B. Dahotre, *Laser surface-engineered vanadium carbide coating for extended die life.* Journal of Materials Processing Technology, 2002. **124**: 105-112.

31. Liang, B. and C. Ding, *Thermal shock resistances of nanostructured and conventional zirconia coatings deposited by atmospheric plasma spraying.* Surface and coating technology, 2005. **197**: 185-192.

32. Shih, D.S. and R.A. Amato, *Interface reaction between gamma TiAl alloys and reinforcements.* Scripta Metallurgica et Materialia, 1990. **24**: 2053-2058.

33. Dixon, D. and J.W. Newkirk. *Gamma-Titanium aluminide reinforced with Al_2O_3 and TiB_2 fibres*. In Proc. of the Materials Research Society Symposium. 1993, 1063-1068.

34. Munro, R.G., *Evaluated material properties for a sintered alpha-Al_2O_3.* Journal of the American Ceramic Society, 1997. **80**(8): 1919-1928.

35. Ai, T.T., F. Wang and X.M. Feng, *Oxidation behaviour of in-situ Al_2O_3/TiAl composites at 900 °C in static air.* International Journal of Minerals, Metallurgy and Materials, 2009. **16**(3): 339-344.

36. Li, Z.W., W. Gao, D.Y. Ying and D.L. Zhang, *Improved oxidation resistance of Ti with a thermal sprayed $Ti_3Al(O)$-Al_2O_3 composite coating.* Scripta Materialia, 2003. **48**(12): 1649-1653.

37. Ludtka, G.M. and V.K. Sikka. *Aluminium soldering performance testing of H13 steel as boron coated by cathodic arc technique*. In Proc. of the 47th Annual SVC Technical Conference. 24th-29th April, 2004. Dallas, USA: Society of Vacuum Coaters.

38. Panjan, P., M. Cekada, R. Kirn and M. Sokovic, *Improvement of die-casting tools with duplex treatment.* Surface and Coatings Technology, 2004. **180-181**: 561-565.

39. Sujata, M., S. Bhargava and S. Sangal, *On the formation of $TiAl_3$ during reaction between solid Ti and liquid Al.* Journal of Materials Science Letters, 1997. **16**(13): 1175-1178.

40. Han, J.C., C.Q. Hong, X.H. Zhang and B.L. Wang, *Thermal shock resistance of TiB_2-Cu interpenetrating phase composites*. Composites Science and Technology, 2005. **65**(11-12): 1711-1718.

41. Pellizzari, M., A. Molinari and G. Straffelini, *Thermal fatigue resistance of plasma duplex-treated tool steel.* Surface and Coatings Technology, 2001. **142-144**: 1109-1115.

Chapter 7

Tribological Properties of $Ti(Al,O)/Al_2O_3$ & $TiAl/Al_2O_3$ Composite Coatings

7.1. Introduction

Die wear and failure are significant issues in die casting. Wear phenomena, as a result of mechanical and thermal loading cycles, are widely observed in the most commonly used AISI H13 die steel [1]. The die life can be improved in a number of ways. The most common methods are, developing new die materials, improving die material heat-treatments, changing the die design, using better lubricants and applying appropriate coatings [1]. The main goal of this work was to investigate the possibility of using thermally sprayed HVOF $Ti(Al,O)/Al_2O_3$ and $TiAl(O)/Al_2O_3$ composite coatings to improve the wear resistance of H13 tool steel for the possible application in Al die casting dies and dummy blocks used in extrusion. Although Al corrosion resistance/soldering and a reduction in the degree of Al wetability are the central issues for the application of these coatings to tool steel die casting dies and dummy blocks used in Al extrusion, Al soldering and wetability behaviour are not necessarily related to the good tribological properties of the coatings. It is important to determine a coating's tribological behaviour along with Al wetability behaviour to make sure that a coating can perform well in both respects for particular applications. A comprehensive study of the tribological properties of candidate coatings for Al die casting die applications is reported by Salas et. al. [2]. There exists a wide variety of wear tests simulating different contact geometry, load and environment. A sand abrasion test is common among thick coatings and it records the wear rate against the abrasive sand particles, which are used against a coating with a specific force. In thin coatings, a scratch adhesion test is the popular one. A scratch test involves moving a thin film against a sharp indenter at a constant speed with increasing load. The load at which film failure occurs is termed the critical load (Lc). The value of Lc is also

termed as the coating adhesion strength. In a reciprocating wear test, an indenter is moved backward and forward across the film under a small fraction of the load (10% of Lc). The amount of material removed under these reciprocating conditions measures the extent of wear. A commonly known pin and disc test is just a variation of a reciprocating wear test. In a pin and disc test a sharp/spherical ended pin is moved across the surface of the coating or film at a constant load in a circular motion. In a pin on disc test (pin or ball against a coated disk), the contact between a spherical ended pin against a flat disc results in a point contact configuration and enable the application of high contact pressure.

Thermal spraying is a well established means of forming relatively thick coatings. Among the thermal spraying techniques, HVOF can be effectively used to prepare metal ceramic coatings with a dense structure at a particle velocity of above 700 m/s. The HVOF spraying has been established into a reliable technique to coat a great variety of metallic surfaces with hard, adherent and tribologically improved composite coatings [3]. Thermally sprayed composites are composed of a matrix and a second reinforcement phase. The matrix is usually a metallic phase and is responsible for the homogenous distribution of the stresses within the composite. The reinforced phase contributes towards increasing the hardness and the wear resistance of the coating [4]. Hard cermet coatings produced by thermal spraying are used in industry to minimize friction, wear and tribological requirements for the base material of protected components [5]. In the literature the use of carbide based composite coatings such as WC-Co, Cr_3C_2-NiCr, WC-CoCr, Mo_2C-Mo, Cr_3C_2-Ni, Cr_3C_2-Mo and WTi-C as wear resistant coatings is well described [5-9]. Coatings with high oxide content are usually harder and more wear resistant. Al_2O_3 is found to be a suitable reinforcement for improving the wear resistance of metal matrix composites (MMCs) due to its excellent chemical and thermal resistance and high hardness [10, 11]. The high hardness of the titanium alloy intermetallics and composites make their application appropriate as wear resistant coating materials.

The wear mechanisms of thermally sprayed coatings are complex due to their lamellar structure. The presence of different phases and microstructural features such as cracks and pores in these coatings make the wear and friction estimation difficult compared with the bulk materials. There are many studies on the friction and wear behaviour of

thermally sprayed coatings. In a detailed study [12, 13] on the sliding wear behaviour of thermally sprayed coatings, delamination of splat structures is described as the dominant mechanism of wear. The coating failure process involves crack initiation from the splat boundaries rather than from inside the splat. A coating's imperfections and splat boundaries act as stress concentrators. Splats adhesion is described as a controlling factor to the coating wear [5].

In Ti(Al,O)/Al_2O_3 and TiAl/Al_2O_3 composite coatings, the ceramic phase Al_2O_3 has excellent high temperature properties, high hardness and is not wetted by the molten aluminium. The intermetallic compounds based on titanium, such as Ti_3Al, TiAl, and $TiAl_3$ have been examined and developed for high temperature applications [14, 15]. Compared with titanium, these titanium aluminides present several advantages; i.e. higher elastic modulus, lower density, higher oxidation resistance, and better mechanical behaviour with increasing temperature [14, 16]. In addition, Ti_3Al and especially TiAl have much better "titanium fire" resistance than titanium and its alloys [17]. Moreover, titanium aluminide coatings show better wear resistance than that of pure Ti [10]. However, low ductility at room temperature is a major obstacle to the use of Ti_3Al, TiAl and $TiAl_3$ as structural materials[16, 18]. Titanium aluminide surface coatings are considered to be another promising application of these intermetallic compounds [10, 18, 19]. One effective way to improve the wear resistance of intermetallic compounds is to obtain a hard phase reinforced intermetallic matrix composite (IMC) which is expected to possess high hardness and subsequently good wear resistance. There is a great interest in intermetallic matrix composites due to the reason that monolithic intermetallic alone can not satisfy the properties required for advance applications. However the processing of intermetallic matrix composites is a critical issue. A number of methods have been explored to fabricate such composites with either continuous or discontinuous reinforcements. The composite with discrete reinforcement provides less improvement in mechanical properties compared to the one with continuous reinforcement. Mechanical alloying provides an economical processing route for composite with discrete reinforcement whereas composite with continuous reinforcement are usually produce by SHS method.

The reciprocating wear properties of plasma and HVOF thermally sprayed TiAl/Al_2O_3 based composite coatings were investigated by Hung [20] under ambient conditions, Results of this study showed that an HVOF sprayed TiAl/Al_2O_3 coating is more wear resistant than a plasma sprayed coating.

In this study the friction and sliding wear behaviour of the composite coatings using alumina and high speed steel pins both at room and high temperature were studied (using a pin on disc test) under lubrication and dry conditions.

7.2. Results and discussion

Besides determining the friction coefficient and wear rate of the composite coatings, the test data was also used to evaluate the approximate coating life. Thus, the particular choice of sliding distance for a given friction test condition is based upon the ultimate coating failure. The specific wear rate of the composite coatings was calculated based on the wear track profile information. All the tests were performed at a constant load of 20 N with a sliding speed of 0.5 m/s.

7.2.1. Friction and wear of composite coatings

7.2.1a. Ti(Al,O)/Al_2O_3 composite coatings (A2)

<u>High temperature tests</u>

At 700 °C, composite coating (A2) failure occurred after approximately 100 m sliding distance with a measured coefficient of friction of about 1.0 (figs. 7.1a,b).

The high fluctuation in coefficient of friction (COF) of the coated sample is likely due to coating debris generated during wear testing and also due to the differences in hardness among the various phases within the composite structure.

The oxidation product/oxidation film (Al_2O_3, TiO_2) at higher temperatures of 700 °C and 800 °C after several hours holding as reported by [21, 22] was not observed in this study due to the short duration of the wear test at 700 °C. So, the role of oxidation is not taken into account during sliding wear. The high coefficient of friction is only due to the interpenetrating hard ceramic oxides in the composite coating. The high

friction and wear of ceramics sliding on ceramics has been reported by others to be generally of the order of 0.5-1.0 [23, 24].

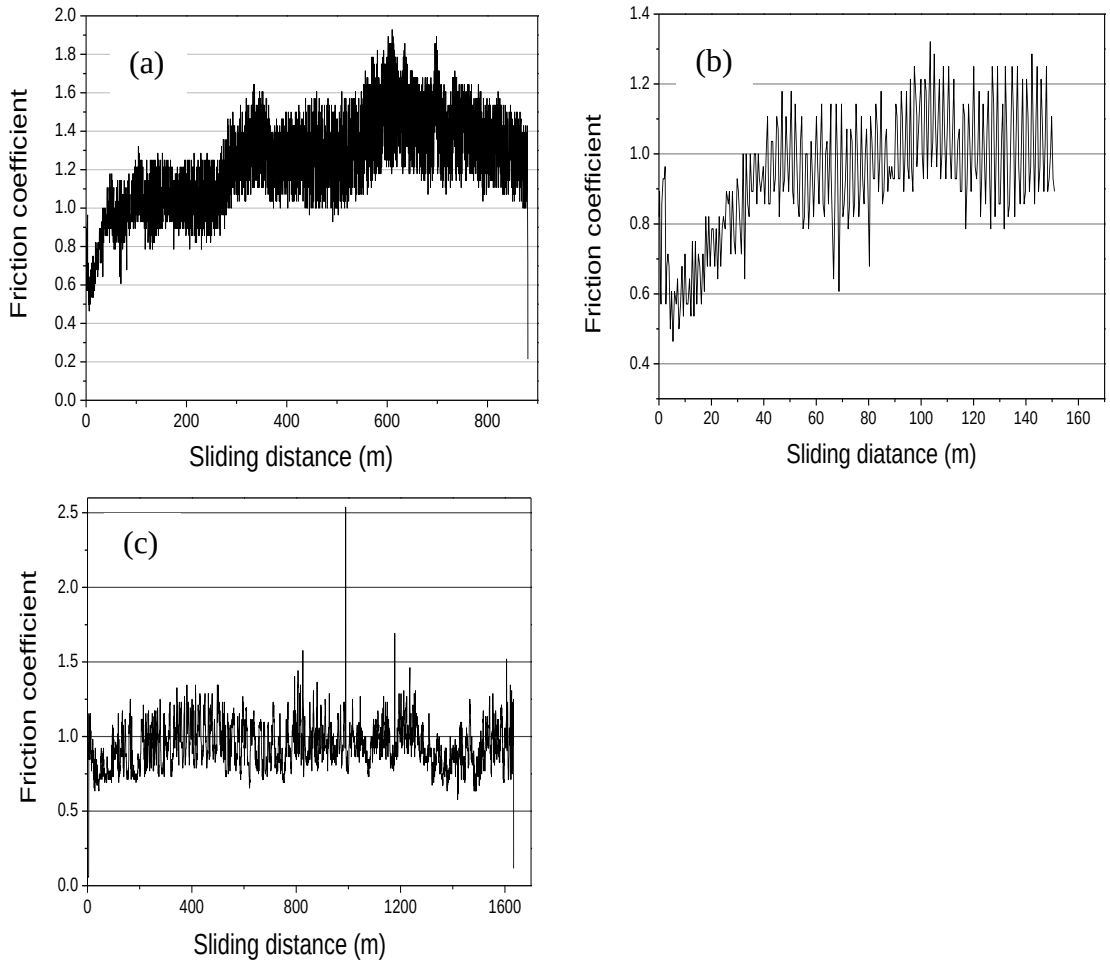

Figure 7.1: Coefficient of friction at high temperature (700 °C) using spherical ended alumina pin, (a, b) coated disc with wear track diameter of 0.028 m, (c) uncoated disc with wear track diameter of 0.052 m

The coefficient of friction for alumina over alumina is reported to be about 1.0 at 700 °C (Air atmosphere, 5 N load, sliding speed 0.38 m/s). The increase in the stable friction coefficient of the coating after 100 m sliding distance is likely due to the combined effect of the coating and H13 tool steel substrate. Figure 7.2 shows the wear track morphology of the coated sample using a spherical ended alumina pin after 115 m sliding distance. No oxidation film is observed over the coating surface at a temperature of 700 °C. However, partial coating failure is observed for the particular sliding distance. The friction coefficient for uncoated H13 tool steel is 0.94 and is stable over the 1600 m sliding distance (fig. 7.1c).

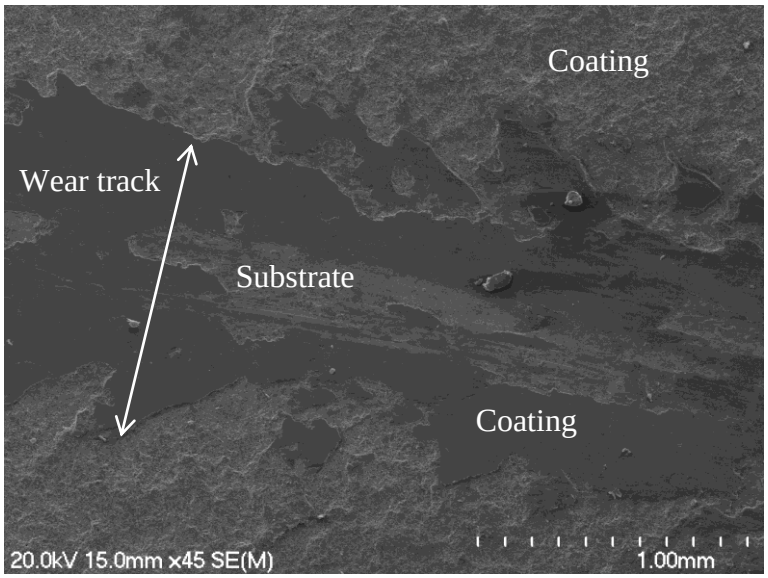

Figure 7.2: Wear track morphology of coated sample after 115m sliding distance at higher temperature (700 °C) using spherical ended alumina pin

An increase in the weight of the pin material was observed during measurements on the uncoated disc due to the sticking of steel onto the pin. This results in more wear/damage of the uncoated steel discs. An oxidation film of iron oxide is reported at 300 °C on ferrous materials. An oxide film of Fe_3O_4 is reported to play a significant role in decreasing the friction and wear rate of alloy steel. The coefficient of friction for the uncoated H13 is slightly less than that measured for the coated disc (till coating failure) due to the lower hardness of the iron oxides /film ($FeO/Fe_2O_3/Fe_3O_4$ with hardness on Mohs scale 3.5/5.5-6.5/5.5-6.5 respectively) than the coating oxides [25, 26]

In tribology, oxidation of a test specimen plays an important role in determining its friction and wear behaviour. At high temperature, Swapnil et al. [27] reported the oxidation kinetics of H13 tool steel in the temperature range of 200-800 °C and found that oxidation is prominent only at high temperatures > 800 °C with less oxidation at temperatures < 800 °C. Studies by Gao et al. [28] have reported excellent oxidation resistance at 700 °C for a $Ti(Al,O)/Al_2O_3$ coating , the oxidation products at 800 °C in these coatings reported to be TiO_2 and Al_2O_3. Due to a remarkably decreased rate of oxidation in these coatings at high temperature, the role of oxidation was not considered to be significant during high temperature tribological testing of coatings. However, a stable value of friction coefficient of H13 tool steel is due to the continuous formation and removal of an oxide film.

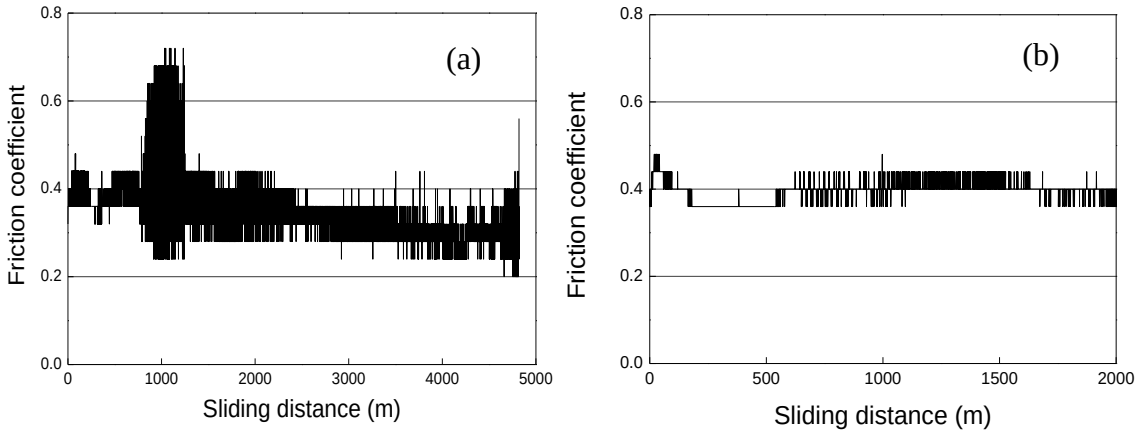

Figure 7.3: Coefficient of friction at 700 °C with a flat ended high speed steel pin (HSS) (a) coated disc with wear track diameter 0.028 m, (b) uncoated disc with wear track diameter 0.025 m

The average value of the coefficient of friction using a flat ended high speed steel pin (fig. 7.3a.) is about 0.30-0.34 and no coating failure was observed until a sliding distance of about 4500 m was reached. The sharp rise in friction coefficient values between 800-1100 m is due to the roughness of the coated disc (run in period). After this period the coating become smoother, some pin material transferred to the disc. The decrease in friction coefficient after 1000 m sliding distance is due to the high temperature oxide film from the transferred material over the coating wear track. The iron oxides have a lower hardness than the coating oxides.

A considerable loss in steel pin weight after the test was also an indication of the pin wear and consequently material transfer to the wear track. SEM imaging and EDAX analysis of the wear track further confirmed the presence of metallic material (Fe) on the wear track without any damage to the coating. Figure 7.4 shows the SEM images of the worn wear track. The average friction coefficient for the uncoated H13 tool steel with a high speed steel pin is 0.40 and is stable throughout the sliding distance (fig. 7.3b).

The average values of friction coefficient for the coated sample at 700 °C using a spherical ended steel pin is 0.39 over a sliding distance of about 180 m (fig. 7.5a). The friction coefficient almost remained stable throughout the sliding distance of the coated specimen in contrast to the uncoated sample. The friction coefficient values for the uncoated specimen (fig. 7.5b) are 0.39-1.10. The increase in the friction coefficient value in the case of the uncoated sample is due to the damage of the

counter pin surface causing pin flattening. The counter steel pin wear (weight loss) was considerably larger in the case of the uncoated sample than the coated one.

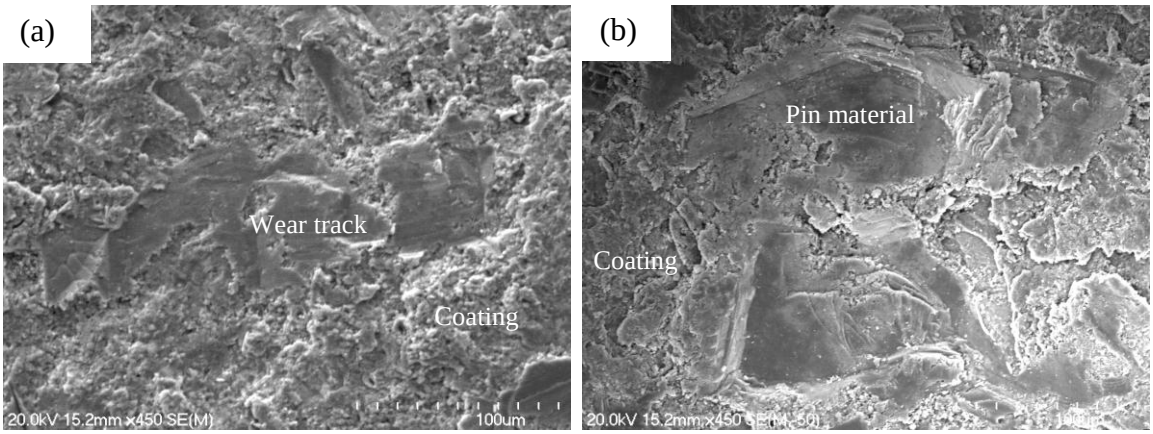

Figure 7.4: (a) Wear track morphology of coated sample after 4819 m sliding distance using flat ended high speed (HSS) steel pin and (b) wear track with pin material

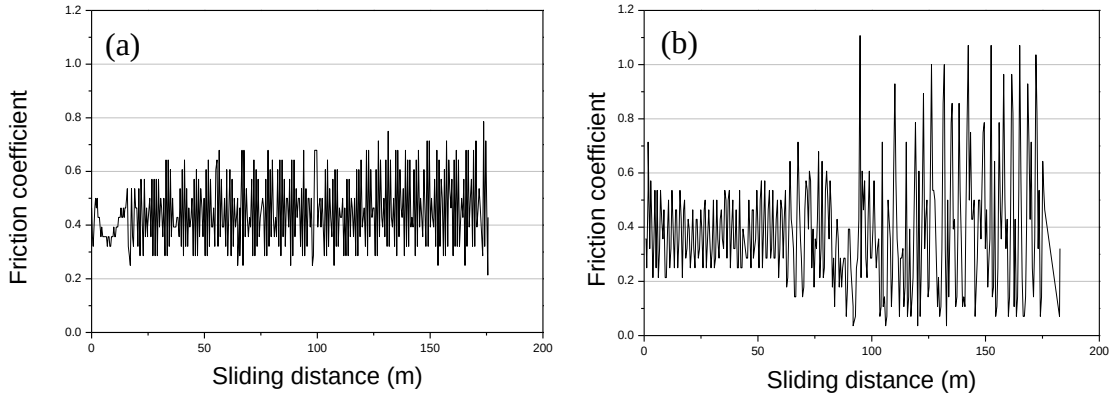

Figure 7.5: Coefficient of friction at 700 °C with a spherical ended steel pin with wear track diameter 0.028 m (a) coated disc (b) uncoated disc

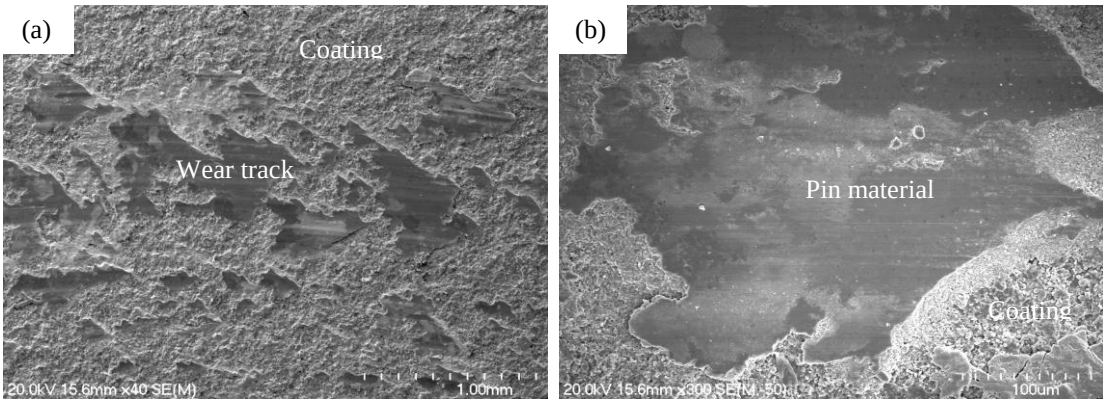

Figure 7.6: (a) Wear track morphology of Ti(Al,O)/Al_2O_3 coated sample tested at 700 °C after 180 m sliding distance using spherical ended steel pin and (b) wear track with steel pin material

Figure 7.6 shows the wear track morphology of the coated sample using a spherical ended steel pin after 180 m sliding distance. No coating failure is observed for the particular sliding distance. However the transfer of counter steel pin material on to the wear track of the coated sample confirmed excessive pin damage/wear.

Room temperature dry sliding tests

At room temperature, using a spherical ended alumina pin, the coating endured a sliding distance of approximately 10 m (fig. 7.7a) with an average coefficient of friction of 0.77. The continuous increase in the friction coefficient after 10 m is due to coating removal and an increase in the surface roughness of the steel substrate underneath due to a cutting action (ploughing action) of the hard alumina pin. The high hardness of the alumina pin caused plastic deformation of the relatively soft matrix/substrate resulting in a cutting action, which removes material from the surface of the steel substrate [29].

In fact, the alumina pin ploughed the steel disc and the steel became harden under the contact force. The hardened steel damaged the alumina pin and consequently the pin damaged the steel. The room temperature friction coefficient for the uncoated tool steel is unstable, with values in the range 0.82-1.8 (fig. 7.7b).

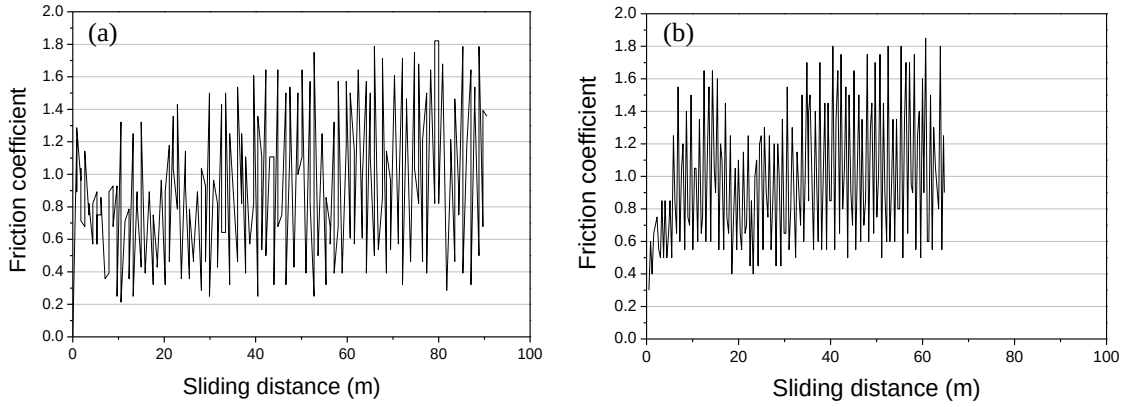

Figure 7.7: Coefficient of friction at room temperature with alumina pin, (a) coated disc with wear track diameter 0.028 m, (b) uncoated disc with wear track diameter 0.020 m

At room temperature, using a flat ended high speed steel (HSS) pin, the coating failure occurred at a sliding distance of about 100 m and the average value of friction coefficient for the particular sliding distance is 0.48 (fig. 7.8a). The friction

coefficient is unstable for the uncoated H13 tool steel sample. The hardened steel damaged the high speed pin and consequently there is more damage to the steel substrate. Friction coefficient values for the uncoated sample are in the range 1.21-2.0 (fig. 7.8b).

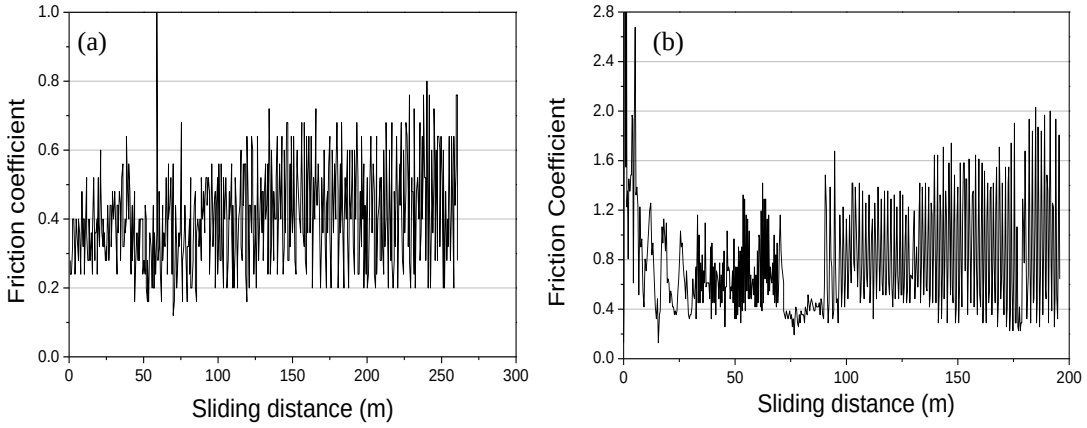

Figure 7.8: Coefficient of friction at room temperature with a high speed steel pin, (a) coated disc with wear track diameter 0.025 m, (b) uncoated disc with wear track diameter 0.031 m

Room temperature lubricated tests

Using an oil lubricant the value of friction coefficient for the coated sample is initially high due to the high surface roughness of the coating (fig. 7.9a). After a run-in period, the surface became smoother and the friction coefficient of the coating decreased to 0.058 and the coating endured a sliding distance of approximately 7800 m. The average value of friction coefficient for the uncoated sample is 0.03 (fig. 7.9b). These values are lower than the friction coefficients obtained with an alumina pin, both at room temperature under dry sliding and at high temperature. The uncoated sample has a lower friction coefficient than the coated sample due to the high surface roughness and lower oil lubrication tendency (boundary film is not easy to form) of the coated sample.

Figure 7.10 shows the worn surface morphology of the coated sample using a spherical ended alumina pin with an oil lubricant after a sliding distance of about 7800m. The SEM clearly shows partial coating failure with exposed metallic substrate.

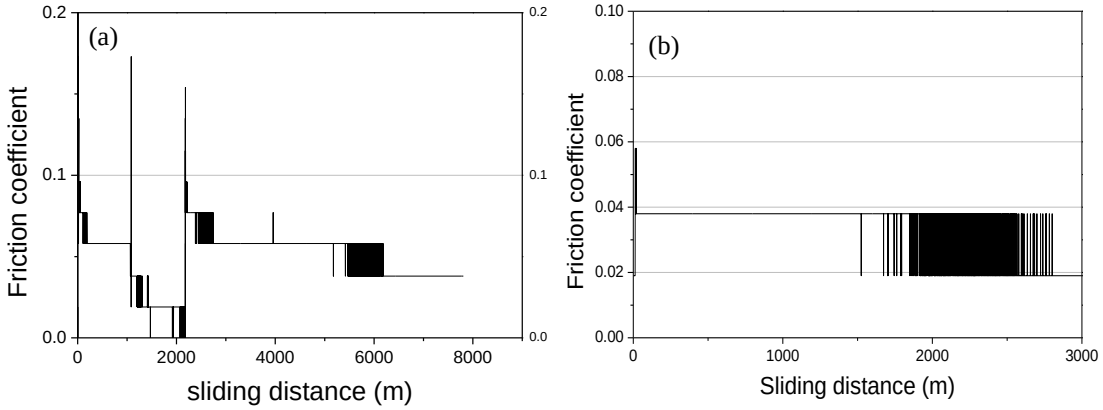

Figure 7.9: Coefficient of friction at room temperature with oil lubrication, wear track diameter 0.052 m, (a) coated sample (b) uncoated sample

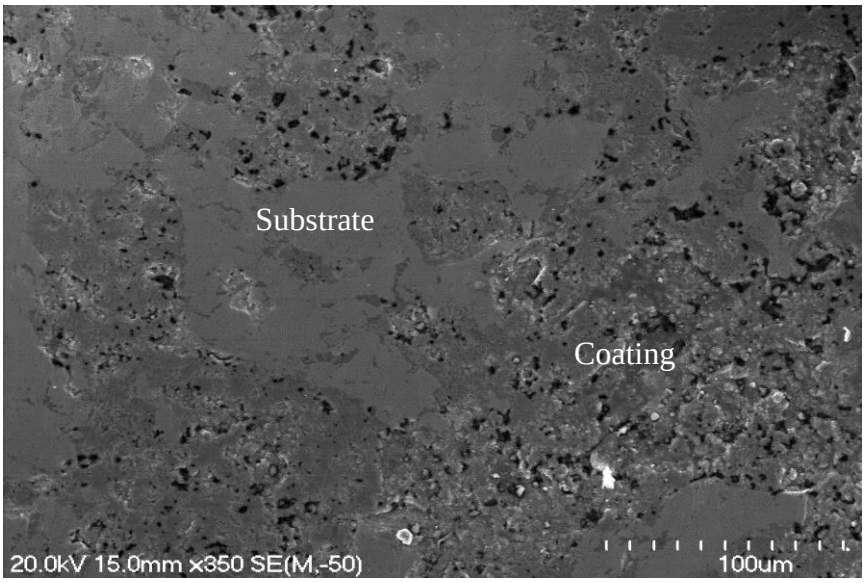

Figure 7.10: Wear track morphology of coated sample after at room temperature after 7800m sliding distance using spherical ended alumina pin with oil lubricant

7.2.1b. $TiAl/Al_2O_3$ composite coatings (B2)

<u>High temperature tests</u>

At high temperature (700 °C), using a spherically ended alumina pin, the composite coating (B2) failure occurred at approximately 100 m sliding distance with an average value of the friction coefficient of about 0.80 (fig. 7.11). The high friction and wear of ceramics sliding on ceramics has been reported by others [23, 24] to be generally of the order of 0.5-1.0. The friction coefficient for uncoated H13 tool steel (fig. 7.1c) is 0.94 and is stable over the 1600 m sliding distance.

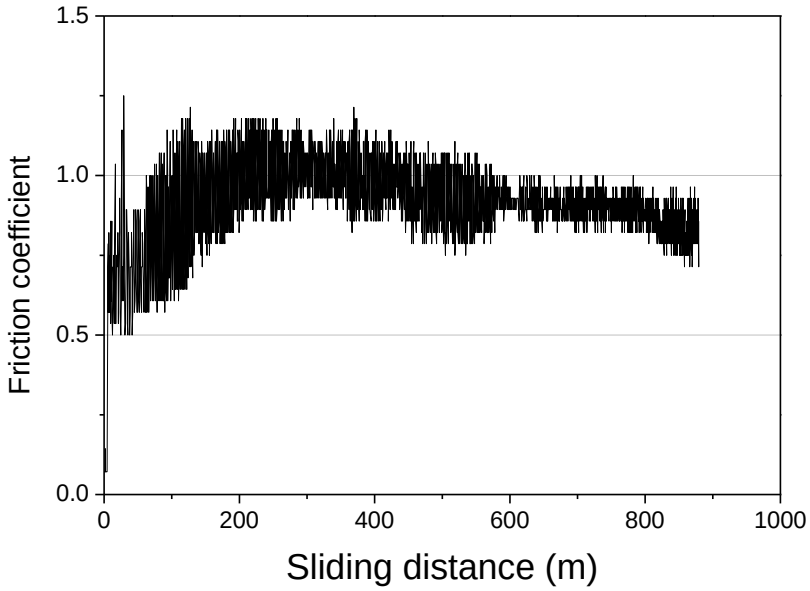

Figure 7.11: Friction coefficient of coated disc at higher temperature (700 °C) using spherical ended alumina pin with wear track diameters 0.028 m

A study [22] has reported a remarkable decreased rate of oxidation and increased spallation resistance of $TiAl/Al_2O_3$ and Ti_3Al/Al_2O_3 coatings at 800 °C. The oxidation products in the coating, after holding for several hours at 800 °C, are reported to be TiO_2 and Al_2O_3. Due to the short duration of a wear test, no oxidation film/product was observed at 700 °C in this study. The role of oxidation is not taken into account during high temperature sliding wear. Figure 7.12 shows the wear track morphology of the coated sample using a spherical ended alumina pin after 175 m sliding distance. No oxidation film is observed over the coating surface at temperature 700 °C. However, partial coating failure is observed along with the exposed substrate surface for the particular sliding distance.

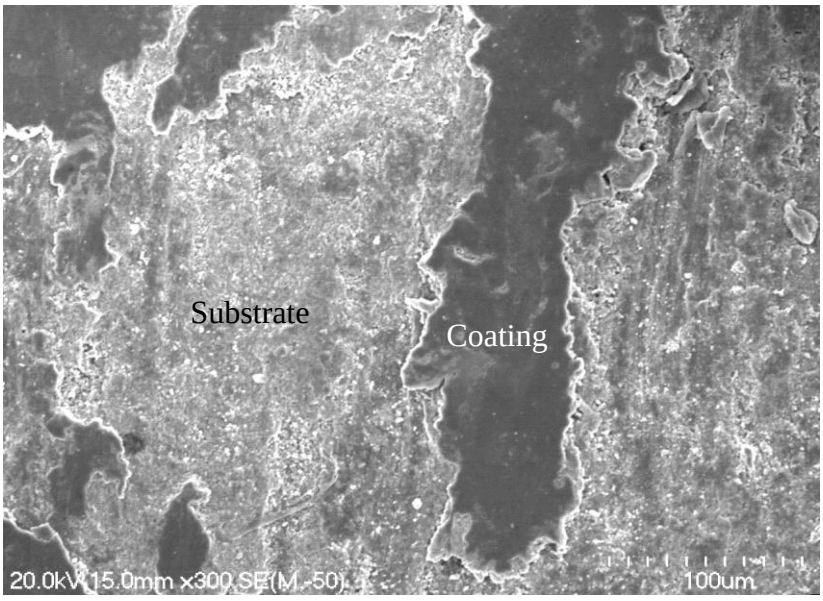

Figure 7.12: Wear surface morphology of coated sample after 175m sliding distance at higher temperature (700 °C) using spherical ended alumina pin

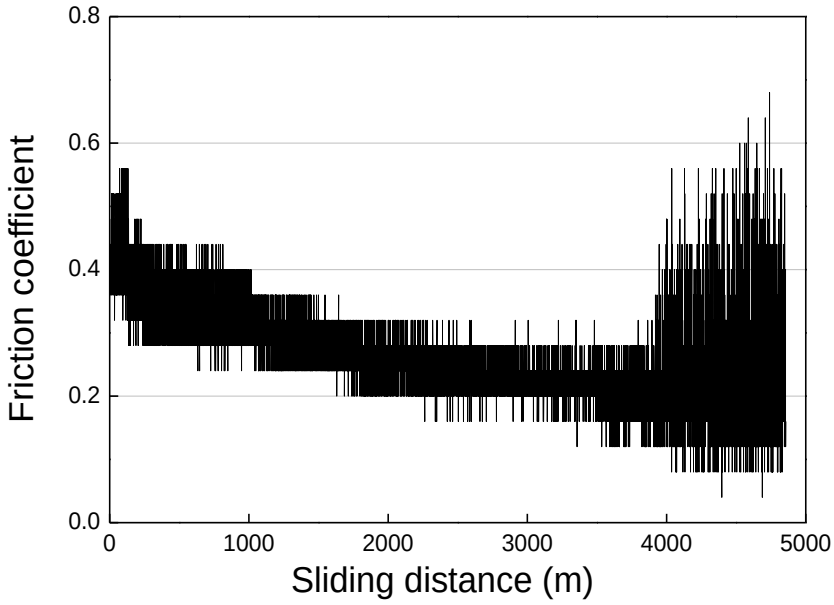

Figure 7.13: Friction coefficient of coated disc at high temperature (700 °C) using HSS pin with wear track diameter of 0.025 m

In the wear tests at 700 °C, using a flat ended high speed steel pin (HSS) (fig. 7.13), the friction coefficient of a coated sample showed a continuous decrease from 0.42 to 0.24 for a sliding distance of about 4000 m. The coating failure occurred at about 4000 m. The continuous decrease in the value of friction coefficient is due to the metallic oxide formed on the wear track due to transfer of pin material.

Room temperature dry sliding tests

The room temperature friction coefficient and coating failure is difficult to predict from the graph shown in fig. 7.14 due to the unstable values of friction coefficient over the measured sliding distance. However, a visual inspection of the wear track showed the complete removal of the coating after 90 m sliding distance. The unstable friction coefficient is due to high surface roughness and quick coating failure. It is due to either an alumina or steel substrate that contacts the pin and results in high and unstable values of friction coefficient. The metallic matrix itself comprises of different phases Ti_3Al and TiAl with varying hardness, so this factor also contributed to the instability of the friction coefficient. Moreover, alumina pulled out of the matrix during the ploughing action of the counter pin, which also acted as an abrasive during testing and thus contributed towards the increased wear rate at room temperature.

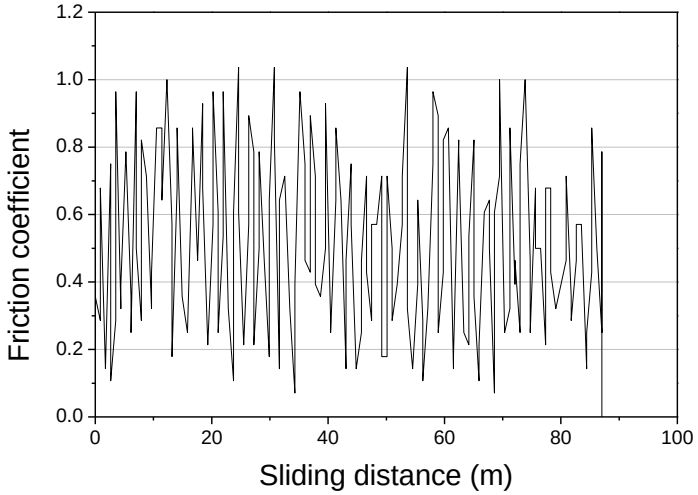

Figure 7.14: Friction coefficients of coating at room temperature using alumina pin with a wear track diameters of 0.028 m

At room temperature, using flat ended high speed steel pin (HSS), the coating failure occurred at about 20 m with a friction coefficient between 0.50-0.80 (fig. 7.15). The friction coefficient was unstable throughout the sliding distance. The continuous increase in the friction coefficient is due to coating removal and an increase in the surface roughness of the tool steel underneath with increased sliding distance. The steel hardened under the contact force and damaged the high speed pin which as a consequence makes the steel surface rougher. Visual inspection of the coating wear after a sliding distance of about 140 m also confirmed the total removal of the coating.

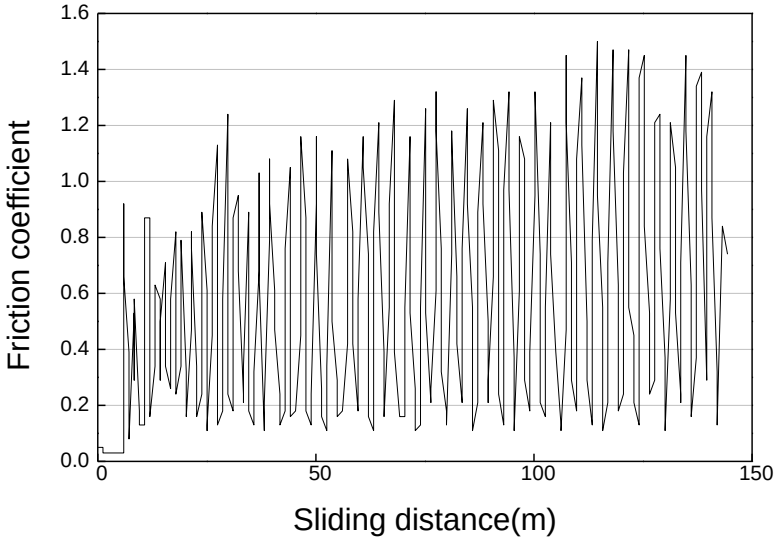

Figure 7.15: Friction coefficient of coated sample at room temperature with flat ended high speed steel pin (HSS) with a wear track diameter 0.038 m

Room temperature lubricated tests

Using an oil lubricant, the value of friction coefficient for the coated sample using an alumina pin is initially high due to the high surface roughness of the coating as shown in (fig. 7.16). After a run-in period, the surface became smoother and the friction coefficient became stable. The average value of friction coefficient for the coated sample is 0.077 and there is oil film failure at about 3500 m which results in an increase in the friction coefficient. However, the coating endured a sliding distance of approximately 4900 m The average value of friction coefficient for the uncoated sample is 0.03 (fig. 7.9b). These values are lower than the friction coefficients with an alumina pin both at room temperature under dry sliding and at high temperature. The uncoated sample has a lower friction coefficient than the coated sample due to the high surface roughness of the coated sample.

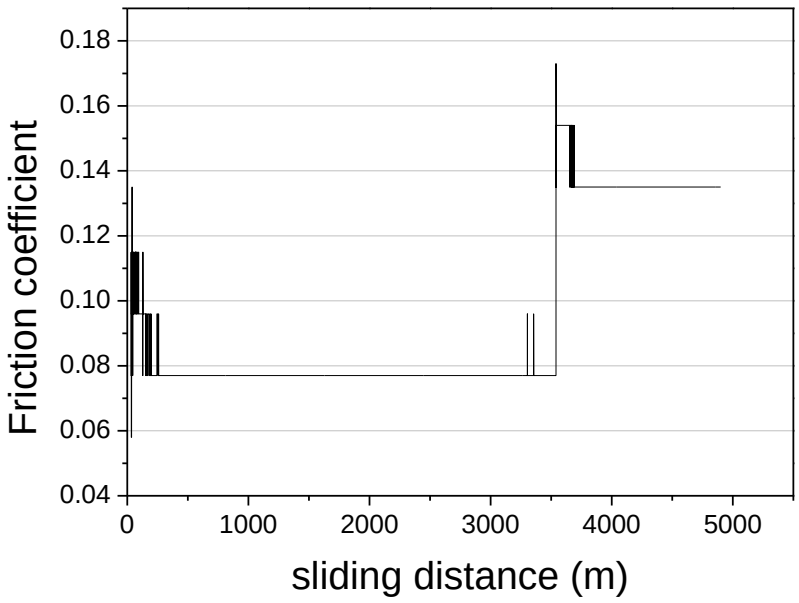

Figure 7.16 Coefficient of the coated sample using alumina pin at room temperature with oil lubrication, wear track diameter 0.052 m

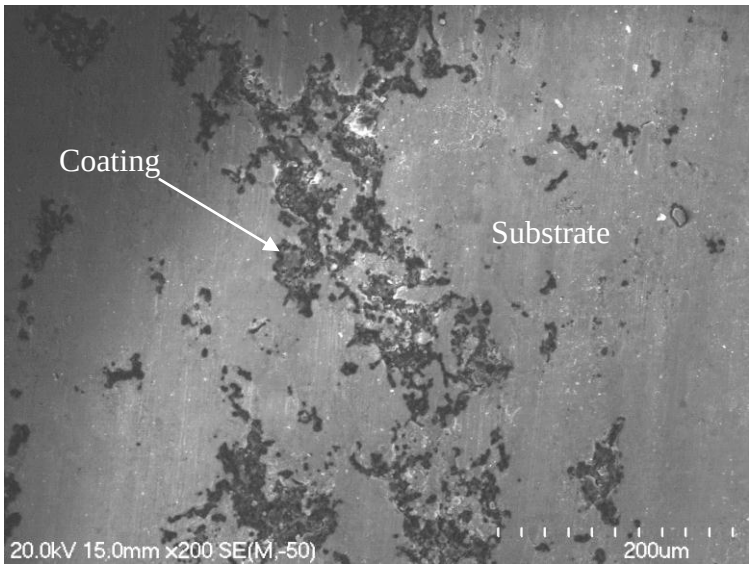

Figure 7.17: Wear track morphology of coated sample at room temperature after 4900 m sliding distance using spherical ended alumina pin with oil lubricant

Figure 7.17 shows the worn surface morphology of the coated sample using a spherical ended alumina pin with an oil lubricant. The SEM clearly shows that there is a significant failure of the coating and the metallic substrate is mostly exposed.

Table 7.1 summarise the friction coefficient and life of both of the composite coatings (A2 and B2) under various test conditions.

Table 7:1: Friction coefficients and composite coating life under sliding wear

Coating	Pin material	Test temperature	Test condition	Coefficient of friction		Coating life (m)
				Coated	Uncoated	
Ti(Al,O)/Al_2O_3 (A2)	Alumia (spherical ended)	HT	Dry	1.0	0.94	100-300
		RT	Dry	0.77	0.82-1.8	10
		RT	Oil lubrication	0.058	0.03	Partial failure/7800
	High speed steel (flat ended)	HT	Dry	0.30-0.34	0.40	No failture/4500
		RT	Dry	0.48	1.21-2.0	100
	Steel (spherical ended)	HT	Dry	0.39	0.39-1.10	No failure/180
TiAl/Al_2O_3 (B2)	Alumina (spherical ended)	HT	Dry	0.80	0.94	100-200
		RT	Dry	Not clear	0.82-1.8	Not clear
		RT	Oil lubrication	0.077	0.03	Partial failure/4900
	High speed steel (flat ended)	HT	Dry	0.24-0.42	0.40	4000
		RT		0.50-0.80	1.21-2.0	20

7.2.2. Specific wear rate of composite coatings

The wear rate of the samples was calculated using Eq. 7.1.

$$K = \frac{V_w}{P \times S} \quad \text{.....7.1}$$

Where K = Specific wear rate mm^3/ N-m; V_w = Worn volume, mm^3; P = Load, N; and S = Sliding distance (m).

For the pin on disc test, a worn volume was calculated using Eq.7.2 from the dimensions of the worn track [30-32].

$$V_w = \frac{\pi r h\left(3h^2 + 4w^2\right)}{3w} \quad \text{.....7.2}$$

Where r = wear track radius, mm; h = depth of worn track, mm; and w = width of worn track, mm.

With the help of the wear track profile, h and w were measured precisely due to the regular profile of the wear track.

For uncoated samples at high temperature (700 °C), the wear track profile data was out of the range (due to higher wear rate) of the equipment measuring limit (-500 µm - 500 µm), so the width of the wear track was measured using an optical microscope (three readings from different locations). From the width of the wear track its depth was calculated using the expression;

$$t = \frac{2R - \sqrt{4R^2 - b^2}}{2} \quad \text{.....7.3}$$

Where R = radius of pin, mm; b = width of the worn track, mm; and t = depth of the wear track, mm.

However, the wear volume calculation based upon the depth of track calculation using Eq. 7.3 could be slightly higher than the one based on actual wear profile track measurements (width and depth) due to plastic deformation.

7.2.2a. Wear track profiles of Ti(Al,O)/Al_2O_3 (A2)

The wear tracks profile of the Ti(Al,O)/Al_2O_3 (A2) composite coatings at different temperatures using a spherically ended alumina pin at load 20N and sliding speed 0.5 m/s are shown in figs. 7.18 - 7.20.

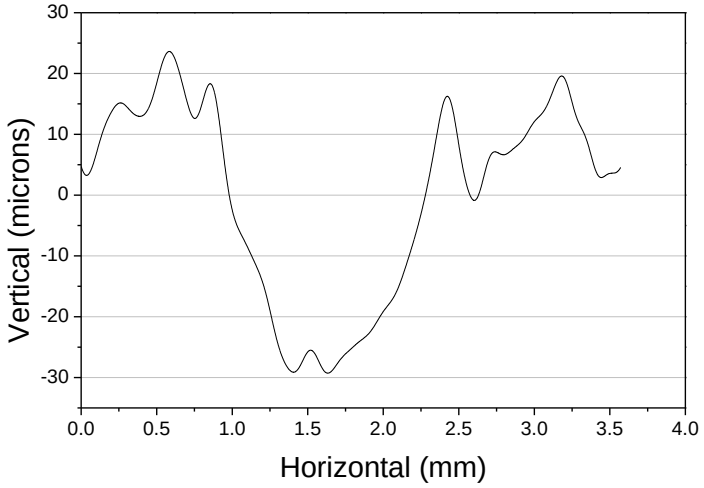

Figure 7.18: Wear track profile of Ti(Al,O)/Al_2O_3 coating sample tested at high temperature 700.°C using spherical ended alumina pin

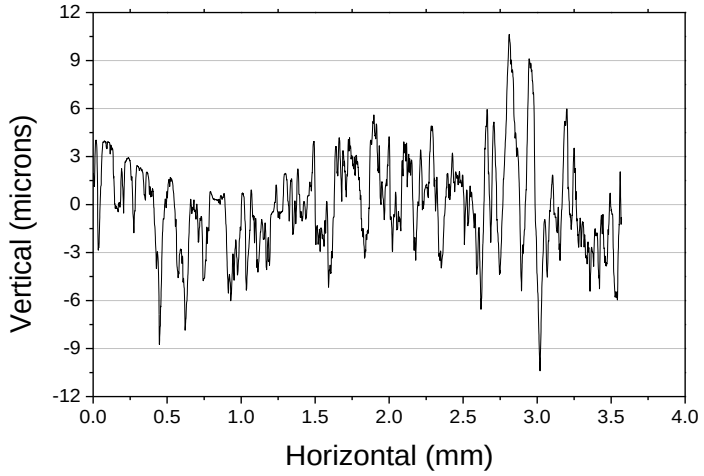

Figure 7.19: Wear track profiles of uncoated samples tested at room temperature using oil lubricant with spherical ended alumina pin

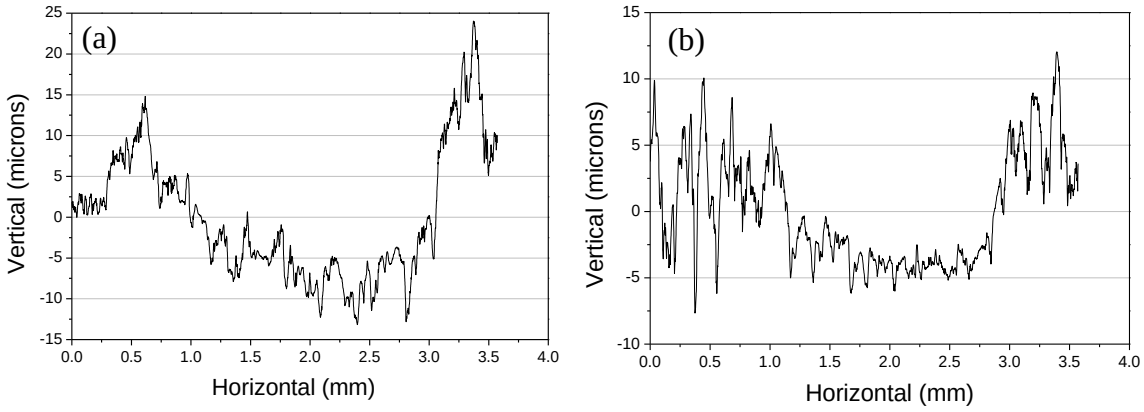

Figure 7.20: Wear track profiles of samples tested at room temperature with spherical ended alumina pin, (a) Ti(Al,O)/Al_2O_3 coated sample (b) uncoated sample

The wear rates of the Ti(Al,O)/Al_2O_3 coated and uncoated materials are compared at room and high temperatures (table 7.3). At high temperature, the wear rate of the Ti(Al,O)/Al_2O_3 coating(A2) was calculated to be $2.36x10^{-4}$ mm^3/N.m which is less than that for the uncoated sample ($2.02x10^{-3}$ mm^3/N.m). The slightly lower wear rate of the uncoated sample under lubrication is due to the lower surface roughness and more stable oil film compared with the coated one. Due to the irregular profile of the coated sample tested under lubrication conditions, the wear rate calculations in this case is based on wear track width measurement (eq.7.3) using an optical microscope. At room temperature, the coated sample has a higher wear rate of about $2.38x\ 10^{-3}$ mm^3/N.m.

7.2.2b. Wear track profiles of TiAl/Al_2O_3 (B2)

The wear track profiles of the TiAl/Al_2O_3 (B2) composite coatings at different temperatures using a spherically ended alumina pin are shown in figures 7.21-7.23.

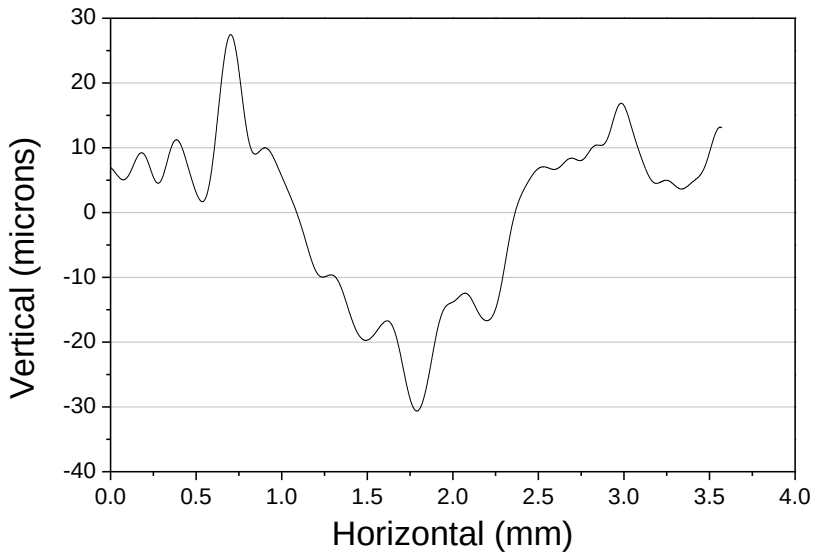

Figure 7.21: Wear track profile of TiAl/Al_2O_3 coated sample tested at high temperature 700 °C using spherical ended alumina pin

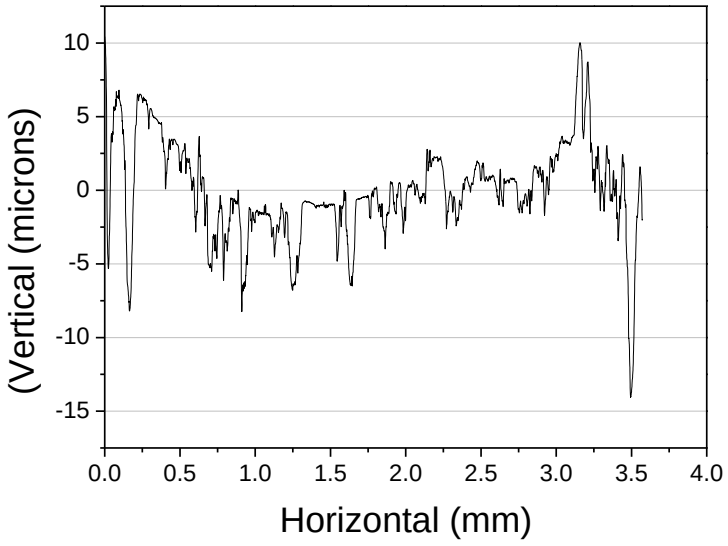

Figure 7.22: Wear track profile of $TiAl/Al_2O_3$ coated sample tested room temperature using oil lubricant with spherical ended alumina pin

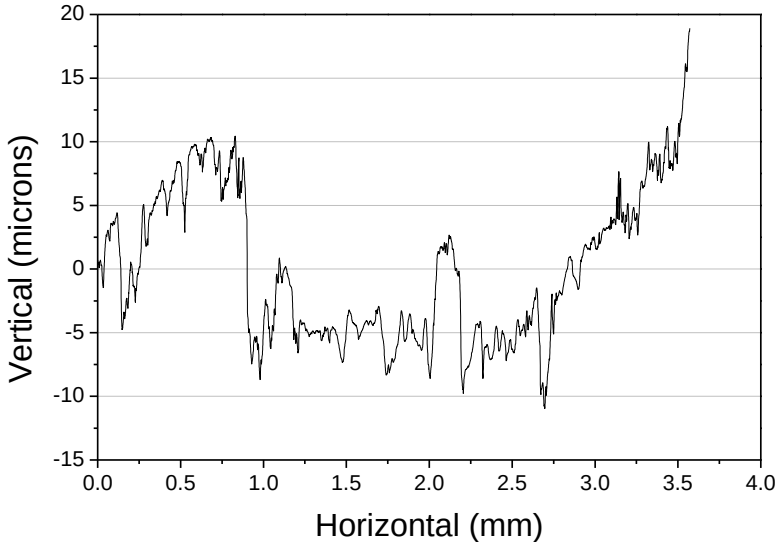

Figure 7.23: Wear track profile of $TiAl(O)/Al_2O_3$ coated sample tested room temperature using spherical ended alumina pin

The table 7.2 presents wear track profile details of coated and uncoated samples.

Table 7:2: Wear track profile details of coated and uncoated samples at room and high temperature (700 °C) using spherically ended alumina pin

Samples	High temp				Room temp				Room temp with oil lubrication			
	r	s	w	h	r	s	w	h	r	s	w	h
Coating A2	14	880.43	1.58	0.045	14	90.56	2.6	0.028	26	7800	1.23	0.038
Coating B2	10	628.69	2.28	0.047	14	87.04	2.7	0.023	26	4899.54	2.93	0.018
Uncoated	26	1633.28	2.37	0.210	10	64.74	2.01	0.012	26	4898.56	1.89	0.014

Where r = wear track radius (mm); s = sliding distance (m); w= wear track width (mm); and h = wear track depth (mm)

The experimental results for the Ti (Al,O)/Al_2O_3 and TiAl/Al_2O_3 coatings (A2, B2) (table 7.3) show that for the un-lubricated test specimens, the wear rate of coated samples at room temperature is an order of magnitude higher than their wear rate at 700 °C, however the wear rate of the uncoated sample at 700 °C is an order of magnitude greater than its wear rate at room temperature. The use of these coating at higher temperatures is therefore beneficial. At room temperature, under lubrication, the results show a decrease in the wear rate of the coated and uncoated samples compared with the un-lubricated room temperature samples, but the recorded wear rate for the coated samples is higher than that for the uncoated samples in both cases. This is probably because of the high surface roughness of the coatings.

Based on the literature, under nearly similar conditions, the composite coatings have a much higher wear rate (of the order of 10^{-4} mm^3/N.m) compared with PVD CrN and multilayered Cr/ CrN coatings for tool steel applications. A wear rate of an order of 10^{-6} mm^3/N.m is reported in case of PVD CrN and multilayered Cr/CrN coatings at a temperature of 700 °C (using alumina ball as a counter pin material, load 5N, sliding speed 0.05m/s, 5000 laps) [33]. The higher wear rate of the composite coating in this

study is more likely due to the brittle nature of these composite coatings which favours easy delamination. Moreover the presence of a metallic binder in the composite coating is also responsible for the higher wear rate in the composite coatings compared with hard ceramic based coatings commonly used in die casting applications.

The literature on tribological properties of die coatings suggests that there is a great need for standardization of wear tests in order to make an adequate comparison among them [2].

Table 7.3: Wear rate comparison of composite coatings (A2, B2) at room and high temperature (700 °C) using spherical ended alumina pin

Samples	Wear Rate ($mm^3/N.m$)		
	High temperature	**Room temperature**	**Room temperature with oil lubrication**
Coated (A2)	2.36×10^{-4}	2.38×10^{-3}	3.26×10^{-5}
Coated (B2)	3.57×10^{-4}	2.01×10^{-3}	5.70×10^{-5}
Uncoated	2.02×10^{-3}	6.95×10^{-4}	2.94×10^{-5}

7.3. Summary

The friction and sliding wear of the $Ti(Al,O)/Al_2O_3$ and $TiAl/ Al_2O_3$ composite coatings were studied at room and higher temperature. The approximate life of the composite coatings was also estimated.

It was found that composite coatings have great potential for high temperature application due to their low wear rate at high temperature.

Room temperature applications of the composite coatings can be improved under lubricated conditions.

The tribological properties of the coating can be improved further by reducing the surface roughness of the as sprayed coatings.

7.4. References

1. Shivpuri, R., Y. L. Chu, K. Venkatesan, J. R. Conrad, K. Sridharan, M. Shamim, and R. P. Fetherston, *An evaluation of metallic coatings for erosive wear resistance in die casting applications.* Wear, 1996. **192**(1-2): p. 49-55.

2. Salas, O., K. Kearns, S. Carrera, and J. J. Moore, *Tribological behavior of candidate coatings for Al die casting dies.* Surface and Coatings Technology, 2003. **172**(2-3): p. 117-127.

3. Dorfman, M., J. DeFalco, and J. Karthikeyan. *Tungsten carbide-cobalt coatings for industrial applications*. in *Proceedings of First International Thermal Spray 2000 Conference*. 2000. Montreal, Canada,471-478.

4. Kim, H.-J., S.-Y. Hwang, C.-H. Lee, and P. Juvanon, *Assessment of wear performance of flame sprayed and fused Ni-based coatings.* Surface and Coatings Technology, 2003. **172**(2-3): p. 262-269.

5. Prchlik, L. and S. Sampath, *Effect of the microstructure of thermally sprayed coatings on friction and wear response under lubricated and dry sliding conditions.* Wear, 2007. **262**(1-2): p. 11-23.

6. Matthews, S., M. Hyland, and B. James, *Microhardness variation in relation to carbide development in heat treated Cr_3C_2–NiCr thermal spray coatings.* Acta Materialia, 2003. **51**(14): p. 4267-4277.

7. Asi, S. K., M. H. Sohi, K. Hokamoto, and M. Uemura, *Effect of heat treatment on wear behavior of HVOF thermally sprayed WC-Co coatings.* Wear, 2006. **260**(11-12): p. 1203-1208.

8. Zhang, W. D., C. T. Lei, and F. J. Li, *Laser cladding of stainless steel with Ni-Cr_3C_2 for improved wear performance.* Wear, 2001. **251**(1-2): p. 1372-1376.

9. Yin, B., G. Liu, H. Zhou, J. Chen, and F. Yan, *Sliding wear behavior of HVOF-sprayed Cr_3C_2–NiCr/CeO_2 composite coatings at elevated temperature up to 800 °C.* Tribology Letters, 2010. **37**(2): p. 463-475.

10. DePoorter, G. L., T. K. Brog, and M. J. Readey, *ASM handbooks online, Structural Ceramics*. Vol. 2. 2002, OH, USA: ASM International.

11. Gunther, R., T. Klassen, B. Dickau, F. Gärtner, A. Bartels, and R. Bormann, *Advanced alumina composites reinforced with titanium-based alloys.* Journal of the American Ceramic Society, 2001. **84**(7): p. 1509-1513.

12. Usmani, S. and S. Sampath, *Time-dependent friction response of plasma sprayed molybdenum.* Wear, 1999. **225-229**: p. 1131-1140.

13. Wayne, S. F., S. Sampath, and V. Anand, *Wear mechanisms in thermally sprayed Mo-based coatings.* Tribology Transactions, 1994. **37**: p. 636-640.

14. Djanarthany, S., J. C. Vialab, and J. Bouixb, *An overview of monolithic titanium aluminides based on Ti_3Al and TiAl.* Materials Chemistry and Physics, 2001. **72**(3): p. 301-319.

15. Weisheit, A., B. L. Mordike, W. Smarsly, and K. H. Richter, *Laser surface remelting and laser surface gas alloying of an intermetallic TiAl alloy.* 2000. **10**(1): p. 63-81.

16. Court, S. A., V. K. Vasudevan, and H. L. Fraser, *Deformation mechanisms in the intermetallic compound TiAl.* Philosophical Magazine A, 1990. **61**(1): p. 141-158.

17. Peters, M., J. Kumpfert, C. H. Ward, and C. Leyens, *Titanium and Titanium Alloys: Fundamentals and Applications*. 2003: Wiley-VCH Verlag GmbH.

18. Matsubara, T., T. Shibutani, K. Uenishi, and K. F. Kobayashi, *Fabrication of thick Intermetallic compound Al_3Ti layer on Ti substrate by reactive - pulsed electric current sintering.* Intermetallics, 2000. **8**: p. 815-822.

19. Guo, B., J. Zhou, S. Zhang, H. Zhou, Y. Pu, and J. Chen, *Tribological properties of titanium aluminides coatings produced on pure Ti by laser surface alloying.* Surface and Coatings Technology, 2008. **202**(17): p. 4121-4129.

20. Hung, J. H., Y. L. Chiu, and J. Liang, *Reciprocating wear properties of thermal sprayed titanium aluminide-alumina composite coatings.* Surface and Coatings Technology, 2008. **202**(22-23): p. 5599-5602.

21. Zhang, D., *Titanium Based Materials Technology (NERF REPORT)*, in *UOWX9909*. 2001-2002.

22. Liang, J., *Application of titanium based composite powders in producing high performance coatings*. 2006, Internal Report,The University of Auckland: Auckland.

23. Sutor, P., *Tribology of silicon nitride and silicon nitride-steel sliding pairs.* Ceramics Engineering and Science Proceedings, 1984. **5**: p. 461-469.

24. Habig, K. H. and M. Woyt, *Sliding friction and wear of Al_2O_3, ZrO_2, SiC, and Si_3N_4.* Procedings of the 5th International Conference on Tribology, 1989. **3**: p. 106-113.

25. Sakrani, S. B. and J. L. Sullivan. *Iron oxide films in tribological surfaces of alloy steel*. in *Third International Conference on Thin Film Physics and Applications*. 1998. Shanghai, China.

26. Douglas, G., *Iron oxides (hydrated Iron oxides) and rust in tribology.* Journal of the Society of Tribologists & Lubrication Engineers, 1999: p. 33-37.

27. Swapnil, V. S. and B. D. Narendra, *Laser surafce engineered vanadium carbide coating for extended die life.* Journal of Materials Processing Technology, 2002. **124**: p. 105-112.

28. Gao, W., Z. Li, and D. Zhang, *New high-temp, oxidation-resistant Ti-based materials.* Oxidation of Metals, 2001. **57**: p. 99-114.

29. Darabaraa, M., L. Bourithisb, S. Diplasc, and G. D. Papadimitrioua, *A TiB_2 metal matrix composite coating enriched with nitrogen: Microstructure and wear properties.* Appied Surafec Science, 2008. **254**(13): p. 4144-4149.

30. Miao, Q., C. E. Cui, and J. D. Pan, *CrN-TiN multilayer coating on magnesium alloy AZ91 by arc-glow plasma depositing process.* Surface and Coatings Technology, 2007. **201**(9-11): p. 5077-5080.

31. Miao, Q., C. Cui, J. Pan, H. Liang, and Y. Liu, *Tribological Behavior of Magnesium alloy AZ91 coated with TiN/CrN by arc-glow Plasma Deposition.* Chinese Journal of Areonautics, 2006. **19**(3): p. 266-270.

32. He, J. A. and Y. W. Wang, *Wear and wear resitance materials*. 2001, China: Northeast University Publish House.

33. Polcar, T., R. Martinez, T. T. Vítu, L. Kopecky, R. Rodriguez, and A. Cavaleiro, *High temperature tribology of CrN and multilayered Cr/CrN coatings.* Surafce and coatings Technology, 2009. **203**: p. 3254-3259.

This page is intentionally left blank

Chapter 8

Conclusions

- A weight to powder ratio (DPR) of 13.2:1 and a milling time of 4 hours is sufficient to produce homogenously inter-mixed composite powders of TiO_2 and Al.

- In combustion reacted powder A, the Ti based metallic and Al_2O_3 based ceramic phases were continuous and exhibited an interpenetrated network. However in powder B powder particles showed a few areas where interpenetrating phases were absent creating a non-homogenous structure.

- Feedstocks of composite powders with good flowability and suitability for thermal spraying were successfully produced by treating the fine feeds with an organic binder consisting of 2% PVA (polyvinyl alcohol).

- The lower temperature of the HVOF spraying process resulted in coatings similar to the original composition of their respective starting feedstock powders. However, some new phases $(Al_2Ti)O_5$ and TiO were also formed in the case of $Ti(Al,O)/Al_2O_3$(A1, A2) and $TiAl/Al_2O$ (B2) coatings respectively due to reactions in the molten particles whilst in flight during the spraying process.

- It was found that the composite coatings change the molten Al attack on H13 tool steel from a generalized to a localized one. The coating blocked, partially blocked or delayed the contact of the aluminium melt and H13 steel, but does not change the mechanism of aluminium attack on the H13 tool steel. The local attack in the coatings caused hemispherical pits on the steel substrate. The process of pit nucleation involved the formation of Fe-Al intermetallic compounds due to the inter-diffusion and reaction between the steel substrate and molten aluminium through the local coating defects.

- The high surface roughness of the as-sprayed coatings, a non uniform coating thickness and coating defects were the most significant contributory factors leading to aluminium soldering. In particular the thinner coating areas were the most vulnerable to aluminium attack.

- It has been found that a Ti(Al,O)/Al_2O_3 (A2) composite coating is a better protective coating than the TiAl/Al_2O_3 (B2) composite coating, due its better stability against molten aluminium attack.

- No reaction between molten aluminium and a Ti(Al,O)/Al_2O_3 (A2) composite coating was identified, the phase constituents of the coating were found to be the same after immersion in molten aluminium. However an inhomogeneous TiAl/Al_2O_3 composite coating microstructure was found to be attacked by molten aluminium as a result of a reaction between the coating and molten aluminium.

- The work suggested that the Ti (Al,O) binder is more resistance to attack by molten aluminium than the intermetallic TiAl binder because it already has aluminium in solid solution.

- A Ti(Al,O)/Al_2O_3 coating (A1) on a hardened H13 steel showed better thermal shock resistance than a Ti(Al,O)/Al_2O_3 and TiAl/Al_2O_3 coatings (A2, B2) under similar test conditions.

- Composite coatings have great potential for high temperature application due to their low wear rate at high temperature. The room temperature wear behaviour of the composite coatings improves under lubricated conditions.

- Successful trials of a Ti(Al,O)/Al_2O_3 composite coated dummy block used in aluminium extrusion revealed that the coating has a potential as an industrial coating.

- The tribological properties of the coating can be improved further by reducing the surface roughness of the as sprayed coatings and by introducing more of the ceramic phase into the coating structure.

- This work suggests that resistance to molten aluminium, coating durability and wear performance may be improved if much more oxide phase could be introduced into the coating.

- The work proposes that the composite coating is suitable for less complex shaped components such as dummy blocks used in aluminium extrusion, dross ladles and other applications where good surface finish is not a stringent requirement.

8.1. Recommendation for future work

- A spray-drying technique could be used to agglomerate fine powder particles and to produce a consistent particle size distribution for the powder feedstock.

- The deposition efficiency of composite powders during thermal spraying should be evaluated.

- The wetability angle of the composite coatings with molten Al should be investigated.

- The coating performance is sensitive to coating thickness therefore the effect of composite coating thickness and surface roughness on molten aluminium soldering should be investigated.

- The spraying method could be modified by using robot manipulation to produce uniform coating thickness. The effect of a shroud attachment to the spray gun warrants further attention.

- The work was conducted using pre-set spraying parameters at Holster Engineering. The effect of changing and optimising these parameters should be investigated.

- The thermal expansion coefficients of the composite coatings should be evaluated to measure the degree of mismatch between the coatings and the steel in order to explain their thermal shock behaviour.

- The thermal conductivity of the composite coatings should be evaluated since it is particularly relevant for their possible application in die casting dies
- The erosive wear behaviour of the composite coating should be assessed for their particular application in die casting dies.
- The soldering evaluation of the composite coatings should be carried out at high pressure to simulate more closely the condition in aluminium die-casting.